# SYNTHESIS AND CHARACTERIZATION OF SCHIFF BASE COMPLEXES OF Cu, Zn, AND Pd; THEIR BIOLOGICAL AND CATALYTIC ACTIVITIES

Thesis Submitted for the Award of the Degree of

## **DOCTOR OF PHILOSOPHY**

in

Chemistry

By

**Ankush Kumar** 

**Registration number: 42000579** 

**Supervised By** 

Co-Supervised by

**Dr. Suman Maji (18432)** 

Dr. Deepak Kumar

**Department of Chemistry (Professor)** 

**Department of Chemistry (Assistant Professor)** 

**Lovely Professional University** 

**GGM Science College, Jammu** 



LOVELY PROFESSIONAL UNIVERSITY, PUNJAB 2025

#### **DECLARATION**

I, hereby declared that the presented work in the thesis entitled "Synthesis and characterization of Schiff Base complexes of Cu, Zn and Pd; Their Biological and Catalytic Activities" in fulfilment of degree of **Doctor of Philosophy (Ph.D.)** is outcome of research work carried out by me under the supervision of DR. SUMAN MAJI, working as Professor, in the Department of Chemistry, School of Chemical Engineering and Physical Sciences, Lovely Professional University, Punjab, India. In keeping with general practice of reporting scientific observations, due acknowledgements have been made whenever work described here has been based on findings of other investigator. This work has not been submitted in part or full to any other University or Institute for the award of any degree.

Revas 5

**Ankush Kumar** 

42000579

Department of Chemistry,

School of Chemical Engineering and Physical Sciences,

Lovely Professional University,

Punjab, India

## **CERTIFICATE**

This is to certify that the work reported in the Ph.D. thesis entitled "Synthesis and characterization of Schiff Base complexes of Cu, Zn and Pd; Their Biological and Catalytic Activities" submitted in fulfillment of the requirement for the award of degree of **Doctor of Philosophy (Ph.D.)** in the in the Department of Chemistry, School of Chemical Engineering and Physical Sciences, is a research work carried out by Ankush Kumar, (Registration No.42000579), is bonafide record of his/her original work carried out under my supervision and that no part of thesis has been submitted for any other degree, diploma or equivalent course.



DR. SUMAN MAJI

(Supervisor)

Professor

Department of Chemistry,

School of Chemical Engineering and Physical

Sciences

Lovely Professional University

Minor

DR. DEEPAK KUMAR

(Co-Supervisor)

**Assistant Professor** 

Department of Chemistry

GGM Science College, Jammu

#### **Abstract**

The effectiveness of Schiff base as a synthetic intermediate in the production of coordination metal complexes has been established. The imine or azomethine (C=N) moiety that is produced as a result of this nucleophilic addition reaction in Schiff base is responsible for their biological actions. A wide range of bacterial, viral, and fungal species have been shown to be effectively inhibited by Schiff base ligands. However, the bio-activity of Schiff base ligands has shown a significant increase when a suitable metal is made to react with these ligands under ambient conditions to form metal complexes. These ligands undergo metalation with almost each of the transition metal via the imine nitrogen. The metal complexes of Schiff base ligands have been reported to exhibit various biomedical and catalytic applications depending upon the type of metal and ligand used in metal complex formation. Upon complexation with transition metals in different oxidation states, these compounds exhibit numerous applications in the field of industry as well as medicine. Metals in different oxidation states from the periodic table have been utilized for complexation with the Schiff base biomolecules, but during the past few decades, transition metal complexes of Cu(II), Zn(II), and Pd(II) engrossed a lot of consideration because of their important biological and catalytic activities. The thrust area of the thesis represents the synthesis of novel homogeneous and heterogeneous Schiff base metal complexes of Copper(II), Zinc(II), and Palladium (II). The synthesised complexes are characterized using various spectroscopic techniques and their applications are tested for biocidal activities, DNA binding tendency and catalysis.

Here in, we have synthesised Salen type Schiff base ligand and corresponding metal complexes of Cu(II), Zn(II) and Pd(II) and their characterization has been done using various spectroscopic techniques. The *in vitro* biological activities i.e., antibacterial, antifungal and DNA binding studies of the Schiff base ligand and corresponding metal complexes of Cu(II), Zn(II) and Pd(II)were assessed through the well disc diffusion method, analytical, and multi-spectroscopic techniques, respectively. To understand the preferential binding modes of the synthesized metal(II) complexes with *ct*-DNA, DNA binding interaction studies were performed using multispectroscopic techniques, including electronic spectroscopy titrations,

fluorescence spectroscopy, ethidium bromide (EB) assay, circular dichroism (CD) studies, and cyclic voltammetry. Circular Dichroism (CD) investigations reveal significant conformational and morphological alterations in the secondary structure of DNA when it interacts with the complexes. The synthesized compounds were also tested for their antibacterial activity against *Escherichia coli*, *Klebsiella pneumonia*, and *Staphylococcus aureus* bacteria, and the anti-fungal activity was tested against *Colletotrichum acutatum* and *Fusarium sp.* fungi. The minimum inhibitory concentration (MIC) and the zone of inhibition (ZOI) values were used to measure the antibacterial activities of the synthesized ligand (L) and metal(II) complexes. Among the synthesized complexes, the Cu(II) complex exhibited the highest activity, while the Pd(II) complex exhibited the least activity. Overall, it was observed that among the synthesized compounds, the Cu(II) complex exhibited the highest biological activities.

Besides, having numerous applications of homogenous transition metal complexes, heterogeneous metal complexes used in catalysis are equally efficient and are meeting the demands due to their easy recovery, recyclability, and sustainability. We have developed a Schiff base functionalized Cu(II) onto L-dopaSB/Al<sub>2</sub>O<sub>3</sub>-Fe<sub>3</sub>O<sub>4</sub> as an efficient magnetic nanocomposite (Cu@L-dopaSB/Al<sub>2</sub>O<sub>3</sub>-Fe<sub>3</sub>O<sub>4</sub>). The developed catalyst has been well characterized by different techniques such as HR-SEM, EDX, TEM, XRD, BET, FTIR, ICP-AES, CHN, TGA, and VSM analysis. Excellent results were obtained when the designed catalyst's catalytic activity was tested for the production of 1,4-Disubstituted-1,2,3-triazoles.

Triazoles have long remained a centre of attraction for researchers owing to their wide range of applicability both in industries as well as in medicines. These acclaimed organic moieties are the most significant and utilitarian set of compounds in the present era. Further, the magnetic nanocomposite showed excellent catalytic activity for the one-pot synthesis of 1,4-Disubstituted-1,2,3-triazoles from aryl/alkyl boronic acids under sustainable reaction conditions. The catalyst could be easily and completely recovered using an external magnet and reused up to seven consecutive runs without any considerable change in catalytic activity, thus making it eco-friendly and economical to use.

Another catalyst system based on Zn(II) onto Chitosan Schiff base metal complex [Zn@CS-SB/Fe<sub>3</sub>O<sub>4</sub>-SiO<sub>2</sub>] has been prepared. The novel catalyst was characterized by numerous techniques like SEM imaging and mapping, EDX, HRTEM, XPS, FTIR, XRD, TGA, BET, VSM, ICP-AES and CHN analysis. One of the main issues facing the modern world is the substantial influence that organic pollutants have on the environment. Dyes, in particular, are a primary contributor to water pollution. A substantial quantity of both man-made and aromatic dyes is used in various industries. Many of these synthetic dyes are highly toxic to humans and aquatic organisms, highlighting the urgent need for effective degradation methods to remove these harmful substances from industrial waste under mild reaction conditions. Keeping in view the above considerations, the applicability of the developed magnetic catalyst, i.e., Zn@CS-SB/Fe<sub>3</sub>O<sub>4</sub>-SiO<sub>2</sub>, has been tested for the degradation of organic dyes. The proposed catalyst showed improved activity for the reduction of a variety of dyes, including methyl red (MR), methyl orange (MO), methylene blue (MB), and pnitrophenol (PNP), using NaBH<sub>4</sub> as the reducing agent under mild reaction conditions. The combination of the magnetic composite's large surface area and better dye adsorption on the catalyst surface is responsible for its increased activity.

Additionally, the catalyst's catalytic activity and selectivity are not significantly reduced throughout its easy recycling and six-time reuse.

In order to continue our work to explore the use of transition metal complexes of Schiff base functionalized magnetic catalysts, we have synthesized another catalyst system i.e., Schiff base functionalized Pd(II) complex onto titania-coated magnetic nanoparticles [Pd@SB/Fe<sub>3</sub>O<sub>4</sub>-TiO<sub>2</sub>]. Numerous techniques, including FE-SEM, EDX, TEM, XPS, BET, XRD, TGA, FT-IR, CHN, VSM, as well as ICP-AES analysis, are used to characterize and thoroughly evaluate the proposed catalytic system. Schiff base functionalization provides excellent support to the palladium, as leaching of the metal was not observed. The catalyst's magnetic core ensures that it is easily recoverable, which keeps the reaction sustainable. The magnetic catalyst demonstrated excellent recyclability up to six cycles with no discernible decrease in catalytic effectiveness, and it was simple to separate with the aid of an external magnet. Suzuki coupling reaction

stands out as one of the most efficient and essential methodologies in organic chemistry for synthesizing biaryls. Its versatility has revolutionized the field, making it nearly impossible to find research in synthetic organic chemistry that does not leverage this powerful technique. Biaryls play a crucial role as building blocks for a myriad of natural products, including polymers, alkaloids, ligands, and vital medicinal drugs. The significance of the biaryl motif is underscored by its widespread occurrence in a diverse array of biologically active compounds and functional groups, highlighting its importance in modern chemistry. Selective hydrogenations, on the other hand, have also attained worldwide significance since they add worth to economical products obtained from diverse processes, and also allow the synthesis of vital compounds for the pharmaceutical, food, petrochemical, and fine chemical industry. Among various hydrogenation reactions, selective catalytic hydrogenation of aromatic nitro compounds finds great importance, since the products obtained are useful in pharmaceutical and medicinal chemistry, and material science. Thus, the catalytic activity of Pd@SB/Fe<sub>3</sub>O<sub>4</sub>-TiO<sub>2</sub> for the Suzuki Miyaura coupling reaction to synthesize biaryls via C-C coupling and for synthesizing aromatic amines by the hydrogenation reaction of aromatic nitro compounds under sustainable reaction conditions was tested, which revealed excellent results.

## Acknowledgement

With heartfelt gratitude, I express my thanks and reverence to **Almighty God**, the most compassionate and generous, who blessed me with the courage and patience necessary to accomplish this work with success.

While my name is the only one displayed on the cover of this thesis, it embodies the invaluable contributions of many individuals who have supported its creation. This long journey would not have been possible without their unwavering support, love, and encouragement. I am profoundly thankful to each of them for their crucial roles in this achievement.

I am truly honored to express my deepest gratitude and heartfelt thanks to my supervisor, **Dr. Suman Maji**, for the continuous support, motivation, and expertise he provided during my doctoral research. His unique approach to handling crises and exemplary guidance made a significant difference in my journey. I couldn't have asked for a better mentor for my Ph.D.

I am also thankful to my Co-Supervisor, **Dr. Deepak Kumar**, for his support, guidance, and help in carrying out my research.

I am also thankful to the **Department of Chemistry** at the **School of Chemical Engineering and Physical Sciences, Lovely Professional University**, for providing me with the necessary facilities to carry out my research work smoothly.

I want to take a moment to express my deep gratitude to my grandparents, **Sh.**Mangal Ram and the late **Smt.** Sumitra Devi, whose blessings and unwavering love have been the foundation of my life. I owe my heartfelt thanks to my parents, **Sh.** Daya Krishan and **Smt.** Raj Kumari, for their relentless support and for creating an environment that nurtured my growth. Their selfless love, care, and countless sacrifices have profoundly shaped my path. Additionally, I am grateful to my inspiring brother, **Dr.** Rahual Kumar, and my supportive sister, **Ms.** Priyia Rani, whose constant motivation has fueled my determination. Their influence has been invaluable to me.

When I think of my in-laws, I truly count my blessings. They have been caring and supportive throughout my research journey. My acknowledgment would not be complete without expressing my gratitude to my father-in-law, **Sh. Madan Lal**, my mother-in-law, **Smt. Kunti Devi**, my brother-in-law, **Mr. Ashish Bhardwaj**, and **Mr. Dheeraj Bhardwaj** for their unwavering support and care during this phase of my life.

Words are too little to thank my loving wife, **Dr. Madhvi Bhardwaj**, without whose sacrifices, support, and guidance this task would not have been completed. She has consistently been my source of inspiration and the sunshine that brightens my days. My kids, **Suryansh Aryan** and **Jivanshi Aryan**, are my little bundles of joy. The innocent smile on their faces acted as a boost and replenished my energy whenever I felt tired and stressed. My children deserve special mention for their sacrifices, including missed bedtime stories and delayed playtime. Nevertheless, this acknowledgment will fall short of words to describe their invaluable presence in my life.

I am highly thankful to Lovely Professional University, University of Jammu, IIIM Jammu, SAIF Chandigarh, Panjab University, AMU Aligarh, CIF Labs (IIT Guwahati, CU Jammu and IIT Jammu), IICT Hyderabad and G.G.M Science College, Jammu for carrying out various characterization studies of the synthesized catalysts.

I express my special thanks to **Dr.Sumeer Choudhary** and **Dr. Shah Imtiaz** for their genuine support throughout this research work.

I genuinely hope that those who have not been mentioned will find it in their hearts to forgive me, as they are always remembered with gratitude. To each of you, I extend my deepest thanks.

Ultimately, despite its ups and downs, this journey has been one of the most rewarding experiences of my life. When rain and sunshine come together, a rainbow is produced. The greatest gifts are the priceless lessons I've learned along the way, and I've shared my greatest victories and worst struggles with the people I care about.

# **Table of Contents**

S.No.	Title	Page No.
1.	Declaration	i
2.	Certificate	ii
3.	Abstract	iii-vi
4.	Acknowledgement	vii-viii
5.	Table of Contents	ix
6.	List of Tables	X
7.	List of Figures	xi-xvi
8.	List of Annexures	xvii-xviii
9.	List of Abbreviations	xix-xxi
10.	Chapter 1 Introduction and Literature Review	1-66
11.	Chapter 2 Synthesis, Characterization and Biological activities of Schiff base ligand and corresponding Cu(II), Zn(II) and Pd(II) metal complexes	67-102
12.	Chapter 3 Synthesis, characterization and application of Schiff base functionalized Cu(II) onto L-dopaSB/Al <sub>2</sub> O <sub>3</sub> -Fe <sub>3</sub> O <sub>4</sub> magnetic composite [Cu@L-dopaSB/Al <sub>2</sub> O <sub>3</sub> -Fe <sub>3</sub> O <sub>4</sub> ]	103-156
13.	Chapter 4 Synthesis, characterization and application of Zn(II) onto Chitosan Schiff base metal complex [Zn@CS-SB/Fe <sub>3</sub> O <sub>4</sub> -SiO <sub>2</sub> ]	157-179
14.	Chapter 5 Synthesis, characterization and application of Schiff base functionalized Pd(II) complex onto titania grafted magnetic nanoparticles [Pd@SB/Fe <sub>3</sub> O <sub>4</sub> -TiO <sub>2</sub> ]	180-233
15.	Summary and Overall Conclusion of the Thesis	234-237
16.	Future Scope	238
17.	List of Publications	239
18.	List of Conferences	240

# **List of Tables**

S.No.	Caption	Page No.
Table 2.1	Cathodic and Anodic potential (V) and current (A)	93
	for the redox couples of complex 1 with ct–DNA in	
	5mM Tris buffer solution (pH 7.2) at a scan rate of	
	100mVs <sup>-1</sup> . Data represent mean ± SEM of three	
	independent trials (n≥ 3)	
Table 2.2	Zone of inhibition for antimicrobial activities of the	95
	Schiff bases ligand (L) and metal(II) complexes (1–	
_	3). Data represent mean $\pm$ SEM.	
Table 3.1	Optimization of reaction conditions for the one-pot	123
_	synthesis of 1,4-disubstituted-1,2,3 triazoles.	
Table 3.2	Optimization of solvent for the one-pot synthesis of	125-126
	1,4-disubstituted-1,2,3 triazole from	
	arylboronicacids and phenylacetylene.	
Table 3.3	Cu@L-dopaSB/Al <sub>2</sub> O <sub>3</sub> -Fe <sub>3</sub> O <sub>4</sub> catalysed synthesis of	126-128
	1,4-disubstituted-1,2,3-triazoles	
Table 3.4	Evaluation of Cu@L-dopaSB/Al <sub>2</sub> O <sub>3</sub> -Fe <sub>3</sub> O <sub>4</sub> catalytic	132
	activity in comparison to other documented catalyst	
	systems for the synthesis of 1,4-disubstituted-1,2,3	
	triazoles	
Table 5.1	Evaluation of the activity of the different catalysts	197
	and their amount at different temperatures for Suzuki	
	coupling reaction	
Table 5.2	Optimization of reaction conditions in terms of	198
	different solvents and amount of base for Suzuki	
	coupling reaction	100 000
Table 5.3	Pd@Fe <sub>3</sub> O <sub>4</sub> -TiO <sub>2</sub> /SB catalyzed Suzuki coupling	199-200
	between arylhalides and boronic acids using water	
Table 5.4	Evaluation of the activity of the different catalysts	217
	and their amount at different temperatures for the	
m 11	reduction of nitrobenzene	• • • • • • • • • • • • • • • • • • • •
Table 5.5	Optimization of different solvents for hydrogenation	218
T 11 7 6	of aromatic nitro compounds	210
Table 5.6	Pd@Fe <sub>3</sub> O <sub>4</sub> -TiO <sub>2</sub> /SB catalysed hydrogenation of	219
m 11 55	aromatic nitrocompounds	222
Table 5.7	Comparison of the catalytic activity of	223
	Pd@SB/Fe <sub>3</sub> O <sub>4</sub> -TiO <sub>2</sub> with other reported Schiff base	
	functionalized catalytic systems for the Suzuki	
	coupling reaction and the hydrogenation of aromatic	
	nitro compounds	

# **List of Figures**

S.No.	Caption	Page No.
	Chapter 1	
Figure 1.1	Structure of Salen type Schiff base Ligand	4
Figure 1.2	Structure of Salophen type Schiff base Ligand	5
Figure 1.3	Structure of Hydrazone type Schiff base Ligands (a and	6
	b)	
Figure 1.4	Structure of Thiosemicarbazone type Schiff base Ligand	6
Figure 1.5	Mechanism of Schiff base formation	9
Figure 1.6	Synthesis of Alumina	13
Figure 1.7	Arrangement of hydroxyl groups on the surface of silica	14
	(a) Free hydroxyl groups (b) Vicinal hydroxyl groups (c)	
	Hydroxyl groups bonded with water by hydrogen	
	bonding.	
Figure 1.8	Structure of Bis-(2-aminobenzaldehyde)] malonoyl	21
	dihydrazone] and metal complexes with Cu(II), Ni(II),	
	Zn(II) and oxovanadium(IV)	
Figure 1.9	Structure of Schiff base (HL)	21
Figure 1.10	Structure of Schiff base complex of Cu(II) metal	22
Figure 1.11	Structure ofCo(II), Cu(II), and Zn(II) complexes of the	23
	Schiff base	
Figure 1.12	Stucture of Schiff base 1,4-bis[(2-	23
	hydroxybenzaldehyde)propyl]piperazine (BHPP) ligand	
Figure 1.13	Structure of Schiff base ligands Pc4PDTC and	24
	Cb4PDTC	
Figure 1.14	Structure of Schiff base ligands (a) H <sub>2</sub> salChx and (b)	25
	H <sub>2</sub> MeOsalChx)	
Figure 1.15	Structure of tetradentate mononuclear copper Schiff base	25
	complex bridged with pyridine	
Figure 1.16	Structure of Salen type Schiff base metal complex	26
Figure 1.17	Structure of Schiff base Cu(II) complex	26
Figure 1.18	Structure of Schiff base ligand (DBAPB)	28
Figure 1.19	Structure of Schiff base Pd(II) complex	30
Figure 1.20	Schiff base complex of Cu(II) and Pd(II)	30
Figure 1.21	Structure Schiff base ligand (B) and corresponding	31
	metal complexes (B <sub>1</sub> -B <sub>4</sub> )	
Figure 1.22	Structure of 5-Imidazole based ligands cenz(1) and	32
	onz(2)	
Figure 1.23	Structure of Schiff base ligand H <sub>2</sub> LB (a) and chelate Cu	32
	metal complex (b)	

Figure 1.24	Structure ofCu(II)-Schiff base/SBA-15 catalyst	33
Figure 1.25	Fe <sub>3</sub> O <sub>4</sub> –Schiff base Cu(II) catalyzed oxidation reaction	33
Figure 1.26	Chitosan attached Copper(II) Schiff base catalyzed	34
	Chan-Lam C-N coupling	
Figure 1.27	Heterogeneous Schiff-base complexes of zirconium	35
	oxide and copper anchored on MCM-41	
Figure 1.28	Pro-chiral Schiff base Copper complex catalyzed	35
	synthesis of β-hydroxy-1,2,3-triazole	
Figure 1.29	Ni or Zn@MCM 41 catalyzed oxidation of sulfides to	36
	sulfoxides and oxidative coupling of thiols to disulfides	
Figure 1.30	Zn-Ag@L-arginine Fe <sub>3</sub> O <sub>4</sub> catalyzed synthesis of	37
	benzimidazoles and pyrimidines	
Figure 1.31	Structure of Palladium based nano-magnetic Schiff base	38
	complex	
Figure 1.32	Pd NPs@Sch-boehmitecatalyzed reduction and Suzuki	39
	coupling reaction	
Figure 1.33	Nanocarbon supported Pd based Schiff base complex	39
Figure 1.34	Fe <sub>3</sub> O <sub>4</sub> @SiO <sub>2</sub> @L-Pd catalysed Suzuki Reaction	39
Figure 1.35	Pd Schiff base complex for the C-C coupling reaction	40
Figure 1.36	Proposed scheme for synthesizing Schiff base type	42
	complexes of transition metals	
Figure 1.37	Proposed scheme for synthesizing Heterogeneous Schiff	43
	base type complexes of transition metals	
Figure 1.38	Applications of Heterogeneous Schiff base metal	43
	complexes	
	Chapter 2	
Figure 2.1	Synthesis and structure of Schiff base Ligand: N, N-	70
	Bis(5-bromo-2-salicylidene) butane 1,4-diamine	
Figure 2.2	General synthetic route for probable structures of Schiff	71
	base metal complexes (1–3).	
Figure 2.3	FT-IR spectra of the ligand and metal complexes of	73
	Cu(II), Zn(II), Pd(II).	
Figure 2.4	UV-Vis. spectra of the ligand and metal complexes of	74
	Cu(II), Zn(II), Pd(II).	
Figure 2.5	XRD spectra of the ligand and metal complexes of	75
	Cu(II), Zn(II), Pd(II).	
Figure 2.6	<sup>1</sup> H NMR spectra of the ligand (L).	76
Figure 2.7	<sup>1</sup> H NMR spectra Zn(II) Schiff base complex	76
Figure 2.8	<sup>1</sup> H NMR spectra Pd(II) Schiff base complex	77
Figure 2.9	ESI mass spectra of ligand L (a), and metal(II) complex	79

	1 (b), 2 (c) and 3 (d).	
Figure 2.10	Mass fragmentation pattern of copper(II) complex (1).	80
Figure 2.11	EPR spectra of copper(II) complex1in solid phase at	80
	room temperature.	
Figure 2.12	Absorption titration curves of synthesized ligand L (a),	88
	and metal(II) complexes 1 (b), 2 (c) and 3 (d) at different	
	concentrations of <i>ct</i> -DNA. Inset: Plots of [DNA]/ $\varepsilon a - \varepsilon f$	
	$(M2 \text{ cm}) \text{ vs } [DNA]. [DNA] = 0.1-0.8 \times 10-5 \text{ M}, [L] =$	
	[Complexes $(1-3)$ ] = $0.5 \times 10-5$ M.	
Figure 2.13	Emission spectra:Plots of 1/F– F0 versus 1/[Metal(II)	89
	complexes $(1-2)$ ], $[DNA] = 0.2 \times 10^{-5} M$ , $[complex 1] =$	
	[complex 2] = [complex 3] $0.1-0.6 \times 10^{-5} M$ .	
Figure 2.14	Emission spectra of EB-DNA system recorded in Tris-	90
	HCl buffer at pH = $7.3$ in presence of synthesized	
	metal(II) complexes 1 (a), 2 (b) and 3 (c). [EB] =	
	$[DNA] = 2 \times 10-6 \text{ M}.$	
Figure 2.15	Emission spectra of synthesized metal (II) complexes 1	91
	(a), 2 (b) and 3 (c) in presence of increasing aliquots of	
	DNA [complex 1] = [complex 2] = [complex 3] = $3 \times$	
	$10^{-6} \text{ M}, [DNA] = 0.1 - 0.5 \times 10^{-5} \text{ M}.$	
Figure 2.16	Cyclic voltammogram curves of Complex 1in the	92
	presence and absence of <i>ct</i> -DNA at a scan rate of 100	
	mVs <sup>-1</sup> in tris HCl buffer of pH=7.2. [Complex] = $4 \times 10^{-1}$	
F: 0.15	$^{6}$ M, [DNA] = $0.6 \times 10^{-6}$ M.	0.4
Figure 2.17	CD spectra of ct-DNA, and metal(II) complexes (1–3) in	94
	Tris-HCl buffer (pH=7.3). [DNA] = $0.4 \times 10^{-5}$ M and	
	[complex 1] = [complex 2] = [complex 2] = $2 \times 10^{-5}$ M.	
Figure 2.18	Comparative antibacterial action of synthesized ligand	96
	(L) and complexes (1–3) against <i>Escherichia coli</i> (a),	
	Klebsiella pneumonia (b) and Staphylococcus aureus (c)	
	bacterial strains.	
Figure 2.19	Comparative antifungal action of synthesized ligand (L)	96
	and complexes (1–3) against Colletotrichum acutatum	
	(a) and Klebsiella pneumonia (b) and Fusarium sp.	
	fungal strains.	
	Chantor 3	
Figure 3.1	Chapter 3  Proposed scheme for the synthesis of Cu@I	104
rigule 3.1	Proposed scheme for the synthesis of Cu@L-dopaSB/Al <sub>2</sub> O <sub>3</sub> -Fe <sub>3</sub> O <sub>4</sub>	104
Figure 3.2	HR-SEM images of Cu@L-dopaSB/Al <sub>2</sub> O <sub>3</sub> -Fe <sub>3</sub> O <sub>4</sub>	107
riguic 3.2	TIN-SENT IMAGES OF CUMPL-GOPASD/AI2O3-TE3O4	107

T: 0.0		100
Figure 3.3	TEM images of Cu@L-dopaSB/Al <sub>2</sub> O <sub>3</sub> -Fe <sub>3</sub> O <sub>4</sub>	108
Figure 3.4	EDX ofCu@L-dopaSB/Al <sub>2</sub> O <sub>3</sub> -Fe <sub>3</sub> O <sub>4</sub>	109
Figure 3.5	EDX Mapping of Cu@L-dopaSB/Al <sub>2</sub> O <sub>3</sub> -Fe <sub>3</sub> O <sub>4</sub>	109
Figure 3.6	BET of Cu@L-dopaSB/Al <sub>2</sub> O <sub>3</sub> -Fe <sub>3</sub> O <sub>4</sub>	110
Figure 3.7	XPS of Cu@L-dopaSB/Al <sub>2</sub> O <sub>3</sub> -Fe <sub>3</sub> O <sub>4</sub> (a) Overall survey	112
	spectrum (b) N 1s region (c) Core level spectrum of Cu	
	2p (Fresh) (d) Core level spectrum of Cu 2p (re-used	
	after 6 runs) (e) Deconvulated XPS spectrum of Cu 2p.	
Figure 3.8	FTIR spectra (a) Al <sub>2</sub> O <sub>3</sub> -Fe <sub>3</sub> O <sub>4</sub> (b) Cu@L-dopaSB/Al <sub>2</sub> O <sub>3</sub> -	113
	Fe <sub>3</sub> O <sub>4</sub> (c) Cu@L-dopaSB/Al <sub>2</sub> O <sub>3</sub> -Fe <sub>3</sub> O <sub>4</sub> (re-used after 6	
	runs).	
Figure 3.9	XRD spectra (a) SB/L-dopa/Al <sub>2</sub> O <sub>3</sub> -Fe <sub>3</sub> O <sub>4</sub> (b) Cu@L-	114
	dopaSB/Al <sub>2</sub> O <sub>3</sub> -Fe <sub>3</sub> O <sub>4</sub> (c) Cu@L-dopaSB/Al <sub>2</sub> O <sub>3</sub> -Fe <sub>3</sub> O <sub>4</sub>	
	(re-used after 6 runs).	
Figure 3.10	TGA curves of (a) Al <sub>2</sub> O <sub>3</sub> -Fe <sub>3</sub> O <sub>4</sub> (b) L-dopaSB/Al <sub>2</sub> O <sub>3</sub> -	115
	Fe <sub>3</sub> O <sub>4</sub> (c) Cu@L-dopaSB/Al <sub>2</sub> O <sub>3</sub> -Fe <sub>3</sub> O <sub>4</sub>	
Figure 3.11	VSM spectra (a)L-dopaSB/Al <sub>2</sub> O <sub>3</sub> -Fe <sub>3</sub> O <sub>4</sub> (b)Cu@L-	116
	dopaSB/Al <sub>2</sub> O <sub>3</sub> -Fe <sub>3</sub> O <sub>4</sub> (c) VSM of Cu@L-dopaSB/Al <sub>2</sub> O <sub>3</sub> -	
	Fe <sub>3</sub> O <sub>4</sub> (re-used after 6 runs).	
Figure 3.12	Drugs containing 1,2,3-triazole motif	120
Figure 3.13	Cu@L-dopaSB/Al <sub>2</sub> O <sub>3</sub> -Fe <sub>3</sub> O <sub>4</sub> catalyzed synthesis of	122
1180110 0110	alkyl/aryl-substituted-1,2,3-triazoles	
Figure 3.14	Plausible mechanism for the Cu@Fe <sub>3</sub> O <sub>4</sub> @Al <sub>2</sub> O <sub>3</sub> /SB	129
	catalyzed synthesis of 1,4-disubstituted - 1,2,3-triazoles	
Figure 3.15	Recyclaibility of Cu@L-dopaSB/Al <sub>2</sub> O <sub>3</sub> -Fe <sub>3</sub> O <sub>4</sub>	130
S	Chapter 4	
Figure 4.1	Proposed Scheme for the synthesis of Zn@CS-	158
	SB/Fe <sub>3</sub> O <sub>4</sub> -SiO <sub>2</sub>	
Figure 4.2	HR-SEM images of (a and b) CS-SB/Fe <sub>3</sub> O <sub>4</sub> -SiO <sub>2</sub> (c and	161
118410 1.2	d) Zn@CS-SB/Fe <sub>3</sub> O <sub>4</sub> -SiO <sub>2</sub>	
Figure 4.3	SEM Elemental Mapping of Zn@CS-SB/Fe <sub>3</sub> O <sub>4</sub> -SiO <sub>2</sub>	162
Figure 4.4	TEM images of Zn@CS-SB/Fe <sub>3</sub> O <sub>4</sub> -SiO <sub>2</sub>	162
Figure 4.5	EDX Spectrum of Zn@CS-SB/Fe <sub>3</sub> O <sub>4</sub> -SiO <sub>2</sub>	163
Figure 4.6	Nitrogen adsorption-desorption isotherm of Zn@CS-	164
1 18410 7.0	SB/Fe <sub>3</sub> O <sub>4</sub> -SiO <sub>2</sub>	107
Figure 4.7	XPS of Zn@CS-SB/Fe <sub>3</sub> O <sub>4</sub> -SiO <sub>2</sub> ; (a) Overall survey	166
riguic 4./	spectrum (b) N 1s region (c) Core level spectrum of Zn	100
	2p (Fresh) (d) Core level spectrum of Zn2p (re-used	
Figure 4.9	after 6 runs) (e) Deconvulated XPS spectrum of Zn2p.	167
Figure 4.8	VSM spectra (a) Fe <sub>3</sub> O <sub>4</sub> -SiO <sub>2</sub> b) Zn@CS-SB/Fe <sub>3</sub> O <sub>4</sub> -SiO <sub>2</sub>	167

E: 4.0	ETID	1/0
Figure 4.9	FTIR spectra (a) Fe <sub>3</sub> O <sub>4</sub> -SiO <sub>2</sub> , (b) CS-SB/Fe <sub>3</sub> O <sub>4</sub> -SiO <sub>2</sub> (c)	168
	Zn@CS-SB/Fe <sub>3</sub> O <sub>4</sub> -SiO <sub>2</sub> (Fresh), (d) Zn@CS-SB/Fe <sub>3</sub> O <sub>4</sub> -	
T' 410	SiO <sub>2</sub> (re-used after 6 runs).	1.60
Figure 4.10	TGA curves (a) Fe <sub>3</sub> O <sub>4</sub> -SiO <sub>2</sub> (b) CS-SB/Fe <sub>3</sub> O <sub>4</sub> -SiO <sub>2</sub> (c)	169
	Zn@CS-SB/Fe <sub>3</sub> O <sub>4</sub> -SiO <sub>2</sub>	
Figure 4.11	XRD spectrum of Zn@CS-SB/Fe <sub>3</sub> O <sub>4</sub> -SiO <sub>2</sub>	170
Figure 4.12	Classification of Dyes	172
Figure 4.13	Zn@CS-SB/Fe <sub>3</sub> O <sub>4</sub> -SiO <sub>2</sub> catalyzed photocatalytic	174
	degradation of Methyl orange Dye under UV-Vis light	
Figure 4.14	Zn@CS-SB/Fe <sub>3</sub> O <sub>4</sub> -SiO <sub>2</sub> catalyzed photocatalytic	175
	degradation of (a) Methylene blue (MB); (b) Methyl red	
	(MR); (c) para-nitrophenol (PNP) under UV-Vis light	
Figure 4.15	Recyclability of Zn@CS-SB/Fe <sub>3</sub> O <sub>4</sub> -SiO <sub>2</sub> for the	176
	degradation of MO dye under optimized reaction	
	conditions.	
	Chapter 5	
Figure 5.1	General scheme for the preparation of Pd@SB/Fe <sub>3</sub> O <sub>4</sub> -	181
	TiO <sub>2</sub>	
Figure 5.2	FEG-SEM images of Pd@SB/Fe <sub>3</sub> O <sub>4</sub> -TiO <sub>2</sub>	183
Figure 5.3	TEM images of Pd@SB/Fe <sub>3</sub> O <sub>4</sub> -TiO <sub>2</sub> (a to c); SAED	184
	pattern (d)	
Figure 5.4	XPS of Pd@SB/Fe <sub>3</sub> O <sub>4</sub> -TiO <sub>2</sub> ; (a) Overall survey	186
	spectrum (b) N 1s region (c) Core level spectrum of Pd	
	3d (Fresh) (d) Core level spectrum of Pd 3d (re-used	
	after 6 runs)(e) Deconvulated XPS spectrum of Pd 3d.	
Figure 5.5	XRD spectra (a) Fe <sub>3</sub> O <sub>4</sub> -TiO <sub>2</sub> , (b) SB/Fe <sub>3</sub> O <sub>4</sub> -TiO <sub>2</sub> (c)	188
	Pd@SB/Fe <sub>3</sub> O <sub>4</sub> -TiO <sub>2</sub> (Fresh), (d)Pd@SB/Fe <sub>3</sub> O <sub>4</sub> -TiO <sub>2</sub> (re-	
	used after 6 runs).	
Figure 5.6	TGA curves (a) Fe <sub>3</sub> O <sub>4</sub> -TiO <sub>2</sub> , (b) SB/Fe <sub>3</sub> O <sub>4</sub> -TiO <sub>2</sub> (c)	189
	Pd@SB/Fe <sub>3</sub> O <sub>4</sub> -TiO <sub>2</sub>	
Figure 5.7	N <sub>2</sub> adsorption-desorption isotherm of Pd@SB/Fe <sub>3</sub> O <sub>4</sub> -	190
	TiO <sub>2</sub>	
Figure 5.8	FTIR spectra (a)Fe <sub>3</sub> O <sub>4</sub> -TiO <sub>2</sub> , (b)Pd@SB/Fe <sub>3</sub> O <sub>4</sub> -TiO <sub>2</sub>	191
	(Fresh), (c) Pd@SB/Fe <sub>3</sub> O <sub>4</sub> -TiO <sub>2</sub> (re-used after 6 runs).	
Figure 5.9	VSM spectra (a)Fe <sub>3</sub> O <sub>4</sub> -TiO <sub>2</sub> , (b) Pd@SB/Fe <sub>3</sub> O <sub>4</sub> -TiO <sub>2</sub>	192
Figure 5.10	EDX spectrum of Pd@SB/Fe <sub>3</sub> O <sub>4</sub> -TiO <sub>2</sub>	193
Figure 5.11	Pd@SB/Fe <sub>3</sub> O <sub>4</sub> -TiO <sub>2</sub> catalyzed Suzuki coupling reaction	196
Figure 5.12	Plausible mechanism for the Pd@SB/Fe <sub>3</sub> O <sub>4</sub> -TiO <sub>2</sub>	201
115010 3.12	catalyzed Suzuki coupling.	201
Figure 5.13	Recyclability of Pd@SB/Fe <sub>3</sub> O <sub>4</sub> -TiO <sub>2</sub>	202
riguic 3.13	Recyclatility of 1 days D/1 c3O4-11O2	202

Figure 5.14	Hydrogenation of nitroarenes	216
Figure 5.15	Plausible Mechanism of Hydrogenation of nitroarenes	220
Figure 5.16	Recyclability of Pd@SB/Fe <sub>3</sub> O <sub>4</sub> -TiO <sub>2</sub>	221

# **List of Annexures**

S.No.	Caption	Page No.
Annexure 3a	<sup>1</sup> H NMR spectrum of 1,4-Diphenyl-1 <i>H</i> -1,2,3	145
	triazole	
Annexure 3b	<sup>13</sup> C NMR spectrum of 1,4-Diphenyl-1 <i>H</i> -1,2,3	145
	triazole	
Annexure 3c	<sup>1</sup> H NMR spectrum of 1-(4-Methoxyphenyl)-4-	146
	phenyl-1 <i>H</i> -1,2,3-triazole	
Annexure 3d	<sup>13</sup> C NMR spectrum of 1-(4-Methoxyphenyl)-4-	146
	phenyl-1 <i>H</i> -1,2,3-triazole	
Annexure 3e	<sup>1</sup> H NMR spectrum of 1-(4-methylphenyl)-4-phenyl-	147
	1 <i>H</i> -1,2,3-triazole	
Annexure 3f	<sup>13</sup> C NMR spectrum of 1-(4-methylphenyl)-4-phenyl-	147
	1 <i>H</i> -1,2,3-triazole	
Annexure 3g	<sup>1</sup> H NMR spectrum of 1-(4-Fluorophenyl)-4-phenyl-	148
	1 <i>H</i> -1,2,3-triazole	
Annexure 3h	<sup>13</sup> C NMR spectrum of 1-(4-Fluorophenyl)-4-phenyl-	148
	1 <i>H</i> -1,2,3-triazole	
Annexure 3i	<sup>1</sup> H NMR spectrum of 1-(2-Bromophenyl)-4-phenyl-	149
	1 <i>H</i> -1,2,3-triazole	
Annexure 3j	<sup>13</sup> C NMR spectrum of 1-(2-Bromophenyl)-4-	149
	phenyl-1 <i>H</i> -1,2,3-triazole	
Annexure 3k	<sup>1</sup> H NMR spectrum of 1-(4-Nitrophenyl)-4-phenyl-	150
	1 <i>H</i> -1,2,3-triazole	
Annexure 31	<sup>13</sup> C NMR spectrum of 1-(4-Nitrophenyl)-4-phenyl-	150
	1 <i>H</i> -1,2,3-triazole	
Annexure 3m	<sup>1</sup> H NMR spectrum of 1-(3-Nitrophenyl)-4-phenyl-	151
	1 <i>H</i> -1,2,3-triazole	
Annexure 3n	<sup>13</sup> C NMR spectrum of 1-(3-Nitrophenyl)-4-phenyl-	151
	1 <i>H</i> -1,2,3-triazole	
Annexure 3o	<sup>1</sup> H NMR spectrum of 4-(4-methoxyphenyl)-1-	152
	phenyl-1 <i>H</i> -1,2,3-triazole	
Annexure 3p	<sup>13</sup> C NMR spectrum of 4-(4-methoxyphenyl)-1-	152
	phenyl-1 <i>H</i> -1,2,3-triazole	
Annexure 3q	<sup>1</sup> H NMR spectrum of 1-Butyl-4-phenyl-1 <i>H</i> -1,2,3-	153
	triazole	
Annexure 3r	<sup>13</sup> C NMR spectrum of 1-Butyl-4-phenyl-1 <i>H</i> -1,2,3-	153
	triazole	
Annexure 3s	<sup>1</sup> H NMR spectrum of 1-Pentyl-4-phenyl-1 <i>H</i> -1,2,3-	154
	triazole	
Annexure 3t	<sup>13</sup> C NMR spectrum of 1-Pentyl-4-phenyl-1 <i>H</i> -1,2,3-	154

	triazole	
Annexure 3u	<sup>1</sup> H NMR spectrum of 1-Hexyl-4-phenyl-1 <i>H</i> -1,2,3-	155
	triazole	
Annexure 3v	<sup>13</sup> C NMR spectrum of 1-Hexyl-4-phenyl-1 <i>H</i> -1,2,3-	155
	triazole	
Annexure 3w	Mass spectrum of1-(3-Nitrophenyl)-4-phenyl-1 <i>H</i> -1,2,3-triazole	156
Annexure 3x	Mass spectrum of1-Hexyl-4-phenyl-1 <i>H</i> -1,2,3-triazole	156
Annexure 5a	<sup>1</sup> H NMR spectrum of 4-Acetylbiphenyl	209
Annexure 5b	<sup>13</sup> C NMR spectrum of 4-Acetylbiphenyl	209
Annexure 5c	<sup>1</sup> H NMR spectrum of Biphenyl-4-carboxaldehyde	210
Annexure 5d	<sup>13</sup> C NMR spectrum of Biphenyl-4-carboxaldehyde	210
Annexure 5e	<sup>1</sup> H NMR spectrum of 4-Phenylbenzonitrile	211
Annexure 5f	<sup>13</sup> C NMR spectrum of 4-Phenylbenzonitrile	211
Annexure 5g	<sup>1</sup> H NMR spectrum of 4'-fluoro-4-acetylbiphenyl	212
Annexure 5h	<sup>13</sup> C NMR spectrum of 4'-fluoro-4-acetylbiphenyl	212
Annexure 5i	<sup>1</sup> H NMR spectrum of 2'-fluoro-4-acetylbiphenyl	213
Annexure 5j	<sup>13</sup> C NMR spectrum of 2'-fluoro-4-acetylbiphenyl	213
Annexure 5k	<sup>1</sup> H NMR spectrum of 2-(4-Acetylphenyl)thiophene	214
Annexure 51	<sup>13</sup> C NMR spectrum of 2-(4-Acetylphenyl)thiophene	214
Annexure 5m	Mass spectrum of4-Acetylbiphenyl	215
Annexure 5n	Mass spectrum of2-(4-Acetylphenyl)thiophene	215
Annexure 50	<sup>1</sup> H NMR spectrum of Aniline	229
Annexure 5p	<sup>13</sup> C NMR spectrum of Aniline	229
Annexure 5q	<sup>1</sup> H NMR spectrum of 4-Methoxyaniline	230
Annexure 5r	<sup>13</sup> C NMR spectrum of 4-Methoxyaniline	230
Annexure 5s	<sup>1</sup> H NMR spectrum of 2-Chloroaniline	231
Annexure 5t	<sup>13</sup> C NMR spectrum of 2-Chloroaniline	231
Annexure 5u	<sup>1</sup> H NMR spectrum of 1-Naphthylamine	232
Annexure 5v	<sup>13</sup> C NMR spectrum of 1-Naphthylamine	232
Annexure 5w	Mass spectrum of 4-Bromoaniline	233
Annexure 5x	Mass spectrum of of4-Chloroaniline	233

# **List of Abbreviations**

Abbreviation	Full name
FTIR	Fourier transform infrared
UV-Vis	Ultra violet visible
XRD	X-ray diffraction
EPR	Electron paramagnetic resonance
DMSO	Dimethyl sulphoxide
CDCl <sub>3</sub>	Deuterated chloroform
DMF	Dimethy formamide
NMR	Nuclear magnetic resonance
Ppm	Parts per million
ESI-MS	Electron spray ionization mass spectroscopy
Cu	Copper
Zn	Zinc
Pd	Palladium
L	Ligand
G	Girade
E.Coli	Escherichia coli
SARS-CoV-2	Severe acute respiratory syndrome coronavirus 2
DNA	Deoxyribonucleic acid
ct-DNA	Calf thymus DNA
MIC	Minimum inhibitory concentration
ADMET	Absorption, distribution, metabolism, excretion and toxicity
IC50	Half maximal inhibitory concentration
TPSA	Topological polar surface area
ZOI	Zone of inhibition
EtBr	Ethidium bromide
CD	Circular Dichroism
NaCl	Sodium chloride
NaOH	Sodium hydroxide
tris-HC1	Tris Hydrochloride
EtOH	Ethanol
CH <sub>3</sub> OH	Methanol
C <sub>2</sub> H <sub>5</sub> OH	Ethanol
CH <sub>3</sub> CN	Acetonitrile
EtOAc	Ethylacetate
H <sub>2</sub> O	Water
pet ether	Petroleum ether
1	

mL	Millilitre
Mmol	Millimole
± SEM	Standard error of mean
IR	Infrared
KBr	Potassium bromide
рН	Power of Hydrogen
MRE	Mean residue ellipticity
i.e.	That is (Latin <i>id est</i> )
Nm	Nanometer
m/z	Mass/charge
S	Singlet
D	Doublet
T	Triplet
G	Gauss
eV	Electron volt
$2\theta$	2 theta
Min	Minutes
Н	Hour
Hz	Hertz
MHz	Mega hertz
J	Coupling constant
Lit. M.Pt	Literature melting point
Anal	Analytical
Calc	Calculated
RBF	Round bottom flask
CaCl <sub>2</sub>	Calcium chloride
SB	Schiff base
L-Dopa	L-3,4-dihydroxyphenylalanine
CS	Chitosan
SiO <sub>2</sub>	Silicon dioxide
TiO <sub>2</sub>	Titanium dioxide
TEOS	Tetraethylorthosilicate
Al <sub>2</sub> O <sub>3</sub>	Aluminium trioxide (Alumina)
EDA	Ethylene diamine
Fe <sub>3</sub> O <sub>4</sub>	Iron oxide
FeCl <sub>3</sub>	Ferric chloride
FeCl <sub>2</sub>	Ferrous chloride
ZnCl <sub>2</sub>	Zinc chloride
ZnO	Zinc Oxide
°C	Degree centigrade

HR-SEM	High resolution scanning electron microscopy
EDX	Energy dispersive X-ray
TEM	Transmission electron microscopy
SAED	Selected area electron diffraction
BET	Brunauer-Emmett-Teller
XPS	X-ray photoelectron spectroscopy
ICP-AES	Inductively coupled plasma atomic emission spectroscopy
CHNS	Carbon hydrogen nitrogen sulphur
TGA	Thermogravimetric analysis
VSM	Vibrating sample magnetometry
Al(OiPr) <sub>3</sub>	Aluminium isopropoxide
Cu(OAc) <sub>2</sub>	Copper acetate
Oe	Oersted
NPs	Nanaoparticles
NaN <sub>3</sub>	Sodium azide
MO	Methyl orange
MB	Methylene blue
MR	Methyl red
PNP	Para nitrophenol

# Chapter 1

#### **Introduction and Review of Literature**

#### 1.1 Introduction

Schiff bases have profoundly shaped the landscape of coordination chemistry, serving as a cornerstone in the growth of inorganic and bioinorganic chemistry, along with the development of cutting-edge optical and nanomaterials. Their remarkable versatility is evident across multiple branches of chemistry spanning inorganic, organic, and analytical domains establishing them as essential components in a wide range of commonly used organic molecules. Schiff bases represent a vital class of compounds that serve as key synthetic intermediates in creating coordination metal complexes [1]. First discovered in 1864 by the renowned German chemist Hugo Schiff, these versatile compounds are generated by the addition of a ketone or an aldehyde to the primary amine in a suitable solvent by the condensation reaction mechanism [2]. While Hugo Schiff first synthesized them over a century ago, it was Pfeiffer in the 1930s, who recognized their potential as effective ligands, paving the way for innovative advancements in the field [3]. Schiff bases can be easily produced through the reaction of aldehydes with primary amines; however, this reaction is substantially more difficult to achieve with ketones [4]. To make this reaction successful with ketones, several factors must be considered, i.e., selection of catalyst, choice of solvents to form azeotropic combination with water, an optimal reaction temperature and the appropriate pH scale [5].

Schiff bases created by the reaction of primary amines and aldehydes are known to have a -C=N-bond, which is called aldimine or azomethine [6]. Ketimine, on the other hand, is the -C=N-bond that is created inside Schiff bases as a result of the interaction of ketones with primary amines [7]. In order to form complexes, the Schiff bases exhibit selectivity towards the transition metal ions. These Schiff bases move electrons from their active sites to the metal ion during complex formation. They are known to be efficient ligands for nitrogen donors (-CH=N-) [8].

During the formation of a coordination compound, these ligands may donate one or more than one pair of electrons to the transition metal ion. Schiff bases can create highly stable chelate complexes having 4-, 5-, and 6-membered rings by donating

multiple electron pairs [9]. For this to occur, the position of the second functional group having displaceable H-atom should be much closer to the azomethine group, with the hydroxyl group being the preferred choice [10]. Schiff base ligands form complexes with transition metals via azomethine nitrogen [11]. These ligands have been broadly studied due to their ease of preparation, obtainability, and electronic and chelating properties. Schiff bases show promising applications in innumerable fields such as catalysis, bioinorganic, electrochemistry, separation process, photography, metallic deactivator, metal refining, analytical chemistry, environmental chemistry, and organic synthesis [12-15]. These assemblies are similar to other biological structures due to the presence of donor atoms such as nitrogen, oxygen, and sulphur in them. Schiff base ligands offer multiple positions for binding with metal which leads to a higher coordination number that results in larger thermodynamic and kinetic steadiness [16]. The biological activity of these compounds is due to -C=N- present in the imines or azomethine derivatives. The nitrogen atom of the imine participates in the bond creation with the metal in the biological systems and thus metal gets attached to biomolecules like amino acids and proteins thus showing bioactivity against microbes [17]. The structure-activity connection of the Schiff bases has also been extensively studied [18]. Schiff bases have lately been used in the development of self-healing covalent hydrogel networks using Click chemistry, the renowned Nobel Prize awarded work [19].

#### Types of Schiff Bases

A thorough examination of the existing literature reveals a rich variety of Schiff bases and numerous synthesis methods available to researchers today. These methods include both traditional techniques and cutting-edge approaches. Among the classical methods, some utilize solvents, while modern alternatives extend to water-suspension mediums and solvent-free conditions. Notably, techniques such as infrared irradiation and ultrasound irradiation offer efficient pathways for synthesizing Schiff bases, enabling rapid reactions while maintaining high yields. Hence, Schiff bases can be synthesized by various methods such as Solvent-free synthesis using microwave irradiation, infrared irradiation, and ultrasound irradiation, Solvent-free synthesis by using a catalyst, Solvent and catalyst-free synthesis, and Solvent-based synthesis [20].

One innovative method, known as one-pot template synthesis, simplifies the process by combining all reactants in a single reaction vessel, streamlining the workflow [21]. During the synthesis of Schiff bases, water is often produced as a byproduct [22]. To manage this, various dehydrating agents can be used to effectively remove excess water. Commonly employed dehydrating agents include magnesium sulphate (MgSO<sub>4</sub>), sodium sulphate (Na<sub>2</sub>SO<sub>4</sub>), and molecular sieves that adsorb moisture [23]. For reactions involving solvents like benzene or toluene, the Dean-Stark apparatus can be utilized to collect and remove water from the reaction mixture, ensuring optimal conditions for the reaction to proceed [24]. Schiff bases can be categorized into several distinct types, each with unique structural and chemical characteristics. These categories include Salen, Salophen complexes, Hydrazones, Semicarbazones, Thiosemicarbazones, and various heterocyclic types [25]. This classification not only emphasizes the diversity of Schiff bases but also highlights their significance and versatility in synthetic organic chemistry, paving the way for their application in multiple scientific domains.

#### Salen type bases

The term "salen" denotes a tetradentate ligand with the chemical formula  $N_2O_2$  [26]. This ligand is synthesized through a condensation reaction involving salicylaldehyde and its derivatives combined with ethylenediamine [27]. In this reaction, the reactants are used in a molar ratio of 2:1, meaning that two moles of salicylaldehyde (or its derivatives) are employed for every mole of ethylenediamine. The resulting salen ligand features two nitrogen atoms and two oxygen atoms that can coordinate with a metal center, making it a versatile building block in coordination chemistry and various catalytic processes (**Figure 1.1**).

Figure 1.1 Structure of Salen type Schiff base Ligand

## Salophen type bases

Just like salen, Salophen based tetradentate ligands (**Figure 1.2**) possess four donor atoms, specifically two oxygen (O) atoms and two nitrogen (N) atoms, arranged as O, N, N, O [28]. Their synthesis is achieved through a carefully controlled reaction between salicylaldehyde-an aromatic aldehyde and various derivatives of this compound, in conjunction with 1,2-phenylenediamines, which are key building blocks in organic chemistry.

Figure 1.2 Structure of Salophen type Schiff base Ligand

#### Hydrazone type ligand

These ligands constitute a significant class of compounds, and their synthesis typically involves a condensation reaction of carbonyl compounds, specifically aldehydes or ketones, with hydrazine or its derivatives [29] (Figure 1.3). It is impossible to overestimate the significance of these ligands in chemistry because of their wide range of biological and pharmacological uses, which have drawn a lot of interest from researchers. Additionally, the changeability of these ligands is reflected in their varied denticities, which can range from monodentate-where the ligand binds through a single donor atom-to multidentate configurations, where the ligand binds through multiple donor sites simultaneously. This flexibility in binding arrangements allows for the formation of robust complexes with different metal ions, further enhancing their utility in numerous chemical and biological contexts [30-33].

**Figure 1.3** Structure of Hydrazone type Schiff base Ligands (a and b)

#### Thiosemicarbazone type ligands

Thiosemicarbazone ligands are a significant class of compounds containing nitrogen and sulphur, first documented in the scientific literature during the 1800s [34]. These ligands have garnered considerable interest due to their unique structural features and their role as biologically active agents. Their exceptional chelating ability allows them to form strong complexes with metal ions, which enhances their potential applications in fields ranging from pharmacology to environmental science. Additionally, their increased lipophilicity contributes to improved bioavailability, making them effective candidates for drug development. The synthesis of thiosemicarbazone ligands typically occurs through a condensation reaction. This involves an aliphatic, aromatic, or heterocyclic aldehyde or ketone reacting with thiosemicarbazide or carbazide [35] (Figure 1.4). This process not only yields various thiosemicarbazone derivatives but also allows for the fine-tuning of their properties to optimize their efficacy in various applications, including antimicrobial, antitumor, and anti-inflammatory activities. The continued research and development of these ligands hold great promise for advancing medicinal chemistry and enhancing our understanding of complex biological systems.

Figure 1.4 Structure of Thiosemicarbazone type Schiff base Ligand

#### Properties of Schiff bases

#### Physical properties

Schiff bases are usually colored solids [36]. Schiff bases are helpful for recognizing the carbonyl compounds and figuring out the metal concentration because of their exact melting points. Because the -C=N-bond rotates more readily than the -C=Cbond, the stereoisomers of Schiff bases interconvert readily [37]. The significant electronegativity difference between carbon and nitrogen causes polarization in the azomethine bond, which results in this phenomenon. Due to the presence of a lone pair on N-atom and the electron-donating properties of the pi-bond in the -C=N-bond, all compounds with an azomethine group display basic behavior [38]. Compared to their comparable amines, Schiff bases with azomethine linkages have lower basic properties [39]. The reason for this discrepancy is the nitrogen atom's hybridization; in amines, it exhibits sp<sup>3</sup> hybridization, whereas in imines, it transitions to sp<sup>2</sup> hybridization. The basic character of Schiff's bases significantly decreased as a result of the hybridization modification, which revealed enhanced s-character. One prominent weak chromophore that exhibits absorption mostly in the UV spectrum is the C=N system [40]. Its visibility is increased when phenyl groups are added because this absorption spreads into the visible spectrum. The wavelength of absorption may, however, decrease if the aromatic ring contains deactivating substituents, such as halogens. Aryl alkyl ketimines usually have absorption values in the middle of dialkyl and diarylketimines. Furthermore, the C=N system's IR stretching frequency falls between 1610 and 1630 cm<sup>-1</sup> [41]. This data highlights the C=N system's fascinating behavior and adaptability in a range of applications.

#### Chemical properties

Depending on the different groups bonded to the azomethine group, Schiff bases display a variety of characteristics. When an electronegative group is linked to the nitrogen atom, these molecules become more stable. For instance, Schiff bases with alkyl or aryl substituents are far less susceptible to hydrolysis than oximes with hydroxyl groups on the nitrogen, phenylhydrazones, and semicarbazones with -NH groups [42–43]. Schiff bases can hydrolyze into amines and carbonyl compounds in

acidic settings, but they remain stable in alkaline ones. One mole of water is produced in the reversible process of Schiff base synthesis [44]. Water can cause the reaction's equilibrium to move to the left. Because of this, these reactions are usually carried out in solvents that enable the distillation of water, frequently resulting in the formation of an azeotrope [45]. The reaction tends to go to completion when it comprises amines that contain electronegative atoms with unpaired electrons on the nitrogen. Because hydrolysis is less likely to happen in certain situations, Schiff bases can be isolated effectively.

## Mechanism of Schiff base formation

The Schiff bases are made by a process that Schiff developed in which the primary amines, which may also be aromatic or aliphatic, undergo a condensation reaction with ketones or aromatic or aliphatic aldehydes. The synthesis of Schiff bases from the reaction of primary amines and carbonyl compounds involves two fundamental stages. To create an intermediate known as carbinolamine, primary amines and carbonyl compounds condense in the first step [46]. This intermediate is dehydrated to produce the Schiff base in the second step [47]. The pH affects the production of Schiff bases. The amine turns into a salt at low pH, which lowers the amount of free amine present [48]. The first fast addition step in the response mechanism becomes the rate-determining step as a result of this slowdown (**Figure 1.5**).

Figure 1.5 Mechanism showing the formation of Schiff base

The stability of Schiff bases is significantly affected by substitution. The aliphatic Schiff base having small-molecular-weight and having no substituents on the N-atom tend to polymerize easily, resulting in limited available information about these imines [49]. Conversely, Schiff bases that include aryl substituents have more stability and are easier to synthesize due to the electron donation from ring conjugation to the imine bond [50]. In contrast, those containing alkyl substituents are relatively unstable, take longer to synthesize, and are prone to polymerization. Aldehydes as compared to ketones readily react with amines to produce imines because aldehydes are more reactive than ketones. This is because of the reason that the carbonyl carbon in aldehydes is less sterically hindered as compared to the ketones. Moreover, the alkyl groups attached to the carbonyl carbon reduces its electrophilic character in ketones by donating electrons to the carbon inductively. This decrease in electrophilicity results in a slower reaction tendency. Consequently, the reaction of primary amines and aldehydes yield Schiff bases easily whereas obtaining Schiff

bases from ketones is quite challenging. A number of parameters need to be taken into account in order to successfully create Schiff bases from ketones. These include picking a suitable catalyst, figuring out the ideal pH range, modifying the reaction temperature, and choosing a solvent that can combine with the water generated during the reaction to form an azeotropic combination [51]. High temperatures, long reaction durations, and the presence of a catalyst are necessary to promote the formation of Schiff bases, especially for aromatic ketones. Ketones and aromatic aldehydes are great options for creating extremely stable Schiff bases [52].

These aldehydes can produce amazing outcomes when they react with amines at low temperatures and in the right solvent environment. Interestingly, the presence of an electron-withdrawing substituent at the aldehyde's para position significantly increased the rate at which aromatic amines reacted with aromatic aldehydes [53]. Conversely, the reaction rate falls if the amine's para position has such a substituent [54]. Eliminating the water created during the reaction is essential when creating Schiff bases from aromatic ketones. Thankfully, this additional step of water removal is not required when synthesizing Schiff bases from aldehydes and dialkyl ketones, which streamlines the procedure and increases efficiency [55].

#### 1.2 Review of Literature

In the expansive and continuously progressing field of modern chemistry, Schiff base complexes are recognized as exceptionally significant compounds. Their distinct properties and remarkable versatility enable them to serve as essential components across a broad spectrum of scientific research and practical applications. Schiff base ligands, characterized by their ability to coordinate metal ions, undergo bonding to form metal coordination complexes. This process can be achieved through a variety of synthesis methods, including direct synthesis, in situ methods, the oxidation of coordinated secondary amines, amine exchange reactions, metal exchange reactions, and ligand exchange reactions [56]. Schiff base is usually refluxed with metal salts, such as metal acetates, metal perchlorates, and metal halides, to create these metal complexes [57]. A suitable solvent is chosen to facilitate this reaction, allowing for efficient complex formation. The resulting Schiff base metal complexes demonstrate

an impressive array of applications within both industrial settings and medicinal science [58]. The geometry and structure of these metal complexes are primarily determined by several factors, including the electronic configuration and ionic radii of the metal ion and the donor properties of the ligands involved [59]. The interplay of these characteristics influences the stability and reactivity of the resulting complexes. Research has shown that metal complexes involving Schiff base ligands exhibit a diverse range of biomedical applications. These include anticancer properties [60], demonstrated through their ability to inhibit tumor growth; antiviral activity [61], which helps combat viral infections; antibacterial effects [62] against a variety of pathogens; antitumor [63] properties that target cancer cells; antimalarial [64] capabilities that offer potential treatment for malaria; antifungal [65] activities that counteract fungal infections; anti-inflammatory effects [66] that alleviate inflammatory conditions; and anticonvulsant properties [67] that can aid in the management of seizure disorders. The efficacy of these applications depends significantly on the specific metal type and the ligand used in forming the metal complex. Moreover, Schiff base complexes are invaluable in industrial applications [68], where they serve as catalysts for some of the most important organic transformations. Their ability to enhance reaction efficiencies and selectivities positions them as key players in chemical manufacturing processes, making advancements in both research and commercial sectors possible [69]. Overall, the multifaceted nature of Schiff base complexes underscores their significance in both scientific exploration and practical implementation.

#### Homogeneous and Heterogeneous Schiff base complexes

Homogeneous and heterogeneous Schiff complexes are two categories of metal complexes with Schiff bases, differing in their composition and applications. Homogeneous complexes are prepared by reacting metal salts with Schiff bases in solvents. Their properties include a well-defined structure, high catalytic activity, and solubility in various solvents [70]. They are used in various applications such as catalysis (oxidation, reduction, C-C bond formation), biomedical applications (antimicrobial, anticancer), and as sensors and imaging agents [71,72]. Heterogeneous complexes of Schiff bases, on the other hand, are synthesized by grafting Schiff bases

onto supports (e.g., silica, titania, polymers, MOF, zeolites) and subsequent metal complexation [73]. The cornerstone of effective heterogeneous catalysts lies in the choice of support material onto which active metals are dispersed. The catalytic performance of transition metals is significantly influenced by the choice of supports [74]. To maximize efficacy, the catalyst support for heterogeneous metal catalysts should encompass key characteristics likelow catalytic activity to ensure the active metal functions optimally, large surface area, optimal porosity and tailored pore size distribution for enhanced reactivity, versatile surface chemical modification properties for adaptable applications, robust resistance to reaction media to maintain integrity under diverse conditions, excellent mechanical properties to withstand operational stresses, superior thermal stability and sintering resistance to enhance longevity, consistent performance during regeneration to ensure reliability, and costeffectiveness to promote economic viability [75-78]. Commonly relied upon supports in the preparation of these advanced catalysts include alumina, silica, titania, clays, zeolites, carbon, biomaterials, and magnetic nanoparticles [79-82]. Selecting the right support can dramatically elevate catalytic performance and project outcomes, making it a crucial decision in catalyst design.

#### Alumina

Alumina with chemical formula  $Al_2O_3$ ·( $H_2O$ )n where n = (0-3) is a popular support material for catalysts, adsorbents, and other applications owing to its exclusive properties such as high surface area, porosity (mesopores, macropores), high thermal stability (up to  $1000^{\circ}$ C), chemical inertness, mechanical strength and low acidity [83]. Alumina is primarily found in its most prevalent crystalline form,  $\alpha$ -aluminium oxide ( $\alpha$ - $Al_2O_3$ ), followed by a metastable $\gamma$ -aluminium oxide ( $\gamma$ - $Al_2O_3$ )having a defect spinel crystal structure. It is a fine-grained polymorphthatconverts to  $\alpha$ - $Al_2O_3$ on heating. $\gamma$ - $Al_2O_3$  is widely utilized as a catalyst support material due to its high surface area. This large surface area enhances catalytic activity and improves efficiency. It is employed in the production of catalysts for various chemical reactions, including hydrogenation, dehydrogenation, and oxidation. Additionally,  $\gamma$ - $Al_2O_3$  is used in the manufacture of adsorbents, desiccants, and as a support material for chromatography. Understanding the composition of alumina is crucial, as it is

influenced by the choice of precursors, temperature, and the method of heating. During the thermolysis process, hydroxyl groups efficiently combine to produce water, highlighting the dynamic chemistry involved. Alumina is synthesized from two key sources: Al(OH)<sub>3</sub> [Al<sub>2</sub>O<sub>3</sub>·(H<sub>2</sub>O)<sub>3</sub>] and AlO(OH) [Al<sub>2</sub>O<sub>3</sub>·(H<sub>2</sub>O)]. This process leads to the formation of three essential surface species: OH<sup>-</sup>, O<sup>2-</sup>, and Al<sup>3+</sup>, both in dehydrated and hydrated states [84] (**Figure 1.6**). Furthermore, the effectiveness of alumina-supported metal catalysts is enhanced through proven preparation techniques such as incipient wetness (IW), grafting (G), and microemulsion methods (ME). These approaches not only optimize performance but also ensure reliability in various applications.

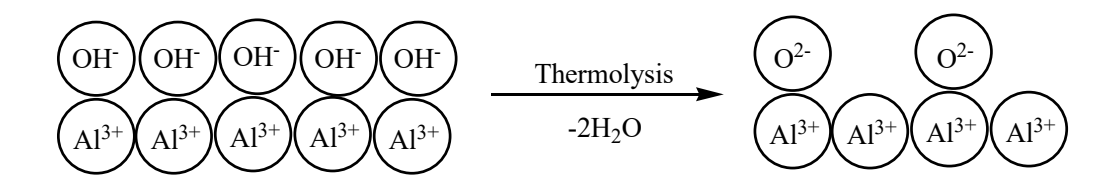
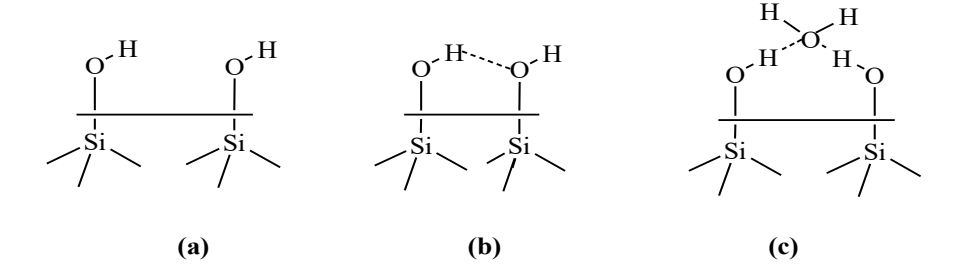


Figure 1.6 Synthesis of Alumina

#### Silica

Silica (SiO<sub>2</sub>), a compound composed of silicon and oxygen, is an exceptionally attractive support material utilized in various applications due to several key characteristics. Its large natural abundance makes it readily available at a low cost, while its stability ensures it can withstand different environmental conditions. Additionally, the commercial availability of silica and its ease of processing further enhance its appeal in industrial applications. In nature, silica typically manifests in three main forms: colloidal, discrete, and agglomerated. The colloidal form consists of nanoparticles ranging from 1 to 100 nanometers, which exhibit unique properties due to their small size and high surface area. The discrete form, known as microparticulate silica, comprises larger, distinct particles. In contrast, the agglomerated form of silica, which includes silica gel, presents a continuous three-dimensional network structure [85]. Silica gel is an example of an amorphous inorganic polymer characterized by its composition of siloxane rings (Si-O-Si). These siloxane rings are interconnected, and the surface of silica gel is adorned with silanol groups (Si-OH). The presence of these silanol groups is significant because they can interact with various substances,

allowing for modifications that enhance the gel's properties. Consequently, the modification of silica gel through the introduction of inorganic or organic functional groups has been a focus of considerable research interest, as it can improve the material's performance in specific applications. In terms of crystalline silica, which includes several well-defined structures, it is important to note that all forms, except for stishovite and fibrous silica, are composed of tetrahedral SiO<sub>4</sub> units [86, 87]. These tetrahedra are connected through shared vertices, leading to a variety of arrangements that define the specific crystalline structure of silica. Regarding the surface characteristics of crystalline silica, hydroxyl groups can be found either as free hydroxyl groups or as bonded hydroxyl groups (**Figure 1.7**). This distinction is crucial, as it influences the chemical reactivity and interaction of crystalline silica with other materials, further demonstrating the versatility of silica as a support material in various scientific and industrial applications.



**Figure 1.7** Arrangement of hydroxyl groups on the surface of silica (a) Free hydroxyl groups (b) Vicinal hydroxyl groups (c) Hydroxyl groups bonded with water by hydrogen bonding.

#### Titania

Titania (TiO<sub>2</sub>) is an incredibly versatile compound, existing in three distinct crystalline forms: anatase, rutile, and brookite. Among these, anatase and rutile are the most prevalent, with rutile generally exhibiting a larger crystalline size than anatase [88]. While brookite, with its orthorhombic structure, is rarely employed in practical applications, rutile stands out for its exceptional thermal stability. Both brookite and anatase undergo a phase transition to rutile when heated above 600°C, capitalizing on the unique properties of each phase. The anatase structure features zigzag chains of

octahedral molecules, while rutile showcases linear chains of edge-shared octahedra [89]. Notably, the transformation from anatase to rutile generally occurs between 600°C and 700°C. However, in specific applications, TiO<sub>2</sub> anatase needs to remain stable at temperatures reaching up to 900°C. Adding cations can effectively stabilize anatase TiO<sub>2</sub> nanoparticles, enhancing their performance. The unique properties of TiO<sub>2</sub>, such as its nontoxicity, long-term photostability, and remarkable effectiveness, make it an ideal solution for mineralizing toxic and nonbiodegradable environmental contaminants [90]. Furthermore, its excellent mechanical resistance and stability in acidic and oxidative environments underscore TiO<sub>2</sub>'s status as a prime candidate for use as a support in heterogeneous catalysis.

### Carbon

Carbon-based materials are increasingly recognized for their versatility as supports in the synthesis of heterogeneous catalysts. One of the most noteworthy supports is activated carbon, whose potential as a catalyst support is attributed to several key properties. Its extraordinary structural characteristics provide a high surface area, enabling better accessibility of reactants to active catalytic sites. Additionally, activated carbon exhibits excellent electronic conductivity [91], which plays a crucial role in facilitating charge transfer during catalytic processes. Moreover, the ability to easily recover and recycle the catalysts makes carbon-supported metals an economically attractive option in various chemical processes. A diverse range of carbon materials can serve as effective support for metals. These include highly ordered pyrolytic graphite (HOPG), which offers a structured framework; amorphous carbon nanomaterials, which provide flexibility; carbon nanotubes (CNT), known for their unique mechanical and electrical properties; fullerenes, which have interesting structural characteristics; as well as graphene and graphene oxide, both of which have attracted a lot of interest because of their remarkable electrical characteristics and substantial surface areas. [92-95]. Collectively, these various carbon materials have been successfully implemented as versatile support frameworks for enhancing the efficacy of transition metals in catalytic applications.

#### **Biomaterials**

Recently, the focus of science and technology has been shifting toward eco-friendly natural product resources and reusable catalysts. Natural biomaterials are gaining attention as environmentally friendly alternatives to traditional inorganic or organic supports due to their biodegradability, biocompatibility, and availability [96]. From a catalysis perspective, these biomaterials offer several appealing features. For instance, they have a high capacity to absorb metal ions and can be shaped into various forms, such as flakes, gel beads, membranes, fibers, hollow fibers, or sponges. These characteristics make them attractive as potential supports for catalysts. In recent years, there has been a concerted effort to utilize several functionalized biopolymers, including cellulose, gelatin, starch, and chitosan derivatives, as supports for catalytic applications [97-99]. These materials are advantageous because they are renewable, biodegradable, relatively inexpensive, and exhibit low toxicity [100].

# Magnetic nanoparticles

Magnetic nanoparticles (MNPs) represent a fascinating class of nanostructured materials that have attracted considerable attention in scientific research and industrial applications due to their unique properties and versatility. These nanoparticles, typically composed of iron oxides such as magnetite or maghemite, exhibit superparamagnetic behaviour [101], which means they can easily respond to external magnetic fields without retaining any magnetization once the field is removed. This characteristic makes them particularly useful in a wide range of applications, including, but not limited to, magnetic resonance imaging (MRI), where they serve as contrast agents, and drug delivery, where they can be utilized to transport therapeutic agents directly to targeted sites in the body [102]. In addition to their biological and medical applications, the development of MNPs for use as catalytic supports and their roles in aqueous catalysis have emerged as important facets of green chemistry [103]. This field of chemistry aims to create processes that minimize environmental impact and promote sustainability. Magnetic nanoparticles facilitate environmentally friendly catalytic processes because of their extremely small size, which drastically increases their surface area relative to their volume [104]. This high surface-to-volume ratio

enhances their catalytic activity and makes them ideal for a variety of reactions in an aqueous environment [105]. One of the standout advantages of using magnetic supports for catalysis is their ability to be easily separated from reaction mixtures. Unlike other solid supports, which often require complex and time-consuming filtration processes, MNPs can be swiftly and effectively extracted from a solution using an external magnetic field [106]. This capability not only simplifies the recovery process but also reduces the risk of contamination and loss of material, thus improving the overall efficiency of the reaction. Moreover, the versatility of magnetic nanoparticles extends to their modification and functionalization. Various strategies, such as surface modification, grafting of specific functional groups, and self-assembly techniques, allow researchers to tailor the properties of MNPs for specific catalytic applications [107]. These approaches create magnetically recoverable heterogeneous catalysts that can be optimized for activity, selectivity, and stability in various chemical reactions [108]. The ability to design and construct these catalysts opens new avenues for innovation in both laboratory and industrial settings, advancing the field of sustainable chemistry.

# Chemistry of Copper, Zinc and Palladium metals Copper

Copper, a reddish-brown metal with atomic number 29, has a rich and varied history of applications, extending from industrial uses to essential roles in biological functions. Dating back to around 3000 BC, the Egyptians discovered the antimicrobial properties of copper and effectively utilized it to sterilize drinking water, helping to prevent the spread of waterborne diseases [109]. By 400 BC, the physician Hippocrates recognized the therapeutic potential of copper and used it to treat leg ulcers linked to varicose veins, showcasing its significance in ancient medicine [110]. As an essential trace element, copper is critical in maintaining the proper functioning of various body tissues and organs. It is a fundamental component of many enzymatic reactions facilitated by copper-dependent enzymes. One prominent example is cytochrome c oxidase, an enzyme that is crucial for cellular respiration, as it helps cells utilize oxygen effectively for energy production [111]. Another important copper-dependent protein is angiogenin, which is instrumental in stimulating

angiogenesis—the process of forming new blood vessels—thereby ensuring that tissues receive an adequate blood supply [112]. In addition to these roles, copper is vital for normal liver function, where it helps metabolize fats and carbohydrates and detoxifies harmful substances. It also plays a significant part in the synthesis of elastin, a protein that provides elasticity to connective tissues, working closely with vitamin C to support this process. A deficiency in copper can have serious health implications. Insufficient copper levels may lead to complications during pregnancy, affecting both the mother and the developing foetus[113]. Additionally, children with low copper levels may be at risk for developing heart diseases, while adults may experience issues related to inadequate iron absorption, potentially leading to anaemia. Therefore, maintaining adequate copper levels is crucial for overall health and well-being. In addition, Copper (Cu) is a widely used metal in catalysis, playing a crucial role in various chemical reactions. Some of the notable Cu catalyzed reactions in catalysis are1. Oxidation reactions (e.g., alcohol oxidation, alkene epoxidation)2. Reduction reactions (e.g., nitroarene reduction, CO<sub>2</sub> reduction)3. C-C bond formation reactions (e.g., Ullmann reaction, Sonogashira coupling)4. Hydrogenation reactions (e.g., alkene hydrogenation)5. Click chemistry (e.g., triazoles synthesis) [114-118].

### Zinc

Zinc, with atomic number 30, is an indispensable trace element that is critical for human health, ranking second only to iron in importance. It plays a crucial role as a structural component in a wide variety of enzymes, frequently residing at their active sites. There are nearly eighty known metalloenzymes containing zinc, each of which performs vital roles in various physiological processes, particularly in tissue repair and the healing of inflammatory conditions [119]. This underscores the element's invaluable contributions to overall health. Zinc is integral to several critical functions within the body, including cell division, growth, wound healing, carbohydrate metabolism, nucleic acid synthesis (DNA and RNA production), and glycolysis (the breakdown of glucose to generate energy) [120]. Its importance cannot be overstated, as zinc directly influences developmental processes and the immune response. Alarmingly, around two billion individuals globally suffer from zinc deficiency. This deficiency can lead to severe health issues, including growth retardation in children,

hair loss, delayed sexual maturation, and a heightened vulnerability to infections, which can diminish quality of life and increase healthcare costs [121]. In addition to its systemic benefits, zinc is commonly incorporated into topical ointments designed to treat a variety of skin conditions. For example, zinc oxide is frequently used in the formulation of products intended for minor burns, diaper rash, and other skin irritations due to its soothing and healing properties. The compound acts as a protective barrier, promoting healing while also reducing inflammation. Recent research has indicated that zinc (II) complexes could potentially play a role in reducing histaminic components found in extracellular fluids or in base cells [122]. This suggests that these complexes might serve as innovative treatments for anaphylactic shocks, a serious and rapidly progressing allergic reaction. Zinc, in addition to its biological significance, has multifold applications in Catalysis. The most important among are 1. Hydrogenation reactions: (reduction of nitro compounds to amines). 2. Alkylation reactions: (production of pharmaceuticals and fine chemicals).3. Carbonylation reactions: Zinc is used as a co-catalyst in carbonylation reactions for the production of aldehydes and ketones. 4. Dye degradation and 5. Organic synthesis: (Reformatsky reaction and the Negishi coupling) [123-127].

#### Palladium

As early as 1700, miners in Brazil encountered a metal they called "ouropodre," which literally means "worthless gold." This term referred to a natural alloy composed of palladium and gold, highlighting its initial lack of perceived value compared to pure gold. It wasn't until 1803 that William Wollaston successfully extracted palladium for the first time, marking a significant milestone in the study and utilization of this metal. Palladium, a lustrous silvery-white metal with atomic number 46, has since become increasingly important in various sectors, particularly in modern technology and fine jewellery. A significant portion of palladium is utilized in catalytic converters [128], which are crucial components of automotive exhaust systems. These converters play a pivotal role in reducing harmful emissions from internal combustion engines, converting toxic gases such as carbon monoxide and nitrogen oxides into less harmful substances like carbon dioxide and nitrogen. This transformation is essential for improving air quality and underscoring the metal's

significance in promoting a cleaner environment. In addition to its automotive applications, palladium is highly valued in the jewelry industry for its ability to enhance both beauty and durability [129]. Its bright, lustrous finish makes it an attractive choice for artisans and consumers alike. Furthermore, palladium is also found in dental materials, such as fillings and crowns, where it contributes to both the aesthetic qualities and the functional longevity of these dental solutions [130]. The electronics sector greatly relies on palladium as well. It is a critical component in the manufacturing of ceramic capacitors, which are essential for the efficient operation of electronic devices such as laptops, smartphones, and tablets. These capacitors consist of layers of palladium intricately sandwiched between ceramic materials, providing exceptional conductivity and reliability that are vital for technology functionality. Moreover, finely divided palladium acts as an outstanding catalyst in chemical reactions, particularly in hydrogenation, dehydrogenation processes and Suzuki coupling [131-133]. Its unique properties allow it to facilitate these reactions efficiently, and its ability to permit the easy diffusion of hydrogen when heated makes it particularly useful in the separation and purification of gases. Overall, embracing palladium is more than just a choice of material; it represents an investment in advanced technology, cleaner emissions, and exquisite craftsmanship that enhances both the functionality and beauty of everyday products.

## Schiff base complexes of Copper, Zinc and Palladium and their applications

One of the most extensively studied Schiff base ligands is the Salen ligand system, which was first reported in 1933 by Pfeiffer et al. [134] By condensing salicylaldehyde compounds with diamine derivatives, molecules with two nitrogen and hydroxyl groups are produced, resulting in Salen Schiff base compounds. These compounds exhibit tetradentate coordination modes and are categorized as Salen ligands. Jian and colleagues [135] have developed Cobalt(II) and copper(II) complexes by using Schiff bases made from valine. The bioactivity of these complexes was examined for their ability to inhibit human pathogenic fungi and both Gram-positive and Gram-negative bacteria. Growth of pathogenic fungi (R. glutinis, C. neoformans, S. cerevisia, Aspergillus spp., Candida spp., and R. nigricans) and (methicillin-resistant S. Aureus, B. subtilis, S. Aureus, and M. luteus) was significantly

inhibited by the copper(II) complex, which demonstrated broad-spectrum activity. Aside from its wide range of activity, the Cu(II) complex showed a moderate level of activity against Gram-negative bacteria, such as *P. vulgaris*, *P. aeruginosa*, *E. aerogenes*, and *E.coli*.

Rajavel et al. [136] synthesized ligands based on the dihydrazone and used these ligands further to synthesize complexes with metalssuch as Nickel(II), Copper(II), Oxovanadium(IV) and Zinc(II) (**Figure 1.8**). All compounds were found to be potential antimicrobial agents. The Copper(II), Zinc(II) and oxovanadium(IV) complexes of ligands based on dihydrazone exhibited higher biological activity against *P. Aeruginosa*, *B. subtilis*, *E. coli* and *S. Aureus* as compared to the Ni(II) complex and chloramphenicol standard.

**Figure 1.8** Structure ofBis-(2-aminobenzaldehyde)] malonoyl dihydrazone] and complexes with Ni(II), Cu(II), oxovanadium(IV) andZn(II) metals.

Gehad et al. synthesized the metal complexes by utilizing the novel Schiff base (HL) as a ligand, which itself was obtained by the condensation reaction of 2-aminophenol and 4-aminoantipyrine (Figure 1.9) [137]. IR spectra revealed that HL here is uninegatively charged and coordinated in tridentate manner from two N and one O sites. N of azomethine, N of amino group, and O of deprotonated phenolic-OH make up the NNO donor sites. Antibacterial activity of metal complexes of HL based ligand, specifically with metals Manganese(II), Nickel(II), Cobalt(II), Zinc(II), Copper(II) and Cadmium(II), was investigated against E. coli, P. putida, Exiguobacteriumacetylicum, and B. simplex. The results showed that these metal complexes were more effective as antibacterial agents compared to the parent Schiff base ligand.

Figure 1.9 Structure of Schiff base (HL)

Bernadette and his coworkers synthesized thirteen quinolin-2(1H)-one derivative which basically act as Schiff bases and then synthesized its complexes with copper(II) [138]. These quinolin-2(1H)-one ligands act as bidentate ligands and are coordinated to the Copper(II) ion through the N-atom of azomethine group and O-atom of deprotonated phenolic oxygen in almost all the cases (**Figure 1.10**). A biological activity analysis of all the produced complexes revealed that they were all inert against S. *aureus* and E. *coli* but had good antifungal activity.

$$R^{2}$$
 $R^{2}$ 
 $R^{2}$ 
 $R^{3}$ 
 $R^{4}$ 
 $R^{2}$ 
 $R^{3}$ 
 $R^{4}$ 
 $R^{3}$ 
 $R^{4}$ 
 $R^{4}$ 
 $R^{4}$ 
 $R^{5}$ 
 $R^{4}$ 
 $R^{5}$ 
 $R^{4}$ 
 $R^{5}$ 
 $R^{6}$ 
 $R^{7}$ 
 $R^{7}$ 
 $R^{8}$ 

Figure 1.10 Structure of Schiff base complex of Copper(II) metal

Metal complexes of novelSchiff base (HL) (HL = 3-(4-ethylazomethinobenzene sulphonamide)-4-methoxy-1,2,5-thiadiazole) followed by metallation with Nickel(II), Cobalt(II), Copper(II), Iron(II) and Zinc(II) was reported by Gehad and his coworkers [139]. *Candida* and *Aspergillus flavus* fungus species, as well as *Escherichia coli* and *S. aureus* bacteria, were tested for the antibacterial properties of the discovered ligand and its metal complexes. The data indicate that the metal complexes exhibit promising

biological activity against both bacterial and fungal species, showing greater efficacy than the Schiff ligand alone.

Novel Schiff base cobalt(II), copper(II) and zinc(II) complexes (**Figure 1.11**) were formed by Xueguang et al. [140] using 2-hydroxy-1-naphthaldehyde and D, L-selenomethionine. Based on the analytical data, the metal complex's composition was determined to be ML(H<sub>2</sub>O), where M represents metal and L represents Schiff baseligand. It has been observed both metal complexes and ligand are active, but CuL(H<sub>2</sub>O) is the most active of them, according to the results of antibacterial and antifungal screening tests against five bacterial and three fungal stains.

Figure 1.11 Structure of cobalt(II), copper(II) and zinc(II) Schiff base complexes

El-Sherif [141] and his colleagues produced the metal complexes of Co(II), Ni(II), and Cu(II) with the Schiff ligand BHPP (**Figure 1.12**). By employing the disc diffusion method, the antimicrobial activity of metal complexes and the ligand was evaluated against specific bacteria and fungi. They were found to work better against Gram-positive bacteria than Gram-negative ones. The antibacterial activity of the copper complex was the strongest when compared to similar compounds that contained nickel(II) and cobalt(II) ions.

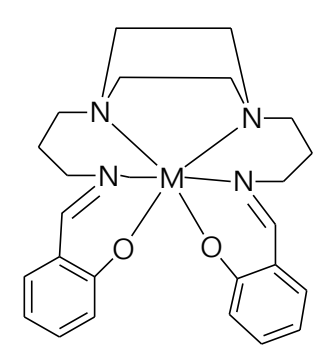


Figure 1.12. Structure of Schiff base BHPP ligand.

Three novel compounds derived from the Cu(II) and Ni(II) metals derived from the Schiffligand [H2pydmedpt]2+·2Cl– were developed by Tirtha et al. [142]. These complexes' competitive DNA binding experiments were conducted at concentrations between 40 and 400  $\mu$ M. According to the binding studies, the binding constants (K) for the Cu(II) and Ni(II) complexes were determined to be 2.9 × 103 and 6.7 × 103 M–1, respectively. These metal complexes were also subjected to HAS binding experiments at concentrations between 800 and 1000  $\mu$ M for Cu(II) and 400 and 500  $\mu$ M for Ni(II). PBS buffer, which has a pH of 7.4, was the buffer utilized in this investigation.

In this work, Nickel(II), Copper(II), Zinc(II), and Cadmium(II) complexes of two Schiff bases (Pc4PDTC) and (Cb4PDTC) were synthesized, according to Teng-Jin and his colleagues [143]. (Figure 1.13). The ligands' cytotoxic, antibacterial, and antioxidant properties were evaluated in vitro together with those of their metal complexes. While Cb4PDTC was inert, the Pc4PDTC Schiff base demonstrated modest cytotoxicity against human promyolicyticleukemia. Pc4PDTC's cytotoxicity against the human promyolicytic leukemic cell line (HL60) was increased when it was complexed with cadmium(II) and copper(II). S4PDTC was inert against fungi but shown outstanding antibacterial action against bacteria. For the majority of the studied bacteria and fungi, the Schiff base complexes of Copper(II) and Cadmium(II) showed distinct inhibitory zones.

Figure 1.13 Structure of Schiff base ligands Pc4PDTC and Cb4PDTC

With tridentate Schiff bases acting as the ligands (H2salChx and H2MeOsalChx), Jindra et al. have successfully synthesized and characterized four new Cu(II)-based and one Zn(II) based Schiff base complexes, demonstrating their significant biological activityby condensation of 1-aminocyclohexane-1-carboxylic acid with

salicylaldehyde or with 3-methoxysalicylaldehyde (**Figure 1.14**). Antimicrobial activity of all five complexes was assayed against *S. aureus* and *E. coli*. Cu(II) complexes also showed significant antiradical activity.

Figure 1.14 Structure of Schiff base ligands (a) H<sub>2</sub>salChx and (b) H<sub>2</sub>MeOsalChx)

The chemical synthesis of a new tetradentate Schiff base ligand, bridged with a pyridine, and its corresponding mononuclear copper complex [145] were reported by Wafa and his colleagues (**Figure 1.15**). The condensation of 5-bromosalicylaldehyde with 2,3-diaminopyridine produced the ligand. By using the disc diffusion method, the anti-bacterial activity of the ligand and copper complex was investigated against strains of Gram-negative bacteria (*P. aeruginosa*, *K. pneumoniae*, *E. coli*, and *P. mirabilis*) and Gram-positive bacteria (*M. luteus*, *S. aureus*, *S. Pyogones* and Methicillin resistant *S. aureus* (MRSA). Compared to the ligand, the copper complex displayedimproved activity.

**Figure 1.15** Structure of tetradentate mononuclear copper Schiff base complex bridged with pyridine

In this study, Alterhoni et al. [146] reported new Schiff bases (H<sub>2</sub>L<sub>1</sub> and H<sub>2</sub>L<sub>2</sub>) and benzimidazolylphenol derivatives (HL<sub>3</sub>-HL<sub>5</sub>) derived from 5-chlorosalicylaldehyde and appropriate aminophenol and o-phenylenediamine derivatives including 4-methyl/4,5-dimethyl/4-chloro-5-nitro groups. CoCl<sub>2</sub>, PdCl<sub>2</sub>, CuCl<sub>2</sub> and

ZnCl<sub>2</sub> complexes of the ligands were synthesized. Three fungal and six bacterial strains were used to assess the compounds' antibacterial properties. Co(II) complexes were shown to have greater activity than the other complexes.

Using Salen type Schiff base ligands (**Figure 1.16**), Karger et al. [147] produced mononuclear Ni(II), Cu(II), and Zn (II) complexes based on 3,5-dihalosalicylaldehyde with polymethylenediamines. The antibacterial qualities of the synthesized compounds were tested on two strains of Gram-positive (*B. cereus* and *S. aureus*) and Gram-negative (*P. aeruginosa* and *E. coli*) bacteria. The size of the zones of inhibition revealed that metal complexes worked better than ligands.

$$X \longrightarrow X \longrightarrow X \longrightarrow X \longrightarrow X$$

Figure 1.16 Structure of Salen type Schiff base metal complex

Schiff-base complexes based on copper(II) were produced by Yusuf et al. [148] and their binding efficacy toward Cytochrome P450 3A4 was examined (**Figure 1.17**). The produced complexes exhibited favorable characteristics and were able to bind to cytochrome P450 3A4 considerably and function as substrates of cytochrome P450 and P-gp i.e., permeability-glycoprotein.

Figure 1.17 Structure of Schiff baseCu(II) complex

Four new symmetrical Schiff base complexes of Fe(II), Zn(II), and Cu(II) complexes derived from salicylaldehyde-based ligands, were synthesized by Tareq. M.A et al.

[149]. The biomedical applications of synthesized compounds were investigated for anticancer and antimicrobial properties. Compounds revealed good amount of activity against *M. luteus*, and *S. aureus* bacterial strains. The majority of the tested substances displayed variable reductions in the ability of the studied cancer cell lines, according to an anticancer analysis.

Sixteen new complexes of Cobalt(II), Nickel(II), Copper(II), and Zinc(II) were developed from four Schiff base ligands (H<sub>2</sub>L<sup>1</sup>), (H<sub>2</sub>L<sup>2</sup>), 1 (H<sub>2</sub>L<sup>3</sup>), and (H<sub>2</sub>L<sup>4</sup>) by Jai et al. [150]. These ligands were obtained from condensation reaction of 4-(benzyloxy)-2-hydroxybenzaldehyde with several aminophenol derivatives. The metal(II) complexes exhibited greater toxicity than the free Schiff base ligands when tested against two fungal strains (*A. niger, C. albicans*) and four bacterial strains (*S. aureus, B. subtilis, P. aeruginosa*, and *E. coli*) for in vitro antibacterial activity.

Fasna and colleagues [151] created new Cu(II) complexes and used them to photocatalytically break down methylene blue and have antibacterial properties against gram-negative bacteria and gram-positive, *E. coli.* and *B.circulans*.

In this study, Sanjeev and colleagues [152] reported synthesizing three Schiff base ligands [H2L1-H2L3] and their metal (II) complexes such as cobalt, nickel, copper and Zinc by stirring their metal salts and Schiff base ligands derived from the of 2-amino-6-chloro-4-nitrophenol condensation reaction with 5-chloro salicylaldehyde. salicylaldehyde/3,5-dibromo salicylaldehyde/3-methoxy-5-nitro Using ciprofloxacin and fluconazole as standards, all of the compounds were investigated for their in vitro antibacterial properties against two gram-positive bacteria, two gram-negative bacteria (S. aureus, B. subtilis, P. aeruginosa, and E. coli), and two fungal strains (A. niger, C. albicans). The findings of the analysis demonstrated that complexes work better than free Schiff base ligands. Of all the chemicals examined, the Cu(L2)(H<sub>2</sub>O)<sub>3</sub> (0.0115 µmol/mL) and Zn(L2)(H<sub>2</sub>O)<sub>3</sub> (0.0115 umol/mL) complexes were determined to be the most active.

A new Schiff base ligand (DBAPB) (**Figure 1.18**) and metal complexes of Copper(II), Chromium (III), Cobalt(II), Manganese(II), Zinc(II), and Nickel(II) were synthesized and described by Mosad et al. [153]. *E. coli, S. aureus*, and *C. albicans* 

were among the bacteria and fungi that were tested for the compounds' antibacterial properties. According to the obtained findings, the metal complexes exhibit higher antibacterial activity than the free ligand. The DNA cleavage study's findings validated the Cu(II) complex's capacity to break down DNA. Strong interactions between the DBAPB ligand and the Copper(II) complex were shown by the docking results, demonstrating their capacity to cleave DNA and their potent to cleavage DNA and their powerful inhibitory effects on tumor cells.

$$\begin{array}{c|c} O \\ HN \\ HC = N \\ OH \\ OH \\ \end{array}$$

Figure 1.18 Structure of Schiff base ligand (DBAPB)

Using phenol-based ligand (HL), Elena et al. [154] examined the antibacterial, anticancer, and antioxidant properties of complexes such as Co(II), Cu(II), Mn(II), Pd(II), Ni(II) and Pt(II). Additional research on the complexes's antibacterial, DNA binding, and protein binding properties was conducted. Additionally, molecular docking research was conducted to assess the drugs' binding affinity to protein targets implicated in bacterial and proliferative activities. Three strains of fungi, two strains of Gram-negative bacteria, and three strains of Gram-positive bacteria were used to test the compounds' antibacterial properties. The best antibacterial effect was shown by the Pt(II) complex on the *Staphylococcus aureus* strain, and as for the inhibitory effect on fungi, it was stronger on the *Candida albicans* strain after treatment with the Co(II) complex.

A newazomethine ligand, HL, and the corresponding complexes VO(II), Cd(II), Mn(II), and Pd(II) were prepared by Mayar and coworkers [155]. The Cd(II) complex showed effective outcomes against various bacterial strains, demonstrating excellent activity that surpassed that of the standard, Gentamicin (108% against *K. pneumoniae*, 100% against *Salmonella*, and 90.47% against *A. fungi*). In contrast, it displayed no cytotoxicity toward the MCF-7 cell line. Nevertheless, in DNA binding studies, the

compound demonstrated noteworthy activity as its concentration increased up to 6 mM, signifying its potential for usage in cancer therapy owing to its ability to prevent DNA replication.

Four novel mono-nuclear metal(II) complexes of Nickel, Palladium, Platinum, and Zinc were synthesized by Tarek et al. [156] employing a bi-dentate Schiff base ligand and bivalent metal ions. Furthermore, the ligand and its complexes were tested against *S. aureus* and *E. coli*, and the results showed that these compounds had exceptional biological activity against both bacterial strains. Unlike binding energies showed good correlation, with Pd showing the strongest binding. Minor energy differences showed high reactivity, with Ni and Pd complexes being the most reactive.

In this study, new azomethine chelate complexes of Zn(II), Pd(II), Cu(II), and Cr(III) with a newly formed tridentate ligand have been reported [157]. The reported complexes were characterized using different techniques. The absorption titration technique was employed to inspect the interaction of metal chelates with *ct*-DNA. Viscometric and gel electrophoresis implied intercalative binding modes of the azomethine metal chelates with DNA.

By reacting palladium(II) chloride with monosodium salts of N-(5-nitro-salicylidene)-Schiff base in aq.DMF solution, Ozlem et al. [158] produced a number of palladium(II) complexes. The obtained physicochemical and analytical data showed that the palladium(II) ion was coordinated squarely. The Pd(II) complexes' in vitro cytotoxicity was tested against the tumor cell lines HeLa and MCF-7 as well as the normal human cell line HEK-293. The complexes showed a moderate antitumor action against HeLa cell lines. All three complexes presented better active cytotoxicity against MCF-7 cancer lines. For HEK-293 lines, a reduction in concentration of the complexes significantly declined their toxicity.

Pd(II) and Pt(II) mixed-ligand complexes were produced and studied by Wesam H. et al. [159]. Complexes were shown to be moderately active against the studied bacterial strains (*Staphylococcus aureus* and *Escherichia coli*) in the antimicrobial activity assay investigations.

Richa et al. [160] reported that Schiff base and its Palladium(II) metal complex (**Figure 1.19**) has antibacterial characteristics. After first preparing sulphathiazole, a novel Schiff base ligand was created using salicylaldehyde. The salt PdCl<sub>2</sub> was used to create the metal complex of the ligand. Both compounds' antifungal and antibacterial properties were also investigated. The Pd(II) complex outperformed the ligand in terms of antibacterial activity.

Figure 1.19 Structure of Schiff base Pd(II) complex

The synthesis of novel salicyl-based Schiff bases from 3,5- dichlorosalicylaldehyde and 4-(chloro/tert-butyl)-2-aminophenols was reported by Dildora and colleagues [161]. To create their Schiff metal complexes, Co(II), Ni(II), Cu(II), Zn(II) perchlorates, and K<sub>2</sub>PdCl<sub>4</sub> were usedand further characterized with elemental analysis, TGA, UV-visible, FT-IR, molar conductivity, magnetic moment, and NMR spectroscopy. The Schiff base complex of Cu(II) and Pd(II) are shown (**Figure 1.20**). The compounds were screened against six bacteria, three fungi and Parainfluenza Type-2 virus. Overall, the compounds showed reasonable antibacterial and antifungal activity. Some metal complexes displayed higher activity against some microbes than the ligands.

$$\begin{bmatrix} CI & & & & & \\ & & & & & \\ & & & & & \\ & & & & & \\ & & & & & \\ & & & & & \\ & & & & \\ & & & & \\ & & & & \\ & & & & \\$$

Figure 1.20 Schiff base complex of Cu(II) and Pd(II)

Novel Copper(I) (B1), Copper(II) (B2), Zinc(II) (B3), and Cadmium(II) (B4) metal complexes of N-phenyl2-(p-tolylglycyl) hydrazine-1-carbothioamide (B) ligand have been described by Aly et al. (Figure 1.21). Several spectroscopic methods have been used to characterize them [162]. Cu(I) and Cd(II) complexes were discovered to be tetrahedral, while Zn(II) and Cu(II) complexes acquired octahedral geometry, according to these investigations. The ability of the ligand and metal complexes to limit the growth of both gram-positive (*Streptococcus pyogenes*) and gram-negative (*Escherichia coli*) bacteria has been studied before and after irradiation. Molecular docking investigation proved that the Zn(II) complex had interesting interactions with active site amino acids of topoisomerase II DNA gyrase enzymes.

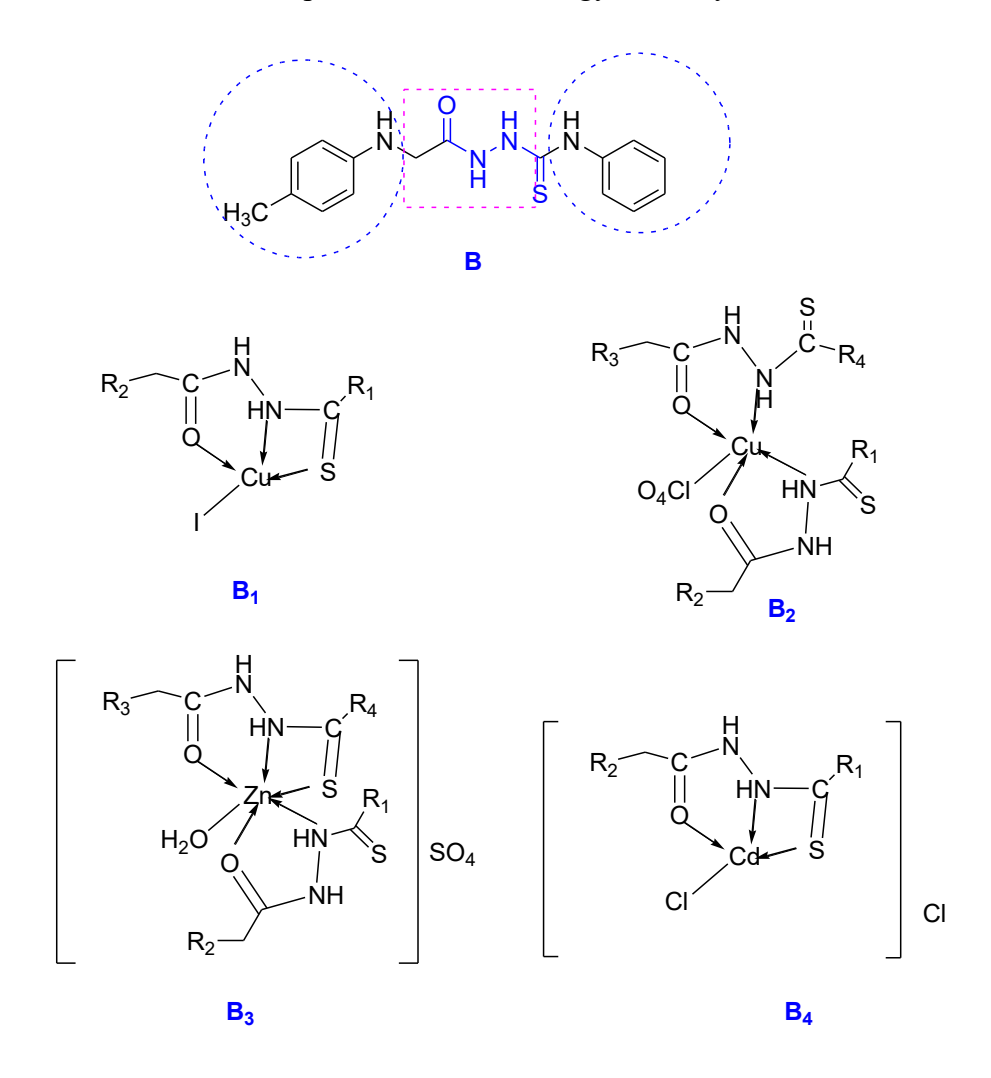


Figure 1.21 Structure of Schiff base ligand (B) and corresponding metal complexes (B<sub>1</sub>-B<sub>4</sub>)

This work reported the synthesis of metal(II) tetrahedral complexes of zinc and copper derived from 5-nitroimidazole derivatives (cenz and onz) and spectroscopically characterized (**Figure 1.22**). The biological activity of these compounds was tested against Toxoplasma gondi and IC50 and lethal dose (LD50) values were determined. The ornidazole copper(II) compounds showed very good antiparasitic activity in its tachyzoite morphology. The spectroscopic data achieved for the two series of complexes (namely with copper(II) and zinc(II) as metal center) agree with the respective DNA-damage features observed by gel electrophoresis [163].

**Figure 1.22** Structure of 5-Imidazole based ligands cenz(1) and onz(2)

In this work, three novel complexes of Pd(II), Cu(II), and Cu(I) metals with new ligand H<sub>2</sub>LB has been reported and characterized using various analytical techniques (**Figure 1.23**). The antimicrobial study was done for the activity of ligands and their chelates and results obtained demonstrated the superior activity of the Cu(I) complex against antifungal species with respect to standard drug Nystatin [164].

Figure 1.23 Structure of Schiff base ligand  $H_2LB$  (a) and chelate Cu metal complex

G.R Bardajee et al. [165] have reported copper (II) Schiff base complex supported on mesoporous silica SBA-15 to afford Cu(II)-Schiff base/SBA-15 catalyst. Under greener conditions, Good catalytic activity in synthesizing pyridopyrazine and quinoxaline derivatives was achieved from diketones and diamines (**Figure 1.24**).

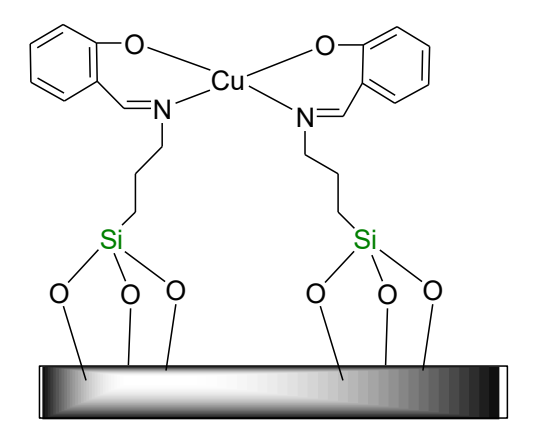


Figure 1.24 Structure of Cu(II)-Schiff base/SBA-15 catalyst

Fe<sub>3</sub>O<sub>4</sub>–Schiff base Cu(II) was synthesized by Ghorbani et al. and employed as a heterogeneous catalyst for the oxidation of several organic molecules [166]. Fe<sub>3</sub>O<sub>4</sub>-Schiff base of Cu(II) is an effective catalyst due to the magnetic nanoparticles' enormous surface area (**Figure 1.25**). It is important to note that the shape of the Fe<sub>3</sub>O<sub>4</sub>-Schiff base of Cu(II) does not alter even after the oxidation reactions, which is a key factor for its reusable property. The main benefit of the developed catalytic system is that its morphology does not alter even after the oxidation reactions, and it can be magnetically separated easily from the product solution.

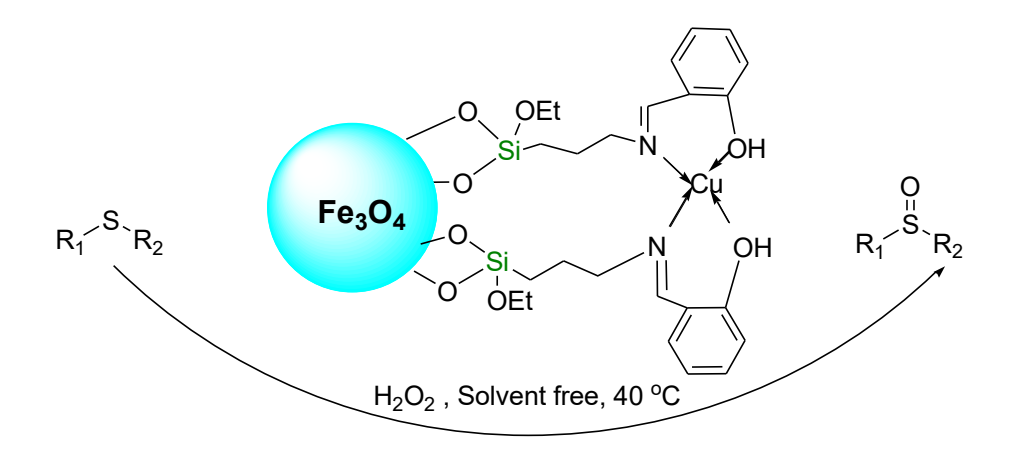


Figure 1.25 Fe<sub>3</sub>O<sub>4</sub>–Schiff base Cu(II) catalyzed oxidation reaction

Shweta et al. synthesized and studied the Schiff base of chitosan, Schiff base ligands, and the resulting Chitosan attached Copper(II) Schiff base complexes using a variety of spectroscopic techniques [167]. For Chan-Lam C-N coupling processes, all three of the Cu complexes were found to be effective heterogeneous catalysts (**Figure 1.26**). The study is innovative since the catalyst is easily filtered out and can be utilized at least five times without experiencing a significant loss of catalytic activity.

**Figure 1.26** Chitosan attached Copper(II) Schiff base catalyzed Chan-Lam C-N coupling

Taskin and coworkers incorporated Cu(I) ions are into the microporous Schiff base network (SNW) structure through coordination with the nitrogen atoms present in the melamine groups. The Cu(I)-incorporated material showed an extremely effective catalytic activity for copper(I)-catalyzed azide–alkyne cycloaddition (CuAAC) reaction [168]. Several azide and alkyne compounds were used to conduct the click reaction by using a small amount of catalyst and almost quantitative yields were attained.

A novel heterogeneous and reusable polyvinyl alcohol immobilized copper(II) Schiff base complex (PVA@Cu(II) Schiff base complex) was synthesized and published by Milad et al. [169]. At room temperature, the produced catalyst is effectively used to synthesize 5-substituted 1H-tetrazoles in a more environmentally friendly solvent, like water.

Nikoorazm et al. have synthesised two new Schiff-base complexes of zirconium oxide and copper anchored on MCM-41 as mesoporous and organometallic catalysts (**Figure 1.27**) under green conditions and tested their catalytic action for the synthesis of tetrazole derivatives and the chemo and homoselective oxidation of sulfides to sulfoxides [170].

**Figure 1.27** Heterogeneous Schiff-base complexes of zirconium oxide and copper anchored on MCM-41

In methanol, Kamroudi et al. created a novel ionic Schiff base macrocycle Cu(II) complex [171]. Several reaction parameters, including solvent effect, reaction temperature, and catalyst quantity, were tuned while the catalytic action of the Cu complex was scrutinized for the click reaction. When a catalyst was present, a high reaction yield of 1,2,3-triazoles was produced in water at 70 °C.

Ajormal and colleagues have reported a pro-chiral Schiff base ligand and its copper complexes (**Figure 1.28**) [172]. The developed chiral Cu(II) complexes employed as catalysts for the synthesis of  $\beta$ -hydroxy-1,2,3-triazole compounds by click reaction under mild conditions. All the products were obtained in excellent yields.

**Figure 1.28** Pro-chiral Schiff base Copper complex catalyzed synthesis of β-hydroxy-1,2,3-triazole

Noori and co-workers have reported two new hybrids, Schiff base composites by anchoring Ni and Zn metals onto amino-modified Ni-MCM-41 and Zn-MCM-41. The catalysts exhibited superb catalytic efficiency in the oxidation of sulfides to sulfoxides and oxidative coupling of thiols to corresponding disulfides by employing urea H<sub>2</sub>O<sub>2</sub> as oxidant under mild conditions [173]. It is simple to re-use the described Schiff base complex without losing its selectivity and catalytic activity. (**Figure 1.29**).

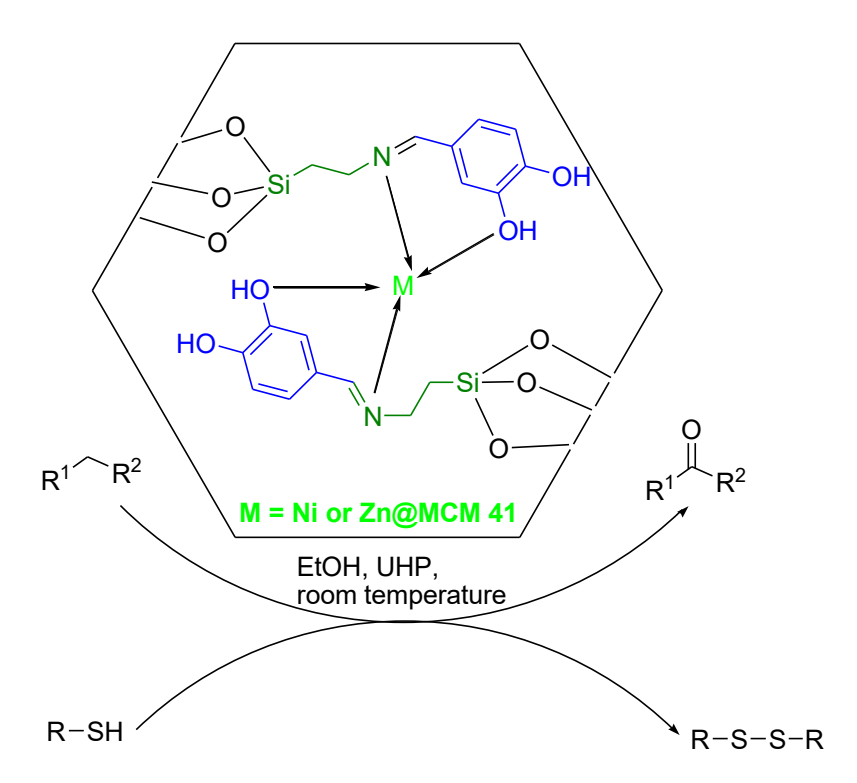


**Figure 1.29** Ni or Zn@MCM 41 catalyzed oxidation of sulfides to sulfoxides and oxidative coupling of thiols to disulfides

Development of polymer-based zinc-salen complex (PS-Zn-salen) has been reported by Balinge et al. [174]. The synthesis of thiohydantoins, hydantoins, and Schiff bases was facilitated by the useful and recyclable heterogeneous catalyst known as the zinc (II)-salen complex. With only a minor drop in activity, the effective catalyst may be readily recovered through filtration and used again for up to six consecutive runs.

Adam et al have reported novel oxovanadium (IV) bis-Schiff base complex (VOL<sub>2</sub>) as useful homogeneous/heterogeneous catalysts for oxidation of alcohols [175]. The deprotonated 4-OH group in VOL<sub>2</sub> caused coating of VOL<sub>2</sub> on mixed oxides of

TiO<sub>2</sub>, successfully forming an anocomposite of TiO<sub>2</sub>–ZnO@VOL<sub>2</sub>. The catalytic applications of both homogeneous as well as VOL<sub>2</sub> and TiO<sub>2</sub>-ZnO@VOL<sub>2</sub> were the of employed in oxygenation reaction benzyl alcohol to chemoselectivebenzaldehyde as the main product and benzoic acidas the overoxidation product.

Dhengale et al. have reported Zn/MCM-41 as a proficient heterogeneous catalyst for the solvent-freeproduction of 1,4-dihydropyridines and polyhydroquinolines under sustainable conditions. The Zn/MCM-41 catalyzed protocol gave an outstanding yield of the anticipated products in a short time with no need for further purification of products [176].

Kulkarni and co-workers [177] have developed Zn-Ag@L-arginine Fe<sub>3</sub>O<sub>4</sub> as a magnetically separable Schiff base catalyst to efficiently synthesize benzimidazoles and pyrimidines. The novel catalyst system can be easily collected using a magnet and recycled without additional treatment up to five consecutive effectively (**Figure 1.30**).

$$\begin{array}{c} \text{NH}_2 \\ \text{NH}_2 \\ \text{NH}_2 \\ \text{R} \end{array} + \begin{array}{c} \text{Zn-Ag @L-arginineFe}_3O_4 \\ \text{Ethanol, 65 °C} \\ \text{Benzimidazoles} \\ \end{array}$$

**Figure 1.30** Zn-Ag@L-arginine Fe<sub>3</sub>O<sub>4</sub>catalyzed synthesis of benzimidazoles and pyrimidines

Mohamed and co-workers [178] have developed modified biomaterial-based chitosan-Schiff base ZnO magnetic complex (Mag-CS-SB/ZnO) bearing active centers for selective removal of malachite green dye and inhibiting the expansion of microorganisms from aqueous environment. The antibacterial activity of the developed complexes was tested for both Gram-negative and Gram-positive bacteria.

The inhibition efficiency of the developed materials displayed excellent bioactivity as comparable to commercially available antibiotics (Streptomycin).

Aghayee and co-workers have reported a newpalladium-based nano-magnetic Schiff base ligand with phosphate spacer using 2-aminoethyl dihydrogen phosphate for coating of magnetic Fe<sub>3</sub>O<sub>4</sub> nanoparticles (**Figure 1.31**). The developed catalyst was successfully employed as a catalyst for the coupling reactions, such as Sonogashira and Mizoroki-Heck [179].

Figure 1.31 Structure of Palladium based nano-magnetic Schiff base complex

Schiff base-functionalized boehmite, Pd NPs@Sch-boehmite, has been reported by Barren and colleagues [180] as a recyclable catalyst for C-C-coupling and for the reduction of2-nitroaniline and 4-nitrophenol at room temperature as well as for the manufacture of biaryls. The catalyst was easily retrieved and may be used repeatedly (**Figure 1.32**).

OH 
$$NO_2$$
  $NH_2$   $NH_2$ 

Figure 1.32 Pd NPs@Sch-boehmitecatalyzed reduction and Suzuki coupling reaction

Noroozi et al. have reported Pd based Schiff base complex by using nanocarbon support materials such as fullerene (C60) (**Figure 1.33**) which helped in the dispersion of catalyst [181]. The obtained catalyst was investigated for their efficacy to catalyze aerobic oxidation of alcohols and Heck coupling reactions.

Figure 1.33 Nanocarbon supported Pd based Schiff base complex

Balali et al. [182] have developed a novel catalyst system, Fe<sub>3</sub>O<sub>4</sub>@SiO<sub>2</sub>@L-Pd, to efficiently catalyzethe Suzuki coupling reaction. In this protocol, aryl halides are made to react effectively with phenylboronic acid to provide arylated alkynes in high amounts (**Figure 1.34**).

$$R_1 \xrightarrow{\hspace*{1cm}} X + \underbrace{\hspace*{1cm}} B(OH)_2 \xrightarrow{\hspace*{1cm}} Fe_3O_4@SiO_2@L-Pd \\ \xrightarrow{\hspace*{1cm}} R_1 \xrightarrow{\hspace*{1cm}$$

Figure 1.34Fe<sub>3</sub>O<sub>4</sub>@SiO<sub>2</sub>@L-Pd catalysed Suzuki Reaction

Baran et al. have developed a new Pd@CS-CeO<sub>2</sub> catalyst system based on Pd stabilized over Schiff base-modified chitosan-CeO<sub>2</sub> support [183]. The activity of the novel catalyst was evaluated towards Heck coupling reactions and for the reduction of 2-nitrophenol and 4-nitrophenol and 4-nitroaniline (4-NA) using NaBH<sub>4</sub>. The catalytic system found to be very efficient and can be reapplied up to 05 runs in the reactions.

The Pd Schiff-based complex that immobilized onto magnetic Fe<sub>3</sub>O<sub>4</sub> nanoparticles was described by Zainul and colleagues [184] as a sustainable and reusable composite for the Suzuki reaction, and the products had high yields. Without losing its stability or activity, the produced catalyst could be retrieved and utilized repeatedly (**Figure 1.35**).

$$\begin{array}{c} Br \\ + \end{array} \begin{array}{c} B(OH)_2 \end{array} \begin{array}{c} Fe_3O_4@SiO_2@APT@BDA \\ @Schiff base-Pd \\ \hline \\ K_2CO_3, H_2O, 80 \ ^{o}C \end{array} \begin{array}{c} \\ R \end{array}$$

Figure 1.35 Pd Schiff base complex for the C-C coupling reaction

## 1.3 Research Gap

The conclusion drawn from a thorough review of the literature is that the Schiff base ligands along with their corresponding transition metal complexes are the most extensively studied subject for a substantial amount of research. Nevertheless, there is always a possibility for adding newer horizons of knowledge to the existing ones. In the earlier reported works slightly harsher conditions such as higher temperatures, lengthier reaction time, and use of various solvents such as acetonitrile, toluene, ethanol, and methanol have been used out of which acetonitrile and toluene are hazardous to use. Furthermore, the Schiff bases that result from the reaction of polyamine derivatives with poly-substituted aldehydes and ketones, as well as their complexes with palladium, zinc, and copper, have received less attention. This field, therefore, provides us ample scope to explore the formation of new ligands and metal complexes of copper, zinc, and palladium using milder reaction conditions and greener solvents for sustainability. There is room for investigation into the DNA binding and cleavage, protein binding, anti-cancer, and anti-germ capabilities of these

ligands and complexes as metal Schiff base complexes demonstrate significant biological and industrial significance. Furthermore, Schiff base metal complexes' catalytic activity can be investigated further for intriguing industrial uses.

## 1.4 Objectives

The proposed research work would be carried out with the following objectives:

- 1. Synthesis of Schiff Base metal complexes of Copper, Zinc and Palladium and their characterization using common spectroscopic techniques.
- 2. To screen the synthesized ligands and their transition metal complexes for various biological activities such as antimicrobial, antifungal, DNA binding activity.
- 3. The catalytic activity of the synthesized Schiff base complexes would also be tested for hydrogenation, C-C, and C-N bond formation reactions.

# 1.5 Research Methodology

In this experimental section, Schiff base type transition metal complexes (Homogeneous) would be prepared by the following steps (Figure 1.36).

- 1) In the first step, the new ligands will be synthesized by condensing substituted aldehydes/ ketones with different amines/diamines under green reaction mediums like ethanol, methanol etc.
- 2) Secondly, metal complexes of the ligands will be synthesized by reacting metal chloride/nitrate or acetate salts with these ligands in a suitable solvent.
- 3) Characterization of transition metal complexes of zinc, copper and palladium with the newly synthesized ligands would be doneusing different spectroscopy techniques like FT-IR, UV-vis, ESI-MS and EPR.
- 4). Structural characterization will be done through <sup>1</sup>H and <sup>13</sup>C spectroscopy
- 5). All the transition metal complexes would be screened for their biological applicability i.e., antibacterial, antifungal, and DNA binding activities.

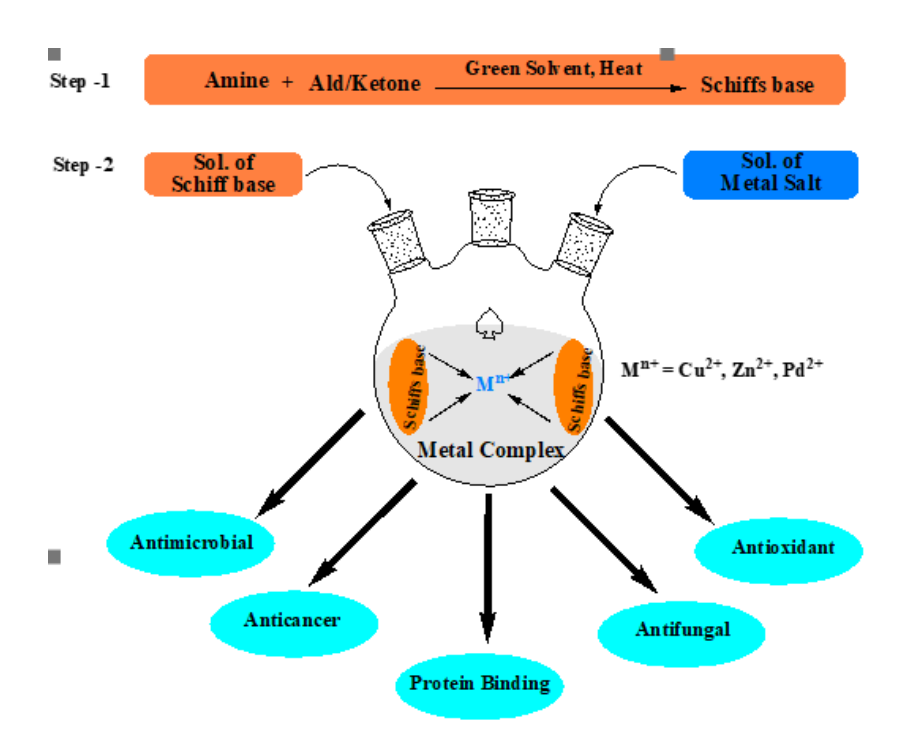


**Figure 1.36** Proposed scheme for synthesizing Schiff base type complexes of transition metals

Another way to synthesize Schiff base metal complexes (Heterogeneous) is by immobilizing these complexes on various supports like silica, titania, alumina etc, using following steps (Figure 1.37).

- 1) Pre-treatment of the support material with suitable solvent to activate the support material as well as to increase surface area for maximization of the active sites.
- 2) Building-up of suitable ligand structure onto the surface of the support material using Schiff base condensation strategy i.e. by introducing an amine functionality on the activated support followed by condensation reaction with suitable aldehyde/ ketone to give an imine.
- 3) Finally, heterogeneous Schiff base metal complex is formed by anchoring of transition metal salts on to the surface of supported imine functionalized ligand in a suitable solvent.

- 4) The characterization of prepared Schiff base metal complexes would be done by various techniques like FTIR, TGA, EDX, SEM, TEM and XRD.
- 5) The application of the heterogeneous Schiff base metal complexes would be tested for different chemical reactions (**Figure 1.38**).

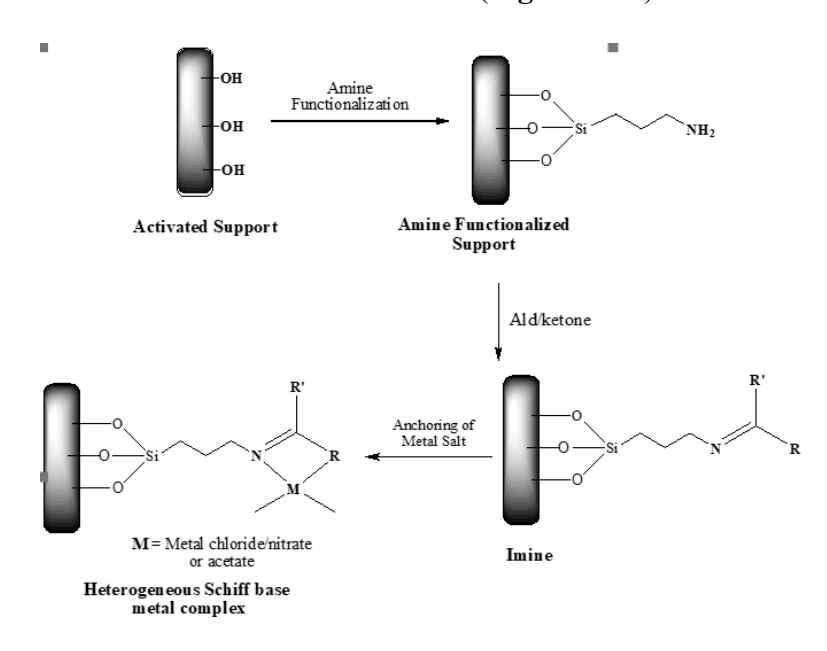


**Figure 1.37** Proposed scheme for synthesizing Heterogeneous Schiff base type complexes of transition metals

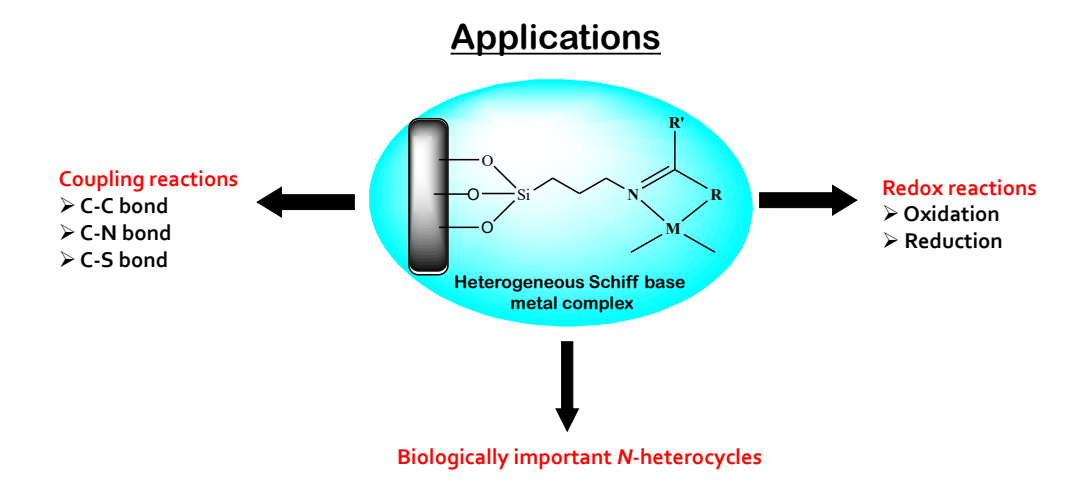


Figure 1.38 Applications of heterogeneous Schiff base metal complexes

#### 1.6 References

- [1]. Sahu, M., Ganguly, M. and Sharma, P., 2024. Recent applications of coinage metal nanoparticles passivated with salicylaldehyde and salicylaldehyde-based Schiff bases. *Nanoscale Advances*, 6(18), pp.4545-4566.
- [2]. Mir, M.A. and Banik, B.K., 2025. Synthesis of Schiff base ligands under environment friendly conditions: A systematic review. *Inorganic Chemistry Communications*, p.113987.
- [3]. Møller, M.S. and McKenzie, C.J., 2023. Structure Activity Relationships for Reversible O<sub>2</sub> Chemisorption by the Solid Phases of Co (salen) and Co (3F-salen). *JACS Au*, 3(5), pp.1484-1495.
- [4]. Gupta, K.C. and Sutar, A.K., 2008. Catalytic activities of Schiff base transition metal complexes. *Coordination Chemistry Reviews*, 252(12-14), pp.1420-1450.
- [5]. El Sonbati, A.Z., Mahmoud, W.H., Mohamed, G.G., Diab, M.A., Morgan, S.M. and Abbas, S.Y., 2019. Synthesis, characterization of Schiff base metal complexes and their biological investigation. *Applied Organometallic Chemistry*, 33(9), p.e5048.
- [6]. Mushtaq, I., Ahmad, M., Saleem, M. and Ahmed, A., 2024. Pharmaceutical significance of Schiff bases: An overview. *Future Journal of Pharmaceutical Sciences*, 10(1), p.16.
- [7]. Rajasekharan Sujatha, A., Anil, A., Deni Raju, P. and Veettil Suneesh, C., 2025. 1, 3, 5-Triformylphloroglucinol Derived β-Ketoenamine-Linked Functional Covalent Organic Frameworks with Enhanced Crystallinity and Stability–Recent Advances. *Chemistry–An Asian Journal*, p.e202401434.
- [8]. Adak, P., Mondal, A. and Chattopadhyay, S.K., 2020. Manganese (ii) complex of an oxygen–nitrogen donor Schiff base ligand showing efficient catechol oxidase activity: synthesis, spectroscopic and kinetic study. *New Journal of Chemistry*, 44(9), pp.3748-3754.

- [9]. Pradeep, C.P. and Das, S.K., 2013. Coordination and supramolecular aspects of the metal complexes of chiral N-salicyl-β-amino alcohol Schiff base ligands: Towards understanding the roles of weak interactions in their catalytic reactions. *Coordination Chemistry Reviews*, 257(11-12), pp.1699-1715.
- [10]. Kachhap, P., Chaudhary, N. and Haldar, C., 2023. Imidazole-modified Merrifield resin supported oxidovanadium (IV) complexes of Schiff-base-ether-based mixed functionality ligands for the catalytic oxidation of light aliphatic alcohols. *Reactive and Functional Polymers*, 189, p.105606.
- [11]. Nasaruddin, N.H., Ahmad, S.N., Tajuddin, A.M., Indriyani, N.P., Sakti, A.W., Permana, Y., Abd Rahman, N.M.M., Yusof, N.S.M. and Bahron, H., 2025. Synthesis, structural characterization, and catalytic performance of Pd (II) complexes with fluorine-and methyl-substituted Schiff bases: Experimental and theoretical insights. *Inorganic Chemistry Communications*, p.114186.
- [12]. Berhanu, A.L., Mohiuddin, I., Malik, A.K., Aulakh, J.S., Kumar, V. and Kim, K.H., 2019. A review of the applications of Schiff bases as optical chemical sensors. *TrAC Trends in Analytical Chemistry*, 116, pp.74-91.
- [13]. Abu-Dief, A.M. and Mohamed, I.M., 2015. A review on versatile applications of transition metal complexes incorporating Schiff bases. *Beni-suef university journal of basic and applied sciences*, 4(2), pp.119-133.
- [14]. Uddin, M.N., Ahmed, S.S. and Alam, S.R., 2020. Biomedical applications of Schiff base metal complexes. *Journal of Coordination Chemistry*, 73(23), pp.3109-3149.
- [15]. Boulechfar, C., Ferkous, H., Delimi, A., Djedouani, A., Kahlouche, A., Boublia, A., Darwish, A.S., Lemaoui, T., Verma, R. and Benguerba, Y., 2023. Schiff bases and their metal Complexes: A review on the history, synthesis, and applications. *Inorganic Chemistry Communications*, 150, p.110451.
- [16]. Abdel Rahman, L.H., Abu Dief, A.M., Moustafa, H. and Hamdan, S.K., 2017. Ni (II) and Cu (II) complexes with ONNO asymmetric tetradentate Schiff base

- ligand: synthesis, spectroscopic characterization, theoretical calculations, DNA interaction and antimicrobial studies. *Applied Organometallic Chemistry*, 31(2), p.e3555.
- [17]. Shahraki, S., 2022. Schiff base compounds as artificial metalloenzymes. *Colloids and Surfaces B: Biointerfaces*, 218, p.112727.
- [18]. Karataş, H., Kiliç, H.K., Tüzün, B. and Kökbudak, Z., 2024. Schiff base derivatives against monkeypox virus: Synthesis, in silico, MM-GBSA and SAR properties. *Journal of Molecular Structure*, 1298, p.137073.
- [19]. George, L. and Varghese, A., 2024. Advancements in thiol-yne click chemistry: Recent trends and applications in polymer synthesis and functionalization. *Materials Today Chemistry*, 38, p.102112.
- [20]. Pathan, I.R. and Patel, M.K., 2023. A comprehensive review on the synthesis and applications of Schiff base ligand and metal complexes: A comparative study of conventional heating, microwave heating, and sonochemical methods. *Inorganic Chemistry Communications*, p.111464.
- [21]. Cantón-Díaz, A.M., Muñoz-Flores, B.M., Moggio, I., Arias, E., De León, A., García-López, M.C., Santillán, R., Ochoa, M.E. and Jiménez-Pérez, V.M., 2018. One-pot microwave-assisted synthesis of organotin Schiff bases: An optical and electrochemical study towards their effects in organic solar cells. *New Journal of Chemistry*, 42(17), pp.14586-14596.
- [22]. Bui, R. and Brook, M.A., 2019. Dynamic covalent Schiff-base silicone polymers and elastomers. *Polymer*, 160, pp.282-290.
- [23]. Gogoi, H.P., Singh, A. and Barman, P., 2023. General Routes of Synthesis. *Schiff Base Metal Complexes: Synthesis and Applications*, pp.53-60.
- [24]. Peralta-Domínguez, D., Rodríguez, M., Ramos-Ortíz, G., Maldonado, J.L., Meneses-Nava, M.A., Barbosa-García, O., Santillan, R. and Farfán, N., 2015. A Schiff base derivative from cinnamaldehyde for colorimetric detection of Ni2+ in water. *Sensors and Actuators B: Chemical*, 207, pp.511-517.

- [25]. Malik, M.A., Dar, O.A., Gull, P., Wani, M.Y. and Hashmi, A.A., 2018. Heterocyclic Schiff base transition metal complexes in antimicrobial and anticancer chemotherapy. *MedChemComm*, 9(3), pp.409-436.
- [26]. Zhang, S., Huang, M., Jiao, L., Weng, Z., Yang, Q., Liao, N., Xu, Q., Li, X. and Wu, Q., 2025. A fluorescence turn-on probe for high SNR monitoring of Mg<sup>2+</sup> ions based on Salen-type Schiff base: Synthesis, characterisation and DFT/TD-DFT studies. *Journal of Molecular Structure*, *1321*, p.140098.
- [27]. Kleij, A.W., 2009. Nonsymmetrical salen ligands and their complexes: synthesis and applications. *European Journal of Inorganic Chemistry*, 2009(2), pp.193-205.
- [28]. Dalla Cort, A., De Bernardin, P., Forte, G. and Mihan, F.Y., 2010. Metal–salophen-based receptors for anions. *Chemical Society Reviews*, 39(10), pp.3863-3874.
- [29]. Kargar, H., Fallah-Mehrjardi, M. and Munawar, K.S., 2024. Metal complexes incorporating tridentate ONO pyridyl hydrazone Schiff base ligands: Crystal structure, characterization and applications. *Coordination Chemistry Reviews*, 501, p.215587.
- [30]. Krishnamoorthy, P., Sathyadevi, P., Butorac, R.R., Cowley, A.H., Bhuvanesh, N.S. and Dharmaraj, N., 2012. Copper (I) and nickel (II) complexes with 1: 1 vs. 1: 2 coordination of ferrocenyl hydrazone ligands: Do the geometry and composition of complexes affect DNA binding/cleavage, protein binding, antioxidant and cytotoxic activities. *Dalton Transactions*, 41(15), pp.4423-4436.
- [31]. Bagherzadeh, M. and Zare, M., 2012. Synthesis and characterization of NaY zeolite-encapsulated Mn-hydrazone Schiff base: an efficient and reusable catalyst for oxidation of olefins. *Journal of Coordination Chemistry*, 65(22), pp.4054-4066.
- [32]. Kitamura, F., Sawaguchi, K., Mori, A., Takagi, S., Suzuki, T., Kobayashi, A., Kato, M. and Nakajima, K., 2015. Coordination structure conversion of hydrazone–palladium (II) complexes in the solid state and in solution. *Inorganic Chemistry*, 54(17), pp.8436-8448.

- [33]. Chew, S.T., Lo, K.M., Sinniah, S.K., Sim, K.S. and Tan, K.W., 2014. Synthesis, characterization and biological evaluation of cationic hydrazone copper complexes with diverse diimine co-ligands. *RSC Advances*, 4(106), pp.61232-61247.
- [34]. Dilworth, J.R. and Hueting, R., 2012. Metal complexes of thiosemicarbazones for imaging and therapy. *InorganicaChimica Acta*, 389, pp.3-15.
- [35]. Verma, C., Quraishi, M.A. and Rhee, K.Y., 2023. Corrosion inhibition relevance of semicarbazides: electronic structure, reactivity and coordination chemistry. *Reviews in Chemical Engineering*, 39(6), pp.1005-1026.
- [36]. Hadjoudis, E. and Mavridis, I.M., 2004. Photochromism and thermochromism of Schiff bases in the solid state: structural aspects. *Chemical Society Reviews*, 33(9), pp.579-588.
- [37]. Padwa, A., 1977. Photochemistry of the carbon-nitrogen double bond. *Chemical Reviews*, 77(1), pp.37-68.
- [38]. Sanjurani, T. and Barman, P., 2023. The versatile nature of indole containing Schiff bases: A mini review. *Polyhedron*, p.116779.
- [39]. Sahu, M., Ganguly, M. and Sharma, P., 2024. Recent applications of coinage metal nanoparticles passivated with salicylaldehyde and salicylaldehyde-based Schiff bases. *Nanoscale Advances*, 6(18), pp.4545-4566.
- [40]. Mandal, P. and Pratihar, J.L., 2023. A review of the photochromic behavior of metal complexes embedded in conjugated (-N= N-C= N-) and non-conjugated azo-imine-based ligands. *Reviews in Inorganic Chemistry*, 43(4), pp.583-625.
- [41]. Clougherty, L., Sousa, J. and Wyman, G., 1957. C= N stretching frequency in infrared spectra of aromatic azomethines. *The Journal of Organic Chemistry*, 22(4), pp.462-462.
- [42]. Rykaczewski, K.A., Wearing, E.R., Blackmun, D.E. and Schindler, C.S., 2022. Reactivity of oximes for diverse methodologies and synthetic applications. *Nature Synthesis*, *1*(1), pp.24-36.

- [43]. Datta, M., 2024. Recent Advances of Deprotection of Oximes, Phenylhydrazones and Semicarbazones. *Tetrahedron*, p.134136.
- [44]. Lei, Z.Q., Xie, P., Rong, M.Z. and Zhang, M.Q., 2015. Catalyst-free dynamic exchange of aromatic Schiff base bonds and its application to self-healing and remolding of crosslinked polymers. *Journal of Materials Chemistry A*, 3(39), pp.19662-19668.
- [45]. Collinson, S.R. and Fenton, D.E., 1996. Metal complexes of bibracchial Schiff base macrocycles. *Coordination Chemistry Reviews*, 148, pp.19-40.
- [46]. Melchiorre, P., 2012. Cinchona based primary amine catalysis in the asymmetric functionalization of carbonyl compounds. *AngewandteChemie International Edition*, 51(39), pp.9748-9770.
- [47]. Cordes, E.H. and Jencks, W.P., 1962. On the mechanism of Schiff base formation and hydrolysis. *Journal of the American Chemical Society*, 84(5), pp.832-837.
- [48]. Nunez, L.J. and Eichhorn, G.L., 1962. On the Mechanism of Formation of the Metal Complexes of Schiff Bases. *Journal of the American Chemical Society*, 84(6), pp.901-906.
- [49]. Di Bernardo, P., Zanonato, P.L., Tamburini, S., Tomasin, P. and Vigato, P.A., 2006. Complexation behaviour and stability of Schiff bases in aqueous solution. The case of an acyclic diimino (amino) diphenol and its reduced triamine derivative. *Dalton Transactions*, (39), pp.4711-4721.
- [50]. Raczuk, E., Dmochowska, B., Samaszko-Fiertek, J. and Madaj, J., 2022. Different Schiff bases—structure, importance and classification. *Molecules*, 27(3), p.787.
- [51]. Metzler, C.M., Cahill, A. and Metzler, D.E., 1980. Equilibriums and absorption spectra of Schiff bases. *Journal of the American Chemical Society*, 102(19), pp.6075-6082.

- [52]. Jia, Y. and Li, J., 2015. Molecular assembly of Schiff base interactions: construction and application. *Chemical reviews*, 115(3), pp.1597-1621.
- [53]. Crugeiras, J., Rios, A., Riveiros, E. and Richard, J.P., 2009. Substituent effects on the thermodynamic stability of imines formed from glycine and aromatic aldehydes: implications for the catalytic activity of pyridoxal-5'-phosphate. *Journal of the American Chemical Society*, 131(43), pp.15815-15824.
- [54]. Witkop, B. and Beiler, T.W., 1954. Studies on Schiff bases in connection with the mechanism of transamination. *Journal of the American Chemical Society*, 76(22), pp.5589-5597.
- [55]. Jain, A., De, S. and Barman, P., 2022. Microwave-assisted synthesis and notable applications of Schiff-base and metal complexes: a comparative study. *Research on Chemical Intermediates*, 48(5), pp.2199-2251.
- [56]. Rana, M.S., Islam, M.A., Islam, M.S., Sarafi, M.S., Kudrat-E-Zahan, M., Hossen, M.F. and Asraf, M.A., 2024. A Review on Synthesis and Biological Activities of 2-Aminophenol-Based Schiff Bases and Their Transition Metal Complexes. *Applied Organometallic Chemistry*, p.e7724.
- [57]. Middya, P., Roy, D. and Chattopadhyay, S., 2023. Synthesis, structures and magnetic properties of end-on pseudo-halide bridged dinuclear copper (II) complexes with N, O-donor salicylaldimine Schiff base blocking ligands: A review. *InorganicaChimica Acta*, 548, p.121377.
- [58]. Jos, S. and Suja, N.R., 2023. Chiral Schiff base ligands of salicylaldehyde: A versatile tool for medical applications and organic synthesis-A review. *InorganicaChimica Acta*, 547, p.121323.
- [59]. Golcu, A., Tumer, M., Demirelli, H. and Wheatley, R.A., 2005. Cd (II) and Cu (II) complexes of polydentate Schiff base ligands: synthesis, characterization, properties and biological activity. *InorganicaChimica Acta*, 358(6), pp.1785-1797.

- [60]. Gou, Y., Li, J., Fan, B., Xu, B., Zhou, M. and Yang, F., 2017. Structure and biological properties of mixed-ligand Cu (II) Schiff base complexes as potential anticancer agents. *European Journal of Medicinal Chemistry*, 134, pp.207-217.
- [61]. Kaushik, S., Paliwal, S.K., Iyer, M.R. and Patil, V.M., 2023. Promising Schiff bases in antiviral drug design and discovery. *Medicinal Chemistry Research*, 32(6), pp.1063-1076.
- [62]. Dinku, D., Demissie, T.B., Beas, I.N., Eswaramoorthy, R., Abdi, B. and Desalegn, T., 2024. Antimicrobial activities and docking studies of new Schiff base ligand and its Cu (II), Zn (II) and Ni (II) Complexes: Synthesis and Characterization. *Inorganic Chemistry Communications*, 160, p.111903.
- [63]. Jiang, M., Su, X., Zhong, X., Lan, Y., Yang, F., Qin, Y. and Jiang, C., 2024. Recent development of Schiff-base metal complexes as therapeutic agents for lung cancer. *Journal of Molecular Structure*, p.139403.
- [64]. Bagul, A.D., Kumar, M., Alanazi, A.M., Tufail, A., Tufail, N., Gaikwad, D.D. and Dubey, A., 2024. Experimental and computational evaluation of anti-malarial and antioxidant potential of transition metal (II) complexes with tridentate schiff base derived from pyrrolopyrimidine. *BioMetals*, pp.1-25.
- [65]. Obradović, R., Joksimović, N., Janković, N., Kosanić, M., Matić, J., Milović, E., Bogdanović, G.A. and Petronijević, J., 2024. Discovery of Schiff bases as potent antibacterial and antifungal agents. *New Journal of Chemistry*, 48(40), pp.17492-17499.
- [66]. Abdel Rahman, L.H., Alzarzah, S.F., Abdel Hameed, M., Shehata, M.R. and El Saghier, A., 2024. A new bio active Schiff base ligand and its Ni (II), Cu (II), Ag (I), Zn (II), Cd (II), and La (III) binuclear complexes: synthesis, DFT analysis, antimicrobial, DNA interaction, COXII inhibition, and molecular docking studies. *Applied Organometallic Chemistry*, 38(9), p.e7631.

- [67]. Sahu, R. and Shah, K., 2024. Schiff Bases: A Captivating Scaffold with Potential Anticonvulsant Activity. *Mini Reviews in Medicinal Chemistry*, 24(18), pp.1632-1650.
- [68]. Kumar, A., Ahmed, S., Bhardwaj, M., Imtiaz, S., Kumar, D., Bhat, A.R., Sood, B. and Maji, S., 2024. In vitro Anti-microbial, DNA-binding, In silico Pharmacokinetics and Molecular Docking Studies of Schiff-based Cu (II), Zn (II) and Pd (II) Complexes. *Journal of Molecular Structure*, p.138695.
- [69]. Juyal, V.K., Pathak, A., Panwar, M., Thakuri, S.C., Prakash, O., Agrwal, A. and Nand, V., 2023. Schiff base metal complexes as a versatile catalyst: A review. *Journal of Organometallic Chemistry*, p.122825.
- [70]. Liu, D.F., Lü, X.Q. and Lu, R., 2014. Homogeneous and heterogeneous styrene epoxidation catalyzed by copper (II) and nickel (II) Schiff base complexes. *Transition Metal Chemistry*, 39, pp.705-712.
- [71]. Al Zoubi, W. and Ko, Y.G., 2017. Schiff base complexes and their versatile applications as catalysts in oxidation of organic compounds: part I. *Applied Organometallic Chemistry*, 31(3), p.e3574.
- [72]. Liu, X., Manzur, C., Novoa, N., Celedón, S., Carrillo, D. and Hamon, J.R., 2018. Multidentate unsymmetrically-substituted Schiff bases and their metal complexes: Synthesis, functional materials properties, and applications to catalysis. *Coordination Chemistry Reviews*, 357, pp.144-172.
- [73]. Kaur, M., Kumar, S., Younis, S.A., Yusuf, M., Lee, J., Weon, S., Kim, K.H. and Malik, A.K., 2021. Post-Synthesis modification of metal-organic frameworks using Schiff base complexes for various catalytic applications. *Chemical Engineering Journal*, 423, p.130230.
- [74]. Li, T., Jia, D., Zhou, S., Liu, Z., Chen, J., Ban, T., Li, A., Li, H. and Gao, H., 2024. Review on recent advances in supported metal catalysts for synthesis of high energy density fuels. *Fuel*, 373, p.132329.

- [75]. Nørskov, J.K., Bligaard, T., Hvolbæk, B., Abild-Pedersen, F., Chorkendorff, I. and Christensen, C.H., 2008. The nature of the active site in heterogeneous metal catalysis. *Chemical Society Reviews*, 37(10), pp.2163-2171.
- [76]. Dhawane, S.H., Kumar, T. and Halder, G., 2018. Recent advancement and prospective of heterogeneous carbonaceous catalysts in chemical and enzymatic transformation of biodiesel. *Energy Conversion and Management*, 167, pp.176-202.
- [77]. Hantoko, D., Khan, W.U., Osman, A.I., Nasr, M., Rashwan, A.K., Gambo, Y., Al Shoaibi, A., Chandrasekar, S. and Hossain, M.M., 2024. Carbon–neutral hydrogen production by catalytic methane decomposition: a review. *Environmental Chemistry Letters*, pp.1-41.
- [78]. Damera, T., Naga Gayatri, S., Pagadala, R., Abbu, V., Palle, K. and Gullapelli, K., 2024. Metal Supported Heterogeneous Catalysts for the Synthesis of Nitrogen Containing Heterocycles: A Comprehensive Review. *ChemistrySelect*, 9(34), p.e202402148.
- [79]. Maurya, A., Singh, S. and Pathak, N.P., 2024. The Importance of Mesoporous Materials (Silica, Alumina, and Zeolite) as Solid Supports for Metal Complex Catalysts in Organic Transformations. *Journal of Inorganic and Organometallic Polymers and Materials*, pp.1-21.
- [80]. Bahuguna, A., Kumar, A. and Krishnan, V., 2019. Carbon support based heterogeneous nanocatalysts: synthesis and applications in organic reactions. *Asian Journal of Organic Chemistry*, 8(8), pp.1263-1305.
- [81]. Govan, J. and Gun'ko, Y.K., 2014. Recent advances in the application of magnetic nanoparticles as a support for homogeneous catalysts. *Nanomaterials*, 4(2), pp.222-241.
- [82]. Nagendrappa, G., 2011. Organic synthesis using clay and clay-supported catalysts. *Applied Clay Science*, 53(2), pp.106-138.
- [83]. Buekenhoudt, A., 2008. Stability of porous ceramic membranes. *Membrane science and technology*, 13, pp.1-31.

- [84]. Kasprzyk-Hordern, B., 2004. Chemistry of alumina, reactions in aqueous solution and its application in water treatment. *Advances in colloid and interface science*, 110(1-2), pp.19-48.
- [85]. Hu, P., Hu, X., Liu, L., Li, M., Zhao, Z., Zhang, P., Wang, J. and Sun, Z., 2024. Dimensional upgrading of 0D silica nanospheres to 3D networking toward robust aerogels for fire resistance and low-carbon applications. *Materials Science and Engineering: R: Reports*, 161, p.100842.
- [86]. Griscom, D.L., 1977. The electronic structure of SiO2: a review of recent spectroscopic and theoretical advances. *Journal of Non-Crystalline Solids*, 24(2), pp.155-234.
- [87]. Bahari, M.B., Bukhari, S.N., Jun, L.N. and Setiabudi, H.D., 2021. Development of fibrous mesoporous silica for catalytic reaction: a short review. *Materials Today: Proceedings*, 42, pp.33-38.
- [88]. Hanaor, D.A. and Sorrell, C.C., 2011. Review of the anatase to rutile phase transformation. *Journal of Materials science*, 46, pp.855-874.
- [89]. Khataee, A.R. and Kasiri, M.B., 2010. Photocatalytic degradation of organic dyes in the presence of nanostructured titanium dioxide: Influence of the chemical structure of dyes. *Journal of Molecular Catalysis A: Chemical*, 328(1-2), pp.8-26.
- [90]. Singh, S., Mahalingam, H. and Singh, P.K., 2013. Polymer-supported titanium dioxide photocatalysts for environmental remediation: A review. *Applied Catalysis A: General*, 462, pp.178-195.
- [91]. Barroso Bogeat, A., 2021. Understanding and tuning the electrical conductivity of activated carbon: a state-of-the-art review. *Critical Reviews in Solid State and Materials Sciences*, 46(1), pp.1-37.
- [92]. Zhou, Y., Neyerlin, K., Olson, T.S., Pylypenko, S., Bult, J., Dinh, H.N., Gennett, T., Shao, Z. and O'Hayre, R., 2010. Enhancement of Pt and Pt-alloy fuel cell catalyst activity and durability via nitrogen-modified carbon supports. *Energy & Environmental Science*, 3(10), pp.1437-1446.

- [93]. Xia, D., Yu, H., Li, H., Huang, P., Li, Q. and Wang, Y., 2022. Carbon-based and carbon-supported nanomaterials for the catalytic conversion of biomass: a review. *Environmental Chemistry Letters*, 20(3), pp.1719-1744.
- [94]. Sharma, A., Sharma, S., Yadav, S., Arora, B., Dutta, S., Dixit, R., Mehta, S. and Sharma, R.K., 2024. Covalently functionalized graphene oxide metal complexes: Versatile nanocatalysts for organic transformations. *Materials Science and Engineering: B*, 310, p.117671.
- [95]. Magdesieva, T.V., 2021. Ni (II) Schiff base complexes as chiral electroauxiliaries and methodological platform for stereoselective electrochemical functionalization of amino acids. *The Chemical Record*, 21(9), pp.2178-2192.
- [96]. Biswal, T., BadJena, S.K. and Pradhan, D., 2020. Sustainable biomaterials and their applications: A short review. *Materials Today: Proceedings*, 30, pp.274-282.
- [97]. Kamel, S. and Khattab, T.A., 2021. Recent advances in cellulose supported metal nanoparticles as green and sustainable catalysis for organic synthesis. *Cellulose*, 28(8), pp.4545-4574.
- [98]. Dohendou, M., Pakzad, K., Nezafat, Z., Nasrollahzadeh, M. and Dekamin, M.G., 2021. Progresses in chitin, chitosan, starch, cellulose, pectin, alginate, gelatin and gum based (nano) catalysts for the Heck coupling reactions: A review. *International journal of biological macromolecules*, 192, pp.771-819.
- [99]. Sadeghi, M., 2024. The untold story of starch as a catalyst for organic reactions. *RSC advances*, 14(18), pp.12676-12702.
- [100]. Lin, Q., Chee, P.L., Pang, J.J., Loh, X.J., Kai, D. and Lim, J.Y., 2024. Sustainable Polymeric Biomaterials from Alternative Feedstocks. *ACS Biomaterials Science & Engineering*, pp.248-256.
- [101]. Shokrollahi, H.J.J.O.M., 2017. A review of the magnetic properties, synthesis methods and applications of maghemite. *Journal of Magnetism and Magnetic Materials*, 426, pp.74-81.

- [102]. Kianfar, E., 2021. Magnetic nanoparticles in targeted drug delivery: a review. *Journal of Superconductivity and Novel Magnetism*, 34(7), pp.1709-1735.
- [103]. Soltys, L., Olkhovyy, O., Tatarchuk, T. and Naushad, M., 2021. Green synthesis of metal and metal oxide nanoparticles: Principles of green chemistry and raw materials. *Magnetochemistry*, 7(11), p.145.
- [104]. Tang, S.C. and Lo, I.M., 2013. Magnetic nanoparticles: essential factors for sustainable environmental applications. *Water research*, 47(8), pp.2613-2632.
- [105]. Kainz, Q.M. and Reiser, O., 2014. Polymer-and dendrimer-coated magnetic nanoparticles as versatile supports for catalysts, scavengers, and reagents. *Accounts of chemical research*, 47(2), pp.667-677.
- [106]. Hemmati, M., Rajabi, M. and Asghari, A., 2018. Magnetic nanoparticle based solid-phase extraction of heavy metal ions: a review on recent advances. *Microchimica Acta*, 185, pp.1-32.
- [107]. Manoj, G.M., Shalini, M., Thenmozhi, K., Ponnusamy, V.K. and Hari, S., 2024. Recent advancements in the surface modification and functionalization of magnetic nanomaterials. *Applied Surface Science Advances*, 21, p.100608.
- [108]. Wang, D., Deraedt, C., Ruiz, J. and Astruc, D., 2015. Magnetic and dendritic catalysts. *Accounts of chemical research*, 48(7), pp.1871-1880.
- [109]. Moellering Jr, R.C., 1995. Past, present, and future of antimicrobial agents. *The American journal of medicine*, 99(6), pp.11s-18s.
- [110]. Medici, S., Peana, M., Nurchi, V.M., Lachowicz, J.I., Crisponi, G. and Zoroddu, M.A., 2015. Noble metals in medicine: Latest advances. *Coordination Chemistry Reviews*, 284, pp.329-350.
- [111]. Villani, G. and Attardi, G., 2000. In vivo control of respiration by cytochrome c oxidase in human cells. *Free Radical Biology and Medicine*, 29(3-4), pp.202-210.
- [112]. Kornblatt, A.P., Nicoletti, V.G. and Travaglia, A., 2016. The neglected role of copper ions in wound healing. *Journal of inorganic biochemistry*, 161, pp.1-8.

- [113]. Keen, C.L., Clegg, M.S., Hanna, L.A., Lanoue, L., Rogers, J.M., Daston, G.P., Oteiza, P. and Uriu-Adams, J.Y., 2003. The plausibility of micronutrient deficiencies being a significant contributing factor to the occurrence of pregnancy complications. *The Journal of nutrition*, 133(5), pp.1597S-1605S.
- [114]. Al Zoubi, W. and Ko, Y.G., 2016. Organometallic complexes of Schiff bases: Recent progress in oxidation catalysis. *Journal of Organometallic Chemistry*, 822, pp.173-188.
- [115]. Ourari, A., Ketfi, B., Malha, S.I.R. and Amine, A., 2017. Electrocatalytic reduction of nitrite and bromate and their highly sensitive determination on carbon paste electrode modified with new copper Schiff base complex. *Journal of Electroanalytical Chemistry*, 797, pp.31-36.
- [116]. Mohajer, F., Heravi, M.M., Zadsirjan, V. and Poormohammad, N., 2021. Copper-free Sonogashira cross-coupling reactions: an overview. *RSC advances*, 11(12), pp.6885-6925.
- [117]. Niu, J., Liu, H., Jin, Y., Fan, B., Qi, W. and Ran, J., 2022. Comprehensive review of Cu-based CO2 hydrogenation to CH3OH: Insights from experimental work and theoretical analysis. *International Journal of Hydrogen Energy*, 47(15), pp.9183-9200.
- [118]. Anand, A., Kumar, R., Maity, J. and Maikhuri, V.K., 2023. Recent progress in the Cu-catalyzed multicomponent synthesis of 1, 4-disubstituted 1, 2, 3-triazoles. *Synthetic Communications*, 53(5), pp.345-375.
- [119]. Lin, P.H., Sermersheim, M., Li, H., Lee, P.H., Steinberg, S.M. and Ma, J., 2017. Zinc in wound healing modulation. *Nutrients*, 10(1), p.16.
- [120]. Zhang, Y., Tian, Y., Zhang, H., Xu, B. and Chen, H., 2021. Potential pathways of zinc deficiency-promoted tumorigenesis. *Biomedicine & Pharmacotherapy*, 133, p.110983.
- [121]. Hambidge, M., 2000. Human zinc deficiency. *The Journal of nutrition*, 130(5), pp.1344S-1349S.

- [122]. Nishida, K. and Uchida, R., 2018. Role of Zinc Signaling in the Regulation of Mast Cell , Basophil , and T Cell Mediated Allergic Responses. *Journal of immunology research*, 2018(1), p.5749120.
- [123]. Tedeeva, M.A., Kustov, A.L., Batkin, A.M., Garifullina, C., Zalyatdinov, A.A., Yang, D., Dai, Y., Yang, Y. and Kustov, L.M., 2024. Catalytic systems for hydrogenation of CO2 to methanol. *Molecular Catalysis*, 566, p.114403.
- [124]. Penner-Hahn, J., 2007. Zinc-promoted alkyl transfer: a new role for zinc. *Current opinion in chemical biology*, 11(2), pp.166-171.
- [125]. Wu, X.F., Fang, X., Wu, L., Jackstell, R., Neumann, H. and Beller, M., 2014. Transition-metal-catalyzed carbonylation reactions of olefins and alkynes: a personal account. *Accounts of Chemical Research*, 47(4), pp.1041-1053.
- [126]. Chopra, L., 2022. Photocatalytic activity of zinc oxide for dye and drug degradation: a review. *Materials Today: Proceedings*, 52, pp.1653-1656.
- [127]. Rubert, R.V. and Paul, R.R., 2023. The applications of organozinc reagents in continuous flow chemistry: Negishi coupling. *Journal of Flow Chemistry*, 13(3), pp.217-246.
- [128]. Cao, Y., Ran, R., Wu, X., Si, Z., Kang, F. and Weng, D., 2023. Progress on metal-support interactions in Pd-based catalysts for automobile emission control. *Journal of Environmental Sciences*, 125, pp.401-426.
- [129]. Sharma, S., Kumar, A.S.K. and Rajesh, N., 2017. A perspective on diverse adsorbent materials to recover precious palladium and the way forward. *Rsc Advances*, 7(82), pp.52133-52142.
- [130]. Givan, D.A., 2007. Precious metals in dentistry. *Dental Clinics of North America*, 51(3), pp.591-601.
- [131]. Bulushev, D.A. and Ross, J.R., 2018. Heterogeneous catalysts for hydrogenation of CO2 and bicarbonates to formic acid and formates. *Catalysis Reviews*, 60(4), pp.566-593.

- [132]. Kumar, S., 2019. Recent advances in the Schiff bases and N heterocyclic Carbenes as ligands in the cross coupling reactions: a comprehensive review. *Journal of Heterocyclic Chemistry*, 56(4), pp.1168-1230.
- [133]. Vinoth Kumar, P., Mohana Roopan, S. and Madhumitha, G., 2024. Recent advances on palladium incorporated clay-based heterogeneous catalyst for carbon-carbon coupling reactions. *Monatshefte für Chemie-Chemical Monthly*, 155(1), pp.1-15.
- [134]. Pfeiffer, P., Breith, E., Lübbe, E. and Tsumaki, T., 1933. *Justus Liebigs Annalen der Chemie*, 503(1), pp.84-130.
- [135]. Lv, J., Liu, T., Cai, S., Wang, X., Liu, L. and Wang, Y., 2006. Synthesis, structure and biological activity of cobalt (II) and copper (II) complexes of valine-derived Schiff bases. *Journal of Inorganic Biochemistry*, 100(11), pp.1888-1896.
- [136]. Rajavel, R., Vadivu, M.S. and Anitha, C., 2008. Synthesis, physical characterization and biological activity of some Schiff base complexes. *Journal of Chemistry*, 5(3),pp.620-626.
- [137]. Mohamed, G.G., Omar, M.M. and Ibrahim, A.A., 2009. Biological activity studies on metal complexes of novel tridentate Schiff base ligand. Spectroscopic and thermal characterization. *European journal of medicinal chemistry*, 44(12), pp.4801-4812.
- [138]. Creaven, B.S., Duff, B., Egan, D.A., Kavanagh, K., Rosair, G., Thangella, V.R. and Walsh, M., 2010. Anticancer and antifungal activity of copper (II) complexes of quinolin-2 (1H)-one-derived Schiff bases. *InorganicaChimica Acta*, 363(14), pp.4048-4058.
- [139]. Mohamed, G.G., Zayed, M.A. and Abdallah, S.M., 2010. Metal complexes of a novel Schiff base derived from sulphametrole and varelaldehyde. Synthesis, spectral, thermal characterization and biological activity. *Journal of Molecular Structure*, 979(1-3), pp.62-71.

- [140]. Ran, X., Wang, L., Lin, Y., Hao, J. and Cao, D., 2010. Syntheses, characterization and biological studies of zinc (II), copper (II) and cobalt (II) complexes with Schiff base ligand derived from 2 hydroxy 1 naphthaldehyde and selenomethionine. *Applied Organometallic Chemistry*, 24(10), pp.741-747.
- [141]. El-Sherif, A.A., Shehata, M.R., Shoukry, M.M. and Barakat, M.H., 2012. Synthesis, characterization, equilibrium study and biological activity of Cu (II), Ni (II) and Co (II) complexes of polydentate Schiff base ligand. *Spectrochimica Acta Part A: Molecular and Biomolecular Spectroscopy*, 96, pp.889-897.
- [142]. Mukherjee, T., Pessoa, J.C., Kumar, A. and Sarkar, A.R., 2013. Synthesis, structure, magnetic properties and biological activity of supramolecular copper (ii) and nickel (ii) complexes with a Schiff base ligand derived from vitamin B 6. *Dalton Transactions*, 42(7), pp.2594-2607.
- [143]. Khoo, T.J., bin Break, M.K., Crouse, K.A., Tahir, M.I.M., Ali, A.M., Cowley, A.R., Watkin, D.J. and Tarafder, M.T.H., 2014. Synthesis, characterization and biological activity of two Schiff base ligands and their nickel (II), copper (II), zinc (II) and cadmium (II) complexes derived from S-4-picolyldithiocarbazate and X-ray crystal structure of cadmium (II) complex derived from pyridine-2-carboxaldehyde. *InorganicaChimica Acta*, 413, pp.68-76.
- [144]. Valentová, J., Varényi, S., Herich, P., Baran, P., Bilková, A., Kožíšek, J. and Habala, L., 2018. Synthesis, structures and biological activity of copper (II) and zinc (II) Schiff base complexes derived from aminocyclohexane-1-carboxylic acid. New type of geometrical isomerism in polynuclear complexes. *InorganicaChimica Acta*, 480, pp.16-26.
- [145]. Benabid, W., Ouari, K., Bendia, S., Bourzami, R. and Ali, M.A., 2020. Crystal structure, spectroscopic studies, DFT calculations, cyclic voltammetry and biological activity of a copper (II) Schiff base complex. *Journal of Molecular Structure*, 1203, p.127313.
- [146]. Alterhoni, E., Tavman, A., Hacioglu, M., Şahin, O. and Tan, A.S.B., 2021. Synthesis, structural characterization and antimicrobial activity of Schiff bases and

benzimidazole derivatives and their complexes with CoCl2, PdCl2, CuCl2 and ZnCl2. *Journal of Molecular Structure*, 1229, p.129498.

- [147]. Kargar, H., Ardakani, A.A., Tahir, M.N., Ashfaq, M. and Munawar, K.S., 2021. Synthesis, spectral characterization, crystal structure and antibacterial activity of nickel (II), copper (II) and zinc (II) complexes containing ONNO donor Schiff base ligands. *Journal of Molecular Structure*, 1233, p.130112.
- [148]. Yusuf, T.L., Oladipo, S.D., Zamisa, S., Kumalo, H.M., Lawal, I.A., Lawal, M.M. and Mabuba, N., 2021. Design of new Schiff-Base Copper (II) complexes: Synthesis, crystal structures, DFT study, and binding potency toward cytochrome P450 3A4. *ACS omega*, 6(21), pp.13704-13718.
- [149]. Al-Shboul, T.M., El-khateeb, M., Obeidat, Z.H., Ababneh, T.S., Al-Tarawneh, S.S., Al Zoubi, M.S., Alshaer, W., Abu Seni, A., Qasem, T., Moriyama, H. and Yoshida, Y., 2022. Synthesis, characterization, computational and biological activity of some Schiff bases and their Fe, Cu and Zn complexes. *Inorganics*, 10(8), p.112.
- [150]. Devi, J., Kumar, S., Kumar, B., Asija, S. and Kumar, A., 2022. Synthesis, structural analysis, in vitro antioxidant, antimicrobial activity and molecular docking studies of transition metal complexes derived from Schiff base ligands of 4-(benzyloxy)-2-hydroxybenzaldehyde. *Research on Chemical Intermediates*, 48(4), pp.1541-1576.
- [151]. Fasna, P.F., Sasi, S., Sharmila, T.B., Chandra, C.J., Antony, J.V. and Raman, V., 2022. Photocatalytic remediation of methylene blue and antibacterial activity study using Schiff base Cu complexes. *Environmental Science and Pollution Research*, 29(36), pp.54318-54329.
- [152]. Kumar, S., Devi, J., Dubey, A., Kumar, D., Jindal, D.K., Asija, S. and Sharma, A., 2023. Co (II), Ni (II), Cu (II) and Zn (II) complexes of Schiff base ligands: Synthesis, characterization, DFT, in vitro antimicrobial activity and molecular docking studies. *Research on Chemical Intermediates*, 49(3), pp.939-965.

- [153]. El-Ghamry, M.A., Elzawawi, F.M., Aziz, A.A.A., Nassir, K.M. and Abu-El-Wafa, S.M., 2022. New Schiff base ligand and its novel Cr (III), Mn (II), Co (II), Ni (II), Cu (II), Zn (II) complexes: spectral investigation, biological applications, and semiconducting properties. *Scientific Reports*, 12(1), p.17942.
- [154]. Pahonţu, E., Dinu Pîrvu, C.E., Vişan, D.C., Socea, L.I., Apostol, T.V., Oprean, C., Păunescu, V., Ungurianu, A., Margină, D.M., Codiţă, I. and Dumitrescu, S., 2024. Evaluation of Antimicrobial, Antitumor, Antioxidant Activities, and Molecular Docking Studies of Some Co (II), Cu (II), Mn (II), Ni (II), Pd (II), and Pt (II) Complexes with a Schiff Base Derived From 2 Chloro 5 (trifluoromethyl) aniline. *Applied Organometallic Chemistry*, p.e7829.
- [155]. Elsherbeny, M., El Ayaan, U., Abou El Reash, Y.G. and Abu El Reash, G.M., 2024. Characterization, DFT, DNA, Biological Applications, and In Silico Studies of Mn (II), VO (II), Pd (II), and Cd (II) Complexes Derived From Chromone Isonicotinic Hydrazone Ligand. *Applied Organometallic Chemistry*, p.e7822.
- [156]. Yousef, T.A. and Al-Janabi, A.S., 2024. Spectroscopic, anti-cancer, anti-bacterial and theoretical studies of new bivalent Schiff base complexes derived from 4-bromo-2, 6-dichloroaniline. *Heliyon*, 10(17).
- [157]. Abu-Dief, A.M., El-Sagher, H.M. and Shehata, M.R., 2019. Fabrication, spectroscopic characterization, calf thymus DNA binding investigation, antioxidant and anticancer activities of some antibiotic azomethine Cu (II), Pd (II), Zn (II) and Cr (III) complexes. *Applied Organometallic Chemistry*, 33(8), p.e4943.
- [158]. Özdemir, Ö., Gürkan, P., Demir, Y.D.Ş. and Ark, M., 2020. Novel palladium (II) complexes of N-(5-nitro-salicylidene)-Schiff bases: Synthesis, spectroscopic characterization and cytotoxicity investigation. *Journal of Molecular Structure*, 1207, p.127852.
- [159]. Khalaf, W.H., Al-Jibori, S.A., Ashfaq, M., Faihan, A.S., Tahir, M.N. and Al-Janabi, A.S., 2024. Synthesis, characterization and biological activity studies of Pd (II) and Pt (II)–2H-benzo [e][1, 3] oxazine-2, 4 (3H)-dione (HBzoxe) complexes. *Chemical Papers*, 78(14), pp.7987-7998.

- [160]. Singh, R., Jain, B., Malik, S., Singh, A., Das, S., Dadoria, A. and Chaturvedi, A., 2024. POTENTIALLY BIOACTIVE SULFATHIAZOLE-BASED LIGAND AND ITS PALLADIUM (II) COMPLEX: SYNTHESIS, CHARACTERIZATION, PHYSICO-CHEMICAL AND ANTIMICROBIAL BEHAVIOR. *Rasayan Journal of Chemistry*, 17(2).1
- [161]. Pardaeva, D., Tavman, A., GÜRBÜZ, D., HACIOĞLU, M., YILMAZ, F., Şahin, O., BİRTEKSÖZ TAN, A. and ÇINARLI, A., 2024. Spectral characterization and antibacterial, antifungal, antiviral activity of salicyl based new Schiff bases and their Co (II), Ni (II), Cu (II), Zn (II), and Pd (II) complexes. *Revue Roumaine de Chimie*, 69(1-2).
- [162]. Aly, S.A., Hassan, S.S., El-Boraey, H.A., Eldourghamy, A., Abdalla, E.M., Alminderej, F.M. and Elganzory, H.H., 2024. Synthesis, biological activity, and the effect of ionization radiation on the spectral, XRD, and TGA analysis of Cu (I), Cu (II), Zn (II), and Cd (II) complexes. *Arabian Journal for Science and Engineering*, 49(1), pp.361-379.
- [163]. Navarro-Peñaloza, R., Anacleto-Santos, J., Rivera-Fernández, N., Sánchez-Bartez, F., Gracia-Mora, I., Caballero, A.B., Gamez, P. and Barba-Behrens, N., 2024. Anti-toxoplasma activity and DNA-binding of copper (II) and zinc (II) coordination compounds with 5-nitroimidazole-based ligands. *JBIC Journal of Biological Inorganic Chemistry*, 29(1), pp.33-49.
- [164]. Hassan, S.S., Aly, S.A., Al-Sulami, A.I., Albohy, S.A., Salem, M.F., Nasr, G.M. and Abdalla, E.M., 2024. Synthesis, characterization, PXRD studies, and theoretical calculation of the effect of gamma irradiation and antimicrobial studies on novel Pd (II), Cu (II), and Cu (I) complexes. *Frontiers in Chemistry*, 12, p.1357330.
- [165]. Bardajee, G.R., Malakooti, R., Jami, F., Parsaei, Z. and Atashin, H., 2012. Covalent anchoring of copper-Schiff base complex into SBA-15 as a heterogeneous catalyst for the synthesis of pyridopyrazine and quinoxaline derivatives. *Catalysis Communications*, 27, pp.49-53.

- [166]. Ghorbani-Choghamarani, A., Darvishnejad, Z. and Norouzi, M., 2015. Cu (II)—Schiff base complex-functionalized magnetic Fe<sub>3</sub>O<sub>4</sub> nanoparticles: a heterogeneous catalyst for various oxidation reactions. *Applied Organometallic Chemistry*, 29(3), pp.170-175.
- [167]. Kumari, S. and Pathak, D.D., 2015. Synthesis and development of Chitosan anchored copper (II) Schiff base complexes as heterogeneous catalysts for N-arylation of amines. *Tetrahedron Letters*, 56(27), pp.4135-4142.
- [168]. Taskin, O.S., Dadashi-Silab, S., Kiskan, B., Weber, J. and Yagci, Y., 2015. Highly efficient and reusable microporous Schiff base network polymer as a heterogeneous catalyst for CuAAC click reaction. *Macromolecular Chemistry and Physics*, 216(16), pp.1746-1753.
- [169]. Kazemnejadi, M. and Sardarian, A.R., 2016. Ecofriendly synthesis of a heterogeneous polyvinyl alcohol immobilized copper (ii) Schiff base complex as an efficient, reusable catalyst for the one-pot three-component green preparation of 5-substituted 1 H-tetrazoles under mild conditions. *RSC advances*, 6(94), pp.91999-92006.
- [170]. Nikoorazm, M., Rezaei, Z., and Tahmasbi, B., 2020, Two Schiff-base complexes of copper and zirconium oxide supported on mesoporous MCM-41 as an organic–inorganic hybrid catalysts in the chemo and homoselective oxidation of sulfides and synthesis of tetrazoles, *Journal of Porous Materials*, 27, pp 671-689.
- [171]. Kamroudi, M.R. and Grivani, G., 2023. Synthesis and characterization of a new Cu (II)-ionic macrocycle Schiff base complex and its use as an efficient catalyst in one pot-multicomponent Click Synthesis of 1, 2, 3-Triazoles in water. *Inorganic Chemistry Communications*, 158, p.111467.
- [172]. Ajormal, F., Bikas, R., Noshiranzadeh, N., Emami, M. and Kozakiewicz-Piekarz, A., 2024. Synthesis of chiral Cu (II) complexes from pro-chiral Schiff base ligand and investigation of their catalytic activity in the asymmetric synthesis of 1, 2, 3-triazoles. *Scientific Reports*, *14*(1), p.10603.

- [173]. Noori, N., Nikoorazm, M. and Ghorbani-Choghamarani, A., 2015. Synthesis and characterization of Ni and Zn Schiff base complexes supported on modified MCM-41 as reusable catalysts for various oxidation reactions. *Journal of Porous Materials*, 22, pp.1607-1615.
- [174]. Balinge, K.R., Khiratkar, A.G., Muskawar, P.N., Thenmozhi, K. and Bhagat, P.R., 2018. Facile access to polymer supported zinc–salen complex: highly efficient heterogeneous catalyst for synthesizing hydantoins, thiohydantoins and Schiff bases in aqueous medium. *Research on Chemical Intermediates*, 44, pp.2075-2097.
- [175]. Adam, M.S.S., Khalil, A., Taha, A., Mostafa, M.M., Makhlouf, M.M. and Mahmoud, H.A., 2023. Facile synthetic route of TiO<sub>2</sub>–ZnOheteronanostructure coated by oxovanadium (IV) bis-Schiff base complex as a potential effective homogeneous/heterogeneous catalyst for alcohols redox systems. *Surfaces and Interfaces*, 39, p.102914.
- [176]. Dhengale, S.D., Naik, V.M., Kolekar, G.B., Rode, C.V. and Anbhule, P.V., 2021. Solvent free, environment benign synthesis of 1, 4-dihydropyridines and polyhydroquinolines by using heterogeneous Zn/MCM-41 catalyst. *Research on Chemical Intermediates*, 47(8), pp.3263-3287.
- [177]. Kulkarni, P.A., Kahandal, S.S., Mirgane, N.A., Satpati, A.K. and Shendage, S.S., 2022. Highly efficient magnetically separable Zn-Ag@ 1-arginine Fe<sub>3</sub>O<sub>4</sub> catalyst for synthesis of 2-aryl-substituted benzimidazoles and multicomponent synthesis of pyrimidines. *Results in Chemistry*, 4, p.100655.
- [178]. Mohamed, E.A., Altalhi, A.A., Negm, N.A., Abo-Shanab, Z.L., Abdelshafi, N.S. and Farag, A.A., 2024. Novel magnetic chitosan Schiff base impregnated with ZnO for removal of malachite green dye from aqueous environment. *International Journal of Environmental Science and Technology*, pp.1-22.
- [179]. Aghayee, M., Zolfigol, M., A., Keypour, H., Yarie, M., & Mohammadi, L., 2016. Synthesis and characterization of a novel magnetic nano-palladium Schiff base complex:application in cross-coupling reactions. *Appl. Organometal. Chem.*, 30 pp 612-618.

- [180]. Baran, N.Y., Baran, T., Nasrollahzadeh, M. and Varma, R.S., 2019. Pd nanoparticles stabilized on the Schiff base-modified boehmite: Catalytic role in Suzuki coupling reaction and reduction of nitroarenes. *Journal of Organometallic Chemistry*, 900, p.120916.
- [181]. Noroozi M. & Sh. G. S., 2021, Synthesis of Schiff Base-functionalized Fullerene Anchored Palladium Complex as a Recyclable Nanocatalyst in the Heck Reaction and Oxidation of Alcohols, *Iran. J. Chem. Chem. Eng*, 40 (5) pp1395-1405.
- [182]. Balali, M., Bagherzadeh, M., Nejat, R. and Keypour, H., 2021. Palladium Supported on Schiff Base Functionalized Magnetite Nanoparticles as an Efficient Catalyst for Coupling Reactions. *Inorganic Chemistry Research*, 5(1), pp.82-93.
- [183]. Çalışkan, M., Güzel, H.D. and Baran, T., 2023. Pd nanoparticles decorated on Schiff base-modified chitosan/CeO2 as a heterogeneous and retriable nanocatalyst for Heck reactions and remediation of environmental pollutants. *International Journal of Biological Macromolecules*, 240, p.124453.
- [184]. Zainul, R., Basem, A., Alfaker, M.J., Ballal, S., Qassem, T.A., Kaur, I., Alaraj, M., Al-khalidi, A. and Elmasry, Y., 2024. Synthesis and characterization of a Pd Schiff base complex anchored on Fe<sub>3</sub>O<sub>4</sub> as a novel and recyclable catalyst for CC cross-coupling reactions. *Journal of Molecular Structure*, *1313*, p.138620.

# Chapter 2

The synthesized Schiff base ligand and related metal complexes of Cu(II), Zn(II), and Pd(II) are described in detail in this chapter, along with their characterization using a variety of spectroscopic techniques and applications.

# Section 2.1 The synthesis and characterisation of Cu(II), Zn(II), and Pd(II) complexes of Schiff base

Schiff base, a product of condensation, formed from a primary amine and an aldehyde or ketone, is an important class of compounds that has successfully been used as a synthetic intermediate in the formation of coordination metal complexes [1]. The imine or azomethine (-C=N-) moiety formed as a result of this nucleophilic addition reaction in Schiff base is accountable for the biological actions shown by them. Schiff base ligands have worked really well in exhibiting the antimicrobial activity against varied strains of fungi, bacteria, and viruses. However, the bio-activity of Schiff base ligands has shown a significant increase when a suitable metal is made to react with these ligands under ambient conditions to form metal complexes. Upon complexation with transition metals in different oxidation states, these compounds exhibit numerous applications in the field of industry as well as medicine [2]. Metals in different oxidation states from the periodic table have been utilized for complexation with these biomolecules, but during the past few decades, the Cu(II), Zn(II), and Pd(II) metal complexes have engrossed a lot of consideration because of their important biological and catalytic activities [3-4].

The present study generated and studied the Cu(II), Zn(II), and Pd(II) complexes of the salen-type Schiff base of Butane1,4-diamine with 5-bromosalicylaldehyde using a variety of spectroscopic techniques.

#### Materials and instrumentation

In this analysis, every chemical and reagent used was of analytical grade and utilized precisely as it was supplied. Sigma Aldrich supplied the 5-bromosalicyaldehyde, 1,4-butanediamine, copper(II) chloride, zinc(II) chloride, and palladium(II) chloride salts, which were used without additional purification.

The elemental analysis (CHN) of the synthesized compounds was carried out with a Carlo Erba model-1106 elemental analyzer. The FT-IR Perkin-Elmer spectrophotometer was used to record each FT-IR spectrum. The D2 PHASER Rigaku X-ray diffractometer was used to record the XRD data in two theta scales ranging from 10 to 80 degrees. The Shimadzu 1900i UV spectrometer was used to record the UV-Vis spectra. Using DMSO/CDCl<sub>3</sub> as solvents, <sup>1</sup>H and <sup>13</sup>C NMR spectra were captured on a Bruker Avance at 100 MHz and 400 MHz.

The electron paramagnetic resonance (EPR) spectral studies of the synthesized compounds were carried out by recording the spectra in solid phase at room temperature on Varian EPR-E 112 spectrometer. Acetonitrile solution was used as a carrier to record the ESI mass spectra on a Q-Tof mass spectrometer. The CH instrument electrochemical analyzer was used to perform cyclic voltammetry. **Figure 2.1-2.11** describes all of the ligand and related metal complex structures and schemes.

# 2.1.1 Synthesis of Schiff base Ligand (L): N, N-Bis(5-bromo-2-salicylidene) butane 1,4-diamine

5-Bromosalicylaldehyde (5 mmol, 1.00 g) was solvated in ethanol (15 mL) and infused to a refluxing solution of 1,4-butanediamine (2.5 mmol, 0.22 g) in ethanol (15 mL) in 2:1 molar ratio and was further refluxed for about 50 min. and then cooled. The light-yellow precipitates formed were separated *via* filtration and cleansed with ethanol and water (20 mL) each successively, and further purified by recrystallising from absolute ethanol and dried under vacuum. TLC was used to track the reaction's development.

Yield: 90%; Colour: Yellow; Melting point: 212 °C: Anal. calc. for  $C_{18}H_{18}N_2O_2Br_2$  (FW: 451.97): C, 47.60; H, 3.99; N, 6.17; Found: C, 48.13; H, 4.05; N, 5.87. Selected IR data (KBr,  $\nu/\text{cm}^{-1}$ ): 1620  $\nu(\text{C=N})$ , 3434  $\nu(\text{-OH})$ , 1500–1400, 1100–1050 and 900–700  $\nu$  (aromatic rings), 1098  $\nu(\text{C-O})$ . UV-Vis: [ $\lambda_{\text{max}}$  (nm) (255)  $\pi \rightarrow \pi^*$  (aromatic), (351)  $n \rightarrow \pi^*(\text{C=N})$ . <sup>1</sup>H-NMR data (δ, ppm; CDCl<sub>3</sub>): 13.55 (bs, 2H, -OH), 8.30 (s, 2H, H-C=N), 7.31-7.41 (m, 2H, H<sub>arom</sub>), 6.91 (d, 2H, H<sub>arom</sub>), 3.68 (t, 4H, =N-CH<sub>2</sub>-C-), 1.83 (q, 2H, =N-C-CH<sub>2</sub>). <sup>13</sup>C-NMR data (δ, ppm; CDCl<sub>3</sub>): 163.28

(-CH=N), 160.29 (-CH-OH), 134.88, 133.39, 120.19, 119.14 (-C=C-), 110.0 (-CH-Br), 59.22, 27.47 (-CH<sub>2</sub>-CH<sub>2</sub>-), ESI-MS (m/z): 451(L)<sup>+</sup>, 453 (L+2)<sup>+</sup>.

**Figure 2.1**: Structure and formation of Schiff base Ligand: N, N-Bis(5-bromo-2-salicylidene) butane 1,4-diamine

### Synthesis of Schiff base metal complexes (1–3)

To create the required metal complexes, Cu(II), Zn(II), and Pd(II) chlorides were used. To each solution of metal salt in ethanol (5mmol, 15 mL) in a separate round bottom flask, an equimolar Schiff base ligand solution was added and immediate precipitation occurred. The refluxing in ethanol (30mL) was continued further for 45 minutes for complete precipitation. After filtering off the precipitated Schiff base metal (II) complexes, they were repeatedly cleaned twice with 20 mL of ethanol before being dried over anhydrous CaCl<sub>2</sub>.

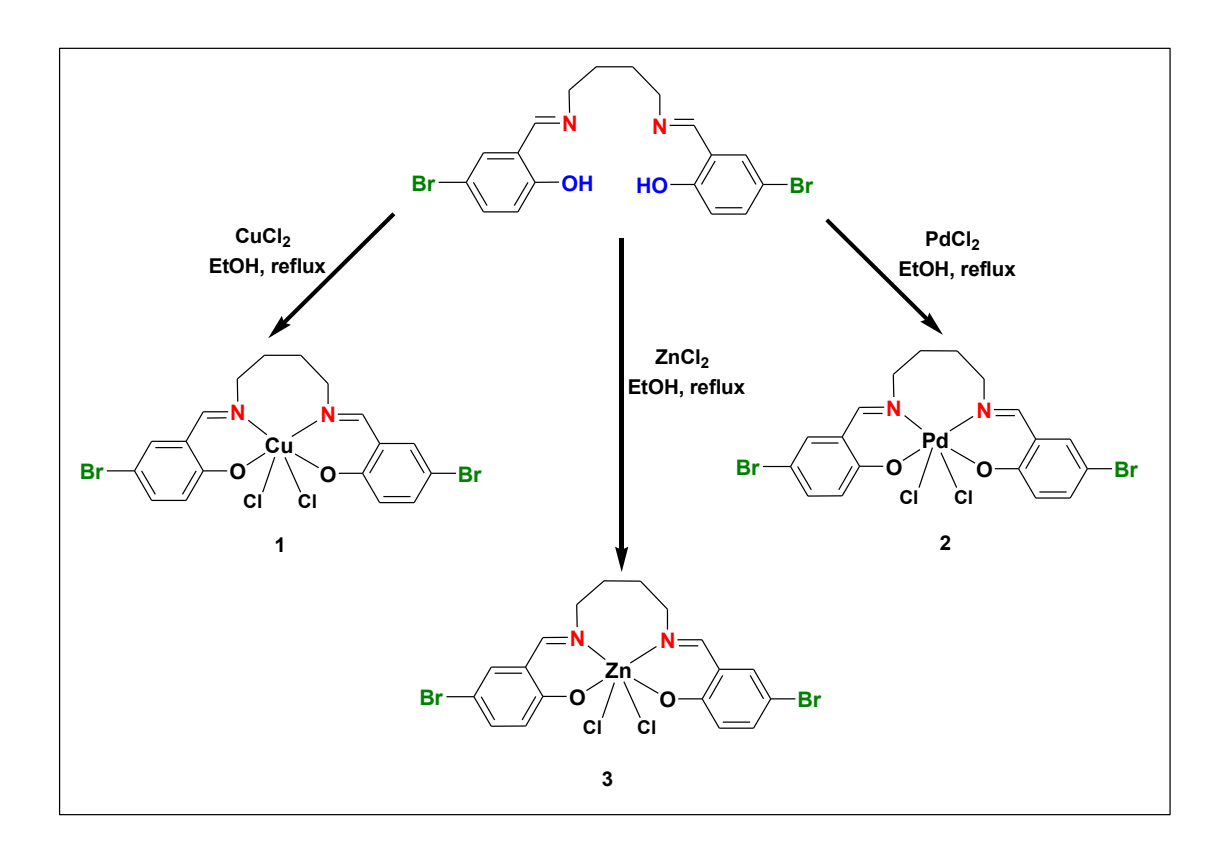


**Figure 2.2.** General synthetic route for probable structures of metal complexes of Schiff base (1–3).

*Synthesis of complex 1 [CuL(Cl)<sub>2</sub>].* Yield: 72%; Colour: Dark green; Melting point: 270 °C Anal. calc. for C<sub>18</sub>H<sub>16</sub>N<sub>2</sub>O<sub>2</sub>Br<sub>2</sub>Cl<sub>2</sub>Cu (FW: 584.82): C, 26.84; H, 2.74; N, 4.78; Found: C, 26.52; H, 2.83; N, 4.68. Selected IR data (KBr,  $\upsilon$ /cm<sup>-1</sup>): 1598  $\upsilon$ (C=N), 1113  $\upsilon$  (C–O), 545  $\upsilon$ (Cu–O),460  $\upsilon$ (Cu–N); UV-Vis: [ $\lambda$ <sub>max</sub> (nm) (265)  $\pi$ → $\pi$ \* (aromatic), (398) n→ $\pi$ \*(C=N); EPR at 298 K:  $g_{\parallel} = 2.19$ ,  $g_{\perp} = 2.01$ ; ESI-MS (m/z): 586.32 [Cu(L)(Cl)<sub>2</sub>]<sup>+</sup>.

Synthesis of complex 2 [ZnL(Cl)<sub>2</sub>]. Yield: 70%; Colour: Pale white; Melting point: 252 °C Anal. calc. for C<sub>18</sub>H<sub>16</sub>N<sub>2</sub>O<sub>2</sub>Br<sub>2</sub>Cl<sub>2</sub>Zn (FW: 588.43): C, 36.74; H, 2.74; N, 4.76; Found: C, 36.63; H, 2.86; N, 4.64. Selected IR data (KBr,  $\upsilon$ /cm<sup>-1</sup>): 1597  $\upsilon$ (C=N), 1105  $\upsilon$  (C-O), 537  $\upsilon$ (Zn-O), 465  $\upsilon$ (Zn-N); UV-Vis: [ $\lambda$ <sub>max</sub> (nm) (245)  $\pi$ → $\pi$ \* (aromatic), (355) n→ $\pi$ \*(C=N); <sup>1</sup>H-NMR data (δ, ppm; DMSO): 8.53 (s, 2H, H-C=N), 7.65-7.66 (d, 2H, H<sub>arom</sub>), 7.44-7.47 (m, 2H, H<sub>arom</sub>), 6.83-6.85 (d, 2H, H<sub>arom</sub>), 3.65 (t, 4H, =N-CH<sub>2</sub>-C-), 1.82 (q, 2H, =N-C-CH<sub>2</sub>).

Synthesis of complex 3 [PdL(Cl)<sub>2</sub>]. Yield: 70%; Colour: Light green; Melting point: 240 °C Anal. calc. for C<sub>18</sub>H<sub>16</sub>N<sub>2</sub>O<sub>2</sub>Br<sub>2</sub>Cl<sub>2</sub>Pd (FW: 629.16): C, 34.35; H, 2.56; N, 4.45; Found: C, 34.28; H, 2.68; N, 4.39. Selected IR data (KBr,  $\nu$ /cm<sup>-1</sup>): 1595  $\nu$ (C=N), 1102  $\nu$  (C-O), 529  $\nu$ (Pd-O),463  $\nu$ (Pd-N); UV-Vis: [ $\lambda$ <sub>max</sub> (nm) (268)  $\pi$ → $\pi$ \* (aromatic), (438) n→ $\pi$ \*(C=N); <sup>1</sup>H-NMR data (δ, ppm; DMSO): 8.56 (s, 2H, H-C=N), 7.67-7.68 (d, 2H, H<sub>arom</sub>), 7.45-7.48 (m, 2H, H<sub>arom</sub>), 6.84-6.86 (d, 2H, H<sub>arom</sub>), 3.64 (t, 4H, =N-CH<sub>2</sub>-C-), 1.79 (q, 2H, =N-C-CH<sub>2</sub>).

### 2.1.2 Description of Schiff base metal complexes (1-3) and Schiff base ligands (L).

Schiff-based ligand (L) of the salen type and novel Cu (II), Zn (II), and Pd (II) complexes of the form [M(L)(Cl)2](1-3) were synthesized in high yield and well characterized using various spectroscopic techniques. It was discovered that every synthetic chemical was soluble in DMF and DMSO and air stable at room temperature.

#### **FTIR**

To investigate the coordination of metal complexes with ligands, the FTIR spectra of the produced ligand (L) and their corresponding metal(II) complexes (1-3) were analyzed(Fig. 2.3). Due to the presence of comparable functional groups, the spectra of the three metal complexes of Cu(II), Zn(II), Pd(II), and the Schiff base showed very identical peaks. The azomethine (C=N) group in the Schiff base causes a distinctively strong band to appear at 1620 cm<sup>-1</sup>. In the produced Schiff base complexes, this band moved to 1598 cm<sup>-1</sup>, suggesting that the azomethine nitrogen and metal ion are coordinated [5]. A wide band at 3434 cm<sup>-1</sup> caused by the ligand's phenolic OH group vanished in the synthesized Schiff-based metal complexes, signifying the participation of the oxygen atom of –OH group in coordination to metal ions [6]. Furthermore, the existence of aromatic rings was confirmed by the characteristic vibrations at 1500-1400, 1100-1050, and 900-700 cm<sup>-1</sup> [7]. The phenolic OH group's oxygen atom's coordination with the metal ion is further proved by the shift in (C–O) band of ligand at 1098 cm<sup>-1</sup> to downfield at 1105 cm<sup>-1</sup> in the metal complexes. The participation of the oxygen atom of phenolic and the nitrogen

atom of the azomethine in complexation are confirmed by the development of two non-ligand peaks in the spectra of complex at 530 cm<sup>-1</sup> and 465 cm<sup>-1</sup> due to (M–O) and (M–N), correspondingly [8].

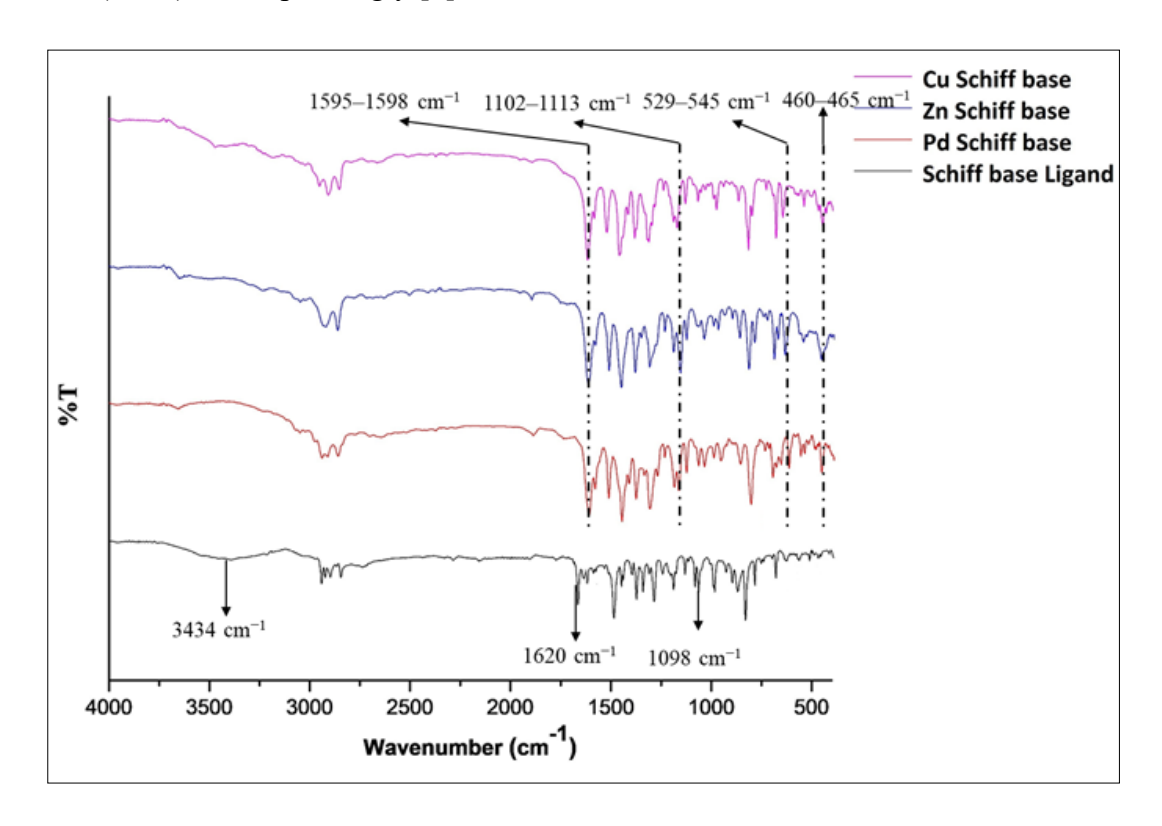


Figure. 2.3 FT-IR spectra of Cu(II), Zn(II), and Pd(II) ligand and metal complexes.

#### UV-Vis

Figure 2.4 displays the UV-vis absorption spectra measured in water for the Schiff base ligand (L) and its matching metal (II) complexes (1-3). In the Schiff base ligand's UV spectrum, the band at 255 nm attributes to the presence of  $\pi \rightarrow \pi^*$  transitions of aromatic region and the absorption bands at the 351 nm corresponds to the  $\pi \rightarrow \pi^*$  transition of the C=N group. These absorption bands were shifted for the metal coordinated complexes 1, 2 and 3 at 265, 245 and 268 nm, respectively, attributing to the presence of intraligand charge transfer ( $\pi \rightarrow \pi^*$ ) transitions and 398, 355, and 438 nm, respectively, corresponding to the interligand charge-transfer with partial contribution from ligand to metal ion of complexes ( $\pi \rightarrow \pi^*$ ) transitions. The ligand's coordination with the relevant metal ions is further supported by these shifts in the absorption bands [9–11].

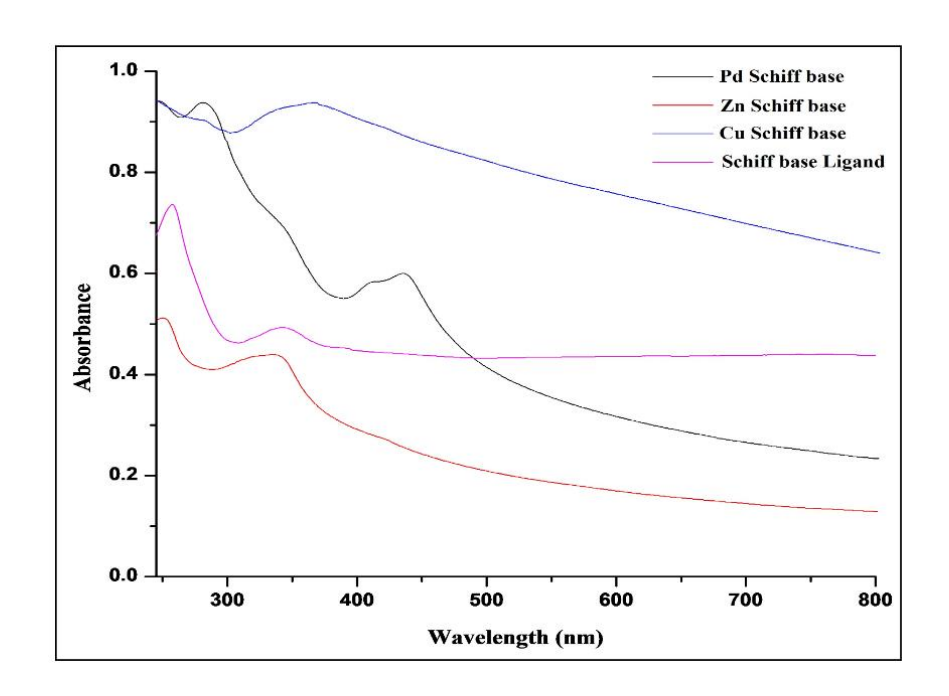


Figure. 2.4 UV-Vis spectra of ligand (L) and metal(II) complexes (1–3).

#### XRD

Attempts to obtain single crystals for the metal complexes were unsuccessful, hence, the X-ray diffraction studies of the produced compounds were inspected (**Figure. 2.5**). A comparison of the XRD patterns of the complexes revealed that the Cu(II) complex (1) shown sharper peaks, indicating the crystalline nature of the complex, while the Zn(II) complex (2) exhibited comparatively fewer sharper peaks than Cu(II) complex indicating comparatively less crystalline nature of the 2. However, the Pd(II) complex (3) shows line broadening of the peaks observed in XRD spectra, confirming the lower crystallinity of the Pd(II) complex in comparison to Zn(II) and Cu(II) metal complexes [12]. Of the metal (II) complexes that were produced, the complex 1 exhibits the most crystalline nature, while the complex 3 exhibits the least crystalline nature.

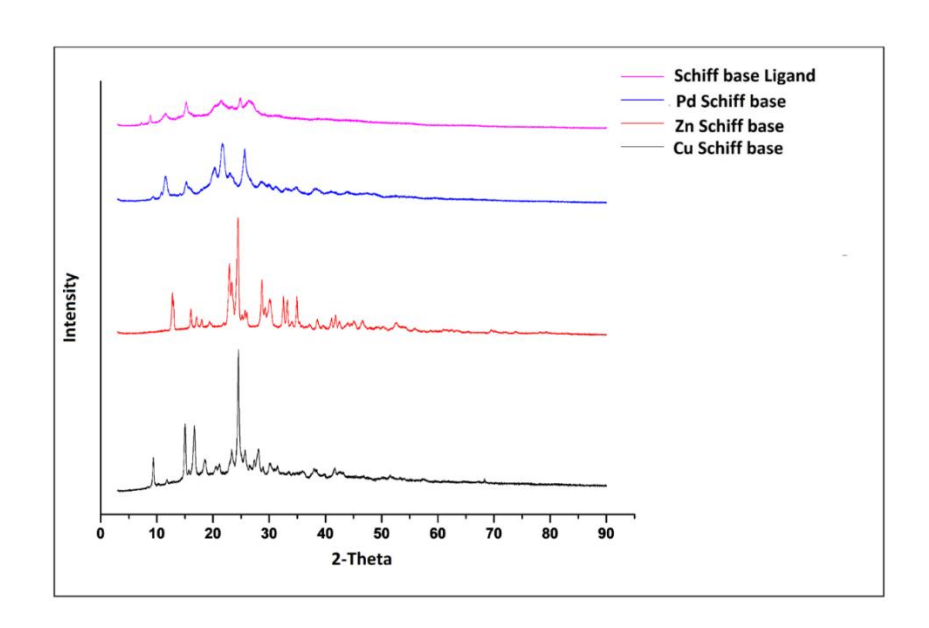


Figure.2.5 XRD spectra of the ligand and Cu(II), Zn(II), Pd(II) metal complexes

### <sup>1</sup>H NMR spectra

The <sup>1</sup>H NMR for the ligand recorded in CDCl<sub>3</sub> displays a broad singlet at 13.55 ppm owing to the 2H protons of -OH groups. Further a sharp signal at 8.30 ppm ascribed to the 2H protons of H-C=N groups. Furthermore, signals in the range of 7.31-6.91 ppm could be due to the aromatic protons of the two phenyl rings and sharp quartets at 1.83 and 3.68 ppm may be assigned to the methylene protons of N-C-CH<sub>2</sub> groups present in the Schiff base (Figure 2.6). The formation of Schiff base metal complexes of Zn(II) and Pd (II) were also confirmed by NMR spectra. Figure 2.7 and 2.8 represents the <sup>1</sup>H spectra of Zn (II) and Pd (II) complexes. Because of the azomethine proton (-CH=N-), the synthesized Schiff base ligand displayed a singlet at 8.30 ppm [13]. But for the Zn(II) and Pd(II) metal complexes, the corresponding –CH=N– peak moved to 8.53 and 8.56 ppm, respectively, suggesting that azomethine nitrogen was coordinated during complexation. The deshielding action brought on by the coordination of azomethine nitrogen with the central metal ion is likewise shown by the downfield shift [14]. Further, in both these complexes, the peak due to hydroxyl (-OH) proton disappears, indicating the deprotonation of -OH group during complexation [9].

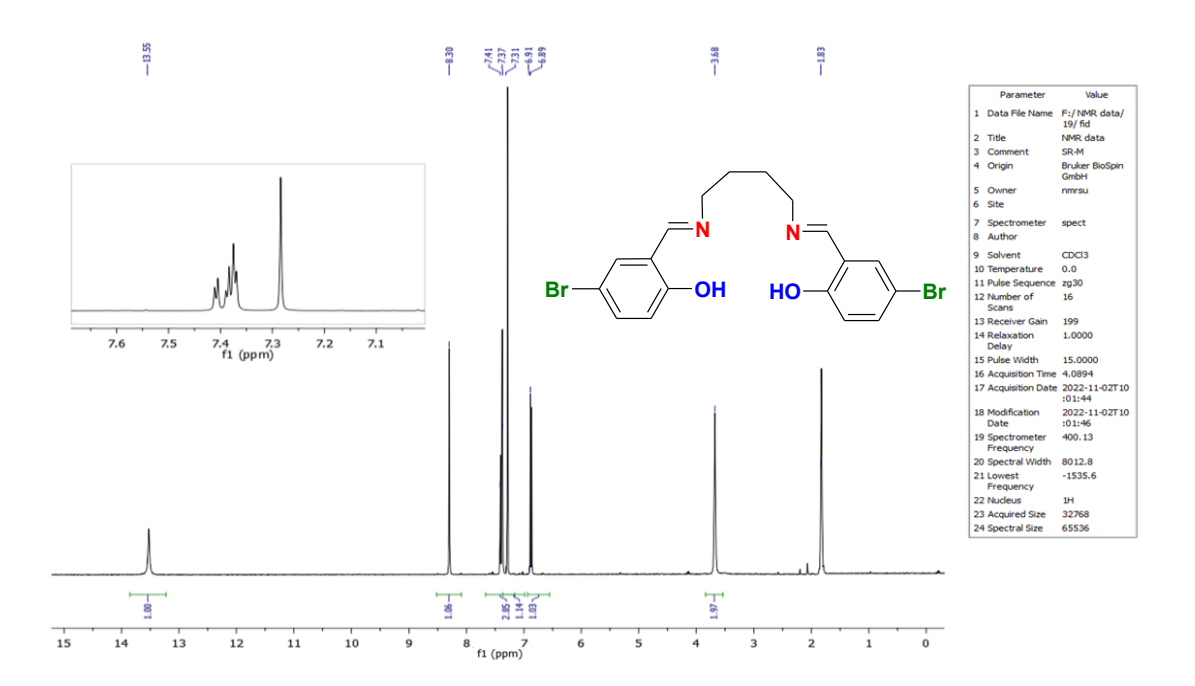


Figure 2.6. <sup>1</sup>H NMR spectra of the ligand (L).

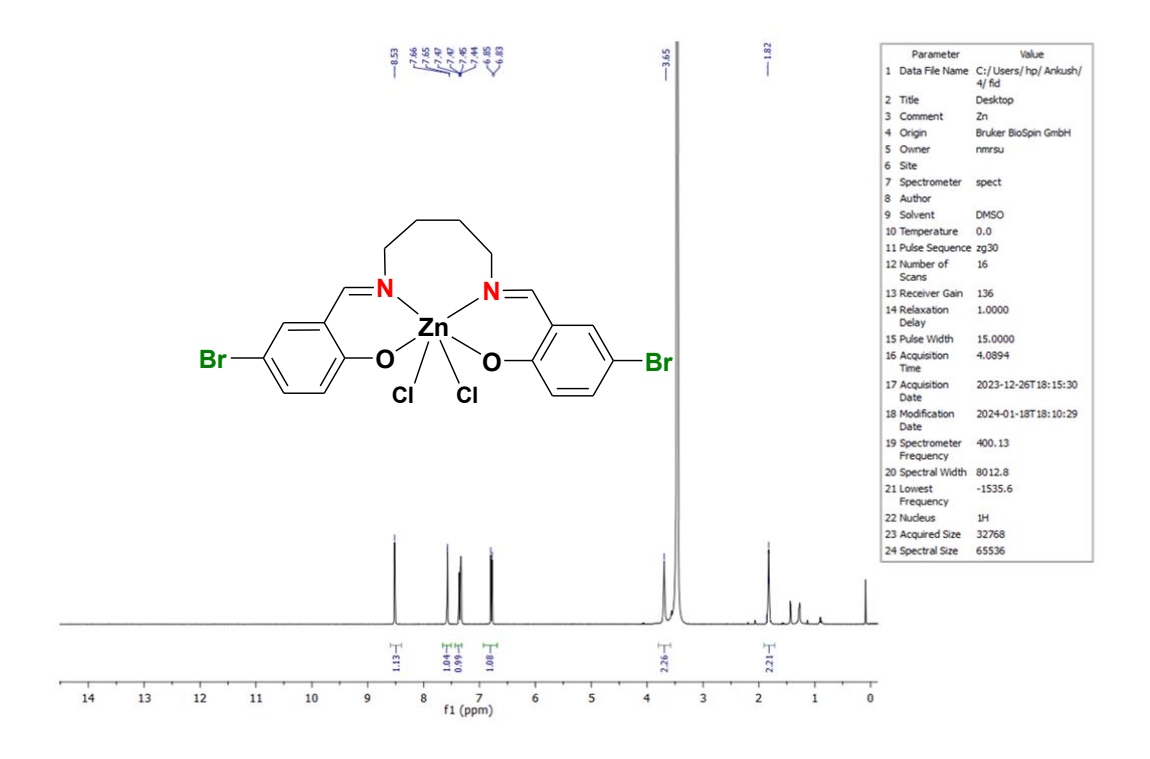


Figure 2.7. <sup>1</sup>H NMR spectra Zn(II) Schiff base complex

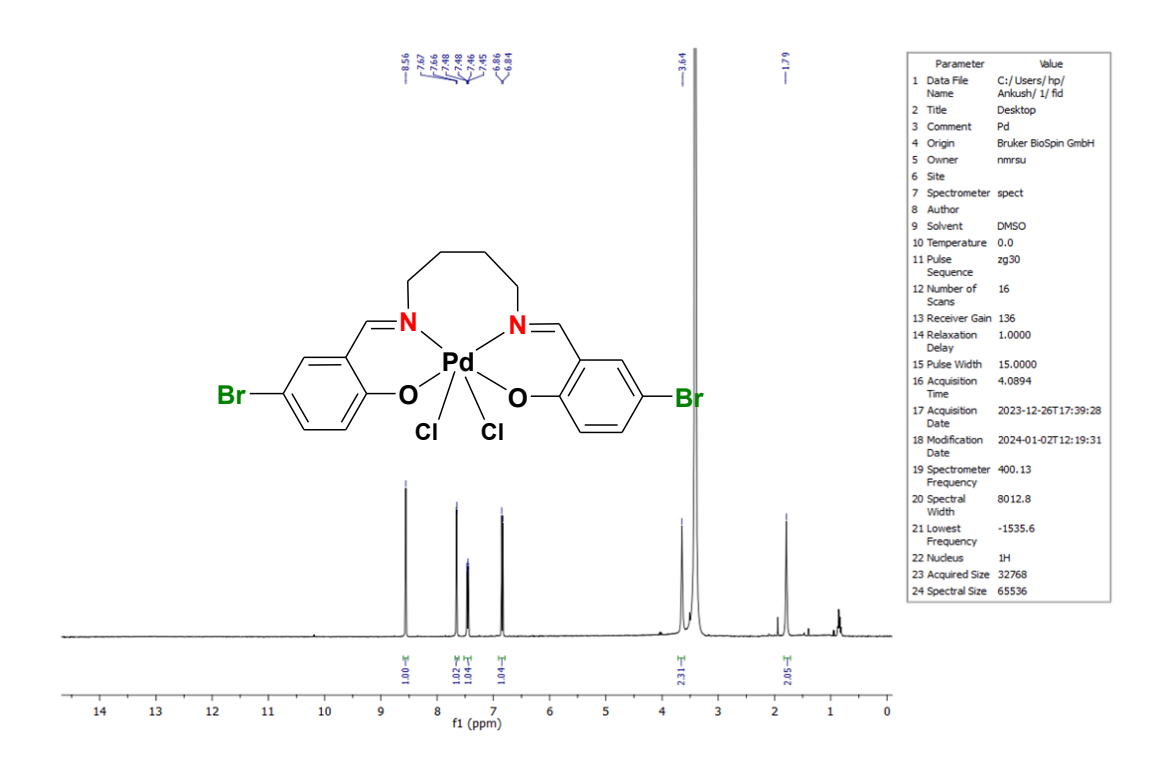


Figure 2.8 <sup>1</sup>H NMR spectra Pd(II) Schiff base complex

### ESI Mass Spectra

The structure of synthesized compounds was further authenticated by analyzing ESI mass spectroscopy (**Figure. 2.9 a-d**). Synthetic ligand (**L**) and Metal(II) complexes 1, 2, and 3 showed molecular ion peaks at m/z 451.95 (M)+, 453.95 (M+2)+, 586.32, 588.43, and 629.16 in their mass spectra consistent with the proposed molecular formulae (L)<sup>+</sup>, (L+H)<sup>+</sup>, [Cu(L)]<sup>+</sup>, [Zn(L)]<sup>+</sup> and [Pd(L)]<sup>+</sup> respectively, and confirmed the stoichiometric composition and formation of the complexes. In addition, the mass fragmentation pattern of the complex **1** was analysed (**Figure 2.10**), which exhibits peaks at m/z 514.63, 451.93 and 357.78 corresponding to [C<sub>18</sub>H<sub>16</sub>Br<sub>2</sub>N<sub>2</sub>O<sub>2</sub>Cu] <sup>+</sup>, [C<sub>18</sub>H<sub>16</sub>Br<sub>2</sub>N<sub>2</sub>O<sub>2</sub>] <sup>+</sup> and [C<sub>18</sub>H<sub>16</sub>N<sub>2</sub>O<sub>2</sub>Cu] <sup>+</sup> fragments, respectively. The other appeared light peaks are attributed to the fragments of different species due to the rupture of bonds inside the molecule. Thus, the results of the ESI mass spectra of the compounds confirmed the proposed chemical formulas of the compounds.

#### **EPR**

The Cu(II) complex's EPR spectrum offers details on the metal ion's surroundings based on hyperfine and super hyperfine structures within the complex (Figure 2.11). Additionally, it provides information with respect to the geometry and characteristics of the ligating sites of both the ligand and the central metal ion. The Cu(II) complex's X-band EPR spectra was captured at ambient temperature in its polycrystalline state using a field set of 3000 G and a frequency of 9.1 GHz. The ground state is determined using the spin Hamiltonian parameters for the Cu(II) complex. In octahedral geometry, the unpaired electron is located in the dz<sup>2</sup> orbital with the gtensor parameter g<sub>1</sub>>g<sub>1</sub>>2.0023, and in the ground state, the unpaired electron is located in the  $d_{x^2-v^2}$  orbital with  $g_{\parallel} > g_{\perp} > 2.0023$  [15]. Cu(II) possesses a  $d_{x^2-v^2}$ ground state indicative of octahedral geometry, and the synthesized complex 1 is axially symmetric, as shown by the measured order of the g-tensor, which was determined to be  $g_{\parallel} > (2.19) > g_{\perp} (2.08) > 2.0$  [16]. The g|| value is a crucial function that indicates the character of the metal-ligand bond; for ionic character, it is greater than 2.3, and for covalent character, it is less than 2.3 [17]. The Cu(II) complex's g<sub>||</sub> value in this investigation is less than 2.3, suggesting a notable covalent nature for the metal-ligand bond. Using g-tensor values, the geometric parameter (G), which measures the magnitude of exchange interactions, is computed using the formula G =  $g_{\parallel}\!\!-\!2.0023/g_{\perp}\!\!-\!2.0023.$  Hathaway and Billing state that an exchange contact between the copper centers is insignificant if the G value is more than 4, but noticeable if it is less than 4 [18]. The Cu(II) complex's computed G value of 5.27 shows that exchange coupling effects are not present in current complexes.

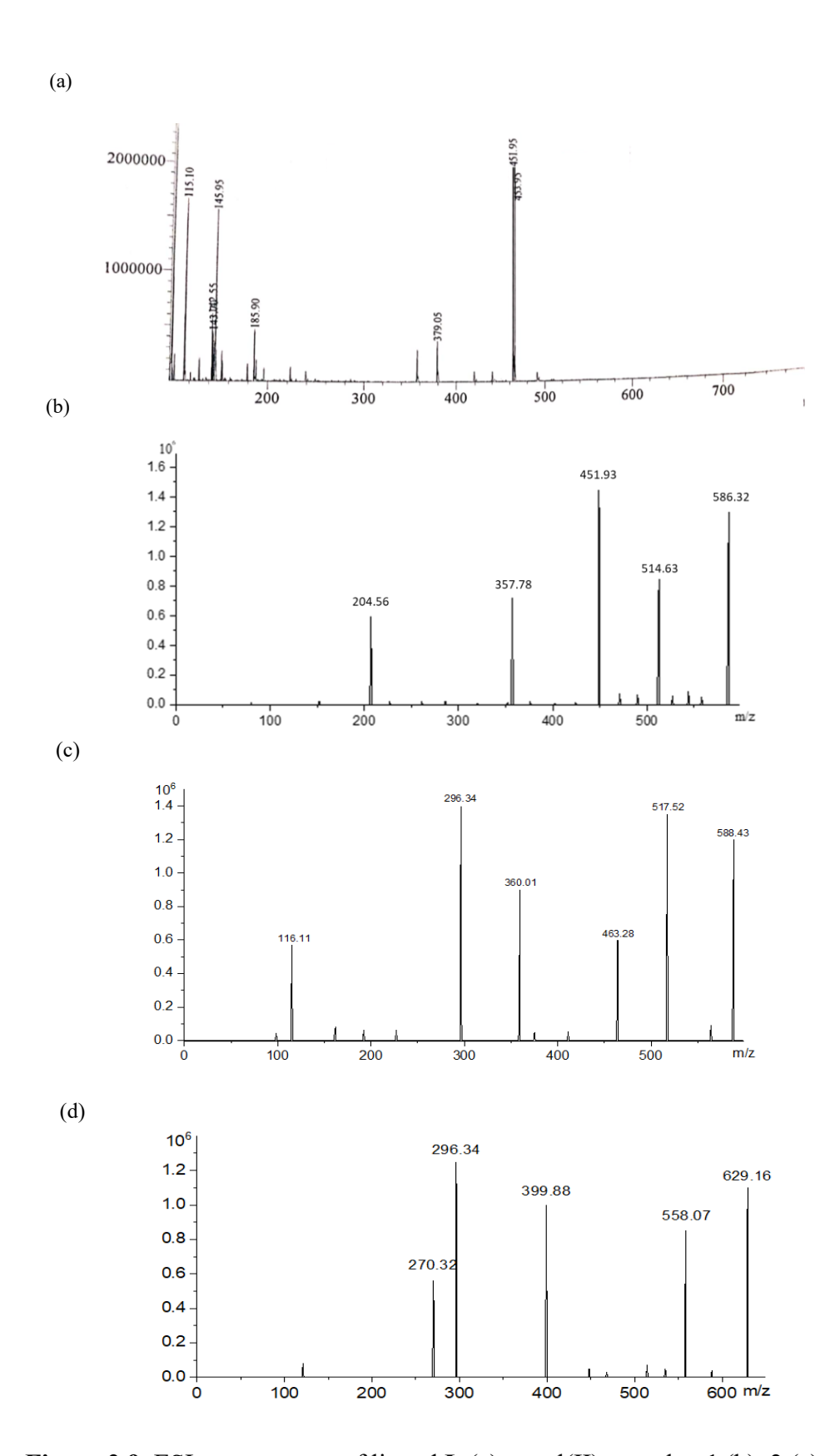


Figure 2.9. ESI mass spectra of ligand L (a) metal(II) complex 1 (b), 2 (c) and 3 (d).

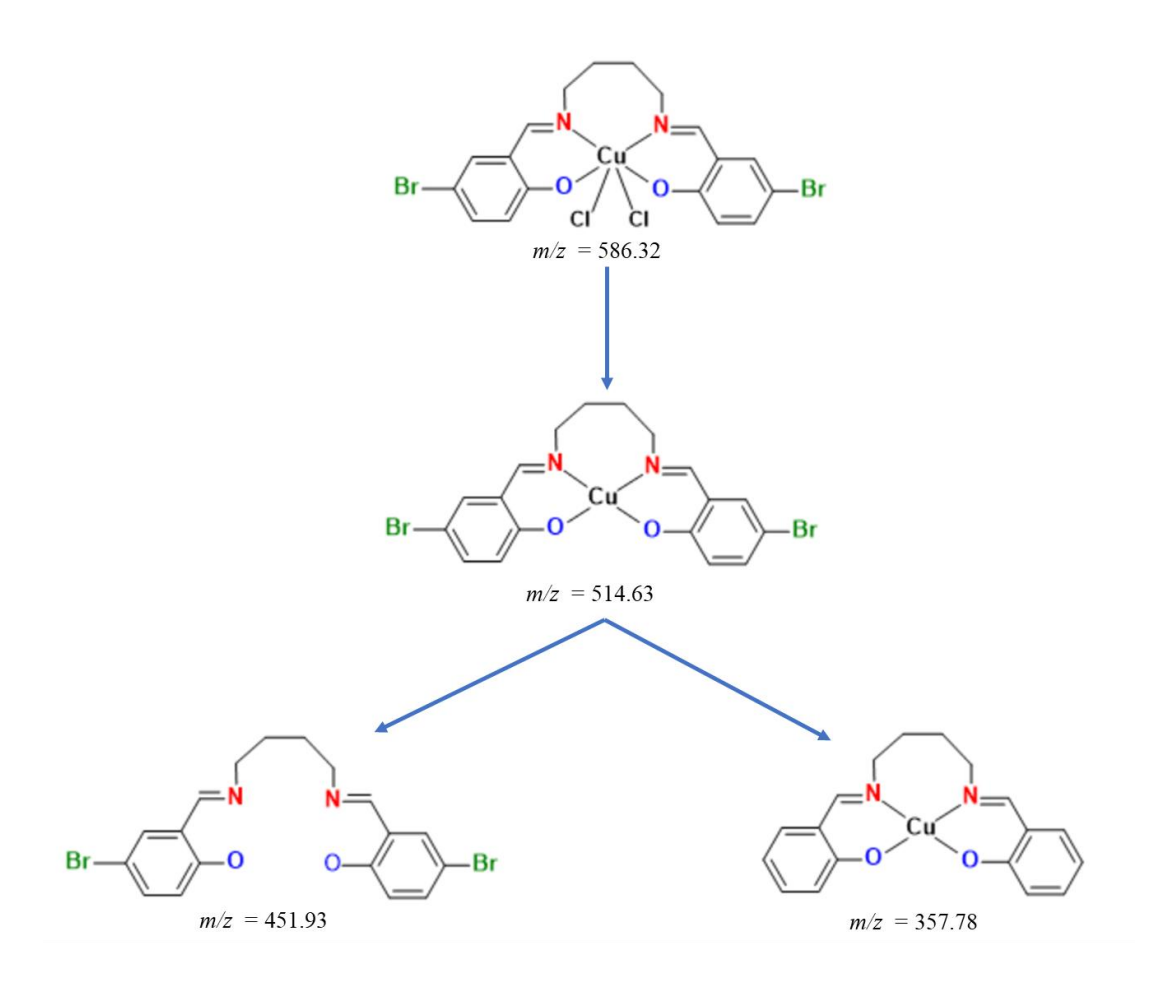


Figure 2.10 Mass fragmentation pattern of copper (II) complex (1).

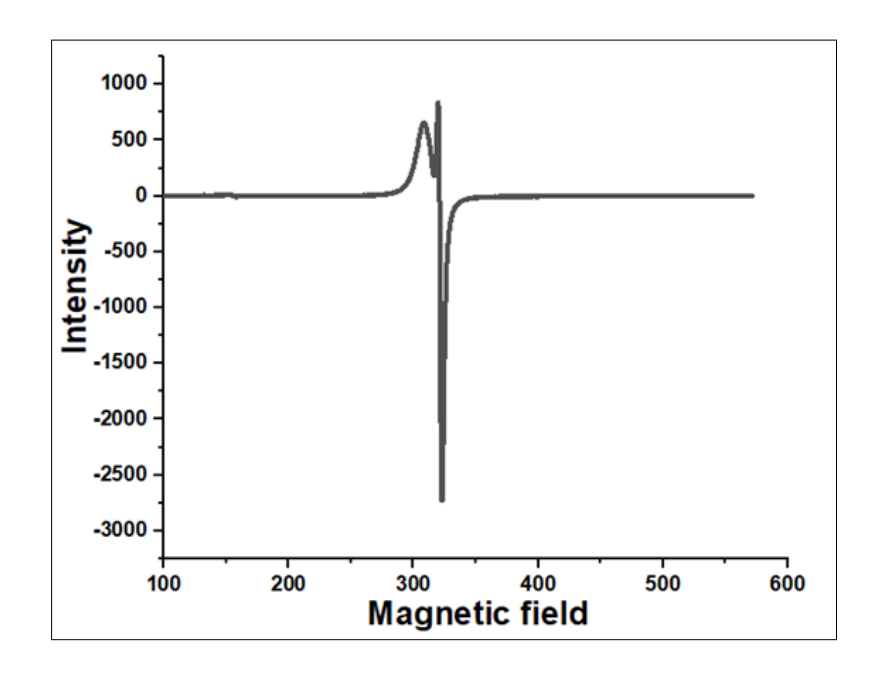


Figure. 2.11 EPR spectra of copper(II) complex 1 in solid phase at room temperature.

#### 2.1.3 References

- 1. Cordes, E. H. and Jencks, W.P., 1962. On the mechanism of Schiff base formation and hydrolysis. *Journal of the American Chemical Society*, 84(5), pp.832-837.
- Abd-El-Aziz, A., Li, Z., Zhang, X., Elnagdy, S., Mansour, M.S., ElSherif, A., Ma, N. and Abd-El-Aziz, A.S., 2025. Advances in Coordination Chemistry of Schiff Base Complexes: A Journey from Nanoarchitectonic Design to Biomedical Applications. *Topics in Current Chemistry*, 383(1), pp.1-102.
- 3. Kurpik, G., Walczak, A., Gołdyn, M., Harrowfield, J. and Stefankiewicz, A.R., 2022. Pd (II) complexes with pyridine ligands: substituent effects on the NMR data, crystal structures, and catalytic activity. *Inorganic Chemistry*, 61(35), pp.14019-14029.
- 4. Manne, R., Kumaradoss, M.M.R.M., Iska, R.S.R., Devarajan, A. and Mekala, N., 2022. Water quality and risk assessment of copper content in drinking water stored in copper container. *Applied Water Science*, *12*(3), p.27.
- 5. Moreno-Narváez, M.E., Arenaza-Corona, A., Lucero, G.S., Ramírez-Apan, M.T.O., Ortega, S.H., Cruz-Navarro, J.A., Alí-Torres, J., Orjuela, A.L., Reyes-Marquez, V., Lomas-Romero, L. and Morales-Morales, D., 2025. Glycoconjugate Pd (II) and Cu (II) complexes of fluorinated N, O Schiff base ligands for targeted cancer therapy: Synthesis, Characterization and In vitro Cytotoxic Activity Evaluation. New Journal of Chemistry.
- 6. Cui, Y., Dong, X., Li, Y., Li, Z. and Chen, W., 2012. Synthesis, structures and urease inhibition studies of Schiff base metal complexes derived from 3, 5-dibromosalicylaldehyde. *European journal of medicinal chemistry*, 58, pp.323-331.
- 7. Yıldız, M., Karpuz, Ö., Zeyrek, C.T., Boyacıoğlu, B., Dal, H., Demir, N., Yıldırım, N. and Ünver, H., 2015. Synthesis, biological activity, DNA binding and anion sensors, molecular structure and quantum chemical studies of a

- novel bidentate Schiff base derived from 3, 5-bis (triflouromethyl) aniline and salicylaldehyde. *Journal of Molecular Structure*, *1094*, pp.148-160.
- 8. Asadi, M., Sepehrpour, H. and Mohammadi, K., 2011. Tetradentate Schiff base ligands of 3, 4-diaminobenzophenone: Synthesis, characterization and thermodynamics of complex formation with Ni (II), Cu (II) and Zn (II) metal ions. *Journal of the Serbian Chemical Society*, 76(1), pp.63-74.
- 9. Sarkar, U., 2014. Emissive bis-salicylaldiminato Schiff baseligands and their zinc (II) complexes: Synthesis, photophysical properties, mesomorphism and DFT studies.
- 10. Mallikarjuna, K., Raju, B.D.P., Park, S. and Kim, H., 2017. Synthesis and catalytic activity of alkylamine-capped ultra-small palladium nanoparticles for organic pollutant degradation. *Journal of Cluster Science*, 28, pp.2833-2846.
- 11. Gopichand, K., Mahipal, V., Rao, N.N., Ganai, A.M. and Rao, P.V., 2023. Co (II), Ni (II), Cu (II), and Zn (II) complexes with Benzothiazole Schiff base ligand: Preparation, Spectral Characterization, DNA Binding, and In Vitro Cytotoxic Activities. *Results in Chemistry*, 5, p.100868.
- 12. Vlasenko, V.G., Burlov, A.S., Milutka, M.S., Koshchienko, Y.V., Uraev, A.I., Lazarenko, V.A., Makarova, N.I., Metelitsa, A.V., Zubenko, A.A. and Garnovskii, D.A., 2023. Cu (II), Ni (II), Co (II), Zn (II), and Pd (II) Complexes with (4 Z)-4-[(2-Furylmethylamino) methylene]-5-methyl-2-phenylpyrazol-3-one: Synthesis, Structures, and Properties. *Russian Journal of Coordination Chemistry*, 49(3), pp.148-157.
- 13. Neelakantan, M.A., Rusalraj, F., Dharmaraja, J., Johnsonraja, S., Jeyakumar, T. and Pillai, M.S., 2008. Spectral characterization, cyclic voltammetry, morphology, biological activities and DNA cleaving studies of amino acid Schiff base metal (II) complexes. *Spectrochimica Acta Part A: Molecular and Biomolecular Spectroscopy*, 71(4), pp.1599-1609.

- 14. Singh, A.K., Pandey, O.P. and Sengupta, S.K., 2012. Synthesis, spectral characterization and biological activity of zinc (II) complexes with 3-substituted phenyl-4-amino-5-hydrazino-1, 2, 4-triazole Schiff bases. *Spectrochimica Acta Part A: Molecular and Biomolecular Spectroscopy*, 85(1), pp.1-6.
- 15. Balasubramanian, S. and Krishnan, C.N., 1986. Synthesis and characterization of five-coordinate macrocyclic complexes of nickel (II) and copper (II). *Polyhedron*, *5*(3), pp.669-675.
- 16. Thaker, B.T., Tandel, P.K., Patel, A.S., Vyas, C.J., Jesani, M.S. and Patel, D.M., 2005. Synthesis and mesomorphic characterization of Cu (II), Ni (II) and Pd (II) complexes with azomethine and chalcone as bridging group.
- 17. Kilveson, D., 1997. Publications of danielkivelson. *Journal of Physical Chemistry B*, 101(43), pp.8631-8634.
- 18. Hathaway, B. and Billing, D.E., 1970. The electronic properties and stereochemistry of mono-nuclear complexes of the copper (II) ion. *Coordination Chemistry Reviews*, 5(2), pp.143-207.

# Section 2.2 *In vitro* Anti-microbial and DNA-binding studies of Cu(II), Zn(II), and Pd(II) Complexes of Schiff base

The Schiff base ligands and their metal complexes have been reported to display various biomedical applications such as anticancer [1], antiviral [2], antibacterial [3-5], antitumor [6], anti-malarial [7], antifungal [8-11], anti-inflammatory [12-13], anticonvulsant [14], anti-depressant, anti-glycation and lipid minimizing activities depending upon the type of metal and ligand used in metal complex formation. Since ancient times copper vessels have been used for storing water, even before their antimicrobial properties were realized by modern science [15]. The touch surfaces of copper-alloy have natural properties that destroy wide range of microorganisms (e.g., E. coli O157:H7), methicillin-resistant Staphylococcus (MRSA), Staphylococcus, Clostridiumdifficile, influenza Α aureus virus, adenovirus, SARS-CoV-2, and fungi) [20]. Zinc supplements in the form of zinc acetate or zinc gluconate lozenges are commonly used for the treatment of the common cold. Recently Schiff complexes of Zn (II) have shown effective anticancer activities as it induced a very similar genotoxic effect as cis-platin and have a very low IC<sub>50</sub> value [16]. Palladium complexes have revealed excellent biological activities in addition to their popular use in catalysis [17]. Over and above, their fascinating coordination properties such as flexible redox chemistry and nonrigidity in the stereochemistry makes them suitable candidates for research in present era.

In the present work, the *in vitro* biological activities i.e., antibacterial, antifungal and DNA binding studies were assessed through well disc diffusion method, analytical and multi-spectroscopic techniques respectively.

#### 2.2.1 Results and Discussion

#### In vitro DNA binding activity

Majority of drugs exert their biological activities by targeting DNA by forming intercalative, electrostatic, and/or groove bonds [18]. To understand the preferential

binding modes of the synthesized metal(II) complexes (1–3) with *ct*-DNA, DNA binding interaction studies were performed using multispectroscopic techniques, including electronic spectroscopy titrations, fluorescence spectroscopy, ethidium bromide (EB) assay, circular dichroism (CD) studies and cyclic voltammetry [19].

Electronic spectroscopy titration studies were carried out by using Perkin Elmer Lambda 25 spectrophotometer and the spectra were recorded in DMSO, in the range of 200–1,100 nm. The stock solution of DNA was prepared by diluting the apposite volume of *ct*-DNA in the buffer solution (containing 5 mM tris–HCl, pH = 7.2, and 50 mM NaCl), stored at 4 °C, and was used by 1 week. The *ct*-DNA concentrations were determined by Beer's law using 6600 M<sup>-1</sup> cm<sup>-1</sup> molar extinction coefficient (ε). Additionally, a stock solution of the tested complexes was generated. Subsequently, the solution was diluted in a buffer solution. The resulting solution was utilized within a maximum time frame of 2 hours [20]. The spectra for the compounds were recorded by adding an equal amount of ct–DNA to both the complex solution and reference solution while performing the experiment. In addition, the magnitude of binding interaction between the synthesized ligand (L) and the metal(II) complexes (1–3) has been measured by calculating the values of binding constant and applying the following equation;

$$\frac{DNA}{(\varepsilon_a - \varepsilon_f)} = \frac{[DNA]}{(\varepsilon_b - \varepsilon_f)} + \frac{1}{K_b(\varepsilon_b - \varepsilon_f)} \dots \dots (Equation 1)$$

Where,

 $\varepsilon_a$  = apparent extinction coefficients (Aabs/[complex]).

 $\varepsilon_b$  = Bound complex extinction coefficients,

 $\varepsilon_f$ = Free complex extinction coefficients,

[DNA] = Conc. of ct-DNA and

 $K_b$ = Intrinsic binding constant value of the synthesized compounds, and was calculated from the ratio of the slope of  $1/(\varepsilon_b - \varepsilon_f)$  to the intercept 1/Kb  $(\varepsilon_b - \varepsilon_f)$  in a plot of [DNA]/ $(\varepsilon_a - \varepsilon_f)$  vs [DNA].

Emission intensity measurements were carried out using a Shimadzu RF–5301PC Spectrofluorophotometer in a 1 cm path–length quartz cell. The emission spectrum is obtained by setting the excitation monochromatic at the maximum excitation wavelength and scanning with the emission monochromatic. Often, an excitation spectrum is first made in order to confirm the identity of the substance and to select the optimum excitation wavelength. Further experiments were carried out to gain support for the binding manner of complexes with *ct*-DNA. Compounds that are not fluorescent or only exhibit faint fluorescence can often be reacted with strong fluorophores, enabling them to be determined quantitatively. On this basis molecular fluorophore EtBr was used, which emits fluorescence in the presence of *ct*-DNA due to its strong intercalation. Quenching of the fluorescence of EB bound to *ct*-DNA was measured with increasing amount of metal complexes as a second molecule, and the Stern–Volmer quenching constant K was attained from the following equation [21].

$$\frac{I_o}{I} = 1 + Kr$$
 (Equation 2)

Where r is the ratio of total concentration of complex to that of DNA and I<sub>o</sub> and I are the fluorescence strengths of EtBr in the absenteeism and existence of complex.

The CD spectra of the complexes with DNA were recorded keeping the molar ratio of 2:1 at the range between 200 and 250 nm, with the scan rate 20 nm min<sup>-1</sup> in the response time of 2 seconds to study the conformational and structural variations in *ct*-DNA secondary structure upon interface with the complexes (1–3). The observed CD spectra are reported in terms of mean residue ellipticity (MRE) value in deg cm<sup>2</sup> dmol<sup>-1</sup>, after subtracting the baseline from the measured spectra for buffer, using the following equation [22];

$$MRE = \left[\frac{Observed \ C_D \ (mdeg)}{C_D \ nl \times 10}\right] (Equation \ 3)$$

Where,

 $C_p$ = molar concentration of the protein,

n = number of amino acid residues (585), and

l =the path length (0.1 cm).

#### In vitro antimicrobial assay

To assess the antimicrobial activity of ligand and complexes, the well diffusion assay was employed. Synthesized ligand (L) and their metal (II) complexes (1–3) were evaluated for antimicrobial action using a range of known concentrations (0.0625, 0.125, 0.25, 0.5, 1, 2, 4, and 6 mg/mL) against *Escherichia coli* (MTCC 441), *Klebsiella pneumonia* (MTCC 741) and *Staphylococcus aureus* (MTCC 902) bacterial strains, and *Colletotrichum acutatum* and *Fusarium sp.* fungal strains whereas Penicillin G and Ciclopiroxolamine were employed as standard reference drugs for antibacterial and fungicidal actions, respectively [23].

#### 2.3.2 Electronic spectroscopy titration technique

One of the most effective experimental methods for examining the interactions between metal ions and DNA is the electronic spectroscopy titration technique. DNA binding with the metal complexes leads to changes in the electronic spectra by perturbing the ligand field transitions. The intercalative and electrostatic binding mode usually results in bathochromism and hypochromism, and hyper- or hypochromism, respectively [49]. When aliquots of ct-DNA (1–8  $\mu$ M) were added to the static concentration of synthesized ligand L (3  $\mu$ M) and metal(II) complexes (1–3) (5  $\mu$ M), the absorbance showed hyperchromism in the spectral bands with a small blue shift of 3–7 nm (**Figure 2.12**). Important confirmation of the electrostatic binding mode was given by the existence of the "hyperchromic effect" with no discernible wavelength change ( $\lambda_{max} = 265$  nm) [50]. Moreover, the creation of hydrogen bonds between the nitrogen and oxygen atoms of the ligand (L) and metal(II) complexes (1–3) with the nucleobases within DNA can improve the steadiness of the binding between the synthesized compounds and ct-DNA [24].

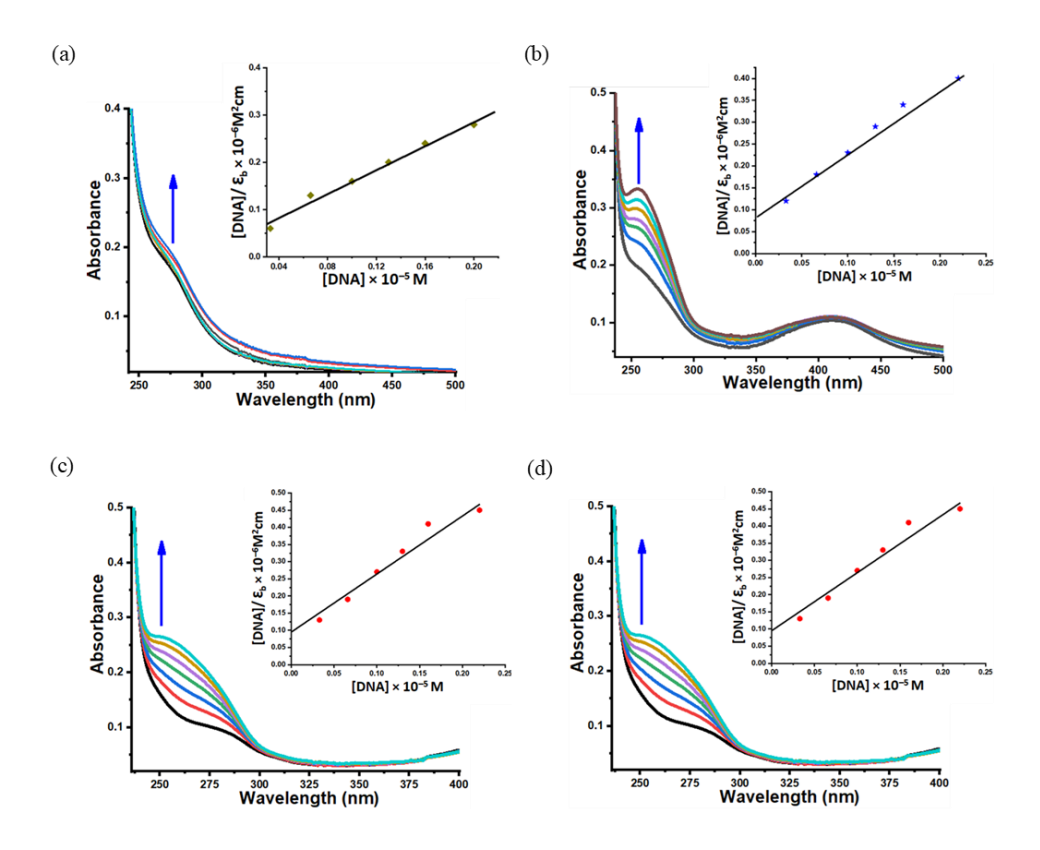


**Figure. 2.12.** Absorption titration curves of synthesized ligand **L** (a), and metal(II) complexes **1** (b), **2** (c) and **3** (d) at varied strength of *ct*-DNA. Inset: Plots of [*ct*-DNA]/ $\varepsilon_a$ - $\varepsilon_f$  (M<sup>2</sup> cm) vs [*ct*-DNA]. [*ct*-DNA] = 0.1–0.8 × 10<sup>-5</sup> M, [**L**] = [Complexes (1–3)] = 0.5 × 10<sup>-5</sup> M.

The binding constant values for synthesized ligand L and metal(II) complexes (1–3) were found to be 3.11 ( $\pm 0.02$ ) x  $10^4$  M<sup>-1</sup>, 8.21 ( $\pm 0.14$ ) x  $10^4$  M<sup>-1</sup>, 7.35 ( $\pm 0.21$ ) x  $10^4$  M<sup>-1</sup>, and 5.11 ( $\pm 0.19$ ) x  $10^4$  M<sup>-1</sup>, respectively, which provides evidence of robust affinity for binding of the complex 1 with the *ct*-DNA, followed by the complex 2 and 3, then and least affinity was shown by ligand L with the *ct*-DNA.

#### Emission spectroscopy

It was further used to illustrate the mode and extent of binding strength of metal complexes upon interaction with ct-DNA. In our recorded spectra, complexes (1–3) exhibit emission maxima at ~430 nm upon excitation by 265 nm wavelength. (**Figure. 2.13**). When ct-DNA (0.1–0.6 × 10<sup>-5</sup> M) was introduced to a fixed concentration of complexes (0.4 × 10<sup>-5</sup> M) in our investigations, a rise in luminescence was observed

without a significant change in emission maxima. The increased intensity observed in the presence of *ct*-DNA may be attributed to the greater nonpolar nature of metal complexes, which demonstrates the strong binding connection between metal(II) complexes and *ct*-DNA. [25]. Furthermore, the binding interaction between the synthesized complexes and *ct*-DNA is responsible for the progressive increase in fluorescence intensity [26].

In addition, the binding constant values evaluated for the tested complexes (1-3) were found to be 6.32 ( $\pm 0.11$ ) x  $10^4$  M<sup>-1</sup>, 5.21 ( $\pm 0.17$ ) x  $10^4$  M<sup>-1</sup>, and 1.78 ( $\pm 0.13$ ) x  $10^4$  M<sup>-1</sup>, correspondingly, demonstrating the intense binding affinity of complex 1 for ct-DNA, while the lowest binding affinity was found to be between the complex 3 and ct-DNA.

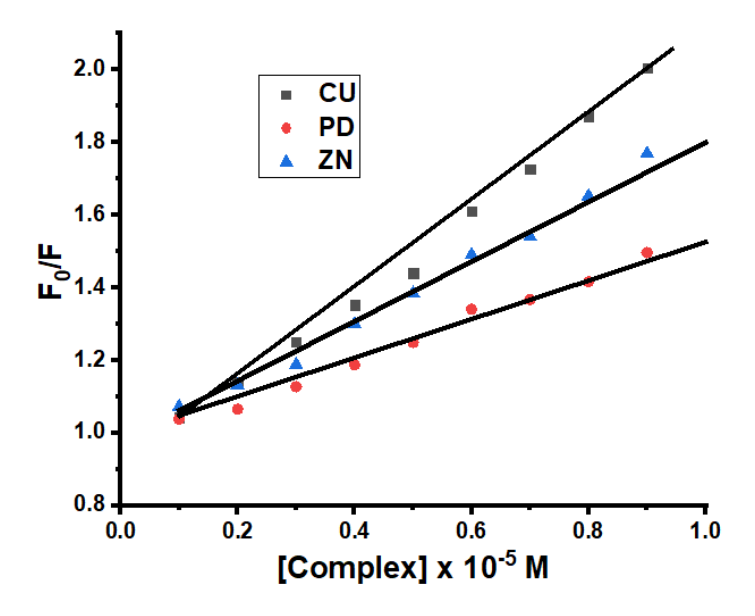
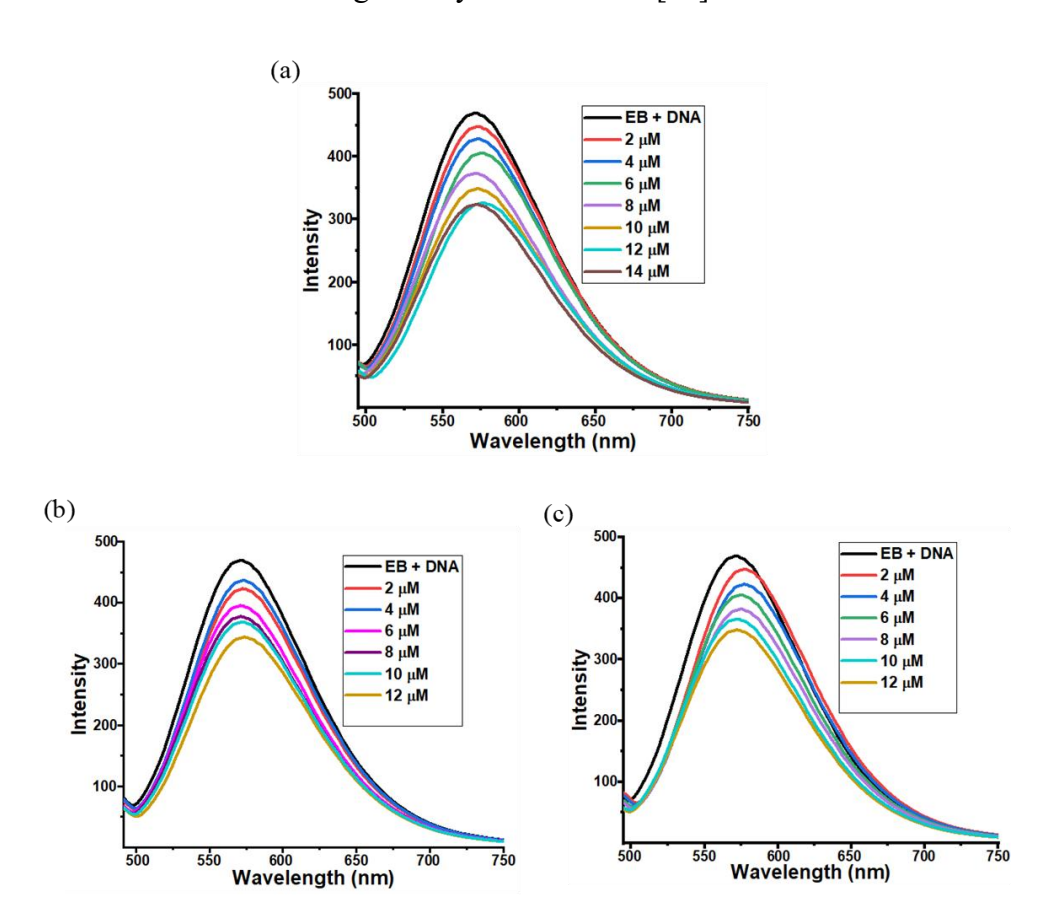


Figure 2.13 Emission spectra:Plots of 1/F– F0 versus 1/[Metal(II) complexes (1–2)], [DNA] =  $0.2 \times 10^{-5} \text{ M}$ , [complex 1] = [complex 2] = [complex 3]  $0.1-0.6 \times 10^{-5} \text{ M}$ .

#### Ethidium bromide assay (EB)

This is a highly sensitive fluorescent probe with a planar shape that binds to DNA through intercalation. The solution exhibits negligible fluorescence when introduced to EB. However, because complex is integrated between the base pairs of the *ct*-DNA, its presence enhances the fluorescence intensity of the complexes. In EB displacement assay, the fluorescence intensity of the EB-DNA system decreases when any molecule

that binds to DNA in the similar manner as EB replaces EB from the DNA helix [27]. The degree of quenching of fluorescence in the EB-DNA system may be employed to calculate the degree of intercalation between the studied complexes and the ct-DNA. The subsequent addition of aliquots of studied complexes exhibits a moderate quenching in the intensity of fluorescence, suggesting that the intercalative mode of binding interaction between synthesized complexes and ct-DNA has been ruled out (**Figure 2.14** and **2.15**). The observed  $K_{sv}$  values for the complexes **1**, **2** and **3** were 7.81 ( $\pm 0.021$ ) x  $10^4$ , 4.43 ( $\pm 0.18$ ) x  $10^4$  and 2.62 ( $\pm 0.32$ ) x  $10^4$  indicating that of complex **1** has the highest binding affinity with ct-DNA, while the complex **3** exhibited the least binding affinity with ct-DNA [28].



**Figure. 2.14.** Emission spectra of EB–DNA system recorded in Tris-HCl buffer at pH = 7.3 in presence of synthesized metal(II) complexes **1** (a), **2** (b) and **3** (c). [EB] =  $[DNA] = 2 \times 10^{-6} M$ .

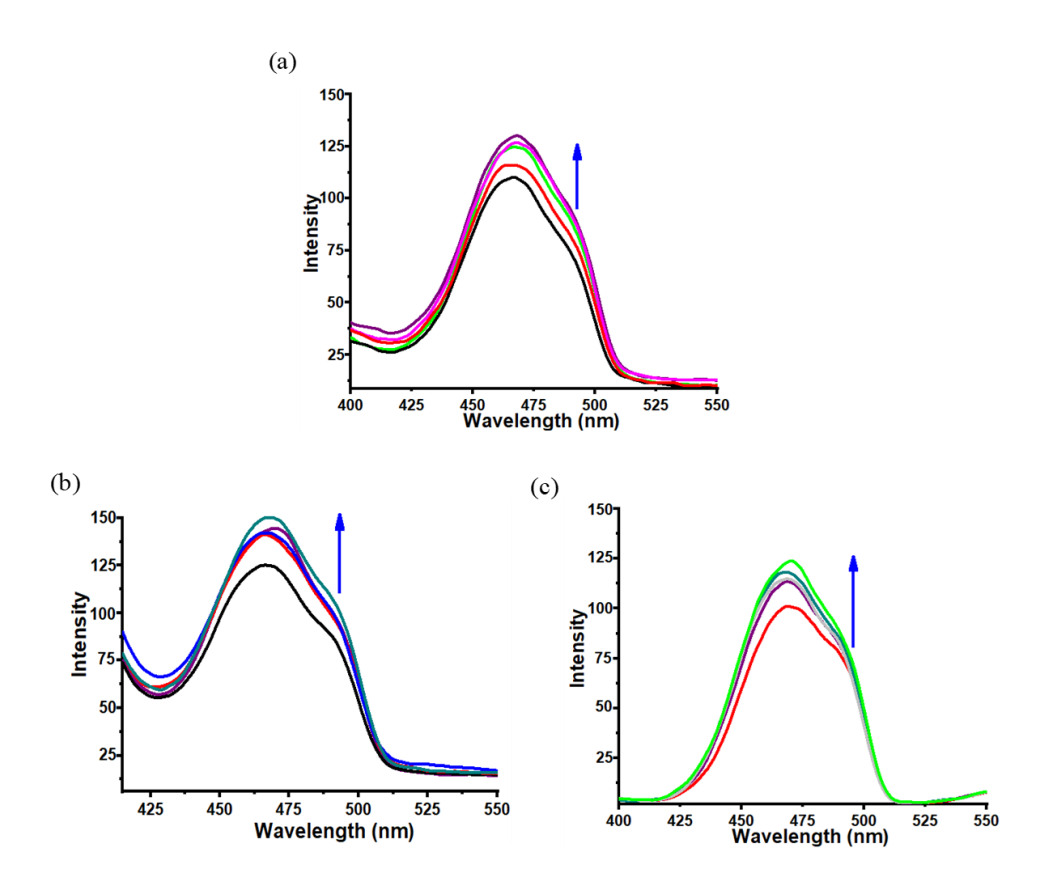


**Figure 2.15.** Emission spectra of synthesized metal (II) complexes **1** (a), **2** (b) and **3** (c) in presence of increasing aliquots of DNA [complex 1] = [complex 2] = [complex 3] =  $3 \times 10^{-6}$  M, [DNA] =  $0.1-0.5 \times 10^{-5}$  M.

#### Electrochemical studies

To examine the alterations in the redox behavior of metal complexes, electrochemical investigations were utilized during interaction with ct-DNA and to further substantiate the DNA binding characteristics revealed by ongoing spectroscopic studies [29]. It has been reported that a positive shift in electrode potential (cathodic and anodic) favours intercalative mode of binding mechanism, while a negative shift in electrode potential favours an electrostatic or groove binding mechanism [30]. We conducted electrochemical analyses of metal complex 1 in a tris-HCl buffer solution at room temperature with a sweep range of -1.0 to 1.5 V. In the absence of ct-DNA, respective cathodic and anodic peaks were found in the range of 0.61-0.64 and 1.23-1.26 V for complex 1, agreeing with redox couple Cu(II)/Cu(I) (Figure 2.16).

In complex 1, cyclic voltammogram have considerable separation between the cathodic and anodic peak potential ( $\Delta E_P$ ) suggesting quasi reversible redox process in the complexes [31]. However, upon titration of complex 1 with small aliquots of ct-DNA, decrease in current intensity was noticed in cathodic and increase in anodic peaks indicate existence of interaction between complex 1 and ct-DNA. Moreover, the negative shift in cathodic and anodic peak potential of complex 1 upon interaction with DNA eliminated the intercalative mode of binding [32]. Additionally, the larger negative shift in both anodic and cathodic potential indicates greater binding affinity of ct-DNA with complex 1 (Table 2.1).

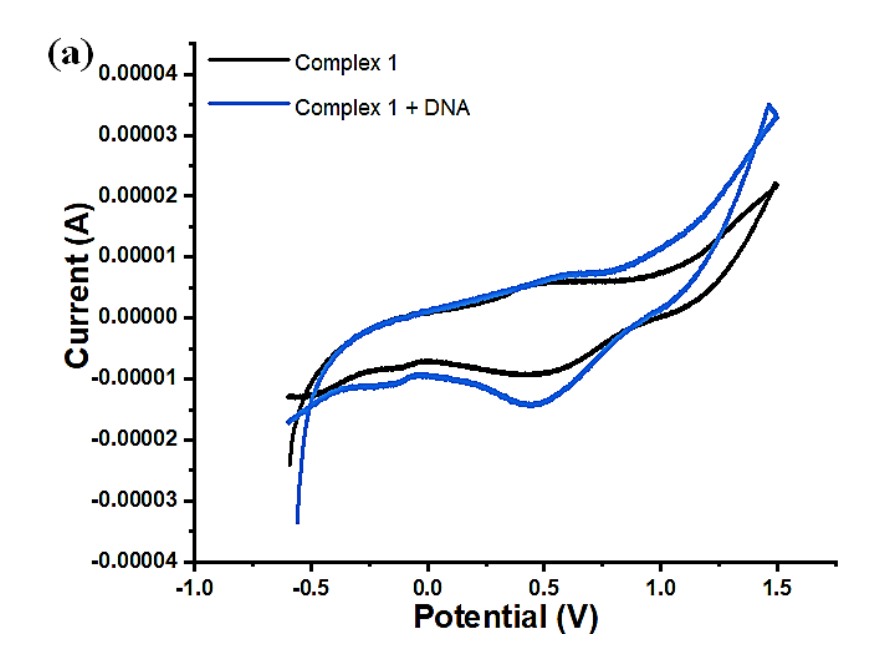


**Figure 2.16.** Cyclic voltametry curves of Complex 1 in the presence and absence of *ct*-DNA at a scanning rate of 100 mVs<sup>-1</sup> in tris HCl buffer having pH=7.2. [Complex] =  $4 \times 10^{-6}$  M, [DNA] =  $0.6 \times 10^{-6}$ M.

**Table 2.1** Cathodic and Anodic potential (V) and current (A) for the redox couples of complex 1 with ct–DNA in 5 mM Tris-buffer solution (pH 7.2) at a scan rate of  $100 \text{mVs}^{-1}$ . The mean  $\pm$  SEM of three separate trials (n $\geq$ 3) is represented by the data.

	<b>Complex Alone</b>		Complex + ct-DNA			
Complexes	Potential	Current	Potential	Current	ΔEpa	$\Delta E_{pc}$
	(V)	(A)	(V)	(A)		
	$E_{pa} = 0.72$	I <sub>pa</sub> = 3.37 ×	E <sub>pa</sub> =0.61	$I_{pa}$ = 2.78 ×		
	$E_{pc} = 1.32$	10 <sup>-5</sup>	E <sub>pc</sub> =1.24	10 <sup>-5</sup>	-1.1	-0.08
[Complex 1]	$E_{1/2} = 0.95$	$I_{pc} = 3.87 \times 10^{-5}$	$E_{1/2} = 0.93$	$I_{pc}=2.91 \times 10^{-5}$		
	$\Delta E_p = 0.71$	$I_{pa}/I_{pc}$ =	$\Delta E_p = 0.65$	$I_{\mathrm{pa}}/I_{\mathrm{pc}}=$		
		0.87		0.953		

#### Circular dichroism

The  $\pi$ - $\pi$ \* and n- $\pi$ \* transitions of the peptide bond are indicated by two separate bands at 276 and 246 nm in the DNA alone's CD spectrum. These two positive and negative bands at 276 and 246 nm are ascribed to base stacking and helicity, respectively, which are quite subtle to the binding of small molecules with DNA. It is reported that electrostatic binding and simple groove binding of complexes can lead to little or no change in the intrinsic CD profile of DNA [33]. Increased spectral band intensity was the result of adding complexes (0.1–0.6 x 10<sup>-6</sup> M) to a constant concentration of DNA (0.3 x 10<sup>-6</sup> M). This interaction with the complexes caused significant conformational and structural variations in the secondary structure of the ct-DNA, disrupting its helicity and confirming the electrostatic mode of interaction between metal(II) complexes (13) and the ct-DNA (**Figure 2.17**) [34].

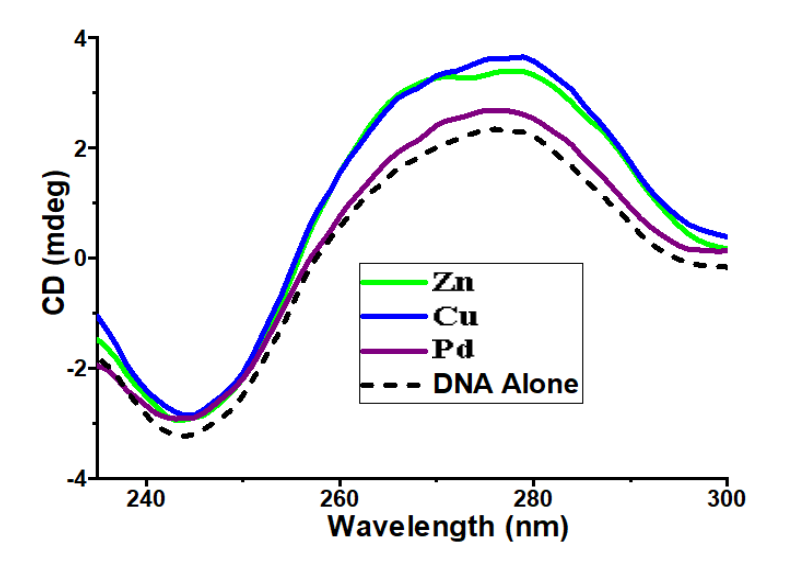


**Figure 2.17.** CD spectra of *ct*-DNA, and metal(II) complexes (1–3) in Tris–HCl buffer system (pH=7.3). [DNA] =  $0.4 \times 10^{-5}$  M and [complex 1] = [complex 2] = [complex 2] =  $2 \times 10^{-5}$  M.

#### In vitro antimicrobial assay

The produced compounds' antibacterial and antifungal properties were evaluated against the bacteria *Klebsiella pneumonia*, *Escherichia coli* and *Staphylococcus aureus*, as well as the fungi *Colletotrichum acutatum* and *Fusarium sp*. The lowest inhibitory concentration and zone of inhibition (ZOI) values were used to evaluate the antibacterial qualities of the produced ligand (L) and corresponding metal (II) complexes(Table 2.2; Figures 2.18 and 2.19) [35]. When tested against the tested microbial strains, the synthesized compounds demonstrated strong antimicrobial activity. The data showed that Cu(II), Zn(II), Pd(II) metal complexes and Schiff base ligand (L) exhibited medium-to-high antibacterial activity against the targeted bacterial strains with mean zones of inhibition that ranged from medium (6.20  $\pm 0.50$ mm) to high (16.37  $\pm$  2.03 mm). The metal complex of Cu(II) and Zn(II) unveiled higher activity compared tothe synthesized Schiff base ligand (L) among the synthesized compounds, with the exception of Pd(II) complex. This suggests that the complexation increases the antimicrobial activity of the synthesized compound. All the experiments were repeated three times with a standard error of deviation.

**Table 2.2:** The Schiff bases ligand (L) and metal (II) complexes' zone of inhibition for antimicrobial activity (1–3). Data represent mean  $\pm$  SEM.

	Zone diameter average (mm)							
Compound	Bacterial strains			Fungal strains				
	Escherichia coli	Klebsiella pneumonia	Staphyloc occus aureus	Colletotrichum acutatum	Fusarium sp.			
L	$8.00 \pm 2.00$	8.50 ±0.65	8.50 ±1.75	9.60 ±1.78	12.00 ±1.50			
1	13.85 ± 1.11	12.65 ± 0.79	16.37 ± 2.03	$10.70 \pm 1.01$	13.97 ±1.78			
2	12.40 ± 1.09	11.50 ±0.84	12.65 ±0.75	11.20 ±0.79	12.85 ±0.96			
3	8.25 ±0.93	7.25±0.84	8.25 ±1.18	8.50 ±0.87	6.20 ±0.50			
SD1	9.00 ±2.01	8.00 ±0.91	11.00 ±1.04	NT	NT			
SD2	NT	NT	NT	12.00 ±1.78	10.00 ±0.95			

SD1:Penicillin G, SD2:Ciclopiroxolamine. NT: Not Tested.

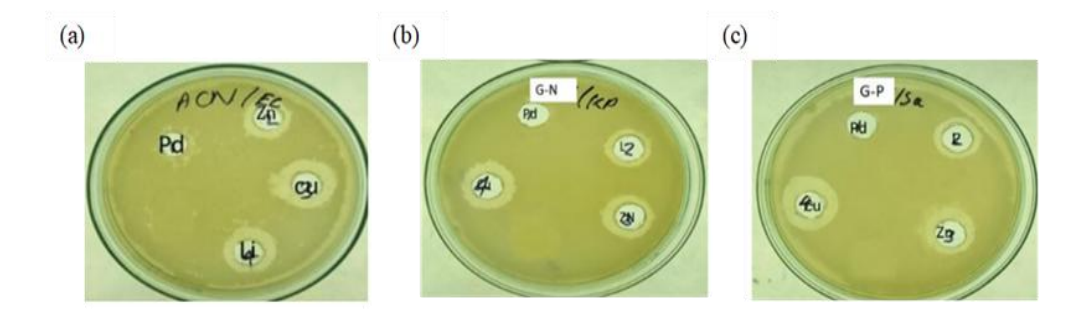


**Figure 2.18** Comparative antibacterial action of synthesized ligand (L) and complexes (1–3) against *Escherichia coli* (a), *Klebsiella pneumonia* (b) and *Staphylococcus aureus* (c) bacterial strains.

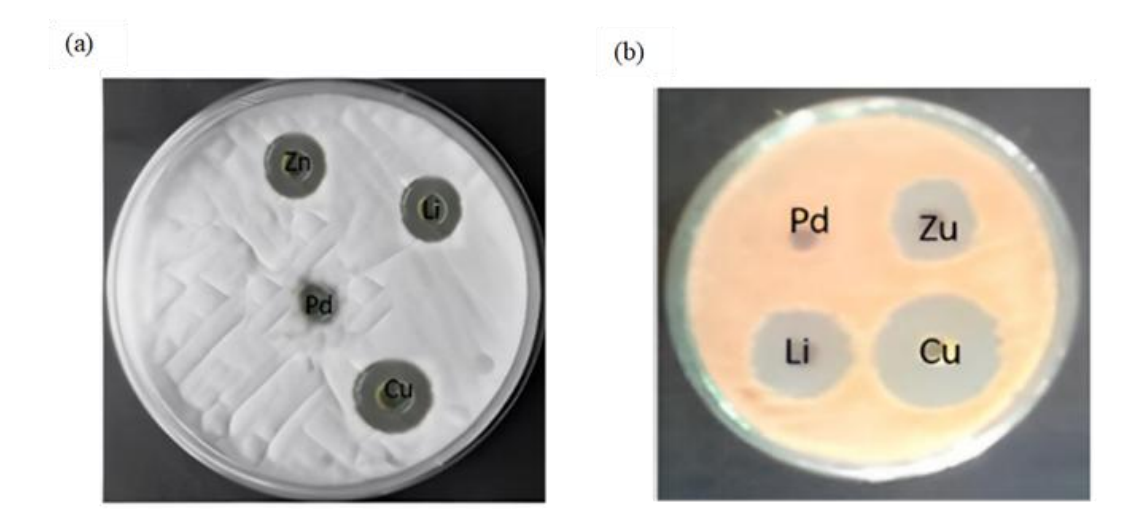


**Figure 2.19** Comparative antifungal action of synthesized ligand (L) and complexes (1–3) against *Colletotrichum acutatum* (a) and *Klebsiella pneumonia* (b) and *Fusarium sp.* fungal strains.

#### 2.2.3 Conclusion

We synthesized and comprehensively characterized the Schiff base ligand (L) and its copper (II), zinc (II), and palladium (II) complexes. The in vitro antimicrobial activity of the synthesized Schiff ligand (L) and its matching metal (II) complexes was tested against strains of the fungi *Colletotrichum acutatum* and *Fusarium sp.*, as well as the bacteria *Escherichia coli*, *Klebsiella pneumonia*, and *Staphylococcus aureus*. The Cu(II) complex (1) was the most active of the synthesized complexes, whereas the

Pd(II) complex (2) was the least active. The synthesized compounds were found to exhibit strong binding affinity with DNA, as demonstrated by electronic spectroscopy titrations and fluorescence quenching spectroscopy. When DNA interacts with the complexes, its structure undergoes notable conformational and morphological changes, as shown by DNA binding studies. Overall, it was observed that among the synthesized compounds the Cu(II) complex (1) exhibited the highest biological activities.

#### 2.2.4 References

- [1]. Uddin, N., Rashid, F., Ali, S., Tirmizi, S.A., Ahmad, I., Zaib, S., Zubair, M., Diaconescu, P.L., Tahir, M.N., Iqbal, J. and Haider, A., 2020. Synthesis, characterization, and anticancer activity of Schiff bases. *Journal of Biomolecular Structure and Dynamics*, 38(11), pp.3246-3259.
- [2]. De Clercq, E., 2002. Strategies in the design of antiviral drugs. *Nature Reviews drug discovery*, *I*(1), pp.13-25.
- [3]. Kaczmarek, M.T., Zabiszak, M., Nowak, M. and Jastrzab, R., 2018. Lanthanides: Schiff base complexes, applications in cancer diagnosis, therapy, and antibacterial activity. *Coordination Chemistry Reviews*, *370*, pp.42-54.
- [4]. Mohamed, G.G., Omar, M.M. and Hindy, A.M., 2005. Synthesis, characterization and biological activity of some transition metals with Schiff derived from 2-thiophene carboxaldehyde and aminobenzoic acid. Spectrochimica A: Molecular and Biomolecular Acta Part *Spectroscopy*, *62*(4-5), pp.1140-1150.
- [5]. Reiss, A., Florea, S., Caproiu, T. and Stanica, N., 2009. Synthesis, characterization, and antibacterial activity of some transition metals with the Schiff base N-(2-furanylmethylene)-3-aminodibenzofuran. *Turkish Journal of Chemistry*, 33(6), pp.775-783.
- [6]. Zhong, X., Yi, J., Sun, J., Wei, H.L., Liu, W.S. and Yu, K.B., 2006. Synthesis and crystal structure of some transition metal complexes with a novel bis-

- Schiff base ligand and their antitumor activities. European journal of medicinal chemistry, 41(9), pp.1090-1092.
- [7]. Shaikh, I., Travadi, M., Jadeja, R.N., Butcher, R.J. and Pandya, J.H., 2022. Crystal feature and spectral characterization of Zn (II) complexes containing Schiff base of Acylpyrazolone ligand with antimalarial action. *Journal of the Indian Chemical Society*, 99(5), p.100428.
- [8]. Joseyphus, R.S. and Nair, M.S., 2008. Antibacterial and antifungal studies on some Schiff base complexes of zinc (II). *Mycobiology*, *36*(2), pp.93-98.
- [9]. Wu, S., Qi, L., Ren, Y. and Ma, H., 2020. 1, 2, 4-triazole-3-thione Schiff bases compounds: Crystal structure, hirshfeld surface analysis, DFT studies and biological evaluation. *Journal of Molecular Structure*, *1219*, p.128591.
- [10]. Nair, M.S., Arish, D. and Joseyphus, R.S., 2012. Synthesis, characterization, antifungal, antibacterial and DNA cleavage studies of some heterocyclic Schiff base metal complexes. *Journal of Saudi Chemical Society*, *16*(1), pp.83-88.
- [11]. Ramesh, R. and Maheswaran, S., 2003. Synthesis, spectra, dioxygen affinity and antifungal activity of Ru (III) Schiff base complexes. *Journal of inorganic biochemistry*, 96(4), pp.457-462.
- [12]. Parashar, R.K., Sharma, R.C., Kumar, A. and Mohan, G., 1988. Stability studies in relation to IR data of some schiff base complexes of transition metals and their biological and pharmacological studies. *Inorganicachimica acta*, 151(3), pp.201-208.
- [13]. Hossain, A.M.S., Méndez-Arriaga, J.M., Xia, C., Xie, J. and Gómez-Ruiz, S., 2022. Metal complexes with ONS donor Schiff bases. A review. *Polyhedron*, *217*, p.115692.
- [14]. Jaisal, P., Fatima, G.N., Vishwakarma, S.K., Kumar, V., Pandey, S. and Saraf, S.K., 2022. Novel 2-aminopyrimidine Schiff bases as possible

- GABA-AT inhibitors: molecular docking, MAOS, and pharmacological screening. *Medicinal Chemistry Research*, *31*(10), pp.1818-1829.
- [15]. Singh, K. and Siwach, P., 2022. Synthesis, spectroscopic, theoretical and biological evaluation of novel Schiff base complexes of divalent transition metals. *Applied Organometallic Chemistry*, 36(3), p.e6553.
- [16]. Rukk, N.S., Kuzmina, L.G., Shamsiev, R.S., Davydova, G.A., Mironova, E.A., Ermakov, A.M., Buzanov, G.A., Skryabina, A.Y., Streletskii, A.N., Vorob'eva, G.A. and Retivov, V.M., 2019. Zinc (II) and cadmium (II) halide complexes with caffeine: Synthesis, X-ray crystal structure, cytotoxicity and genotoxicity studies. *InorganicaChimica Acta*, 487, pp.184-200.
- [17]. Kurpik, G., Walczak, A., Gołdyn, M., Harrowfield, J. and Stefankiewicz, A.R., 2022. Pd (II) complexes with pyridine ligands: substituent effects on the NMR data, crystal structures, and catalytic activity. *Inorganic Chemistry*, 61(35), pp.14019-14029.
- [18]. Bashir, M., Dar, A.A. and Yousuf, I., 2023. Syntheses, structural characterization, and cytotoxicity assessment of novel Mn (II) and Zn (II) complexes of aroyl-hydrazone Schiff base Ligand. *ACS omega*, 8(3), pp.3026-3042.
- [19]. Yousuf, I., Usman, M., Ahmad, M., Tabassum, S. and Arjmand, F., 2018. Single X-ray crystal structure, DFT studies and topoisomerase I inhibition activity of a tailored ionic Ag (I) nalidixic acid–piperazinium drug entity specific for pancreatic cancer cells. *New Journal of Chemistry*, 42(1), pp.506-519.
- [20]. Lakowicz, J.R. and Weber, G., 1973. Quenching of fluorescence by oxygen. Probe for structural fluctuations in macromolecules. *Biochemistry*, *12*(21), pp.4161-4170.
- [21]. Kumar, A., Ahmed, S., Bhardwaj, M., Imtiaz, S., Kumar, D., Bhat, A.R., Sood, B. and Maji, S., 2024. In vitro Anti-microbial, DNA-binding, In

- silico Pharmacokinetics and Molecular Docking Studies of Schiff-based Cu (II), Zn (II) and Pd (II) Complexes. *Journal of Molecular Structure*, p.138695.
- [22]. Yousuf, I., Mantoo, I.A., Bashir, M. and Bhat, S.A., 2022. Structure elucidation of a bimetallic μ-hydroxo-bridged Cu (II)-flufenamate-bpy complex and cytotoxic evaluation against MDA-MB-231 and A549 carcinoma cell lines. *Applied Organometallic Chemistry*, 36(12), p.e6906.
- [23]. Hassan, S.A., Aziz, D.M., Abdullah, M.N., Bhat, A.R., Dongre, R.S., Hadda, T.B., Almalki, F.A., Kawsar, S.M., Rahiman, A.K., Ahmed, S. and Abdellattif, M.H., 2024. In vitro and in vivo evaluation of the antimicrobial, antioxidant, cytotoxic, hemolytic activities and in silico POM/DFT/DNA-binding and pharmacokinetic analyses of new sulfonamide bearing thiazolidin-4-ones. *Journal of Biomolecular Structure and Dynamics*, 42(7), pp.3747-3763.
- [24]. Sivakova, S. and Rowan, S.J., 2005. Nucleobases as supramolecular motifs. *Chemical Society Reviews*, *34*(1), pp.9-21.
- [25]. Karami, K., Mehvari, F., Ramezanzade, V., Zakariazadeh, M., Kharaziha, M. and Ramezanpour, A., 2022. The interaction studies of novel imine ligands and palladium (II) complexes with DNA and BSA for drug delivery application: the anti-cancer activity and molecular docking evaluation. *Journal of Molecular Liquids*, 362, p.119493.
- [26]. Al-Raqa, S.Y., Khezami, K., Kaya, E.N. and Durmuş, M., 2021. A novel water soluble axially substituted silicon (IV) phthalocyanine bearing quaternized 4-(4-pyridinyl) phenol groups: Synthesis, characterization, photophysicochemical properties and BSA/DNA binding behavior. *Polyhedron*, 194, p.114937.
- [27]. Sarwar, T., Husain, M.A., Rehman, S.U., Ishqi, H.M. and Tabish, M., 2015. Multi-spectroscopic and molecular modelling studies on the interaction of esculetin with calf thymus DNA. *Molecular BioSystems*, 11(2), pp.522-531.

- [28]. Rehman, S.U., Yaseen, Z., Husain, M.A., Sarwar, T., Ishqi, H.M. and Tabish, M., 2014. Interaction of 6 mercaptopurine with calf thymus DNA–deciphering the binding mode and photoinduced DNA damage. *PLoS one*, *9*(4), p.e93913.
- [29]. Rodriguez, M. and Bard, A.J., 1990. Electrochemical studies of the interaction of metal chelates with DNA. 4. Voltammetric and electrogenerated chemiluminescent studies of the interaction of tris (2, 2'-bipyridine) osmium (II) with DNA. *Analytical chemistry*, 62(24), pp.2658-2662.
- [30]. Perontsis, S., Hatzidimitriou, A.G., Papadopoulos, A.N. and Psomas, G., 2016. Nickel-diflunisal complexes: synthesis, characterization, in vitro antioxidant activity and interaction with DNA and albumins. *Journal of Inorganic Biochemistry*, 162, pp.9-21.
- [31]. Johansson, F.B., Bond, A.D., Nielsen, U.G., Moubaraki, B., Murray, K.S., Berry, K.J., Larrabee, J.A. and McKenzie, C.J., 2008. Dicobalt II– II, II– III, and III– III complexes as spectroscopic models for dicobalt enzyme active sites. *Inorganic chemistry*, 47(12), pp.5079-5092.
- [32]. Loganathan, R., Ramakrishnan, S., Suresh, E., Palaniandavar, M., Riyasdeen, A. and Akbarsha, M.A., 2014. Mixed ligand μ-phenoxo-bridged dinuclear copper (II) complexes with diimine co-ligands: efficient chemical nuclease and protease activities and cytotoxicity. *Dalton Transactions*, 43(16), pp.6177-6194.
- [33]. Yang, Q., Liang, J. and Han, H., 2009. Probing the interaction of magnetic iron oxide nanoparticles with bovine serum albumin by spectroscopic techniques. *The Journal of Physical Chemistry B*, 113(30), pp.10454-10458.
- [34]. Xiang, Y. and Wu, F., 2010. Study of the interaction between a new Schiff-base complex and bovine serum albumin by fluorescence spectroscopy. *Spectrochimica Acta Part A: Molecular and Biomolecular Spectroscopy*, 77(2), pp.430-436.

[35]. Colinas, I.R., Rojas-Andrade, M.D., Chakraborty, I. and Oliver, S.R., 2018. Two structurally diverse Zn-based coordination polymers with excellent antibacterial activity. *CrystEngComm*, 20(24), pp.3353-3362.

## Chapter 3

This chapter give details about the synthetic procedure of Cu@L-dopaSB/Al<sub>2</sub>O<sub>3</sub>-Fe<sub>3</sub>O<sub>4</sub>, its characterization and Applications.

### Section 3.1 Synthesis and characterisation of a Schiff base functionalized Cu(II) onto L-dopaSB/Al<sub>2</sub>O<sub>3</sub>-Fe<sub>3</sub>O<sub>4</sub> magnetic composite [Cu@L-dopaSB/Al<sub>2</sub>O<sub>3</sub>-Fe<sub>3</sub>O<sub>4</sub>]

In this section, a novel magnetic nanocomposite, Cu@L-dopaSB/Al<sub>2</sub>O<sub>3</sub>-Fe<sub>3</sub>O<sub>4</sub>, was prepared by anchoring Cu(II) ions to L-dopa functionalized Schiff base on an Al<sub>2</sub>O<sub>3</sub>-Fe<sub>3</sub>O<sub>4</sub> support. The schematic illustration of the synthesis of the developed magnetic catalyst is presented in **Figure 3.1**. Fe<sub>3</sub>O<sub>4</sub> nanoparticles were synthesized by coprecipitating Fe<sup>3+</sup> and Fe<sup>2+</sup> salts in alkaline medium. Thereafter, Fe<sub>3</sub>O<sub>4</sub> nanoparticles were coated by a layer of Al<sub>2</sub>O<sub>3</sub> in order to avoid their agglomeration using aluminium isopropoxide via ultrasonication process followed by calcination at 500 °C. The surface of Al<sub>2</sub>O<sub>3</sub> coated magnetic nanoparticles was further functionalized using L-dopa. The surface -NH<sub>2</sub> groups of Fe<sub>3</sub>O<sub>4</sub>-Al<sub>2</sub>O<sub>3</sub>/L-dopa were then condensed with thiophene-2-carboxaldehyde to give Schiff base functionalized Al<sub>2</sub>O<sub>3</sub> coated magnetic nanoparticles. Finally, treatment with copper (II) acetate resulted in Cu@L-dopaSB/Al<sub>2</sub>O<sub>3</sub>-Fe<sub>3</sub>O<sub>4</sub> as the heterogeneous magnetic nanocomposite. The synthesised catalyst has been thoroughly described utilizing a number of techniques, including HR-SEM, EDX, TEM, XRD, BET, FTIR, ICP-AES, CHN, TGA, and VSM.

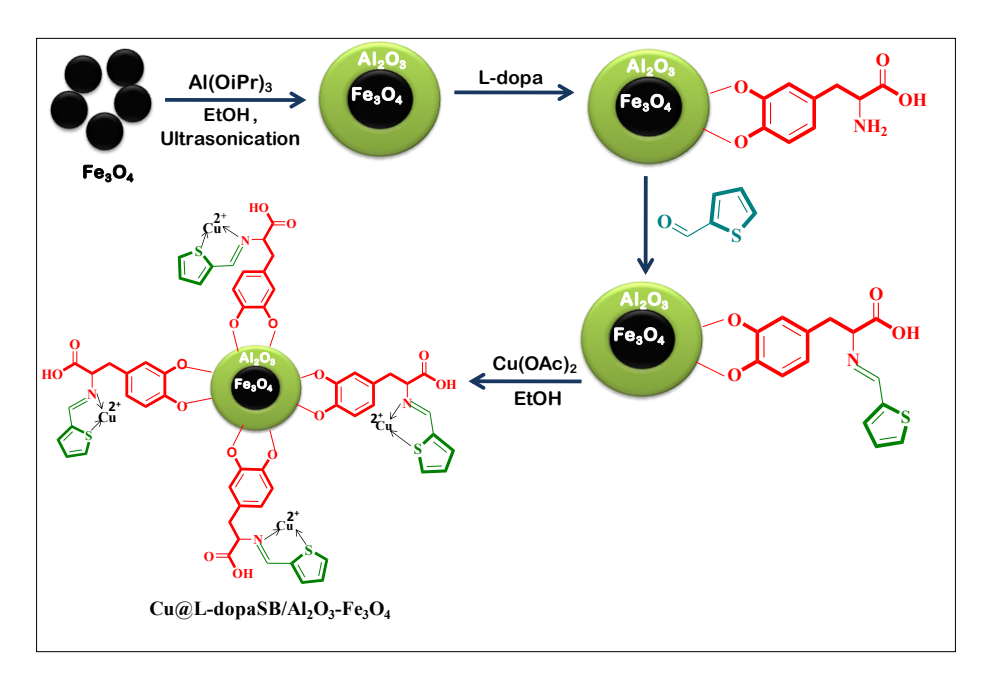


Figure 3.1. Proposed scheme for the synthesis of Cu@L-dopaSB/Al<sub>2</sub>O<sub>3</sub>-Fe<sub>3</sub>O<sub>4</sub>

#### **Materials and Instrumentation**

All reagents used in this study were procured from Merck or Aldrich Chemical Companies. The FTIR i.e., Fourier Transform Infrared spectra, were documented using PerkinElmer FTIR spectrophotometer. X-ray Diffraction (XRD) data were collected with a D2 PHASER Rigaku X-ray diffractometer over a 2-theta range of 10° to 80°. X-ray Photoelectron Spectroscopy (XPS) spectra of the prepared catalyst were obtained using a Thermo Scientific NEXA Surface Analyzer. Carbon, Hydrogen, Nitrogen, and Sulfur (CHNS) analysis was performed using an Elementar UNICUBE model, while thermal behavior (TGA) was examined with a Perkin Elmer Diamond TG/DTA at a heating rate of 10 °C per minute. FEG-SEM analysis and EDX were conducted using a Hitachi S-3000N scanning electron microscope. TEM analysis was performed on an FEI Talos model. The amount of metal loading was determined through ICP-AES analysis using the ARCOS simultaneous ICP spectrometer. Magnetism (magnetic moment) was calculated using a vibrating sample magnetometer (VSM), Model 7410 series from Lakeshore, at room temperature within a range of -10,000 to +15,000 Oe. The ^1H and ^13C NMR data were recorded using a Bruker Avance spectrometer operating at 100 MHz and 400 MHz.

#### 3.1.1 Overall procedure for the preparation of Cu@L-dopaSB/Al2O3-Fe3O4

#### Preparation of Fe<sub>3</sub>O<sub>4</sub>NPs

Fe<sub>3</sub>O<sub>4</sub>-nanoparticles were synthesized by using a previously reported protocol [1]. In a beaker, 5 g of FeCl<sub>3</sub> and 2.5 g of FeCl<sub>2</sub> were dissolved in 30 ml of distilled H<sub>2</sub>O. To this, an aq. NaOH sol. was added drop by drop under continuous stirring. Precipitation thus occurred and the metal salt was transformed into corresponding hydroxides which gets converted into nano ferrites. The precipitated nano ferrites were separated after 15 minutes using external magnet and subsequently washed so as to maintain its pH at 7.0 using distilled water and vacuum dried at 60° C.

#### Preparation of Fe<sub>3</sub>O<sub>4</sub>-Al<sub>2</sub>O<sub>3</sub>

For the preparation of Fe<sub>3</sub>O<sub>4</sub>- Al<sub>2</sub>O<sub>3</sub>, 1g of aluminium isopropoxide was dissolved in ethanol (50 mL) and to it 0.5g of as prepared Fe<sub>3</sub>O<sub>4</sub> nanoparticles were added and the

mixture was ultrasonicated for 40 minutes. Subsequently, a water and ethanol mixture (1:5, 20 mL) was added dropwise to the above solution under vigorous stirring over a period of 20 minutes. Finally, the product was magnetically separated and extracted with ethanol, dried at 80°C for 12 h and calcined at 500°C for 2.5 h.

#### Preparation of L-Dopa/Fe<sub>3</sub>O<sub>4</sub>-Al<sub>2</sub>O<sub>3</sub>

For grafting L-dopa over the surface of Fe<sub>3</sub>O<sub>4</sub>- Al<sub>2</sub>O<sub>3</sub> nanoparticles, Fe<sub>3</sub>O<sub>4</sub>- Al<sub>2</sub>O<sub>3</sub> (1 g) and L-dopa (0.5 g) was added in a flask and the mixture was stirred in deionized water (50 mL) at  $120^{\circ}$ C for 3 h. The precipitates of L-dopa/Fe<sub>3</sub>O<sub>4</sub>-Al<sub>2</sub>O<sub>3</sub>were collected magnetically, washed with deionized water (3 × 10 mL) and dried under vacuum.

#### Preparation of L-dopaSB/Fe<sub>3</sub>O<sub>4</sub>-Al<sub>2</sub>O<sub>3</sub>

To the suspension of L-dopa/Fe<sub>3</sub>O<sub>4</sub>-Al<sub>2</sub>O<sub>3</sub> (1 g) in ethanol (40 mL), thiophene-2 carboxaldehyde (1.5 mmol, 0.18 g) was added and the resultant mixture undergo refluxing for 24 h. Schiff base of L-dopa functionalized Al<sub>2</sub>O<sub>3</sub> coated Fe<sub>3</sub>O<sub>4</sub> nanocomposite (L-dopaSB/Al<sub>2</sub>O<sub>3</sub>-Fe<sub>3</sub>O<sub>4</sub>) thus obtained after the condensation reaction of amine groups of L-dopa/Fe<sub>3</sub>O<sub>4</sub>-Al<sub>2</sub>O<sub>3</sub> with thiophene-2 carboxaldehyde was separated using magnet and washed with EtOH and H<sub>2</sub>O and dried under vacuum.

#### Synthesis of Cu@L-dopaSB/Al<sub>2</sub>O<sub>3</sub>-Fe<sub>3</sub>O<sub>4</sub>

To 1 g of L-dopa/Fe<sub>3</sub>O<sub>4</sub>-TiO<sub>2</sub>, a sol. of Cu(OAc)<sub>2</sub>in toluene (0.1 g, 25 mL) was incorporated. Vigrous stirring of the reaction mixture was done for 16 hours under a controlled nitrogen atmosphere at 70°C. The reaction mixture undergoes stirring for 16 h under nitrogen atmosphere at 70°C. The resulting Cu@L-dopaSB/Al<sub>2</sub>O<sub>3</sub>-Fe<sub>3</sub>O<sub>4</sub> complex so obtained was separated via magnet followed by washing with EtOH and H<sub>2</sub>O and vacuum dried overnight.

#### 3.1.2 Characterization of Cu@L-dopaSB/Al<sub>2</sub>O<sub>3</sub>-Fe<sub>3</sub>O<sub>4</sub>

#### HR-SEM

HR-SEM images of Cu@L-dopaSB/Al<sub>2</sub>O<sub>3</sub>-Fe<sub>3</sub>O<sub>4</sub> were recorded to investigate the surface morphology of the catalyst. SEM micrographs (**Figure. 3.2**) clearly infers that

the developed catalyst consists of tiny quasi-spherical particles with slightly rough structure.

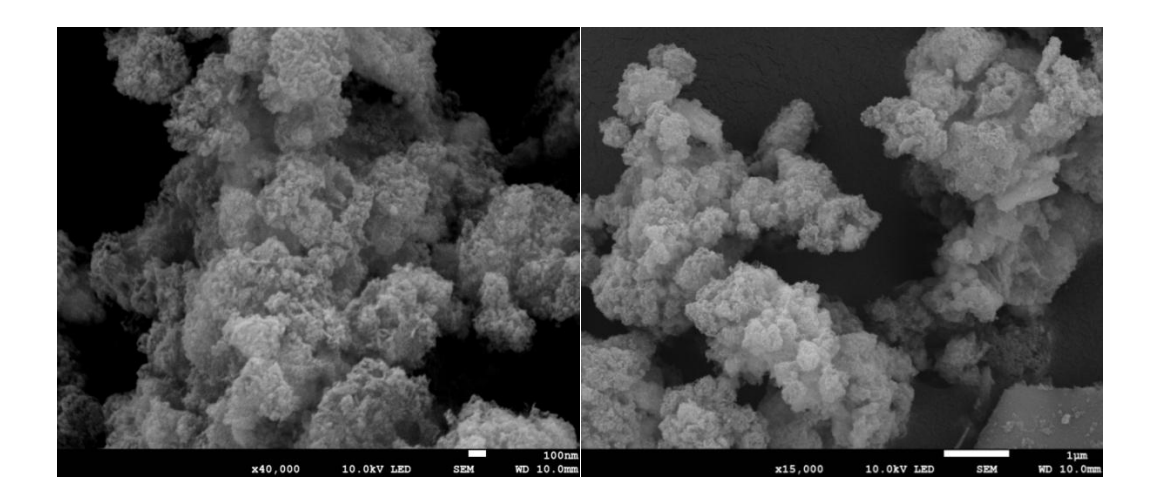


Figure. 3.2 HR-SEM images of Cu@L-dopaSB/Al<sub>2</sub>O<sub>3</sub>-Fe<sub>3</sub>O<sub>4</sub>

#### **TEM**

To get more insights about the morphology and the crystalline properties of Cu@L-dopaSB/Al<sub>2</sub>O<sub>3</sub>-Fe<sub>3</sub>O<sub>4</sub>, TEM and selected area electron diffraction (SAED) patterns were collected and analysed (**Figure 3.3**). The development of thin fibers on the catalyst's surface was visible in the TEM pictures (**Figure 3.3a** and **3.3b**), which represent the Al<sub>2</sub>O<sub>3</sub> moieties, while the black dots represent the uniformly distributed Cu(II) particles. Moreover, the light grey area behind the black dots confirms the presence of Fe<sub>3</sub>O<sub>4</sub> nanoparticles. The average size distributions of Cu@L-dopaSB/Al<sub>2</sub>O<sub>3</sub>-Fe<sub>3</sub>O<sub>4</sub> werefound to be in the range of 40 to 50 nm (Inset image, **Figure 3.3e**), which was analyzed by plotting a histogram. Using TEM images, we have also calculated the lattice fringe spacing measuring 2.93 and 3.09 Å, which represents the (220) and (111) lattice planes of Fe<sub>3</sub>O<sub>4</sub> [2] and Cu [3], respectively.

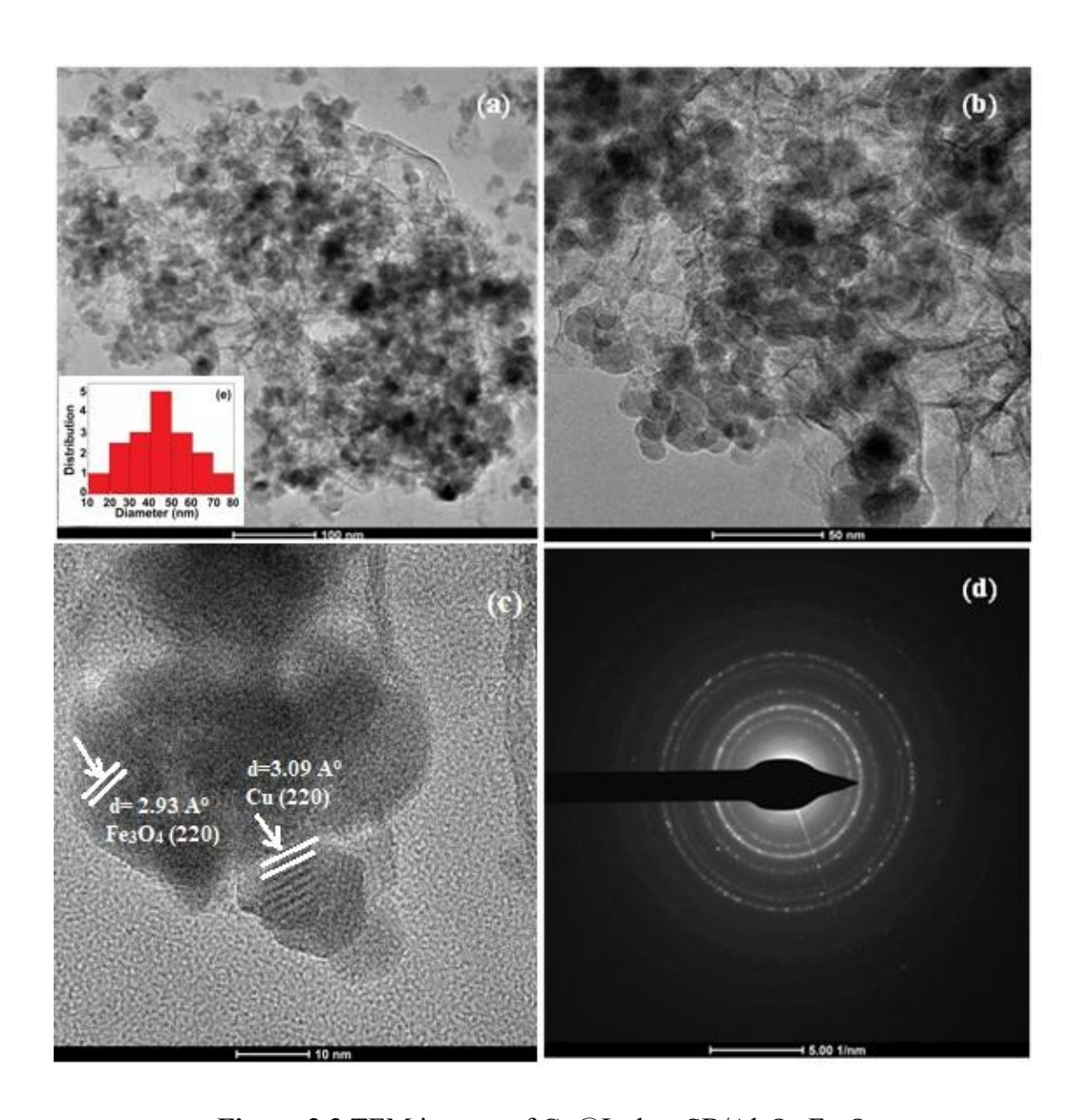


Figure 3.3 TEM images of Cu@L-dopaSB/Al<sub>2</sub>O<sub>3</sub>-Fe<sub>3</sub>O<sub>4</sub>

#### **EDX**

The elemental composition of the developed catalyst was explored by carrying out the EDX analysis and the results revealed the occurrence of Fe, Al, O, N, S, and Cu, hence, corroborating with the high purity of Cu@L-dopaSB/Al<sub>2</sub>O<sub>3</sub>-Fe<sub>3</sub>O<sub>4</sub> by the absence of any other extra element in the EDX spectrum (**Figure 3.4**). Moreover, EDX mapping demonstrated the uniform dispersion of Fe, Al, N, O, S, and Cu within the catalyst structure (**Figure 3.5**).

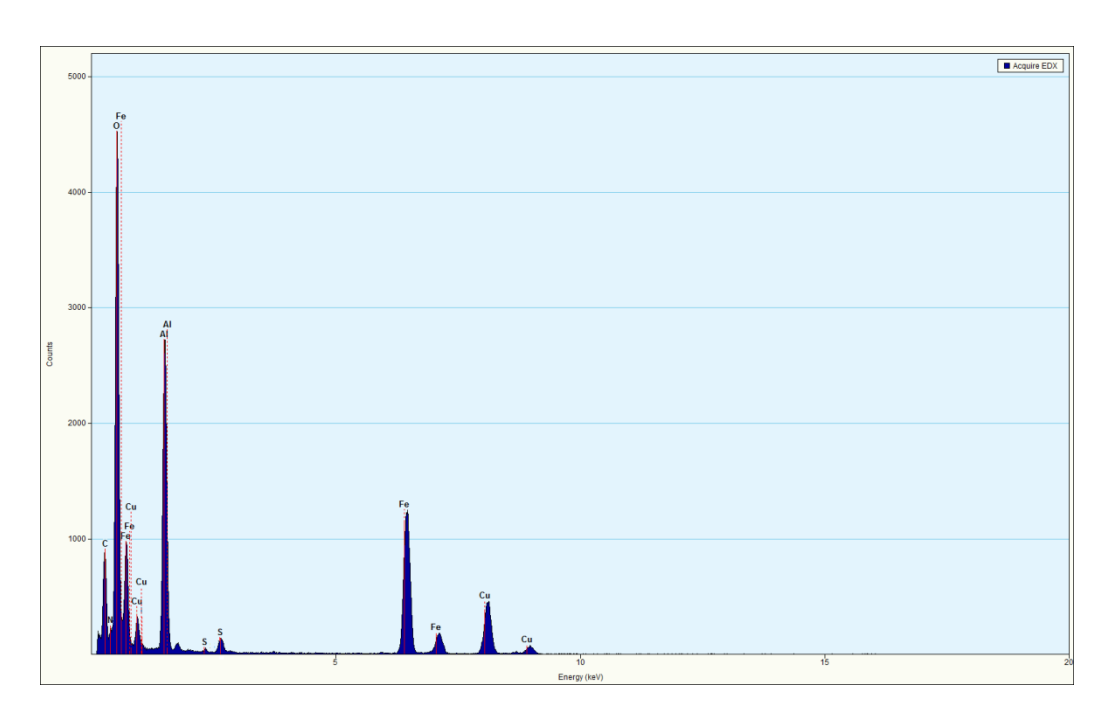


Figure 3.4 EDX of Cu@L-dopaSB/Al<sub>2</sub>O<sub>3</sub>-Fe<sub>3</sub>O<sub>4</sub>

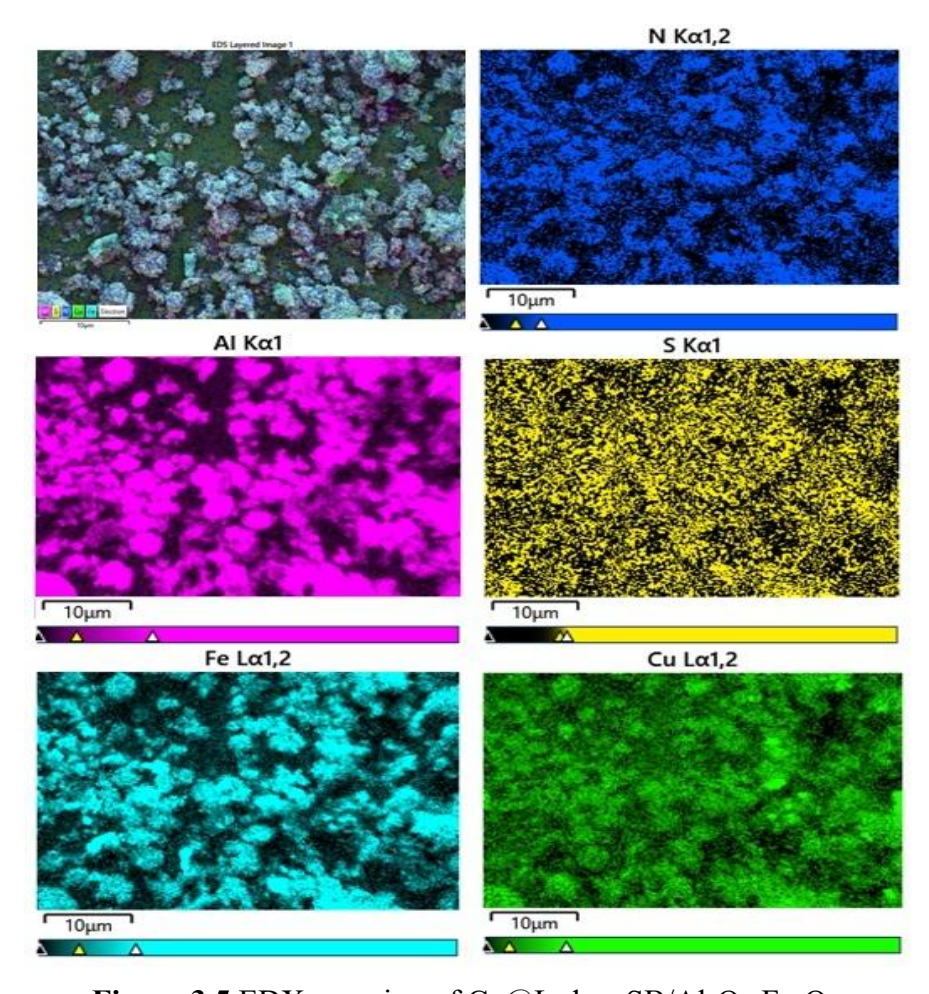


Figure 3.5 EDX mapping of Cu@L-dopaSB/Al<sub>2</sub>O<sub>3</sub>-Fe<sub>3</sub>O<sub>4</sub>.

#### **BET**

The surface area as well as the porosity Cu@L-dopaSB/Al<sub>2</sub>O<sub>3</sub>-Fe<sub>3</sub>O<sub>4</sub> was done using the N<sub>2</sub> adsorption-desorption measurements by BET analysis. According to the IUPAC classification, the plot of Cu@L-dopaSB/Al<sub>2</sub>O<sub>3</sub>-Fe<sub>3</sub>O<sub>4</sub> exhibited type IV isotherm [4], suggesting the mesoporous nature of the catalyst (**Figure 3.6**). As inferred from the BET data, Cu@L-dopaSB/Al<sub>2</sub>O<sub>3</sub>-Fe<sub>3</sub>O<sub>4</sub> has specific surface area of 197.40 m<sup>2</sup> g<sup>-1</sup>, mean pore diameter of 13.63 nm and total pore volume 0.67 cm<sup>3</sup>/g respectively.

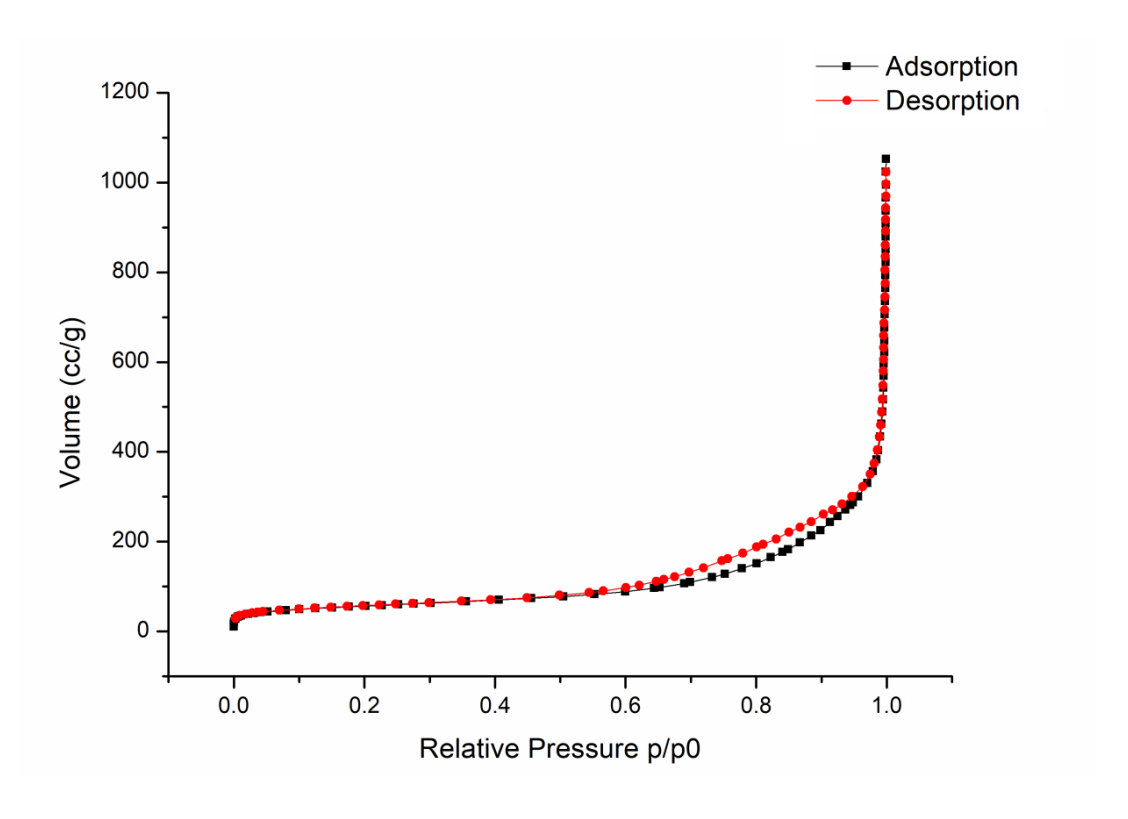


Figure 3.6 BET of Cu@L-dopaSB/Al<sub>2</sub>O<sub>3</sub>-Fe<sub>3</sub>O<sub>4</sub>

#### XPS

The electronic properties i.e. binding energy and chemical potential of various metals present in Cu@L-dopaSB/Al<sub>2</sub>O<sub>3</sub>-Fe<sub>3</sub>O<sub>4</sub> were analyzed by XPS analysis. **Figure 3.7a** depicts the overall survey spectrum which confirms the presence of all the expected elements. The binding energy peaks corresponding to Fe 2p (711 eV), Al 2p (74 eV), O 1s (531 eV), N 1s (399 eV), S 2p (162 eV) and Cu 2p (934 eV) are well observed. The existence of Cu(II) species is confirmed by the observation of two characteristic

absorption peaks at 934 eV and 953 eV corresponding to  $2p_{3/2}$  and  $2p_{1/2}$ ,respectively [5]. Furthermore, the deconvoluted XPS spectrum of Cu 2p also showed two doublets of peaks at 934.6 and 953.4 eV, attributed to the +2 oxidation state of Cu for  $2p_{3/2}$  and  $2p_{1/2}$ ,respectively. The XPS curve of N 1s shows peaks corresponding to the imine bond present in Schiff base functionalized support. Further, a significant shift of the binding energy of the 398.1 eV (398.1 $\rightarrow$ 399.18 eV) was also observed, which confirmed that nitrogen is coordinated to Cu(II) ion [30]. This phenomenon was observed because a lone pair of electrons of the nitrogen atom is coordinated with Cu(II) ions, and as a consequence, the electron cloud density of the nitrogen atom is reduced, resulting in a higher binding energy [6]. Moreover, the shift in the binding energy of the S 2p (161.4  $\rightarrow$ 162 eV) also signifies that Cu(II) was successfully bonded to the Sulphur and Nitrogen elements of Schiff base functionalized support (L-dopaSB/Al<sub>2</sub>O<sub>3</sub>-Fe<sub>3</sub>O<sub>4</sub>) [7].

The XPS of the reused catalyst (after six runs) was also done and the results indicated no significant changes in their binding energy patterns in comparison to the fresh catalyst, and thus representing a stable electronic structure around Cu (II) in recycled catalyst (**Figure 3.7d**), indicating the excellent recyclability of Cu@L-dopaSB/Al<sub>2</sub>O<sub>3</sub>-Fe<sub>3</sub>O<sub>4</sub>.

#### **FTIR**

FTIR of Cu@L-dopaSB/Al<sub>2</sub>O<sub>3</sub>-Fe<sub>3</sub>O<sub>4</sub> shows the existence of various functionalities present in it. The spectra of Al<sub>2</sub>O<sub>3</sub>-Fe<sub>3</sub>O<sub>4</sub> (**Figure 3.8a**) shows the presence of characteristic bands at 585 cm<sup>-1</sup> and 644 cm<sup>-1</sup> indicating the presence of metallic Fe-O and Al-O stretching vibrations [8], while the presence of a broad absorption peak at 3450 cm<sup>-1</sup> corresponds to the -OH stretching frequency of the absorbed water molecules [9]. FTIR spectrum of Cu@L-dopaSB/Al<sub>2</sub>O<sub>3</sub>-Fe<sub>3</sub>O<sub>4</sub> (**Figure 3.8b**) showed the advent of a new absorption peak at 1636 cm<sup>-1</sup>, which corresponds to the stretching vibrations of the C=N group, which confirms the successful binding of L-dopa functionalized Schiff base onto the surface of Al<sub>2</sub>O<sub>3</sub>-Fe<sub>3</sub>O<sub>4</sub> magnetic nanoparticles. Moreover, the observation of characteristic vibrations around 1520-1300cm<sup>-1</sup> and 1110-1055 cm<sup>-1</sup> due to the C=C stretching frequencies thereby confirms the existence of phenyl rings in Cu@L-dopaSB/Al<sub>2</sub>O<sub>3</sub>-Fe<sub>3</sub>O<sub>4</sub>. Further, the FTIR spectra (**Figure** 

**3.8c**) of the reused catalyst (after six consecutive runs) for the synthesis of 1,4-Disubstituted 1,2,3-triazoles was carried out and the outcome clearly indicated no

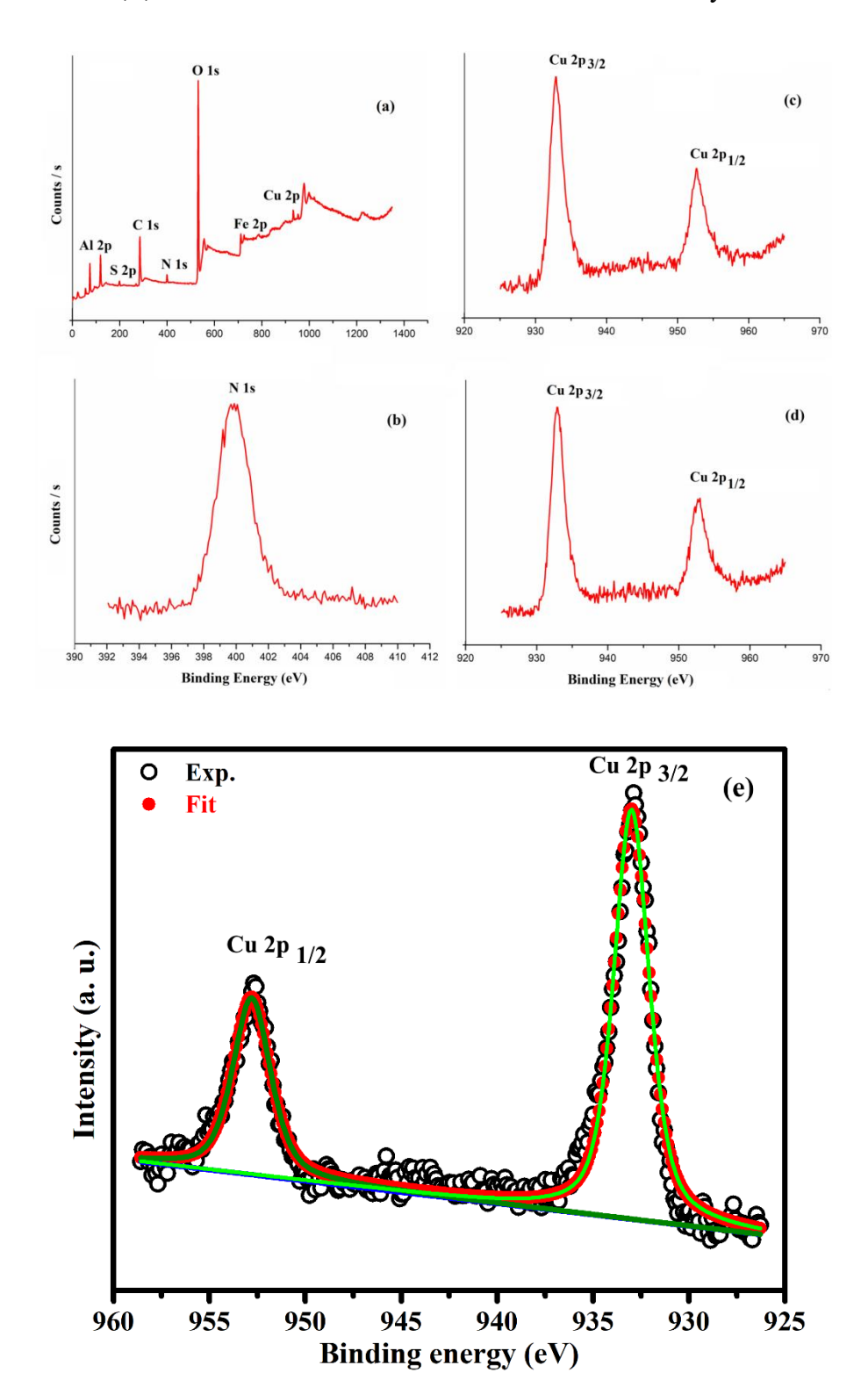


**Figure 3.7** XPS of Cu@L-dopaSB/Al<sub>2</sub>O<sub>3</sub>-Fe<sub>3</sub>O<sub>4</sub> (a) Overall survey spectrum (b) N 1s region (c) Core level spectrum of Cu 2p (Fresh) (d) Core level spectrum of Cu 2p (reused after 6 runs) (e) Deconvulated XPS spectrum of Cu 2p.

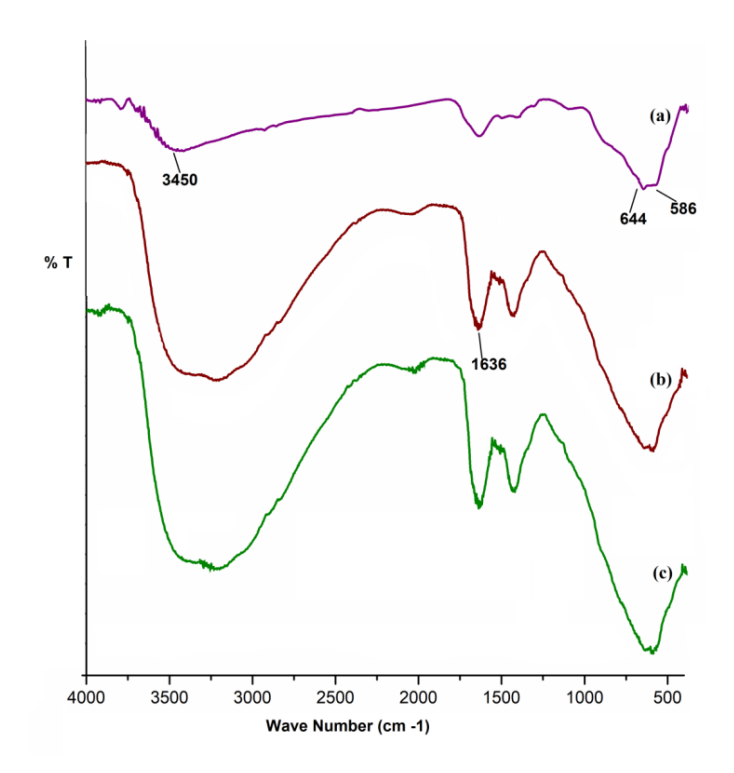


**Figure 3.8** FTIR spectra (a)Al<sub>2</sub>O<sub>3</sub>-Fe<sub>3</sub>O<sub>4</sub>(b)Cu@L-dopaSB/Al<sub>2</sub>O<sub>3</sub>-Fe<sub>3</sub>O<sub>4</sub> (c) Cu@L-dopaSB/Al<sub>2</sub>O<sub>3</sub>-Fe<sub>3</sub>O<sub>4</sub> (re-used after 6 runs).

#### XRD

The synthesised materials' crystallinity and phase composition were ascertained using XRD examination. The comparative XRD patterns of (a) L-dopaSB/Al<sub>2</sub>O<sub>3</sub>-Fe<sub>3</sub>O<sub>4</sub> (b) Cu@L-dopaSB/Al<sub>2</sub>O<sub>3</sub>-Fe<sub>3</sub>O<sub>4</sub> and (c) Cu@L-dopaSB/Al<sub>2</sub>O<sub>3</sub>-Fe<sub>3</sub>O<sub>4</sub> (re-used after 6 runs) are represented in **Figure 3.9**. The XRD pattern of L-dopaSB/Al<sub>2</sub>O<sub>3</sub>-Fe<sub>3</sub>O<sub>4</sub> (**Figure3.9a**) exhibited diffraction peaks at 30.3°, 35.6°, and 63.1°, attributable to the (220), (311), and (440) planes of Fe<sub>3</sub>O<sub>4</sub> nanoparticleswhich was confirmed by the JCPDS card No. 75–1609 [2] while the diffraction peaks at 25.3°, 43.2° and 57.4° corresponds to the (012), (113) and (116) planes of Al<sub>2</sub>O<sub>3</sub> [10]. Further, the XRD spectra of Cu@L-dopaSB/Al<sub>2</sub>O<sub>3</sub>-Fe<sub>3</sub>O<sub>4</sub> (**Figure3.9b**), showed two new diffraction peaks at  $2\theta = 28.7^{\circ}$  and  $40.8^{\circ}$  which correspond to the (111) and (221)

Cu(II) crystalline planes [11]. It is clearly observed that the introduction of Cu (II) does not interfere the crystalline phases of Fe<sub>3</sub>O<sub>4</sub> and Al<sub>2</sub>O<sub>3</sub> although their intensities had been slightly reduced. This confirmed that the crystalline core nature of Fe<sub>3</sub>O<sub>4</sub> and Al<sub>2</sub>O<sub>3</sub> remain intact even after the grafting of L-dopa functionalized Schiff base on them. Besides, the XRD (**Fig 3.9c**) of the reused catalyst (after six consecutive runs) indicated no considerable changes in peak positions in contrast to the fresh catalyst.

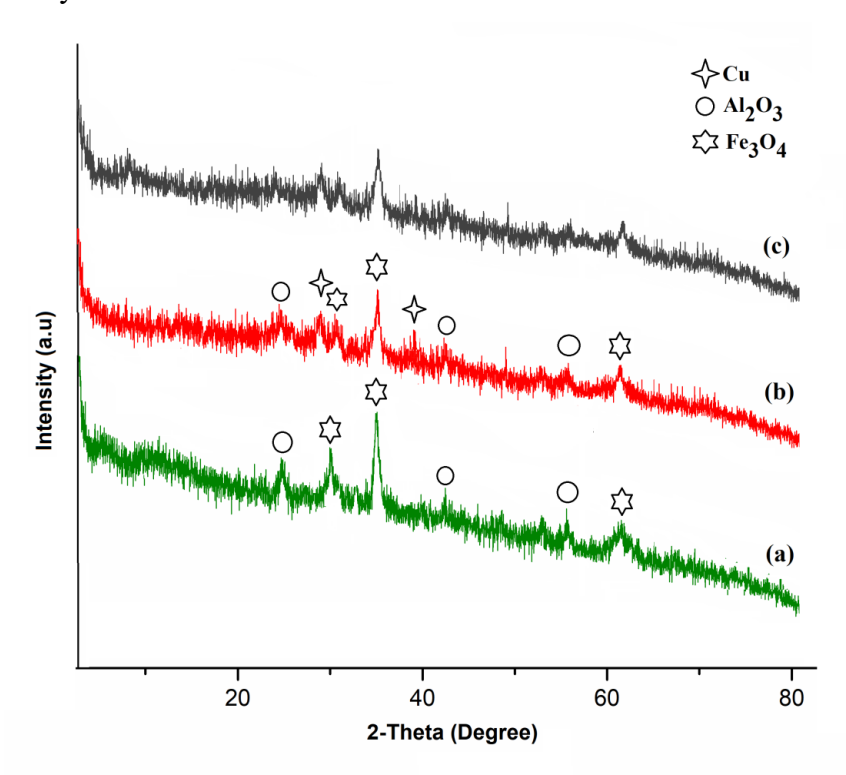


**Figure 3.9** XRD spectra (a) SB/L-dopa/Al<sub>2</sub>O<sub>3</sub>-Fe<sub>3</sub>O<sub>4</sub>(b) Cu@L-dopaSB/Al<sub>2</sub>O<sub>3</sub>-Fe<sub>3</sub>O<sub>4</sub> (c) Cu@L-dopaSB/Al<sub>2</sub>O<sub>3</sub>-Fe<sub>3</sub>O<sub>4</sub> (re-used after 6 runs).

#### **TGA**

The thermal stability of the developed catalyst Cu@L-dopaSB/Al<sub>2</sub>O<sub>3</sub>-Fe<sub>3</sub>O<sub>4</sub> was evaluated by carrying out thermogravimetric analysis (TGA). **Figure3.10** shows the comparison of TGA curves of (a) Al<sub>2</sub>O<sub>3</sub>-Fe<sub>3</sub>O<sub>4</sub> (b) L-dopaSB/Al<sub>2</sub>O<sub>3</sub>-Fe<sub>3</sub>O<sub>4</sub> (c) Cu@L-dopaSB/Al<sub>2</sub>O<sub>3</sub>-Fe<sub>3</sub>O<sub>4</sub>. The primary weight loss of about 5 wt% below 150 °C in all the TGA curves accounts to the loss of residual solvents and moisture content from the surface of catalyst. Additionally, except the TGA curve of Al<sub>2</sub>O<sub>3</sub>-Fe<sub>3</sub>O<sub>4</sub> (**Figure3.10a**), the other two TGA curves (**Figure3.10b** and **3.10c**) exhibits two-stage

decomposition between 200 °C and 500 °C. In the initial stage of thermal decomposition, weight loss of 14.5 wt% in the temperature range below 350 °C, could be attributed to the loss of covalently bonded moieties onto Al<sub>2</sub>O<sub>3</sub>-Fe<sub>3</sub>O<sub>4</sub>magnetic nanoparticles. In the second stage, weight loss of 8.5 wt% in the temperature above 420 °C, corresponds to the decomposition of aromatic framework and unreacted molecules from the developed catalyst. It has been observed that anchoring of Cu (II) onto the surface of L-dopaSB/Al<sub>2</sub>O<sub>3</sub>-Fe<sub>3</sub>O<sub>4</sub> decreased the overall thermal constancy of Cu@L-dopaSB/Al<sub>2</sub>O<sub>3</sub>-Fe<sub>3</sub>O<sub>4</sub> which could be ascribed to the thermal degrading of the metal species resulting in the lowering of the activation energy [12]. After 600 °C, no significant thermal decomposition or weight loss was notified in all the three curves indicating the thermal stability of developed materials at elevated temperatures.

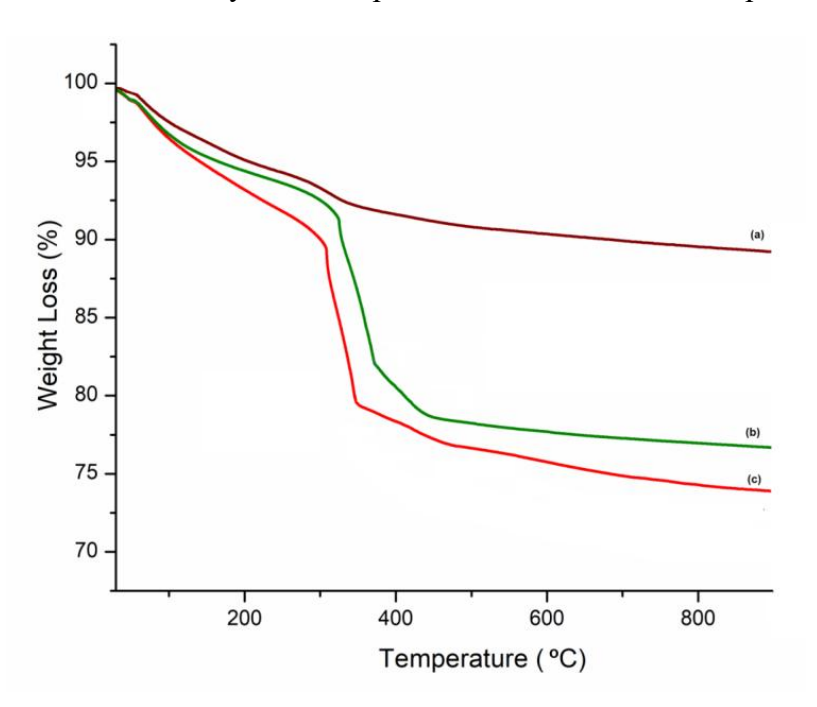


**Figure 3.10** TGA curves of (a) Al<sub>2</sub>O<sub>3</sub>-Fe<sub>3</sub>O<sub>4</sub> (b) L-dopaSB/Al<sub>2</sub>O<sub>3</sub>-Fe<sub>3</sub>O<sub>4</sub> (c) Cu@L-dopaSB/Al<sub>2</sub>O<sub>3</sub>-Fe<sub>3</sub>O<sub>4</sub>

#### **VSM**

The magnetic characteristics of the newly synthesized materials were explored using VSM i.e., Vibrating Sample Magnetometry at room temperature (**Figure 3.11**). The saturation magnetization value of L-dopaSB/Al<sub>2</sub>O<sub>3</sub>-Fe<sub>3</sub>O<sub>4</sub> (**Figure 3.11a**), Cu@L-dopaSB/Al<sub>2</sub>O<sub>3</sub>-Fe<sub>3</sub>O<sub>4</sub> (**Figure 3.11b**) and Cu@L-dopaSB/Al<sub>2</sub>O<sub>3</sub>-Fe<sub>3</sub>O<sub>4</sub> (re-

used after 6 runs) (**Figure 3.11c**) are found to be 16.25 and 11.72 emu g<sup>-1</sup>and 8.81 emu g<sup>-1</sup>respectively, which are comparatively lower than the reported value of saturation magnetization for Fe<sub>3</sub>O<sub>4</sub> nanoparticles [13]. This decrease in the saturation value accounts to the grafting of non-magnetic components (Cu@L-dopaSB/Al<sub>2</sub>O<sub>3</sub>-Fe<sub>3</sub>O<sub>4</sub>) on the surface of Fe<sub>3</sub>O<sub>4</sub> nanoparticles which mediates metal charge transfer effect, thus quenching the unpaired d-electrons of Fe<sup>3+</sup> ions. Nevertheless, the novel catalyst and the re-used catalyst after 6 runs are still magnetically strong enough to be detached using external magnet.

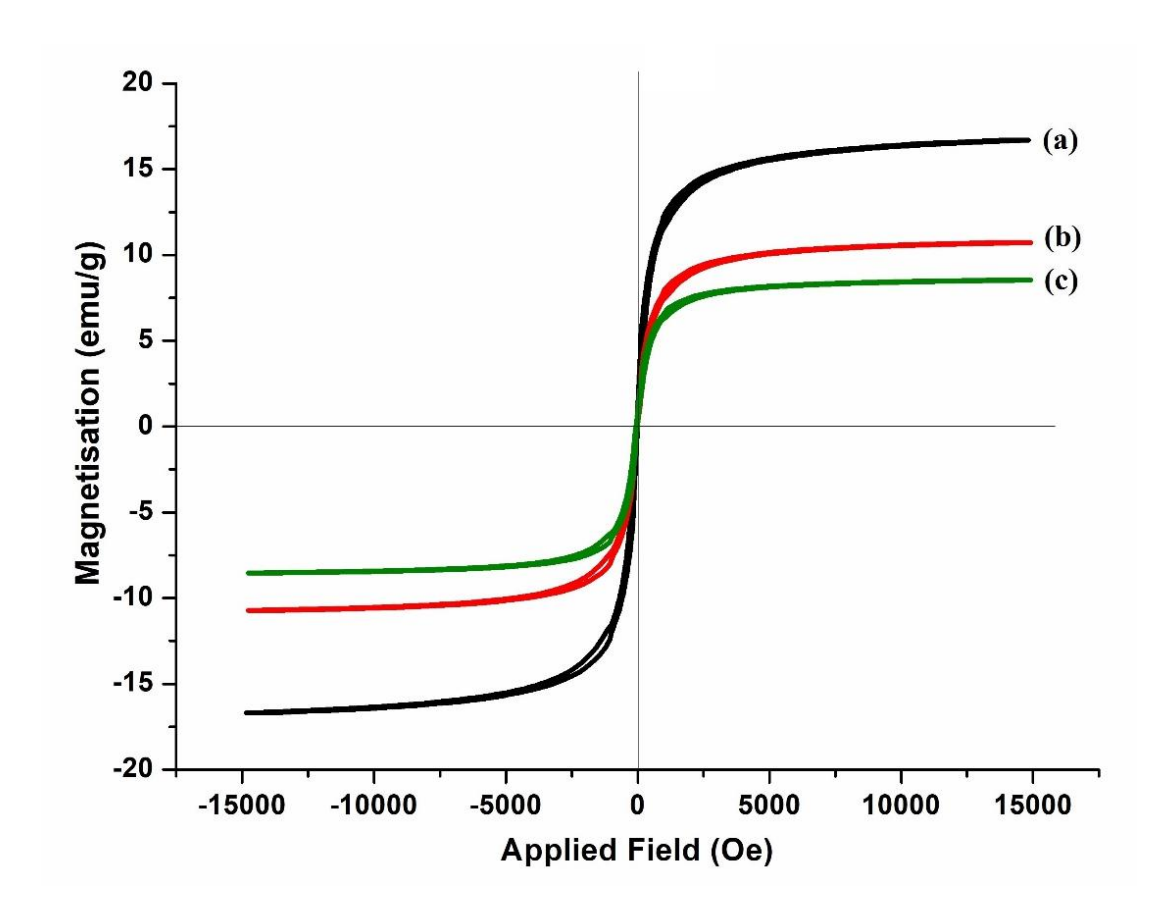


**Figure 3.11** VSM spectra (a)L-dopaSB/Al<sub>2</sub>O<sub>3</sub>-Fe<sub>3</sub>O<sub>4</sub> (b) Cu@L-dopaSB/Al<sub>2</sub>O<sub>3</sub>-Fe<sub>3</sub>O<sub>4</sub> (c) Cu@L-dopaSB/Al<sub>2</sub>O<sub>3</sub>-Fe<sub>3</sub>O<sub>4</sub> (re-used after 6 runs).

#### **CHNS**

The successful functionalization of L-dopa based Schiff Base over the surface of Al<sub>2</sub>O<sub>3</sub>-Fe<sub>3</sub>O<sub>4</sub>was also confirmed by CHNS analysis and the result inferred that

Cu@L-dopaSB/Al<sub>2</sub>O<sub>3</sub>-Fe<sub>3</sub>O<sub>4</sub> is composed of 6.57 % of Carbon, 1.60 % of Hydrogen, 1.48 % of Nitrogen and 1.32 % Sulphur element.

#### **ICP-AES**

The amount of copper loaded onto Cu@L-dopaSB/Al<sub>2</sub>O<sub>3</sub>-Fe<sub>3</sub>O<sub>4</sub>, was evaluated by ICP-AES analysis. The outcomes revealed that the Cu content loaded onto 0.1 g of Fe<sub>3</sub>O<sub>4</sub>-TiO<sub>2</sub>/SB was 3.10 wt%. Moreover, the ICP-AES of recovered catalyst after Six catalytic runs was also recorded to ensure any possibility of Cu leaching from the surface of support (L-dopaSB/Al<sub>2</sub>O<sub>3</sub>-Fe<sub>3</sub>O<sub>4</sub>) and the corresponding results established the stability of the developed catalyst and no considerable loss of the Cu was observed even after Six catalytic cycles (3.06 wt% Cu).

#### 3.1.3 References

- [1].Bhardwaj, M., Sharma, H., Paul, S. and Clark, J.H. 2016. Fe<sub>3</sub>O<sub>4</sub>@ SiO<sub>2</sub>/EDAC–Pd (0) as a novel and efficient inorganic/organic magnetic composite: sustainable catalyst for the benzylic C–H bond oxidation and reductive amination under mild conditions. *New Journal of Chemistry*, 40(6), pp 4952-4961.
- [2]. Hasan, K., Joseph, R.G., Shehadi, I.A. and Patole, S.P., 2023. Fe<sub>3</sub>O<sub>4</sub>-chitosan immobilized Cu (II) Schiff base catalyst for the microwave-assisted amination of aryl halides in water. *Arabian Journal of Chemistry*, *16* (12), pp 105317.
- [3]. Han, M.S., Lee, B.G., Ahn, B.S., Moon, D.J. and Hong, S.I., 2003. Surface properties of CuCl2/AC catalysts with various Cu contents: XRD, SEM, TG/DSC and CO-TPD analyses. *Applied surface science*, 211(1-4), pp 76-81.
- [4]. Kaur, M., Sharma, S., Choudhary, A., and Paul, S., 2023. Tuning the catalytic performance of a Cu supported silica modified γ-Al 2 O 3 nanocatalyst via cobalt-doping for A 3-coupling. *Reaction Chemistry & Engineering*, 8(9), pp 2141-2155.
- [5]. Martínez, J.M.L., Rodriguez-Castellón, E., Sánchez, R.M.T., Denaday, L.R., Buldain, G.Y. and Dall'Orto, V.C., 2011. XPS studies on the Cu (I, II)-

- polyampholyte heterogeneous catalyst: An insight into its structure and mechanism. *Journal of Molecular Catalysis A: Chemical*, 339(1-2), pp 43-51.
- [6]. Fun, H.K., Yip, B.C., Lu, Z.L., Duan, C.Y., Tian, Y.B. and You, X.Z., 1996. Synthesis, characterization and crystal structure of a tris (2-aminoethyl) amine copper complex with a imidazole coligand. *Transition Metal Chemistry*, 21, pp 193-196.
- [7]. Nasr-Esfahani, M., Mohammadpoor-Baltork, I., Khosropour, A.R., Moghadam, M., Mirkhani, V. and Tangestaninejad, S., 2013. Synthesis and characterization of Cu (II) containing nanosilica triazine dendrimer: A recyclable nanocomposite material for the synthesis of benzimidazoles, benzothiazoles, bis-benzimidazoles and bis-benzothiazoles. *Journal of Molecular Catalysis A: Chemical*, 379, pp 243-254.
- [8]. Kumar, A., Verma, S. and Pathak, D. D., 2021. Synthesis and characterization of a recyclable graphene oxide-surface-engineered copper (II) Schiff base complex: Catalytic application in synthesis of 1, 2, 3-triazoles and 2H-indazoles. *Journal of Environmental Chemical Engineering*, 9(4), pp 105791.
- [9].Karimi, M.A., Mohammadi, S.Z., Mohadesi, A., Hatefi-Mehrjardi, A., Mazloum-Ardakani, M., Korani, L.S. & Kabir, A.A., 2011. Determination of silver (I) by flame atomic absorption spectrometry after separation/preconcentration using modified magnetite nanoparticles. *Scientia Iranica*, 18(3), pp 790-796.
- [10]. Tekiye, E.S., Aghajani, Z. & Sharif, M.A., 2017. Synthesis and characterization of Fe<sub>3</sub>O<sub>4</sub>@Al<sub>2</sub>O<sub>3</sub> nanoparticles and investigation its catalyst application. *Journal of Materials Science: Materials in Electronics*, 28, pp 5360-5365.
- [11]. Benykhlef, S., Bekhoukh, A., Berenguer, R., Benyoucef, A. &Morallon, E., 2016. PANI-derived polymer/Al<sub>2</sub>O<sub>3</sub> nanocomposites: synthesis, characterization, and electrochemical studies. *Colloid and Polymer Science*, 294, pp 1877-1885.

- [12]. Lee, J.Y., Liao, Y., Nagahata, R. & Horiuchi, S., 2006. Effect of metal nanoparticles on thermal stabilization of polymer/metal nanocomposites prepared by a one-step dry process. *Polymer*, 47(23), pp 7970-7979.
- [13]. Veisi, H., Gholami, J., Ueda, H., Mohammadi, P. and Noroozi, M., 2015. Magnetically palladium catalyst stabilized by diaminoglyoxime-functionalized magnetic Fe<sub>3</sub>O<sub>4</sub> nanoparticles as active and reusable catalyst for Suzuki coupling reactions. *Journal of Molecular Catalysis A: Chem*, 396, pp 216-223.

# Section 3.2 Cu@L-dopaSB/Al<sub>2</sub>O<sub>3</sub>-Fe<sub>3</sub>O<sub>4</sub>as an efficientSchiff base functionalized magnetically recoverable catalyst for the single pot production of 1,4-Disubstituted-1,2,3-Triazoles using Boronic Acids under sustainable conditions

Triazoles have long been remained a centre of attraction for the researchers owing to their wide range of applicability both in industries as well as in medicines [1]. These acclaimed organic moieties are the most significant and utilitarian set of compounds in the present era [2]. The 1,2,3-triazoles display extensive biological actionsfor instance, anticancer 6 antifungal [3], anti-HIV [4], antioxidant [5] and antimalarial [6]. Numerous drugs like rufinamide, cefatrizine, carboxyamidotriazole and tazobactam contain 1,2,3-triazole in their composition. (Figure 3.12) [7-8]. Additionally, these 1,4-disubstituted-1,2,3-triazoles also employed as ligation tool in the making of multivalent dendrimeric peptides, neoglyco-conjugates [9], triazolophanes [10], cyclic peptides [11], peptidomimetics [12] and ionic receptors [13] etc.

**Figure 3.12** Drugs containing 1,2,3-triazole motif.

In 2002, Sharpless and Meldal made significant contributions to the field of organic chemistry by independently synthesizing the highly regarded 1,2,3-Triazoles through the innovative 1,3-dipolar cycloaddition of azide-alkyne click reaction. [14]. With the winning of noble prize for click chemistry in the year 2022, the one pot synthesis reactions have once again garnered the attention of the chemists all around the world. Mostly, methodologies reported for the 1,4-disubstituted-1,2,3-triazoles productionare very competent, yet they suffer severe drawbacks. These transformations generally involve the usage of organic azides or sodium azides, which are highly toxic. Although these organic azides are usually stable at normal reaction conditions, but, high temperatures results in decomposition of aryl azides[15]. Also, lower molecular weight derivatives of azide can be explosive at times. Hence, more methodologies are advantageous which involve one-pot procedures for 1,2,3-triazoles synthesis via *in situ* production of aryl azides in the company of the alkynes.

A thorough literature review indicated that while azide and phenylacetylene are common reactants for triazole synthesis, the inclusion of a third component, such as aryl halides, boronic acids, or amines, has proven effective, leading to high product yields in all cases [16-18]. It is however, the boronic acids which have been chosen for the synthesis of triazoles via click chemistry due to their mild behaviour and low toxicity compared to others. Furthermore, boronic acids have been shown to accelerate triazole formation in one-pot processes by serving as precursors for in situ azide generation [19-21].

In light of these factors, we synthesized a Schiff base functionalized copper(II) complex supported on L-dopa and combined with Al<sub>2</sub>O<sub>3</sub>-Fe<sub>3</sub>O<sub>4</sub>, as an effective magnetic nanocomposite for the single-pot production of 1,4-disubstituted-1,2,3-triazoles using aryl/alkyl boronic acids (**Figure 3.13**). To date, most of the work that has been described for the synthesis of 1,2,3-triazoles with alkyl substituents gives very low yields [22-25], so we have made substantial efforts to develop a sustainable Cu@L-dopaSB/Al<sub>2</sub>O<sub>3</sub>-Fe<sub>3</sub>O<sub>4</sub> catalyzed protocol for the synthesis of alkyl/aryl-substituted-1,2,3-triazoles in high yields.

$$R=B(OH)_2 + NaN_3 + = R' \qquad \frac{Cu@L-dopaSB/Al_2O_3-Fe_3O_4}{EtOH:H_2O (1:1), 60 °C} \qquad R=N$$

**Figure 3.13** Cu@L-dopaSB/Al<sub>2</sub>O<sub>3</sub>-Fe<sub>3</sub>O<sub>4</sub> catalyzed synthesis of alkyl/aryl-substituted-1,2,3-triazoles.

#### 3.2.1 Results and discussion

#### Optimization of the reaction conditions

To optimize the reaction conditions, phenylacetylene, phenyl boronic acids, and sodium azide were used as test substrate in the model reaction. Several parameters like catalyst, catalyst amount, solvent, time and temperature were optimized and the findings are listed in Table 3.1 & 3.2. First, the reaction was performed without the catalyst but no desired product could be obtained even after 12 h stirring at 60°C (Table 3.1, entry 1). To explore the role of support, the reaction under the similar conditions was performed using 0.05 g of various supports as catalyst such as Al<sub>2</sub>O<sub>3</sub>, Fe<sub>3</sub>O<sub>4</sub>, Al<sub>2</sub>O<sub>3</sub>-Fe<sub>3</sub>O<sub>4</sub>, L-dopa@Al<sub>2</sub>O<sub>3</sub>-Fe<sub>3</sub>O<sub>4</sub> and LdopaSB/Al<sub>2</sub>O<sub>3</sub>-Fe<sub>3</sub>O<sub>4</sub> and yields 15%, 25%, 30%, 37% and 49% were obtained respectively (Table 3.1, entry 2-6). Thereafter, various copper (II) salts such as Copper oxide (CuO), Copper Chloride (CuCl<sub>2</sub>) and Copper Acetate [Cu(OAc)<sub>2</sub>] in the same amounts were also tested for catalyzing the model reaction and an appreciable increase in the amount of yield was noticed in all the cases (Table 3.1, entry 7-9). From the results, it has been concluded that among all the supports, Schiff base functionalized support catalyzes the reaction to form highest amount of desired product whereas Cu(OAc)<sub>2</sub> provides the highest amount of yield among all the copper(II) salts. Thereafter, while keeping other conditions unaltered, the test reaction was conducted by using 0.05 g of the synthesized catalytic system at room temperature, which afforded 70% of the product in 8 h, however the yield marginally increased to 76% when the same reaction was run for 12h (**Table 3.1**, entry 10-11). The reaction was then proceeded at 60°C and the yield significantly increased to 97% in 4h (Table 3.1, entry 12), however when the reaction was further carried for 6 h, no considerable change in the amount of yield was noticed. To check whether the variation in the amount of catalyst can alter the yield percentage, the reaction was first carried by doubling the amount of the catalyst (0.1 g) and secondly by taking half of the amount of catalyst (0.025 g). In the former case, a slight increase while in the latter case a decrease in the product yield was obtained (**Table 3.1**, **entry 13-14**). Thus, the amount 0.05 g (0.85 mol% Cu) of developed catalyst i.e., Cu@L-dopaSB/Al<sub>2</sub>O<sub>3</sub>-Fe<sub>3</sub>O<sub>4</sub> has been found to be enough to catalyze the reaction to give best results (**Table 3.1**, **entry 12**).

**Table 3.1.** Optimization of reaction conditions for the one-pot synthesis of 1,4-disubstituted -1,2,3 triazoles.

Entry	Catalyst	Amount	Temp	Time	Yield
		(g)	(°C)	(h)	(%) <sup>b</sup>
1.	Without catalyst	-	60	12	Nil
2.	$Al_2O_3$	0.05g	60	12	15
3.	Fe <sub>3</sub> O <sub>4</sub>	0.05g	60	12	25
4.	$Al_2O_3$ - $Fe_3O_4$	0.05g	60	12	30
5.	L-dopa@Al <sub>2</sub> O <sub>3</sub> -Fe <sub>3</sub> O <sub>4</sub>	0.05g	60	12	37
6.	L-dopaSB/Al <sub>2</sub> O <sub>3</sub> -Fe <sub>3</sub> O <sub>4</sub>	0.05g	60	12	49
7.	$Cu(OAc)_2$	0.05g	60	08	67
8.	$CuCl_2$	0.05g	60	08	62
09.	CuO	0.05g	60	08	52
10.	Cu@L-dopaSB/Al <sub>2</sub> O <sub>3</sub> -Fe <sub>3</sub> O <sub>4</sub>	0.05g	RT	08	70
11.	Cu@L-dopaSB/Al <sub>2</sub> O <sub>3</sub> -Fe <sub>3</sub> O <sub>4</sub>	0.05g	RT	12	76
12.	Cu@L-dopaSB/Al <sub>2</sub> O <sub>3</sub> -Fe <sub>3</sub> O <sub>4</sub>	0.05g	60	04	97
13.	Cu@L-dopaSB/Al <sub>2</sub> O <sub>3</sub> -Fe <sub>3</sub> O <sub>4</sub>	0.1g	60	04	98
14.	Cu@L-dopaSB/Al <sub>2</sub> O <sub>3</sub> -Fe <sub>3</sub> O <sub>4</sub>	0.025g	60	04	90
14.	Cu@L-dopaSB/Al <sub>2</sub> O <sub>3</sub> -Fe <sub>3</sub> O <sub>4</sub>	0.025g	60	04	9

<sup>&</sup>lt;sup>a</sup>Reaction conditions: Arylboronic acid (1 mmol), Phenylacetylene (1.5 mmol), NaN<sub>3</sub> (2 mmol), Cu@L-dopaSB/Al<sub>2</sub>O<sub>3</sub>-Fe<sub>3</sub>O<sub>4</sub> (0.05g, 0.85 mol% Cu), EtOH:H<sub>2</sub>O (1:1, 5mL) at 60 °C.

<sup>&</sup>lt;sup>b</sup>Isolated yields.

We have also examined the effects of several solvents on the model reaction in order to better optimize the reaction conditions. (Table 3.2, entries 1-14). Keeping in consideration the environment-friendly protocols for carrying out the reaction, various solvents such as water, methanol, acetonitrile, ethanol and the mixture of these solvents in different ratios was used. To begin with, the reaction was carried out at room temperature. in solvent free conditions and then at a temperature of 60°C for 4h, both of which gave desired products in good yield; nevertheless higher amount of product was obtained when the reaction is carried out at 60°C (Table 3.2, entry 1). In the same pattern, reaction was performed in the presence of solvents such as H<sub>2</sub>O, CH<sub>3</sub>OH, C<sub>2</sub>H<sub>5</sub>OH, and CH<sub>3</sub>CN. In all the cases, conversion was more efficient for the reaction performed at 60°C (Table 3.2, entries 2-5). In the wake of the recent approaches in green chemistry, the role of co-solvents cannot be undermined for carrying out the reactions. In this regard, the model reaction was performed in different ratios of solvents, and it was observed that a (1:1) ratio of H<sub>2</sub>O with CH<sub>3</sub>OH, C<sub>2</sub>H<sub>5</sub>OH and CH<sub>3</sub>CN, respectively, gives the highest yield (**Table 3.2**, entries 6-14). Among all of them, EtOH:H<sub>2</sub>O (1:1) combination of solvent was observed as most appropriate for the required transformation at 60°C (Table 3.2, entry 9). The best results using EtOH:H<sub>2</sub>O (1:1) solvent system may be due to greater solubility of reactants in this co-solvent system or due to an increase in the number of collisions between the substrates which resulted in enhancement of their ground state energy and hence greater reaction rates. So the EtOH:H<sub>2</sub>O (1:1) co-solvent system has been found to be most effective, convenient and efficient for the required transformation. Hence, it could be concluded that the best results for the formation of triazoles can be achieved using 0.05 g (0.85 mol% Cu) of Cu@L-dopaSB/Al<sub>2</sub>O<sub>3</sub>-Fe<sub>3</sub>O<sub>4</sub>as a catalyst, in EtOH:H<sub>2</sub>O co-solvent system at 1:1 ratiofor 4 h at 60°C (**Table 3.2**, entry 9).

After establishing the optimal reaction conditions, we observed the successful formation of 1,4-disubstituted-1,2,3-triazoles using variously substituted aryl boronic acids and aryl alkynes (**Figure 3.13**). The effect of electron donating groups such as -CH<sub>3</sub>, -OCH<sub>3</sub> (**Table 3.3**, entry 2 and 3) and electron-withdrawing groups such as -Cl, -F, -Br and -NO<sub>2</sub>(**Table 3.3**, entry 4 to 9) were also investigated for the reaction and the products were obtained in excellent yield. Next, the reaction of differently substituted aryl alkynes with aryl boronic acids was carried out, and an excellent yield

was afforded (**Table 3.3**, **entries 10** and **11**). Furthermore, with these optimized reaction conditions, the activity of the catalyst was also tested to perform the reaction between various alkyl boronic acids and phenylacetylene, and the results showed a good conversion rate in all the cases (**Table 3.3**, **entries 12** to **15**). <sup>1</sup>H-NMR and <sup>13</sup>C-NMR spectroscopy were used to identify the isolated derivatives of 1,4-disubstituted 1,2,3-triazole.

**Table 3.2.** Optimization of solvent for the one-pot synthesis of 1,4-disubstituted-1,2,3 triazole from arylboronicacids and phenylacetylene.

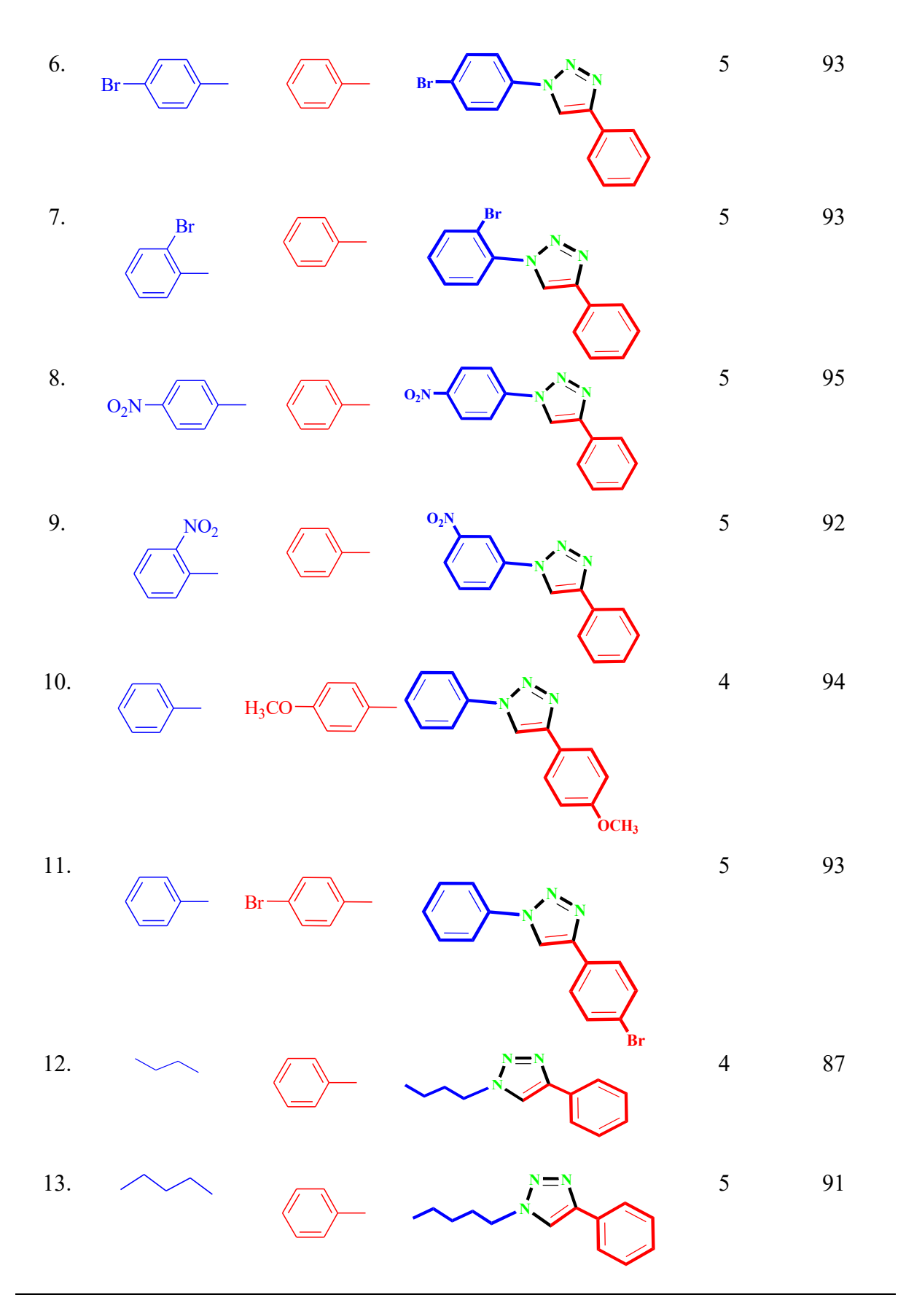
Entry	Solvent	Temperature	Time (h)	Yield (%)
1.	Neat	RT		25
		60	4h	40
2.	$H_2O$	RT		55
		60	4h	76
3.	СН <sub>3</sub> ОН	RT		50
		60	4h	68
4.	C <sub>2</sub> H <sub>5</sub> OH	RT		52
		60	4h	72
5.	CH <sub>3</sub> CN	RT		45
		60	4h	62
6.	H <sub>2</sub> O:CH <sub>3</sub> OH(1:1)	60	4h	84
7.	H <sub>2</sub> O:CH <sub>3</sub> OH(2:1)	60	4h	78
8.	H <sub>2</sub> O:CH <sub>3</sub> OH(1:2)	60	4h	72
9.	H <sub>2</sub> O:C <sub>2</sub> H <sub>5</sub> OH(1:1)	60	4h	97
10.	H <sub>2</sub> O:C <sub>2</sub> H <sub>5</sub> OH(2:1)	60	4h	92

11.	$H_2O:C_2H_5OH(1:2)$	60	4h	89	
12.	H <sub>2</sub> O:CH <sub>3</sub> CN(1:1)	60	4h	64	
13.	H <sub>2</sub> O:CH <sub>3</sub> CN(2:1)	60	4h	59	
14.	H <sub>2</sub> O:CH <sub>3</sub> CN(1:2)	60	4h	55	

 $<sup>^</sup>aReaction$  conditions: Arylboronic acid (1 mmol), Phenylacetylene (1.5 mmol), NaN₃ (2 mmol), Cu@L-dopaSB/Al₂O₃-Fe₃O₄ (0.05g, 0.85 mol% Cu).  $^bIsolated\ yields.$ 

 $\textbf{Table 3.3} \ \ \text{Cu@L-dopaSB/Al}_2\text{O}_3\text{-Fe}_3\text{O}_4 \ \text{catalysed synthesis of 1,4-disubstituted-1,2,3-triazoles}^a$ 

Entry	R	R'	Product	Time (h)	Yield (%) <sup>b</sup>
1.				5	96
2.	H <sub>3</sub> CO		H <sub>3</sub> CO-NNNNNNNNNNNNNNNNNNNNNNNNNNNNNNNNNNNN	5	94
3.	H <sub>3</sub> C		H <sub>3</sub> C	5	93
4.	F———		F-NNNN	3.5	95
5.	Cl			5	94



<sup>a</sup>Reaction conditions: Aryl/Alkylboronic acid (1 mmol), aryl alkyne (1.5 mmol), NaN<sub>3</sub> (2 mmol), Cu@L-dopaSB/Al<sub>2</sub>O<sub>3</sub>-Fe<sub>3</sub>O<sub>4</sub> (0.05g, 0.85 mol% Cu), EtOH:H<sub>2</sub>O (1:1, 5mL) at 60 °C.

Isolated Yields.

#### Proposed mechanism

Designed for the manufacture of 1,4-disubstituted-1,2,3-triazoles by usingcatalyst, Cu@L-dopaSB/Al<sub>2</sub>O<sub>3</sub>-Fe<sub>3</sub>O<sub>4</sub> [26–27], a tenable reaction mechanism has been suggested (**Figure 3.14**). It is hypothesized that initiallyformed Cu (I) complex is formed when sodium azide first coordinates with Cu@L-dopaSB/Al<sub>2</sub>O<sub>3</sub>-Fe<sub>3</sub>O<sub>4</sub>. After that, an intermediate (II) is formed by adding aryl azide, which is created in situ when arylboronic acid and sodium azide combine. The intermediate product (III) is then produced by adding phenylacetylene. After that, the nitrogen atom of the azide successfully attacked the C-2 carbon of the Cu-acetylidine, forming a 6-membered copper metallacycle (IV) intermediate. This crucial step is pivotal, as the metallacycle's ring contraction regenerates the catalyst and leads to the production of a Cu(I)-triazolide complex (V). This complex plays a vital role in ultimately facilitating the synthesis of the triazole (VI), showcasing the elegance of this catalytic process.

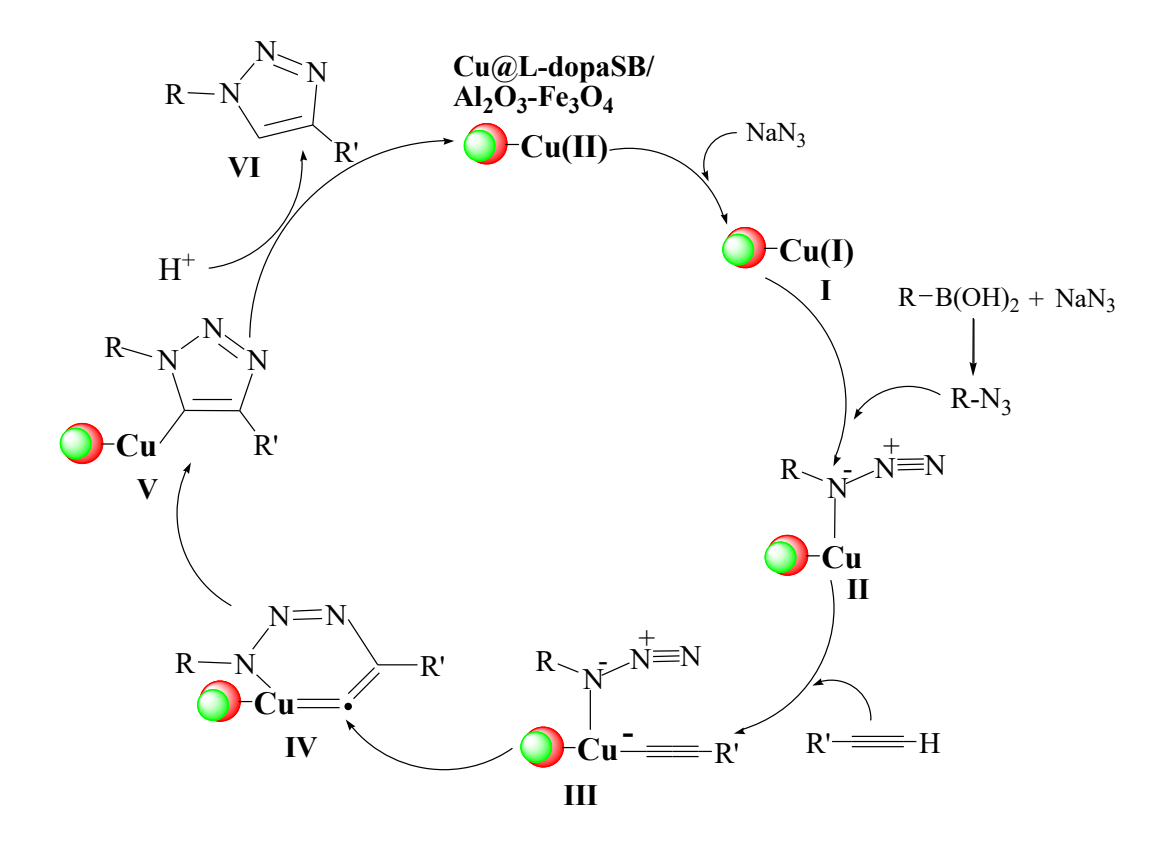


**Figure 3.14** Plausible mechanism for the Cu@Fe<sub>3</sub>O<sub>4</sub>@Al<sub>2</sub>O<sub>3</sub>/SBcatalyzed synthesis of 1,4-disubstituted 1,2,3-triazoles

#### Recyclability and Heterogeneity

The recyclability of  $Cu@Fe_3O_4@Al_2O_3/SB$ was rigorously assessed for the synthesis of 1,4-disubstituted-1,2,3-triazoles to confirm that the established catalytic system adheres to sustainability standards. As illustrated in **Table 3.1**, **entry 1**, this evaluation highlighted the catalyst's impressive recyclability. After the reaction concluded, by applying magnetic separation using an external magnet, we were able to effectively remove the catalyst from the reaction composition. Following this, we meticulously washed the catalyst with ethyl acetate (3 × 10 mL) and deionized water (3 × 10 mL), dried it thoroughly, and prepared it for reapplication in the subsequent cycle. This process underscores our commitment to sustainable practices in chemical synthesis. The catalytic activity of the catalyst was probed for six repeated runs, and no substantial decline in activity was detected (**Figure 3.15**), which reveals that the catalyst is recyclable and thus can be efficiently employed for more than six runs. In

order to further inspect the stability of the recovered catalyst after the 6<sup>th</sup> run, we examined its structure using XPS, FTIR, XRD, and ICP-AES analysis, and the results pointed towards insignificant structural change compared to the fresh catalyst.

A hot filtration test was conducted to investigate and confirm the heterogeneity of the catalytic system. The model reaction was made to progress in the presence of the catalyst under optimized conditions, awaiting the conversion was 48 %. The reaction was stopped, and after the catalyst was removed from the reaction mixture, the reaction was continued for four hours. Afterwards, no change in the yield of the product was noticed. The result obtained thus rules out the homogeneity of the catalyst as no leaching of the catalyst was observed.

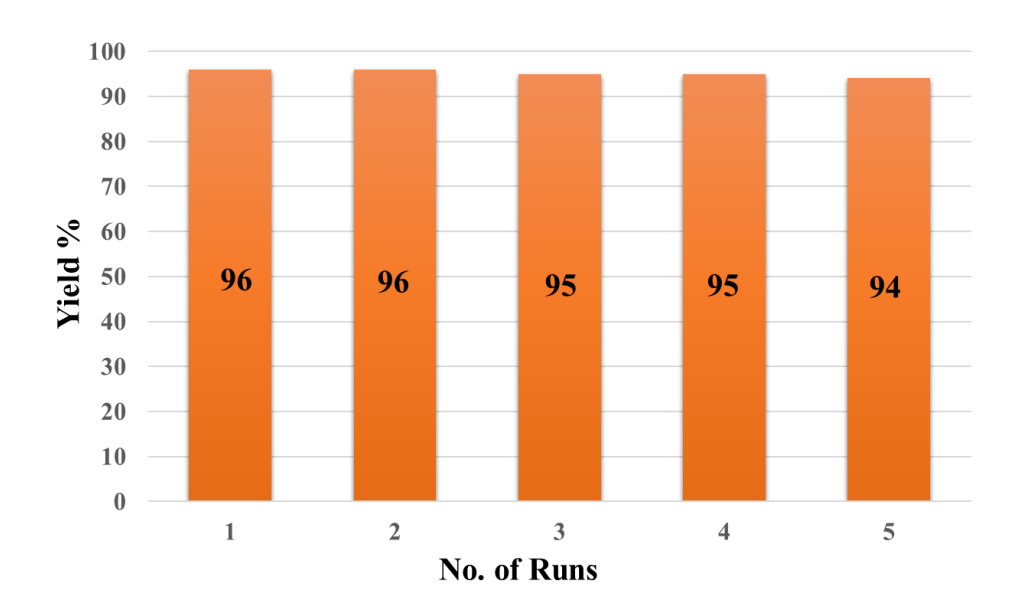


**Figure 3.15** Recyclability ofCu@L-dopaSB/Al<sub>2</sub>O<sub>3</sub>-Fe<sub>3</sub>O<sub>4</sub>; Reaction conditions: Arylboronic acid (1 mmol), Phenylacetylene (1.5 mmol), NaN<sub>3</sub> (2 mmol), Cu@L-dopaSB/Al<sub>2</sub>O<sub>3</sub>-Fe<sub>3</sub>O<sub>4</sub> (0.05g, 0.85 mol% Cu), EtOH:H<sub>2</sub>O (1:1, 5mL) at 60 °C. <sup>b</sup>Isolated yields.

#### 3.2.2 Conclusion

Starting from aryl/alkyl boronic acids, for which there are only a few catalytic systems documented in the literature, we have created a unique Schiff Base functionalized Cu@L-dopaSB/Al<sub>2</sub>O<sub>3</sub>-Fe<sub>3</sub>O<sub>4</sub>as an effective magnetic nanocomposite for the three-component one-pot synthesis of 1,4-disubstituted-1,2,3-triazoles. We

have used aryl/alkyl boronic acids as the substrates for the synthesis of triazoles due to their economical and mild nature and low toxicity as compared to other substrates. Most importantly, our method purifies the product by straightforward crystallization from an environmentally acceptable solvent and does not call for the use of an external reducing agent when sodium azide is present in the reaction media. Moreover, this protocol offers several advantages like simplicity in operation, easy separation, and recyclability, which asserts its high activity for click reaction. The catalyst's magnetic properties enable straightforward recovery from the reaction mixture, allowing it to be reused up to six times while maintaining its full catalytic potential.

## Comparison with catalysts documented in the literature for the synthesis of 1,4-disubstituted 1,2,3-triazoles

We have conducted a comprehensive comparison of the catalytic activity of Cu@L-dopaSB/Al<sub>2</sub>O<sub>3</sub>-Fe<sub>3</sub>O<sub>4</sub> against other catalyst systems documented in the literature for the production of 1,4-disubstituted 1,2,3-triazoles. The results establish the dominance of our innovative catalytic system. This protocol is not only more effective but also embodies a highly sustainable approach compared to existing catalysts for 1,4-disubstituted 1,2,3-triazoles. It demonstrates a significantly reduced reaction time, utilizes environmentally friendly solvents, employs cost-effective and less toxic aryl/alkyl boronic acids, operates at lower temperatures, achieves impressive yields, and facilitates magnetic separation and recyclability (**Table 3.4**).

**Table 3.4** Evaluation of catalytic activity of Cu@L-dopaSB/Al<sub>2</sub>O<sub>3</sub>-Fe<sub>3</sub>O<sub>4</sub>in comparison to other documented catalyst systems for the production of 1,4-disubstituted-1,2,3 triazoles.

Catalyst system	Set up conditions	Time (h)	Yield (%)	Ref.
$Cu_2$ – $\beta$ - $CD$	Boronic acid, Phenylacetylene, NaN <sub>3</sub> ,	04	94	20
	water, r.t.			
CuI/II@Cys-MGO	Boronic acid, Phenylacetylene,NaN <sub>3</sub> ,	05	85	28
	H <sub>2</sub> O:EtOH, 60°C.			
Cu-PsIm	Aniline, NaNO2, NaN3, HCl:H2O, r.t.	7-8	97	29
$Cu(OAc)_2$	Aniline, N-tosylhydrazone, PivOH,	12	73	30
	toluene, 100°C.			
Go-SB-Cu	Benzyl halide, Phenylacetylene, NaN <sub>3</sub> ,	4-6	91	31
	CH <sub>3</sub> OH, r.t.			
CuFe <sub>2</sub> O <sub>4</sub> nanoparticles	Boronic acid, Phenylacetylene, NaN <sub>3</sub> ,	12	86	32
	water, r.t.			
PAN <sub>S2</sub> FCu (0.5 mol %)	Benzyl halide, Phenylacetylene, NaN <sub>3,</sub>	3.5	78	33
	water, 60°C.			
CuNPs@agarose	Aniline, t-BuONO, NaN3,	12	82	34
	Phenylacetylene, H <sub>2</sub> O and t-BuOH			
	(1:1), 40°C.			
CuI (5 mol %)	Phenylacetylene, phenacyl bromide,	8	81	35
,	NaN <sub>3</sub> , water or water:acetone (1:1), r.t.	1.6	0.7	2.6
Cu(II) SBA-15	Phenylacetylene, Azide,CH <sub>2</sub> Cl <sub>2</sub> , r.t.	16	87	36
Silica-APTS-Cu(I)	Phenylacetylene, benzylhalide, NaN <sub>3</sub> , EtOH, 78°C.		92	37
Cu@L-dopaSB/Al <sub>2</sub> O <sub>3</sub> -	Phenylacetylene, boronic acid, NaN <sub>3</sub> ,	4	97	This
Fe <sub>3</sub> O <sub>4</sub>	H <sub>2</sub> O:EtOH, 60°C.			work

## General Procedure for the Cu@L-dopaSB/Al<sub>2</sub>O<sub>3</sub>-Fe<sub>3</sub>O<sub>4</sub> catalyzedone-pot synthesis of 1,4- Disubstituted 1,2,3-Triazoles from aryl/alkylboronic acids

After adding Cu@L-dopaSB/Al<sub>2</sub>O<sub>3</sub>-Fe<sub>3</sub>O<sub>4</sub>(1.2 mol%, 0.05 g) and stirring for 10 minutes at room temperature, sodium azide (2 mmol) and aryl/alkylboronic acid (1 mmol) in H<sub>2</sub>O/EtOH (5 mL, 1:1) were added to a 50 mL round-bottom flask and stirred for an additional 20 minutes. Phenyl acetylene (1.1 mmol) was added to it, and the mixture was agitated for the proper amount of time at 60 °C (as observed by TLC). Following reaction completion, the catalyst was separated using a magnet and then cleaned with 2×10 mL of EtOAc, 2×10 mL of distilled H<sub>2</sub>O, and 2×10 mL of EtOH. It was reused for further reactions after being vacuum-dried. Thereafter, 1,4-disubstituted 1,2,3-triazoles were obtained in high purity by diluting the above reaction mixture with H<sub>2</sub>O and EtOAc to separate the phases. Carefully isolate the organic layer, then dry it over sodium sulfate to remove moisture. After the solvent was removed under low pressure, the final product was produced by recrystallizing it using n-hexane/EtOAc.

By using <sup>1</sup>H and <sup>13</sup>C NMR and comparing them to real samples that were either prepared using methods from the literature or purchased commercially, the structures of the products were verified.

#### 3.2.3 Characterization data of synthesized compounds (entry 1-15)

#### 1,4-diphenyl-1H-1,2,3 triazole



**M.pt.**176-178°C (Lit. M. pt. 175-177°C) [38]; <sup>1</sup>H NMR (400 MHz, CDCl<sub>3</sub>+ DMSO):  $\delta 6.52$ -6.55 (1H, t, J = 8.0 Hz), 6.63-6.67 (3H, m), 6.75-6.79 (2H, t, J = 8.0 Hz), 7.12-14 (4H, d, J = 8.0 Hz), 8.35 (1H, s); <sup>13</sup>C NMR (100 MHz, DMSO + CDCl<sub>3</sub>):  $\delta 117.6$ , 120.5, 125.8, 128.4, 128.8, 128.9, 129.8, 130.2, 137.1, 148.4. MS-ESI: m/z = 222 (M+1)<sup>+</sup>.

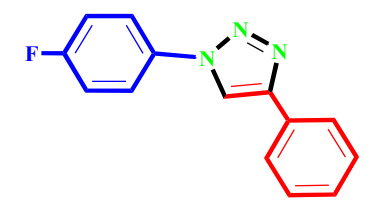
#### 1-(4-methoxyphenyl)-4-phenyl-1H-1,2,3-triazole

**M.pt.**168-169°C (Lit. M. pt. 167-168 °C[38]; <sup>1</sup>**H NMR (400 MHz, DMSO)**: $\delta$  3.05 (s, 3H), 6.37-6.39 (2H, d, J = 8.0 Hz), 6.57-6.60 (1H, t, J = 8.0 Hz), 6.68-6.72 (2H, t, J = 8.0 Hz), 7.05-7.08 (2H, d, J = 12.0 Hz), 7.13-7.15 (2H, d, J = 8.0 Hz), 8.4 (1H, s); <sup>13</sup>**C NMR (DMSO, 100 MHz)**: $\delta$  56.0, 115.4, 120.0, 122.1, 125.7, 128.6, 129.4, 130.5, 130.8, 147.5, 159.7. **MS-ESI**: m/z = 252 (M+1)<sup>+</sup>.

#### 1-(4-methylphenyl)-4-phenyl-1H-1,2,3-triazole

**M.pt.**157-159°C (Lit. M. pt. 159-160 °C[39]; <sup>1</sup>**H NMR (400 MHz, CDCl<sub>3</sub>):** $\delta$  2.46 (3H, s), 7.35-7.41 (3H, m), 7.47-7.51 (2H, t, J = 8.0 Hz), 7.68-7.70 (2H, d, J = 8.0 Hz), 7.93-7.95 (2H, d, J = 8.0 Hz), 8.19 (1H, s); <sup>13</sup>**C NMR (100 MHz, CDCl<sub>3</sub>)**:  $\delta$ 148.2,138.9, 134.7, 130.33, 130.30, 128.9, 128.3, 125.8, 120.4, 117.6, 21.1; **MS-ESI**: m/z = 236 (M+1)<sup>+</sup>.

#### 1-(4-Fluorophenyl)-4-phenyl-1H-1,2,3-triazole



**M.pt.**220-221°C (Lit. M. pt. 221-222[40]; <sup>1</sup>**H NMR (400 MHz, DMSO)**:  $\delta 6.54$ -6.58 (t, J = 8.0 Hz, 1H), 6.61-6.69 (m, 4H), 7.12-7.14 (d, J = 8.0 Hz, 2H), 7.17-7.21 (m,

2H), 8.42 (s, 1H); <sup>13</sup>C NMR (**400 MHz, DMSO**):  $\delta$  116.9, 117.2, 120.0, 122.5, 122.6, 125.7, 128.5, 129.2, 130.6, 147.8.**MS-ESI**: m/z = 240 (M+1)<sup>+</sup>.

#### 1-(4-chlorophenyl)-4-phenyl-1H-1,2,3-triazole (3e)

**M.pt.**184-185°C (Lit. M. pt. 185-186 °C[41]; <sup>1</sup>**H NMR (400 MHz, DMSO)**:  $\delta$  7.47-7.52 (3H, m), 7.77-7.80 (2H, d, J = 12.0 Hz), 7.92-7.94 (2H, d, J = 8.0 Hz), 8.01-8.02 (2H, d, J = 4.0 Hz), 8.20 (1H, s); <sup>13</sup>**C NMR (400 MHz, DMSO)**:  $\delta$  121.6, 117.4, 125.9, 127.7, 128.9, 128.6, 129.6, 130.0, 136.4, 142.6.**MS-ESI**: m/z = 256 (M)<sup>+</sup>, 258 (M+2)<sup>+</sup>.

#### 1-(4-Bromophenyl)-4-phenyl-1H-1,2,3-triazole

**M.pt.**229-230 °C (Lit. M. pt. 228-230 °C[41]; <sup>1</sup>**H NMR (400 MHz, DMSO)**:  $\delta$  7.38-7.43 (2H, m), 7.48-7.52, (2H, t, J = 8.0 Hz), 7.70-7.74 (3H, t, J = 8.0 Hz), 7.92-7.94 (2H, d, J = 8.0 Hz), 8.21 (1H, s); <sup>13</sup>**C NMR (400 MHz, DMSO)**:  $\delta$  120.5, 121.8, 122.8, 125.7, 126.2, 128.8, 130.4, 132.1, 135.4, 155.4.**MS-ESI**: m/z = 300 (M)<sup>+</sup>, 302 (M+2)<sup>+</sup>.

#### 1-(2-Bromophenyl)-4-phenyl-1H-1,2,3-triazole

**M.pt.**129-130 °C (Lit. M. pt. 128-129 °C[41]; <sup>1</sup>**H NMR (400 MHz, DMSO)**:  $\delta$  7.38-7.42 (t, J = 8.0 Hz, 1H), 7.48-7.51 (t, J = 8.0 Hz, 4H), 7.62-7.64 (m, 1H), 7.70-7.72 (m, 1H), 7.94-7.96 (d, J = 8.0 Hz, 2H), 8.24 (s, 1H); <sup>13</sup>**C NMR (400 MHz, DMSO)**:  $\delta$  121.6 , 125.9 ,127.8 ,128.0 ,128.4 ,128.6 ,128.9 ,130.1 ,130.8 ,134.9 ,147.6 .**MS-ESI**: m/z = 300 (M)<sup>+</sup> ,302 (M+2)<sup>+</sup>.

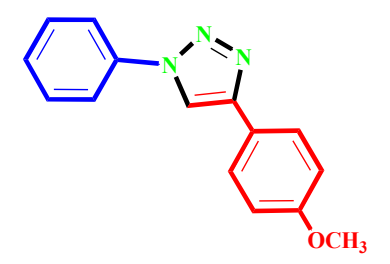
#### 1-(4-Nitrophenyl)-4-phenyl-1H-1,2,3-triazole

**M.pt.**234-235 °C (Lit. M. pt. 233-235°C[41]; <sup>1</sup>**H NMR (400 MHz, DMSO)**:  $\delta = 6.61$ -6.64 (1H, t, J = 8.0 Hz), 6.72-6.75 (2H, t, J = 8.0 Hz), 7.16-7.18 (2H, d, J = 8.0 Hz), 7.47-7.49 (2H, d, J = 8.0 Hz), 7.71-7.73 (2H, d, J = 8.0 Hz),8.74 (1H, s); <sup>13</sup>**C NMR (400 MHz, DMSO)**:  $\delta = 114.4$ , 120.1, 120.5, 126.0, 126.2, 131.7, 141.8, 144.5, 147.1.**MS-ESI**: m/z = 267 (M+1)<sup>+</sup>.

#### 1-(3-Nitrophenyl)-4-phenyl-1H-1,2,3-triazole

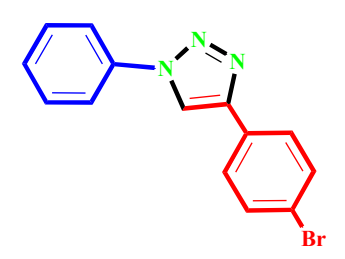
**M.pt.**202-203°C (Lit. M. pt. 201-203°C[41]; <sup>1</sup>**H NMR (400 MHz, DMSO)**:  $\delta$ 6.59-6.63 (t, J = 8.0 Hz, 1H), 6.71-6.74 (t, J = 8.0 Hz, 2H), 7.12-7.17 (m, 3H), 7.55-7.57 (d, J = 8.0, 1H), 7.65-7.67 (d, J = 8.0, 1H), 8.77 (s, 1H); <sup>13</sup>**C NMR (400 MHz, DMSO)**: $\delta$  115.0, 120.5, 123.6, 125.7, 126.3, 128.9, 129.5, 130.3, 132.1, 137.6, 148.1, 149.0.**MS-ESI**: m/z = 267 (M+1)<sup>+</sup>.

#### 4-(4-Methoxyphenyl)-1-phenyl-1H-1,2,3-triazole



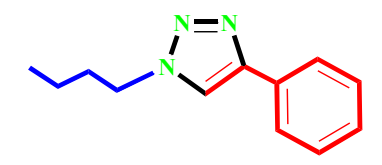
**M.pt.**195-196 °C (Lit. M. pt. 196-198 °C[42]; <sup>1</sup>**H NMR (400 MHz, DMSO)**: $\delta$  3.79 (s, 3H), 6.93-6.95 (d, J = 8.0 Hz, 2H), 7.24-7.28 (t, J = 8.0 Hz, 2H), 7.79-7.81 (d, J = 8.0 Hz, 2H), 7.87-7.90 (m, 2H), 8.78 (s, 1H); <sup>13</sup>**C NMR (400 MHz, DMSO)**:  $\delta$  55.3, 114.4, 116.6, 116.8, 118.3, 122.2, 122.3, 123.1, 127.0, 133.5, 147.9, 159.6.**MS-ESI**: m/z = 267 (M+1)<sup>+</sup>.

#### 4-(4-Bromophenyl)-1-phenyl-1H-1,2,3-triazole



**M.pt.**211-212 °C (Lit. M. pt. 212-214 °C[41]; <sup>1</sup>**H NMR (DMSO, 400 MHz)**:  $\delta$  7.05-7.08 (t, J = 8.0 Hz, 1H), 7.26-7.29 (t, J = 8.0 Hz, 2H), 7.47-7.49 (d, J = 8.0 Hz, 2H), 7.56-7.60 (t, J = 8.0 Hz, 4H), 8.06 (s, 1H); <sup>13</sup>**C NMR (DMSO, 400 MHz)**:  $\delta$  120.6, 124.7, 127.4, 128.8, 129.8, 131.9, 132.2, 134.5, 137.3, 147.6. **MS-ESI**: m/z = 300 (M)<sup>+</sup>, 302 (M+2)<sup>+</sup>.

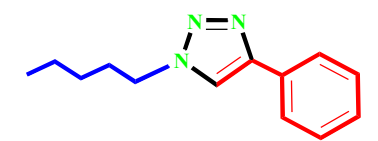
#### 1-Butyl-4-phenyl-1H-1,2,3-triazole



**M.pt.** 45-46°C (Lit. M. pt. 46-47°C[43]; <sup>1</sup>**H NMR (400 MHz, CDCl<sub>3</sub>)**:  $\delta\delta$ 0.90-0.94 (t, J= 8.0 Hz, 3H), 1.25-1.31 (m, 2H), 1.69-1.78 (m, 2H), 4.48-4.52 (t, J= 8.0 Hz, 2H), 7.33-7.37 (t, J= 8.0 Hz, 1H), 7.43-7.47 (t, J= 8.0 Hz, 2H), 7.76 (s, 1H), 7.82-7.84 (d,

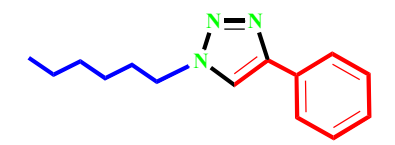
2H, J=8.0 Hz, H<sub>arom</sub>); <sup>13</sup>C NMR(100 MHz, CDCl<sub>3</sub>):  $\delta$  14.05, 22.70, 30.71, 52.14, 127.16, 128.13, 128.74, 128.99, 130.39, 148.90.MS-ESI: m/z = 202 (M+1)<sup>+</sup>.

#### 1-Pentyl-4-phenyl-1H-1,2,3-triazole



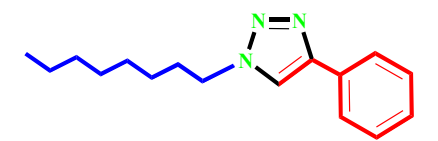
**M. pt.** 68-69 °C (Lit. M. pt. 70-71°C[44]; ¹H NMR (400 MHz, CDCl<sub>3</sub>): δ 0.88-0.92 (t, J= 8.0 Hz, 3H), 1.21-1.27 (m, 4H), 1.66-1.70 (m, 2H), 4.40-4.44 (t, J= 8.0 Hz, 2H), 7.34-7.38 (t, J= 8.0 Hz, 1H), 7.44-7.48 (t, J= 8.0 Hz, 2H), 7.75 (s, 1H), 7.80-7.82 (d, J= 8.0 Hz, 2H); ¹³C NMR(100 MHz, CDCl<sub>3</sub>): δ 13.89, 22.25, 28.41, 30.15, 53.34, 125.54, 128.23, 128.69, 130.92, 132.69, 148.22.MS-ESI: m/z = 216 (M+1)<sup>+</sup>.

#### 1-Hexyl-4-phenyl-1H-1,2,3-triazole



**M. pt.** 78-79 °C (Lit. M. pt. 79-80°C [43]; <sup>1</sup>**H NMR (CDCl<sub>3</sub>, 100 MHz,)**:  $\delta$  0.86-0.90 (3H, t, J= 8.0 Hz), 1.23-1.28 (6H, m), 1.66-1.71 (2H, m), 4.38-4.42 (2H, t, J= 8.0 Hz), 7.33-7.37 (1H, t, J= 8.0 Hz), 7.44-7.48 (2H, t, J= 8.0 Hz), 7.71 (1H, s), 7.81-7.83 (d, J= 8.0 Hz, 2H); <sup>13</sup>**C NMR(CDCl<sub>3</sub>, 100 MHz)**:  $\delta$  13.92, 22.59, 27.20, 28.08, 31.15, 52.95, 126.92, 128.23, 128.70, 130.93, 131.29, 148.30.**MS-ESI**: m/z = 230 (M+1)<sup>+</sup>.

#### 1-Octyl-4-phenyl-1H-1,2,3-triazole



**M. pt.** 73-74°C (Lit. M. pt. 74-78°C[44]; <sup>1</sup>**H NMR (CDCl<sub>3</sub>, 400 MHz)**: δ 0.81-0.85 (t, 3H, J= 8.0 Hz, 3H), 1.21-1.24 (m, 10H), 1.65-1.71 (m, 2H), 4.32-4.36 (t, J= 8.0 Hz, 2H), 7.32-7.36 (t, J= 8.0 Hz, 1H), 7.45-7.48 (t, J= 8.0 Hz, 2H), 7.67 (s, 1H), 7.75-7.79 (t, J= 8.0 Hz, 2H); <sup>13</sup>**C NMR (CDCl<sub>3</sub>, 100 MHz)**: δ 14.06, 22.91, 27.03, 27.77, 29.10,

29.21, 31.71, 52.03, 127.12, 128.18, 128.63, 128.96, 130.38, 148.74. **MS-ESI**: m/z = 258 (M+1)<sup>+</sup>.

#### 3.2.4 References

- [1]. Ghara, S., Barik, P., Ghosh, S., Ghosh, S., Mandal, A., Pramanik, C., Ikbal, M., Dhara, S. and Samanta, S., 2025. UV/Visible Light Promoted External Photocatalyst Free Transformations: One Decade Journey to N-Heterocycles and its Functionalisation. *Organic Chemistry Frontiers*.
- [2]. Gorachand, B., Surendra Reddy, G. and Ramachary, D.B., 2024. Direct Organocatalytic Chemoselective Synthesis of Pharmaceutically Active 1, 2, 3-Triazoles and 4, 5'-Bitriazoles. *ACS Organic & Inorganic Au*, 4(5), pp.534-544.
- [3].Raj, R., Singh, P., Singh, P., Gut, J., Rosenthal, P.J. and Kumar, V., 2013. Azide-alkyne cycloaddition en route to 1H-1, 2, 3-triazole-tethered 7-chloroquinoline-isatin chimeras: Synthesis and antimalarial evaluation. *European journal of medicinal chemistry*, 62, pp 590-596.
- [4]. Tavassoli, M., Landarani-Isfahani, A., Moghadam, M., Tangestaninejad, S., Mirkhani, V. and Mohammadpoor-Baltork, I., 2015. Polystyrene-supported ionic liquid copper complex: A reusable catalyst for one-pot three-component click reaction. *Applied Catalysis A: General*, 503, pp 186-195.
- [5].Mady, M.F., Awad, G.E. and Jørgensen, K.B., 2014. Ultrasound-assisted synthesis of novel 1, 2, 3-triazoles coupled diaryl sulfone moieties by the CuAAC reaction, and biological evaluation of them as antioxidant and antimicrobial agents. *European journal of medicinal chemistry*, 84, pp 433-443.
- [6]. Soltis, M.J., Yeh, H.J., Cole, K.A., Whittaker, N., Wersto, R.P. and Kohn, E.C., 1996. Identification and characterization of human metabolites of CAI [5-amino-1-1 (4'-chlorobenzoyl-3, 5-dichlorobenzyl)-1, 2, 3-triazole-4-carboxamide. *Drug metabolism and disposition*, 24(7), pp 799-806.
- [7]. Agalave, S.G., Maujan, S.R. and Pore, V.S., 2011. Click chemistry: 1, 2, 3-triazoles as pharmacophores. *Chemistry–An Asian Journal*, 6(10), pp 2696-2718.

- [8]. Wheless, J.W. and Vazquez, B., 2010. Rufinamide: a novel broad-spectrum antiepileptic drug. *Epilepsy Currents*, 10(1), pp 1-6.
- [9]. Kumar, A. and Pandey, P.S., 2008. Anion recognition by 1, 2, 3-triazolium receptors: application of click chemistry in anion recognition. *Organic Letters*, 10(2), pp 165-168.
- [10]. Haridas, V., Lal, K., Sharma, Y.K. and Upreti, S., 2008. Design, synthesis, and self- assembling properties of novel triazolophanes. *Organic Letters*, 10(8), pp 1645-1647.
- [11]. Turner, R.A., Oliver, A.G. and Lokey, R.S., 2007. Click chemistry as a macrocyclization tool in the solid-phase synthesis of small cyclic peptides. *Organic letters*, 9(24), pp 5011-5014.
- [12]. Angell, Y.L. and Burgess, K., 2007. Peptidomimetics via copper-catalyzed azide–alkyne cycloadditions. *Chemical Society Reviews*, *36*(10), pp 1674-1689.
- [13]. Huisgen, R., Szeimies, G. and Möbius, L., 1967. 1.3-Dipolar cycloadditions, XXXII. *Chemical Reports*, 100(8), pp 2494-2507.
- [14]. Chen, Z., Yan, Q., Liu, Z., Xu, Y. and Zhang, Y., 2013. Copper-mediated synthesis of 1, 2, 3-triazoles from N-tosylhydrazones and anilines. *Angew. Chem., Int. Ed*, 52(50), pp 13324-13328.
- [15]. Baig, R.N. and Varma, R.S., 2013. Magnetically retrievable catalysts for organic synthesis. *Chemical Communications*, 49(8), pp 752-770.
- [16]. Hudson, R., Li, C.J. and Moores, A., 2012. Magnetic copper–iron nanoparticles as simple heterogeneous catalysts for the azide-alkyne click reaction in water. *Green chemistry*, 14(3), pp 622-624.
- [17]. Mukherjee, N., Ahammed, S., Bhadra, S., & Ranu, B. C., 2013. Solvent-free one-pot synthesis of 1, 2, 3-triazole derivatives by the 'Click'reaction of alkyl halides or aryl boronic acids, sodium azide and terminal alkynes over a Cu/Al<sub>2</sub>O<sub>3</sub> surface under ball-milling. *Green chemistry*, 15(2), pp 389-397.
- [18]. Wei, F., Li, H., Song, C., Ma, Y., Zhou, L., Tung, C. H., & Xu, Z., 2015. Cu/Pd-catalyzed, three-component click reaction of azide, alkyne, and aryl

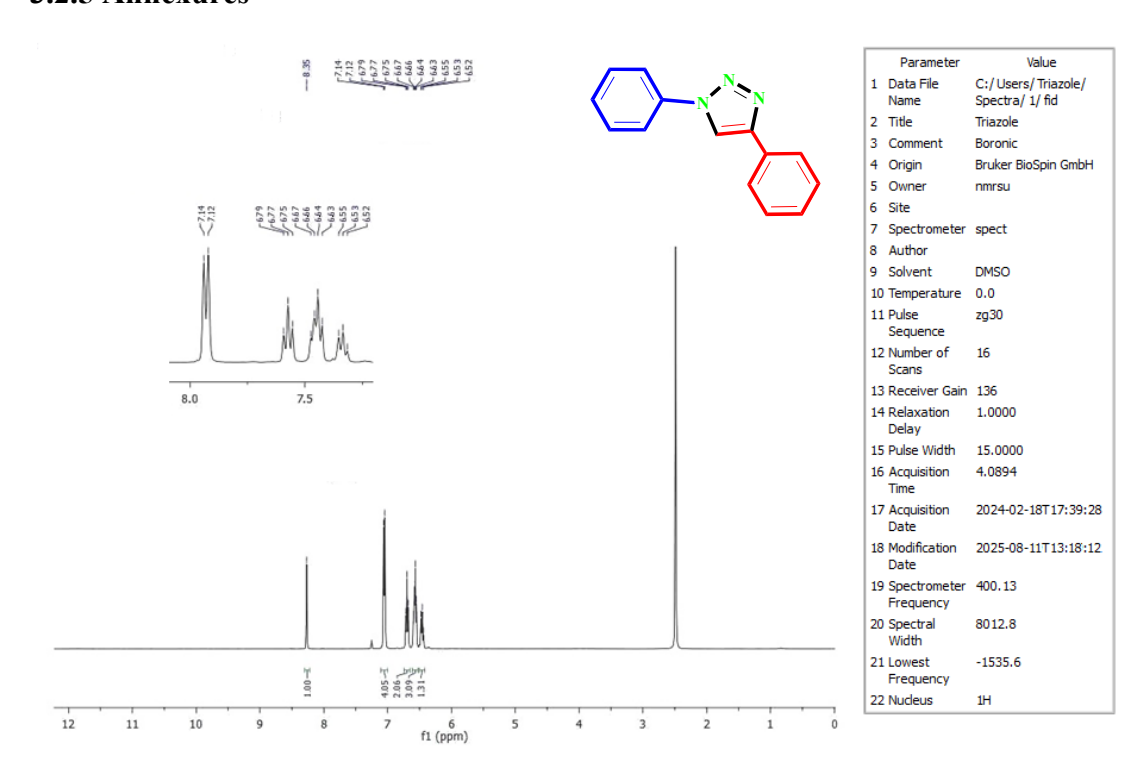
- halide: One-pot strategy toward trisubstituted triazoles. *Organic letters*, 17(11), pp 2860-2863.
- [19]. Lv, L., Gao, G., Luo, Y., Mao, K., & Li, Z., 2021. Three-Component Reactions of α-CF3 Carbonyls, NaN3, and Amines for the Synthesis of NH-1, 2, 3-Triazoles. *The Journal of Organic Chemistry*, 86(23), pp 17197-17212.
- [20]. Kaboudin, B., Abedi, Y., & Yokomatsu, T. 2012. One-pot synthesis of 1, 2, 3-triazoles from boronic acids in water using Cu (II)–β-cyclodextrin complex as a nanocatalyst. *Organic & biomolecular chemistry*, 10(23), pp 4543-4548.
- [21]. Krishnaveni, T., Kadirvelu, K., & Kaveri, M. V., 2022. Facile one pot 'click'synthesis of 1, 4 disubstituted-1, 2, 3-trizole derivatives catalyzed by green chemically prepared CuO nanoparticles. *Materials Science and Engineering: B*, 278, pp 115618.
- [22]. Antonio, J. P., Russo, R., Carvalho, C. P., Cal, P. M., & Gois, P. M., 2019. Boronic acids as building blocks for the construction of therapeutically useful bioconjugates. *Chemical Society Reviews*, 48(13), pp 3513-3536.
- [23]. Nie, R., Sang, R., Ma, X., Zheng, Y., Cheng, X., Li, W., Guo, L., Jin, H. and Wu, Y., 2016. Copper-γ-cyclodextrin complexes immobilized on hexagonal boron nitride as an efficient catalyst in the multicomponent synthesis of 1, 2, 3-triazoles. *Journal of Catalysis*, 344, pp 286-292.
- [24]. Mishra, A., Rai, P., Srivastava, M., Tripathi, B.P., Yadav, S., Singh, J.& Singh, J., 2017. A peerless aproach: organophotoredox/Cu (I) catalyzed, regioselective, visible light facilitated, click synthesis of 1, 2, 3-Triazoles via Azide-Alkyne [3+2] Cycloaddition. *Catalysis Letters*, (147) pp 2600-2611.
- [25]. Sharma, C., Kaur, M., Choudhary, A., Sharma, S. & Paul, S., 2020. Nitrogen doped carbon-silica based Cu (0) nanometal catalyst enriched with well-defined N-moieties: synthesis and application in one-pot synthesis of 1, 4-disubstituted-1, 2, 3-triazoles. *Catalysis Letters*, *150*, pp 82-94.

- [26]. Worrell, B.T., Malik, J.A. and Fokin, V.V., 2013. Direct evidence of a dinuclear copper intermediate in Cu (I)-catalyzed azide-alkyne cycloadditions. *Science*, *340*(6131), pp 457-460.
- [27]. Mohammed, S., Padala, A.K., Dar, B.A., Singh, B., Sreedhar, B., Vishwakarma, R.A. and Bharate, S.B., 2012. Recyclable clay supported Cu (II) catalyzed tandem one-pot synthesis of 1-aryl-1, 2, 3-triazoles. *Tetrahedron*, 68(39), pp 8156-8162.
- [28]. Rafiee, F., & Khavari, P., 2020. Preparation of aryl azides of aryl boronic acids and one-pot synthesis of 1, 4-diaryl-1, 2, 3-triazoles by a magnetic cysteine functionalized GO–CuI/II nanocomposite. *Applied Organometallic Chemistry*, 34(9), pp 5789.
- [29]. Roy, S., Chatterjee, T., & Islam, S. M. 2013. Polymer anchored Cu (II) complex: an efficient and recyclable catalytic system for the one-pot synthesis of 1, 4-disubstituted 1, 2, 3-triazoles starting from anilines in water. *Green chemistry*, 15(9), pp 2532-2539.
- [30]. Chen, Z., Yan, Q., Liu, Z., Xu, Y. and Zhang, Y., 2013. Copper-mediated synthesis of 1, 2, 3-triazoles from N-tosylhydrazones and anilines. *Angew. Chem., Int. Ed*, 52(50), pp 13324-13328.
- [31]. Kumar, A., Verma, S. and Pathak, D. D., 2021. Synthesis and characterization of a recyclable graphene oxide-surface-engineered copper (II) Schiff base complex: Catalytic application in synthesis of 1, 2, 3-triazoles and 2H-indazoles. *Journal of Environmental Chemical Engineering*, 9(4), pp 105791.
- [32]. Kumar, A. S., Reddy, M. A., Knorn, M., Reiser, O., & Sreedhar, B., 2013. Magnetically Recoverable CuFe2O4 Nanoparticles: Catalyzed Synthesis of Aryl Azides and 1, 4-Diaryl-1, 2, 3-triazoles from Boronic Acids in Water. *European Journal of Organic Chemistry*, 2013 (21), pp 4674-4680.
- [33]. Li, P., Liu, Y., Wang, L., Xiao, J., & Tao, M., 2018. Copper (II)-Schiff base complex-functionalized polyacrylonitrile fiber as a green efficient heterogeneous catalyst for one-pot multicomponent syntheses of 1, 2,

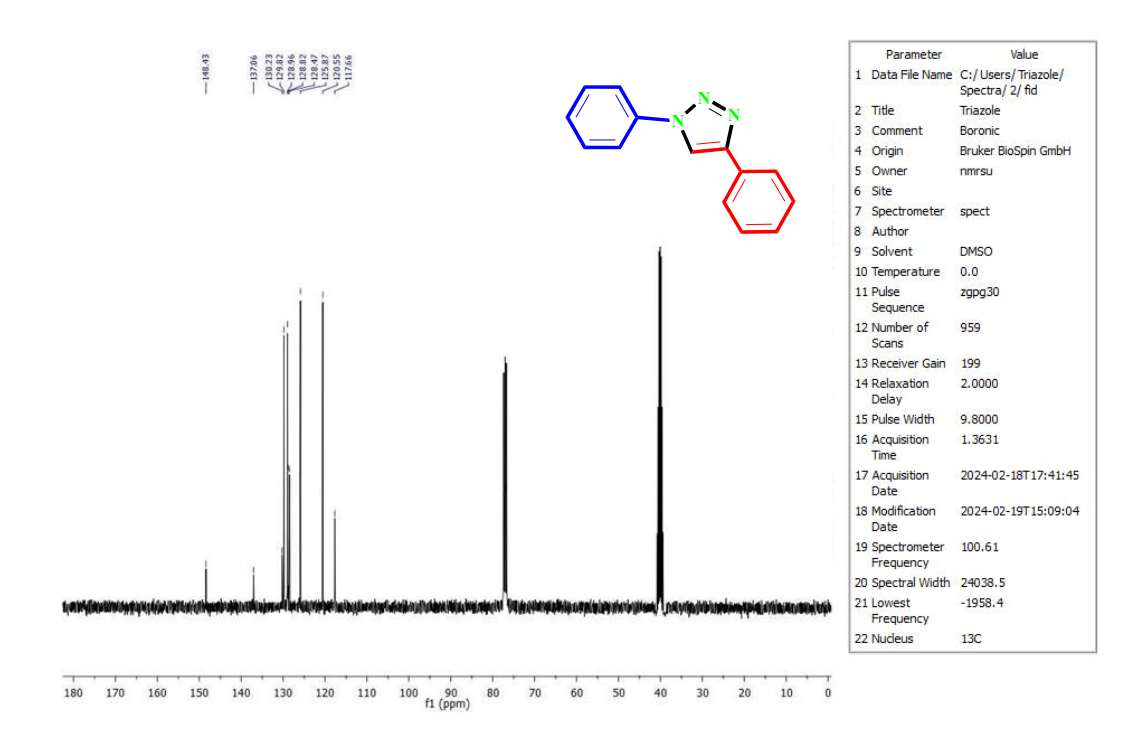
- 3-triazoles and propargylamines. *Advanced Synthesis & Catalysis*, *360*(8), pp 1673-1684.
- [34]. Gholinejad, M. and Jeddi, N., 2014. Copper nanoparticles supported on agarose as a bioorganic and degradable polymer for multicomponent click synthesis of 1, 2, 3-triazoles under low copper loading in water. *ACS Sustainable Chemistry & Engineering*, 2(12), pp 2658-2665.
- [35]. Vantikommu, J., Palle, S., Reddy, P.S., Ramanatham, V., Khagga, M. and Pallapothula, V.R. 2010. Synthesis and cytotoxicity evaluation of novel 1, 4-disubstituted 1, 2, 3-triazoles via CuI catalysed 1, 3-dipolar cycloaddition. *European journal of medicinal chemistry*, 45(11), pp 5044-5050.
- [36]. Jlalia, I., Gallier, F., Brodie-Linder, N., Uziel, J., Augé, J., & Lubin-Germain, N., 2014. Copper (II) SBA-15: A reusable catalyst for azide-alkyne cycloaddition. *Journal of Molecular Catalysis A: Chemical*, 393, pp 56-61.
- [37]. Miao, T. and Wang, L., 2008. Regioselective synthesis of 1, 2, 3-triazoles by use of a silica-supported copper (I) catalyst. *Synthesis*, pp 363-368.
- [38]. Sheldrick, G.M., 2008. A short history of SHELX. *Acta Crystallographica Section A: Foundations of Crystallography*, 64(1), pp 112-122.
- [39]. Farrugia, L.J., 1999. WinGX suite for small-molecule single-crystal crystallography. *journal of Applied Crystallography*, 32(4), pp 837-838.
- [40]. Nardelli, M., 1995. PARST95–an update to PARST: a system of Fortran routines for calculating molecular structure parameters from the results of crystal structure analyses. *Applied Crystallography*, 28(5), pp 659-659.
- [41]. Spek, A.L., 2009. Structure validation in chemical crystallography. *Acta Crystallographica Section D: Biological Crystallography*, 65(2), pp 148-155.

- [42]. Mohammed, S., Padala, A.K., Dar, B.A., Singh, B., Sreedhar, B., Vishwakarma, R.A. and Bharate, S.B., 2012. Recyclable clay supported Cu (II) catalyzed tandem one-pot synthesis of 1-aryl-1, 2, 3-triazoles. *Tetrahedron*, 68(39), pp 8156-8162.
- [43]. Cai, Z.J., Lu, X.M., Zi, Y., Yang, C., Shen, L.J., Li, J., Wang, S.Y. and Ji, S.J., 2014. I2/TBPB mediated oxidative reaction of N-tosylhydrazones with anilines: Practical construction of 1, 4-disubstituted 1, 2, 3-triazoles under metal-free and azide-free conditions. *Organic letters*, *16*(19), pp 5108-5111.
- [44]. Liu, J., Liu, M., Yue, Y., Yao, M. and Zhuo, K., 2012. Environmental Friendly Azide-Alkyne Cycloaddition Reaction of Azides, Alkynes, and Organic Halides or Epoxides in Water: Efficient" Click" Synthesis of 1, 2, 3-Triazole Derivatives by Cu Catalyst. *Chinese Journal of Chemistry*, 30(3), pp 644-650.

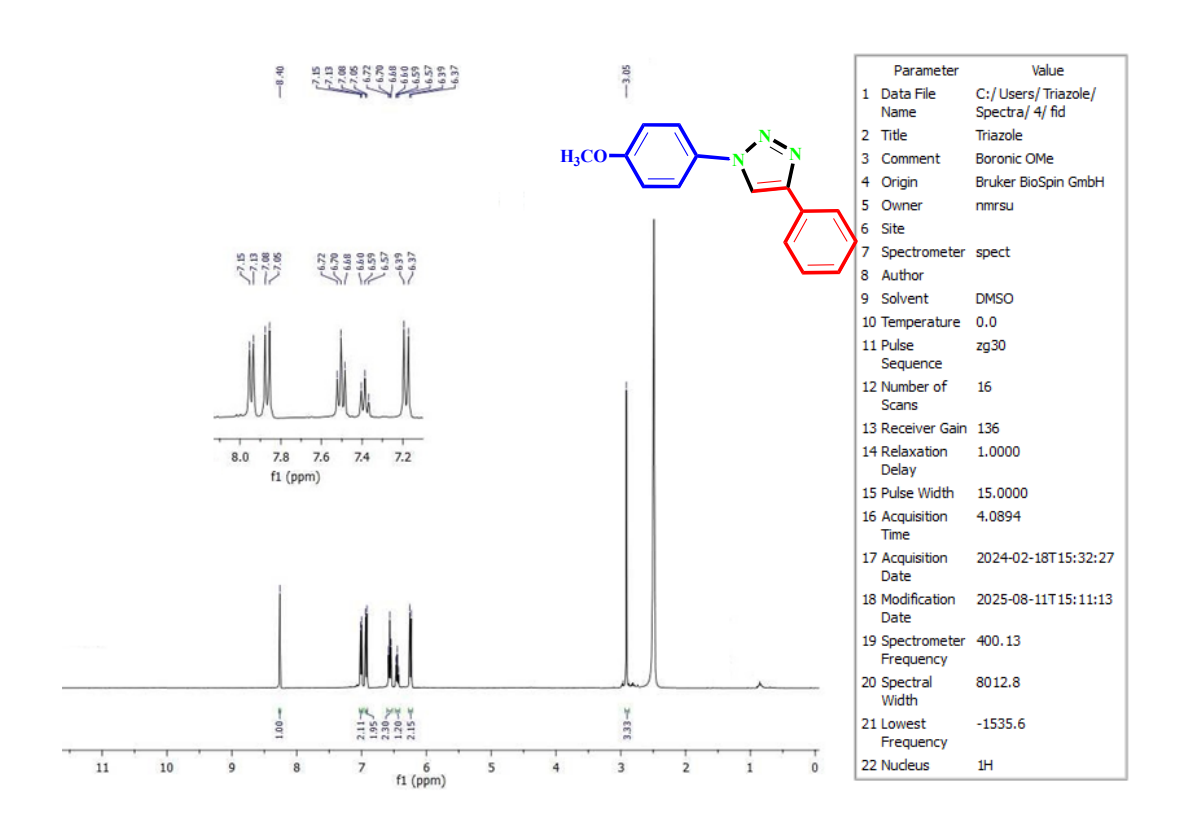
#### 3.2.5 Annexures



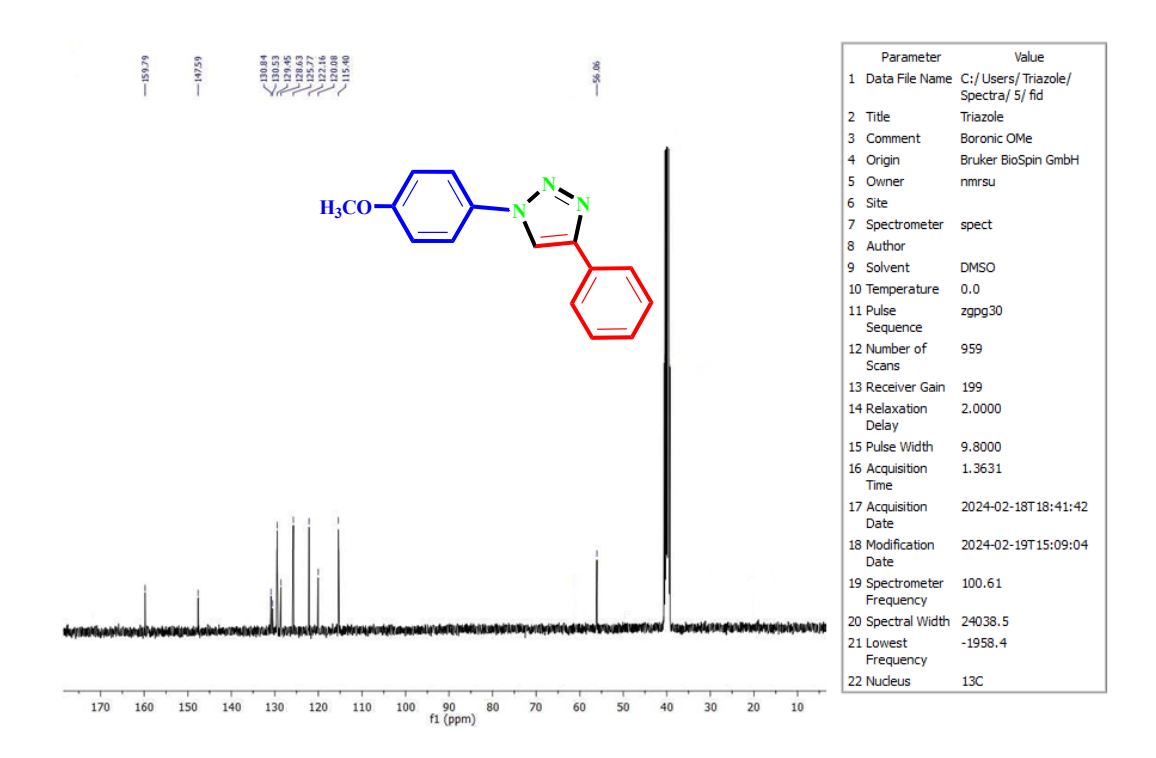
Annexure 3(a) <sup>1</sup>H NMR spectrum of 1,4-Diphenyl-1*H*-1,2,3 triazole



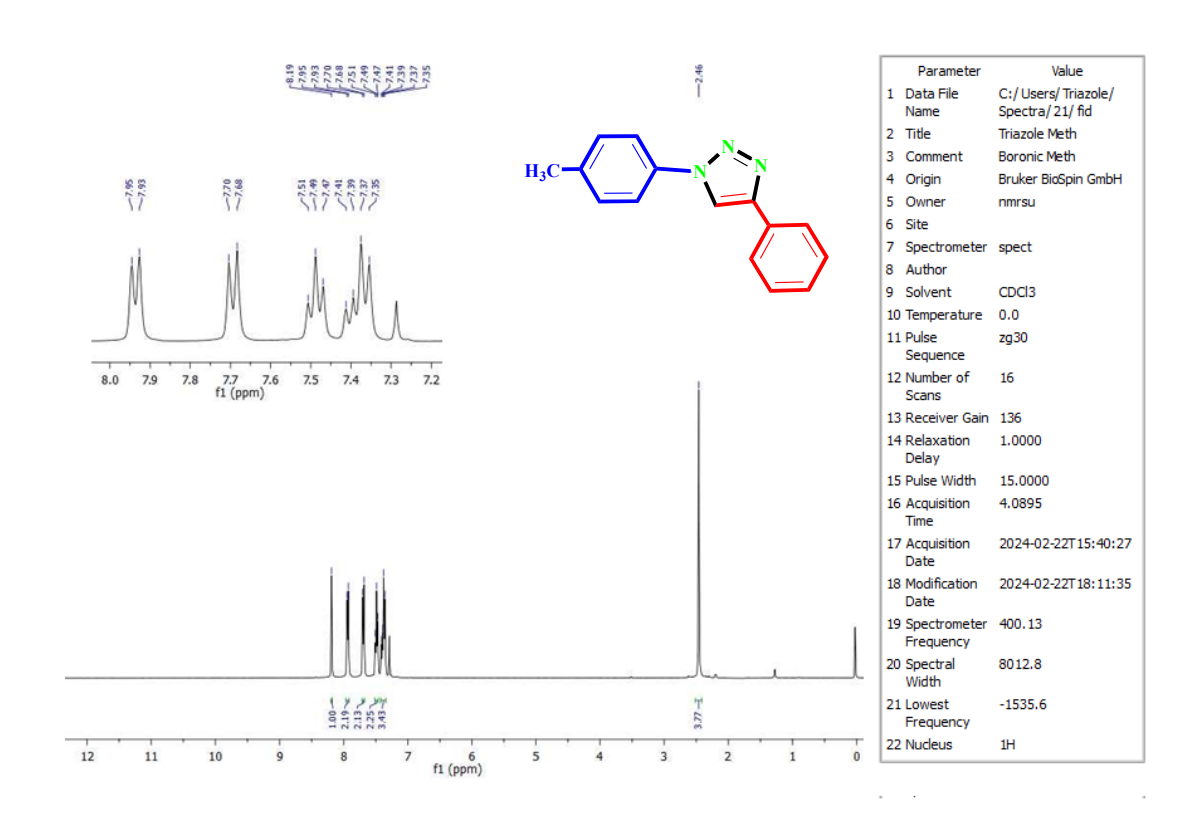
Annexure 3(b) <sup>13</sup>C NMR spectrum of 1,4-Diphenyl-1*H*-1,2,3 triazole



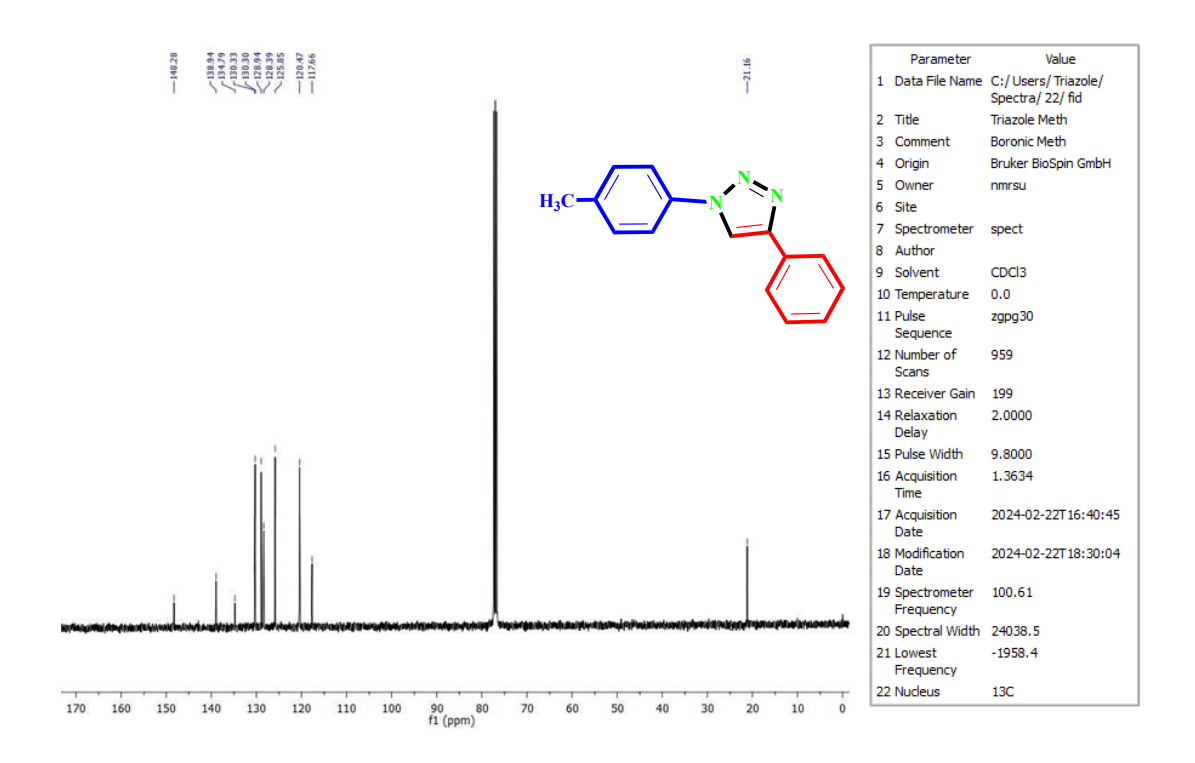
**Annexure 3(c)** <sup>1</sup>H NMRspectrum of 1-(4-Methoxyphenyl)-4-phenyl-1*H*-1,2,3-triazole



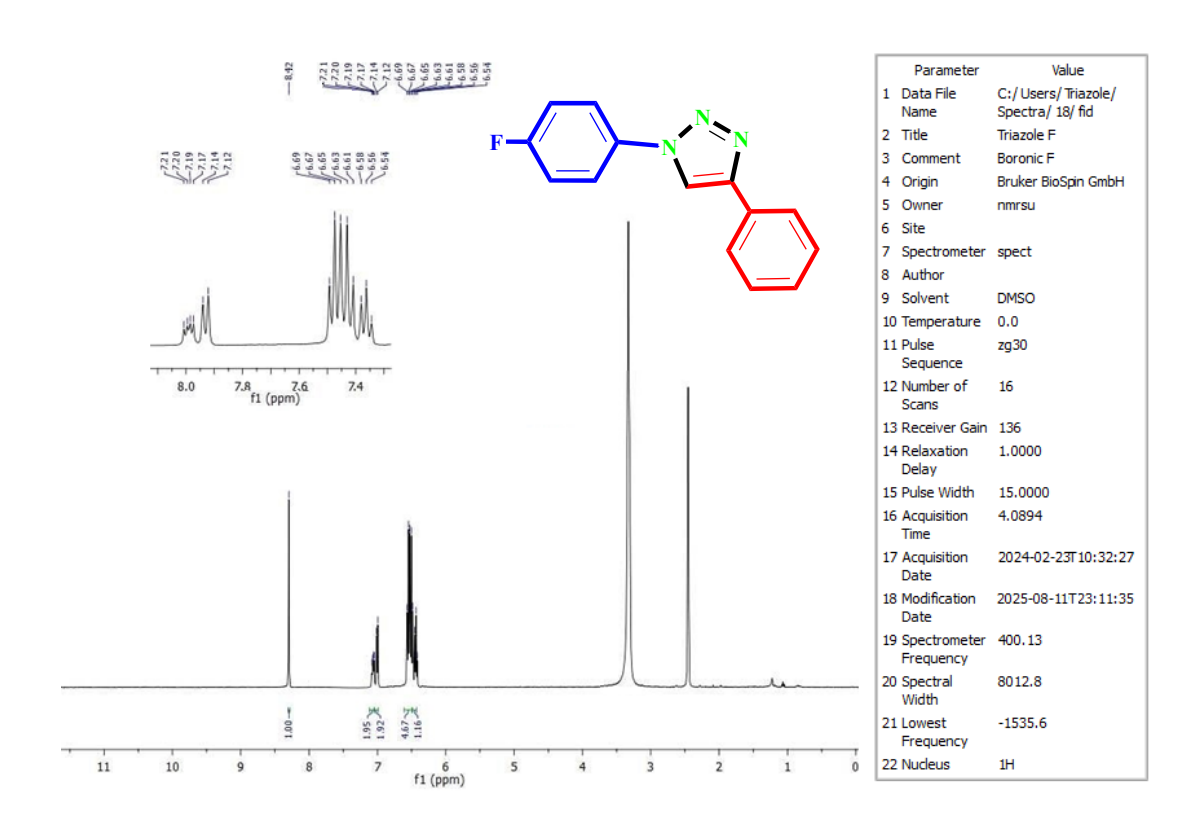
**Annexure 3(d)** <sup>13</sup>C NMRspectrum of 1-(4-Methoxyphenyl)-4-phenyl-1*H*-1,2,3-triazole



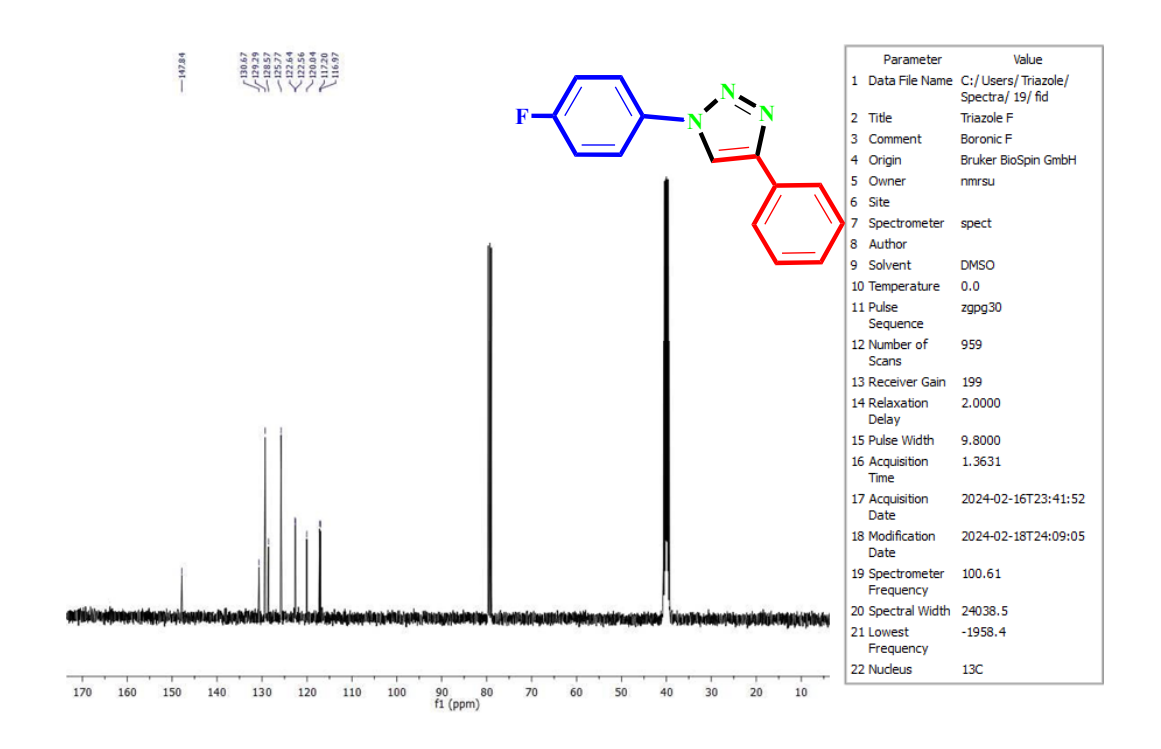
Annexure 3(e) <sup>1</sup>HNMRspectrum of 1-(4-methylphenyl)-4-phenyl-1*H*-1,2,3-triazole



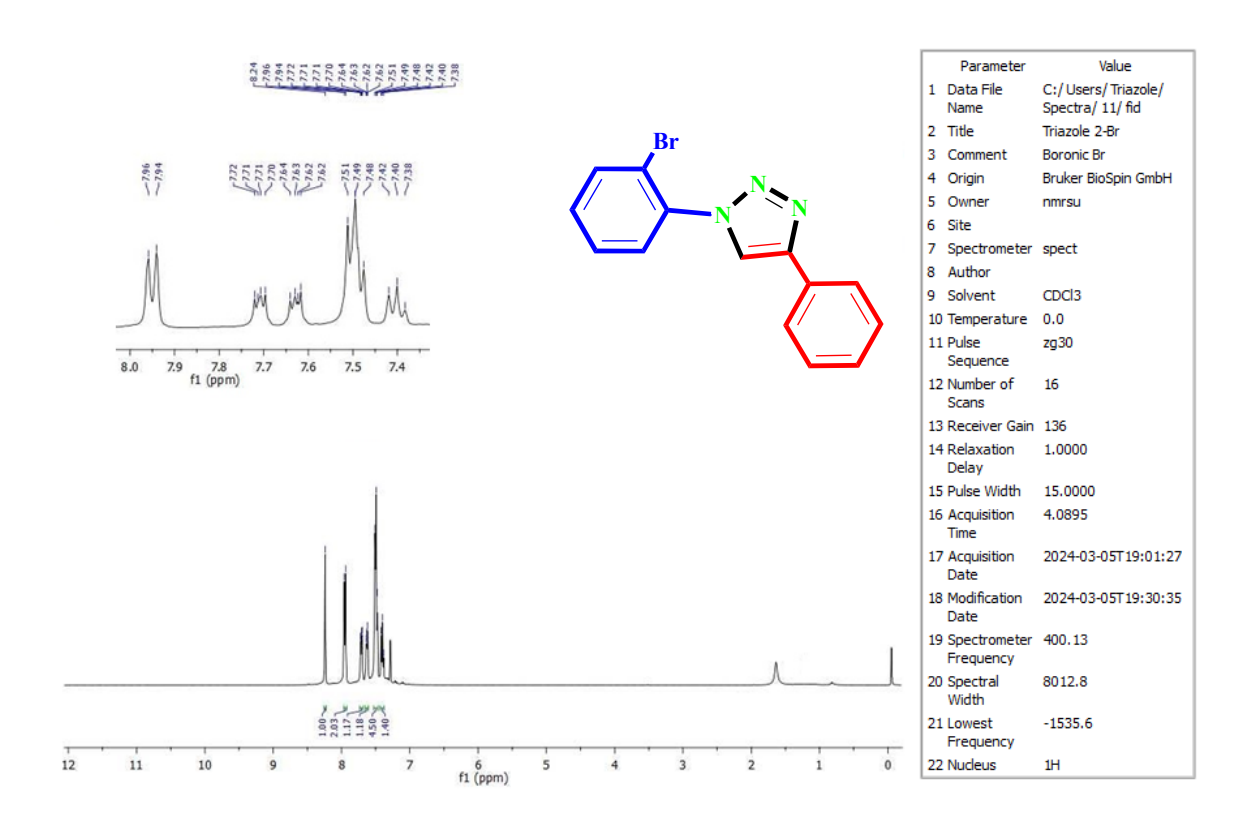
Annexure 3(f) <sup>13</sup>C NMRspectrum of 1-(4-methylphenyl)-4-phenyl-1*H*-1,2,3-triazole



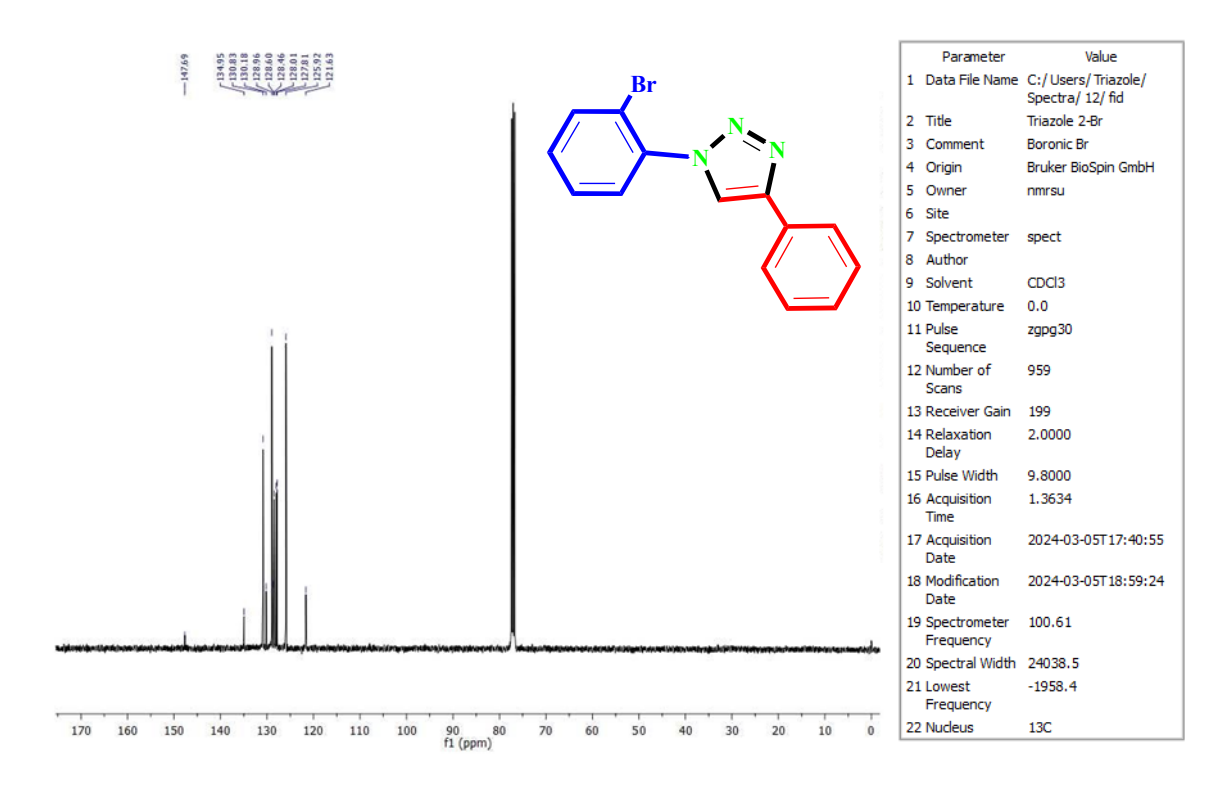
Annexure 3(g) <sup>1</sup>H NMRspectrum of 1-(4-Fluorophenyl)-4-phenyl-1*H*-1,2,3-triazole



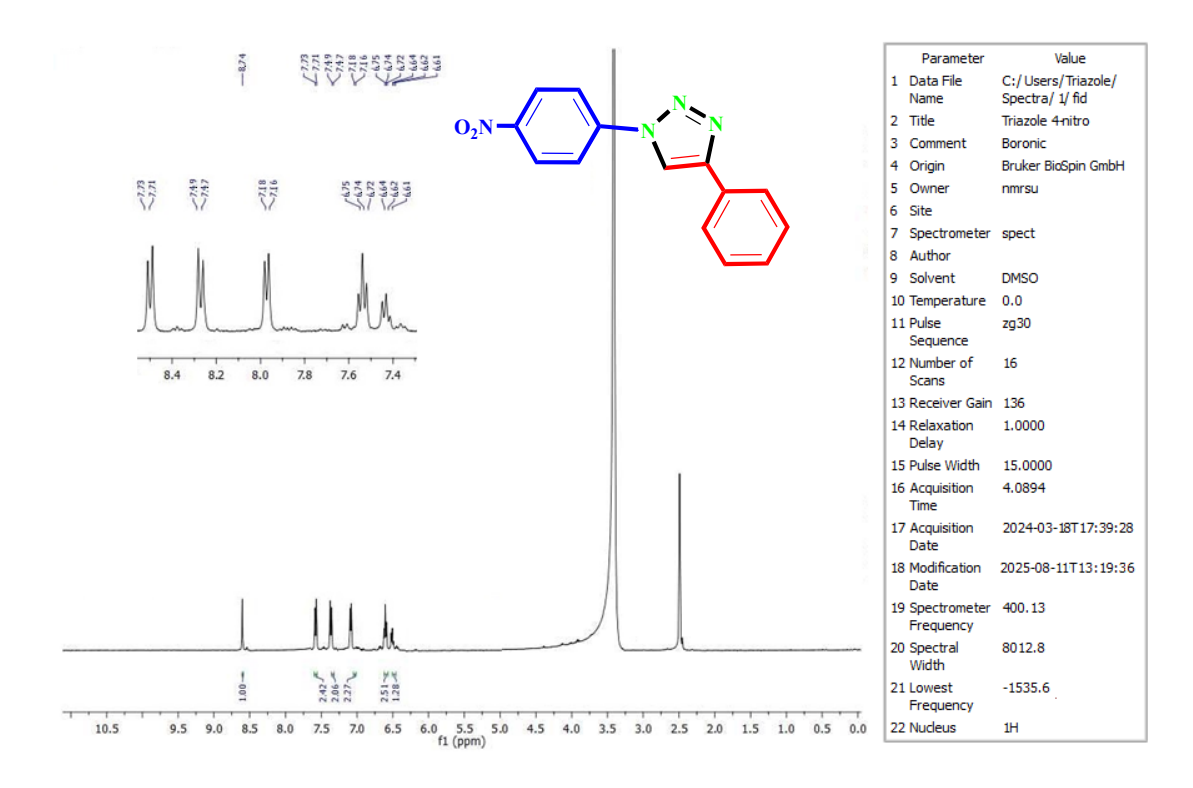
**Annexure 3(h)** <sup>13</sup>CNMRspectrum of 1-(4-Fluorophenyl)-4-phenyl-1*H*-1,2,3-triazole



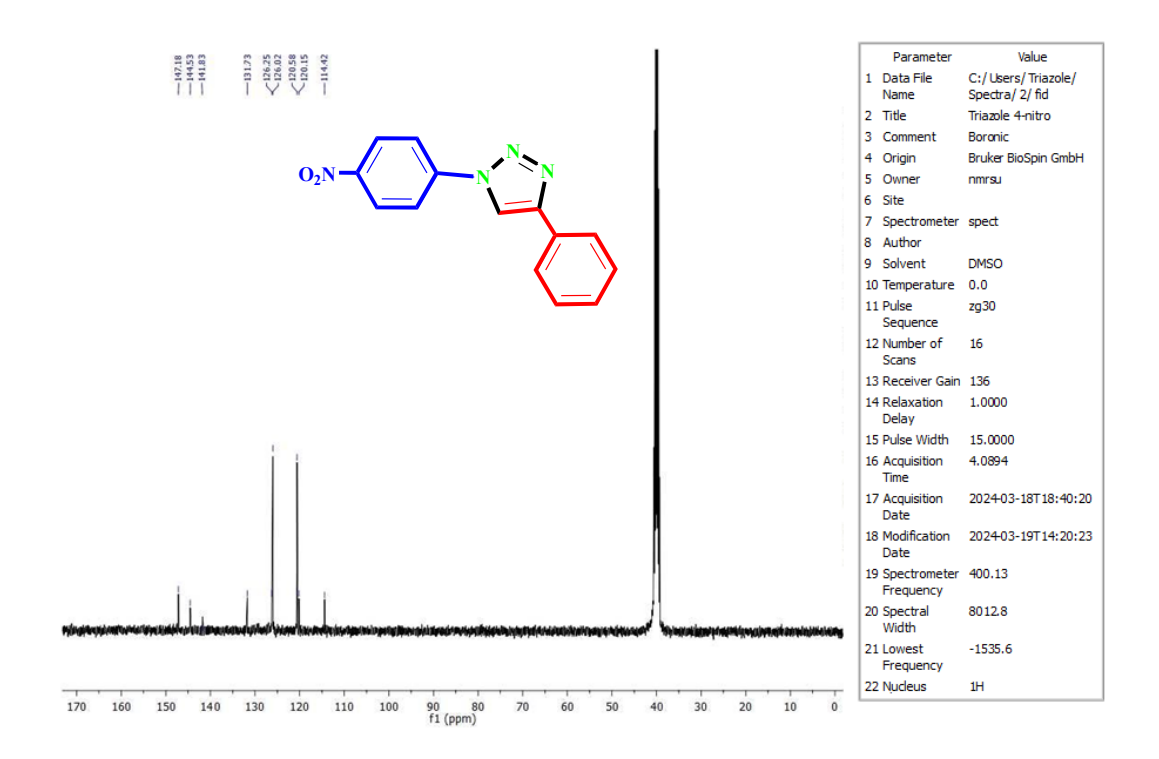
Annexure 3(i) <sup>1</sup>H NMRspectrum of 1-(2-Bromophenyl)-4-phenyl-1*H*-1,2,3-triazole



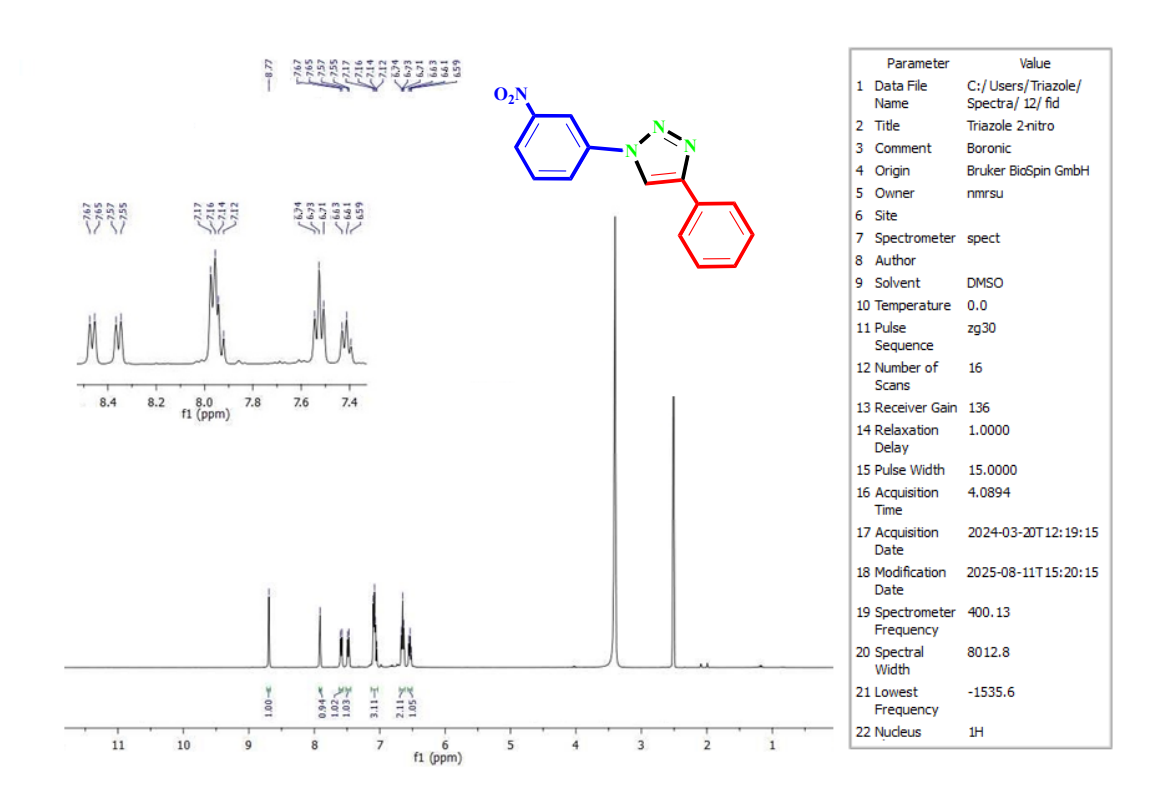
**Annexure 3(j)** <sup>13</sup>CNMRspectrum of 1-(2-Bromophenyl)-4-phenyl-1*H*-1,2,3-triazole



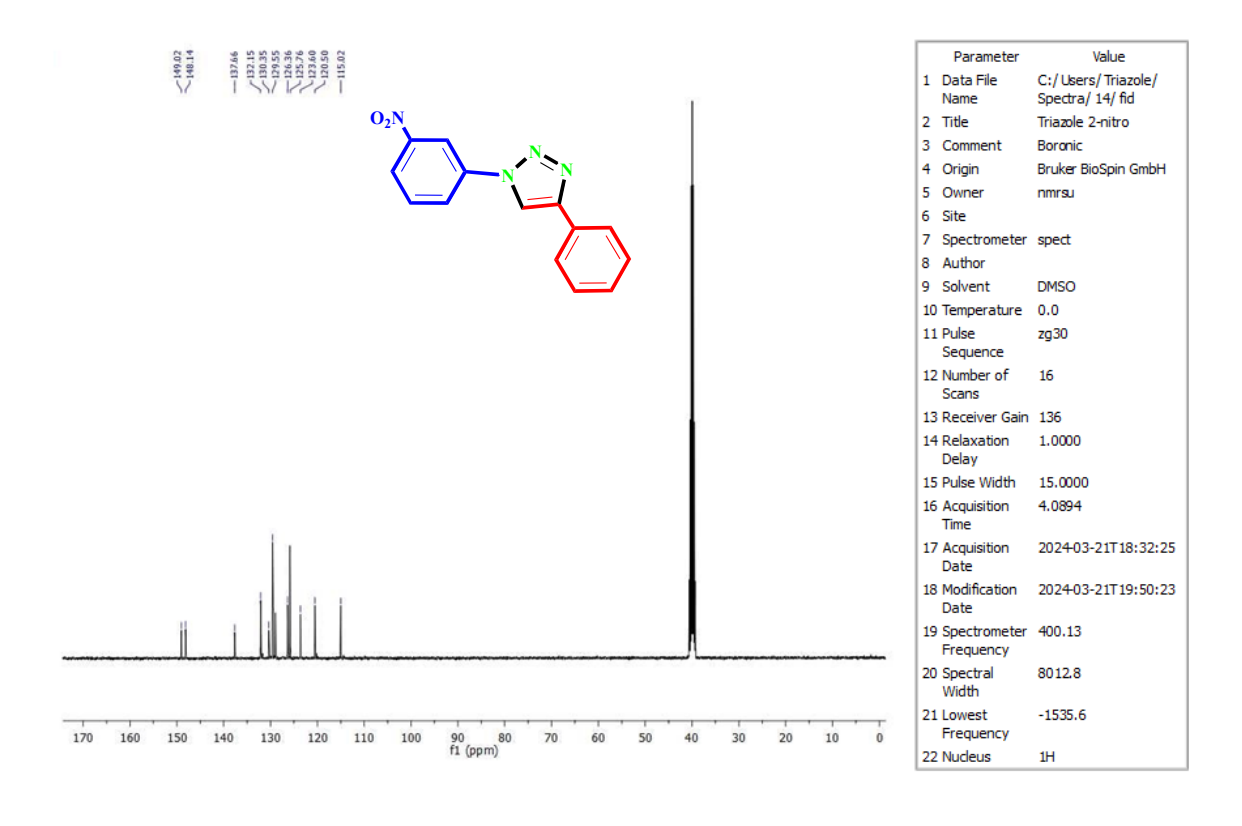
Annexure 3(k) <sup>1</sup>H NMRspectrum of 1-(4-Nitrophenyl)-4-phenyl-1*H*-1,2,3-triazole



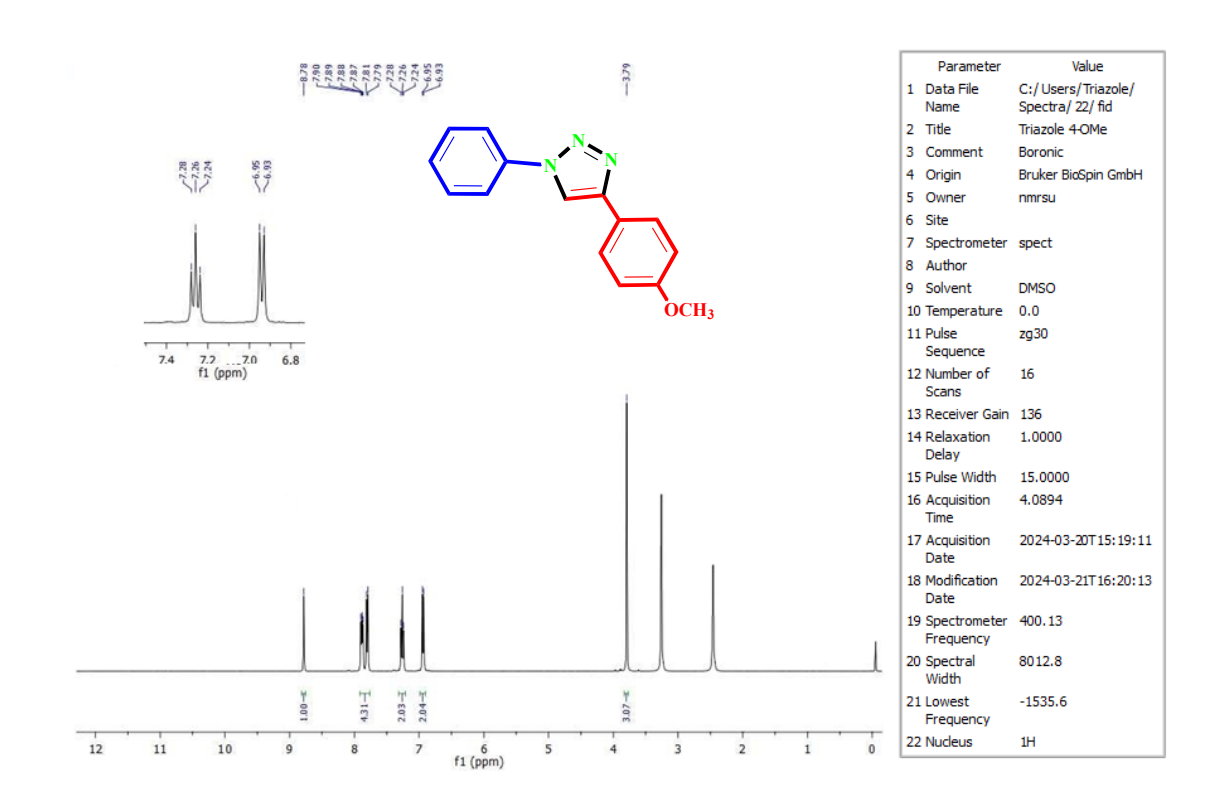
**Annexure 3(1)** <sup>13</sup>CNMRspectrum of 1-(4-Nitrophenyl)-4-phenyl-1*H*-1,2,3-triazole



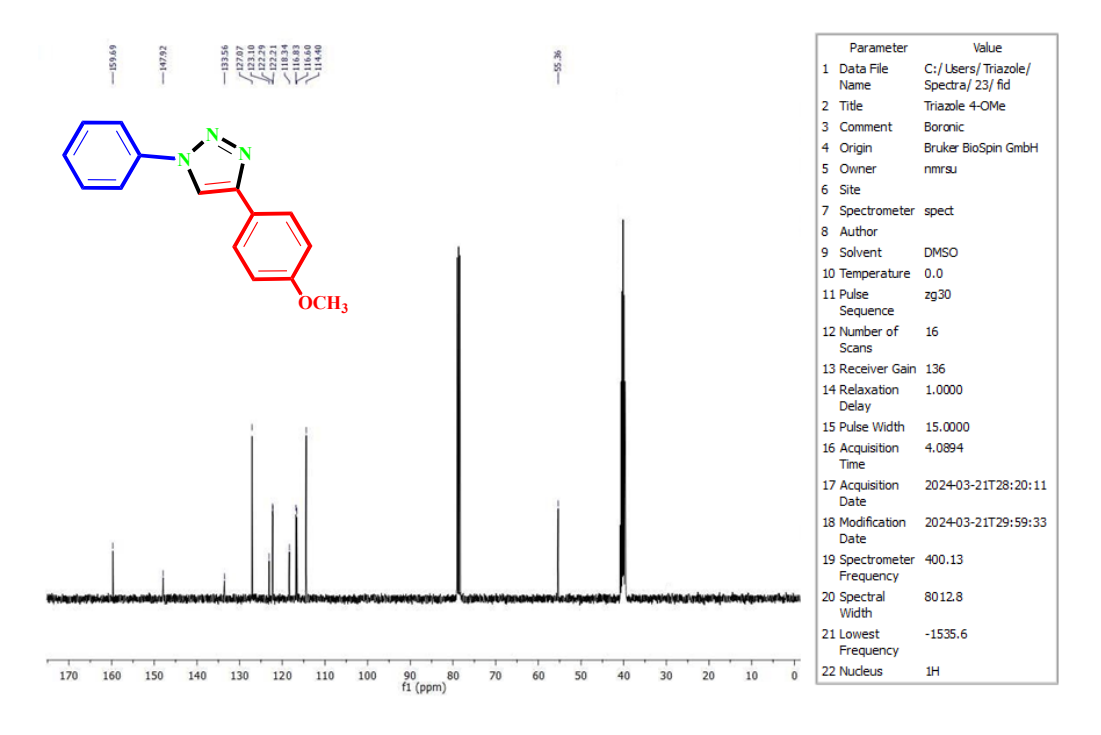
Annexure 3(m) <sup>1</sup>H NMR spectrum of 1-(3-Nitrophenyl)-4-phenyl-1*H*-1,2,3-triazole



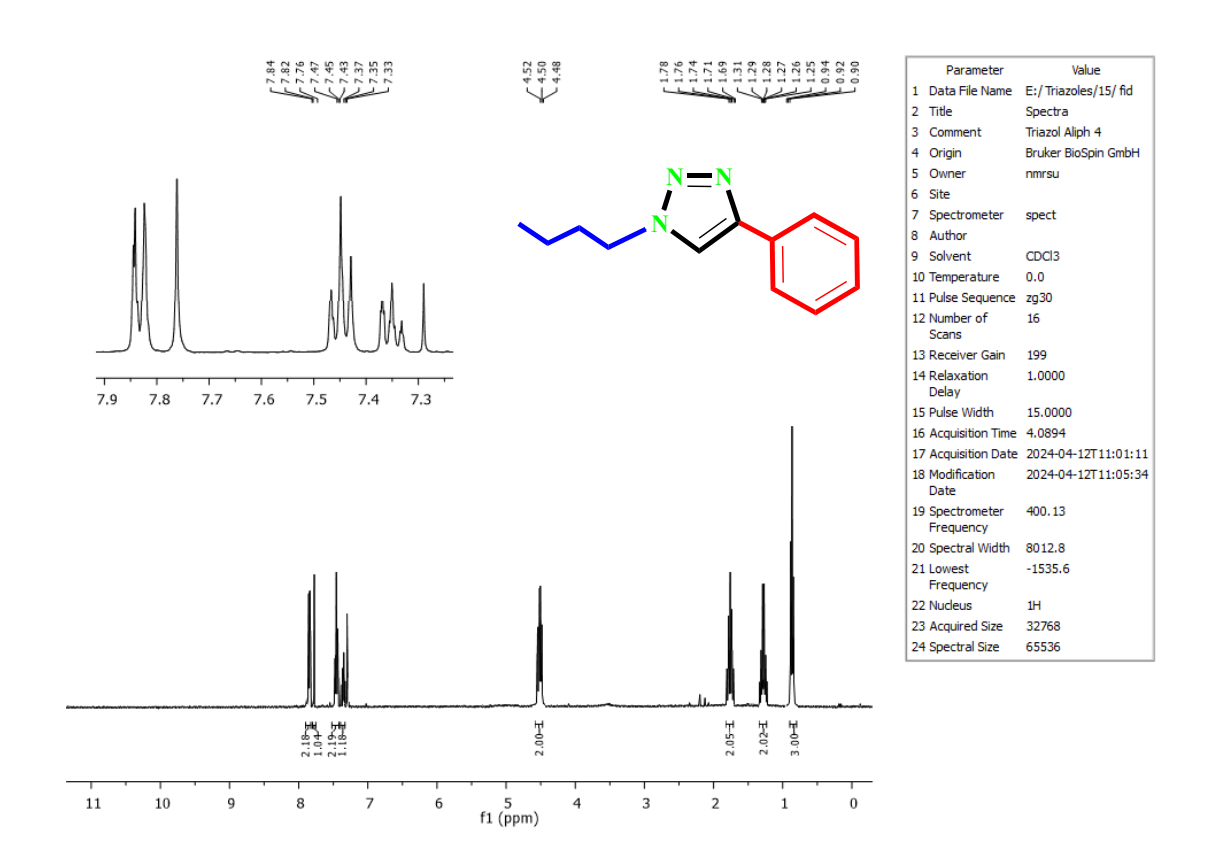
Annexure 3(n) <sup>13</sup>CNMR spectrumof 1-(3-Nitrophenyl)-4-phenyl-1*H*-1,2,3-triazole



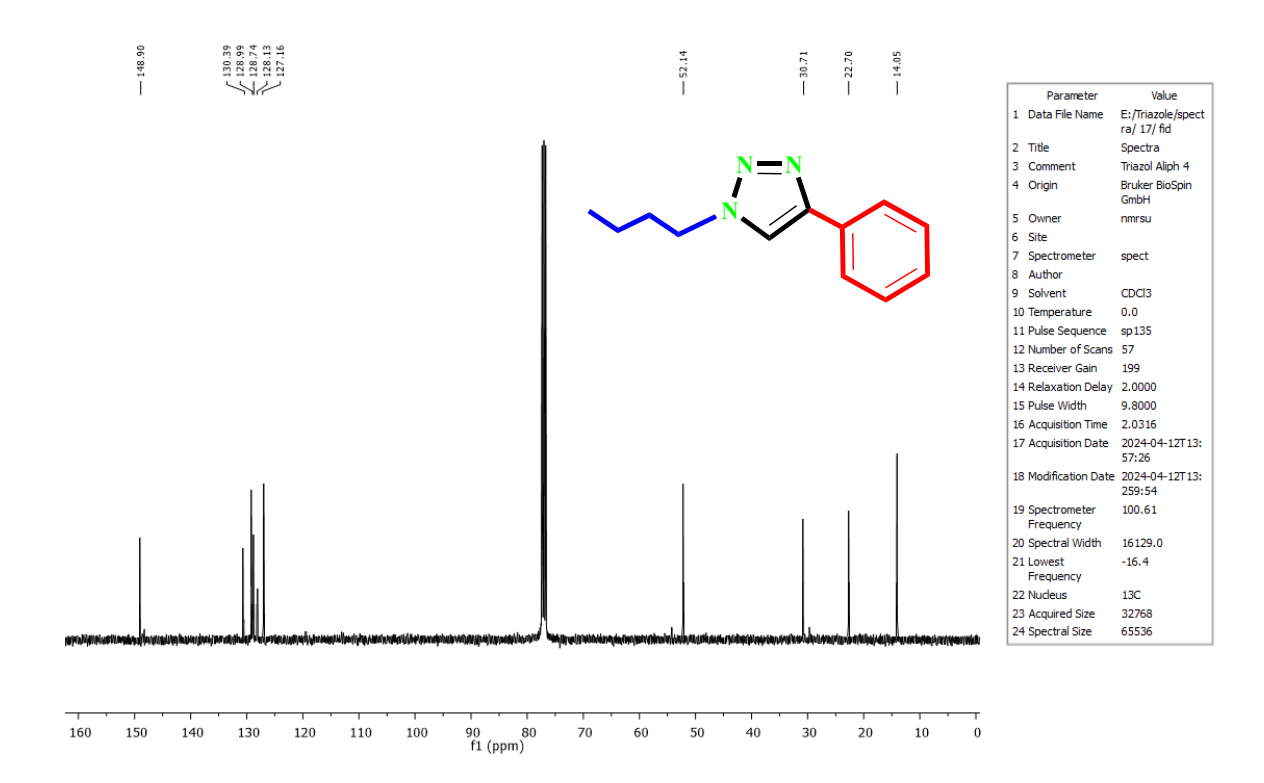
**Annexure 3(o)** <sup>1</sup>HNMRspectrum of 4-(4-methoxyphenyl)-1-phenyl--1*H*-1,2,3-triazole



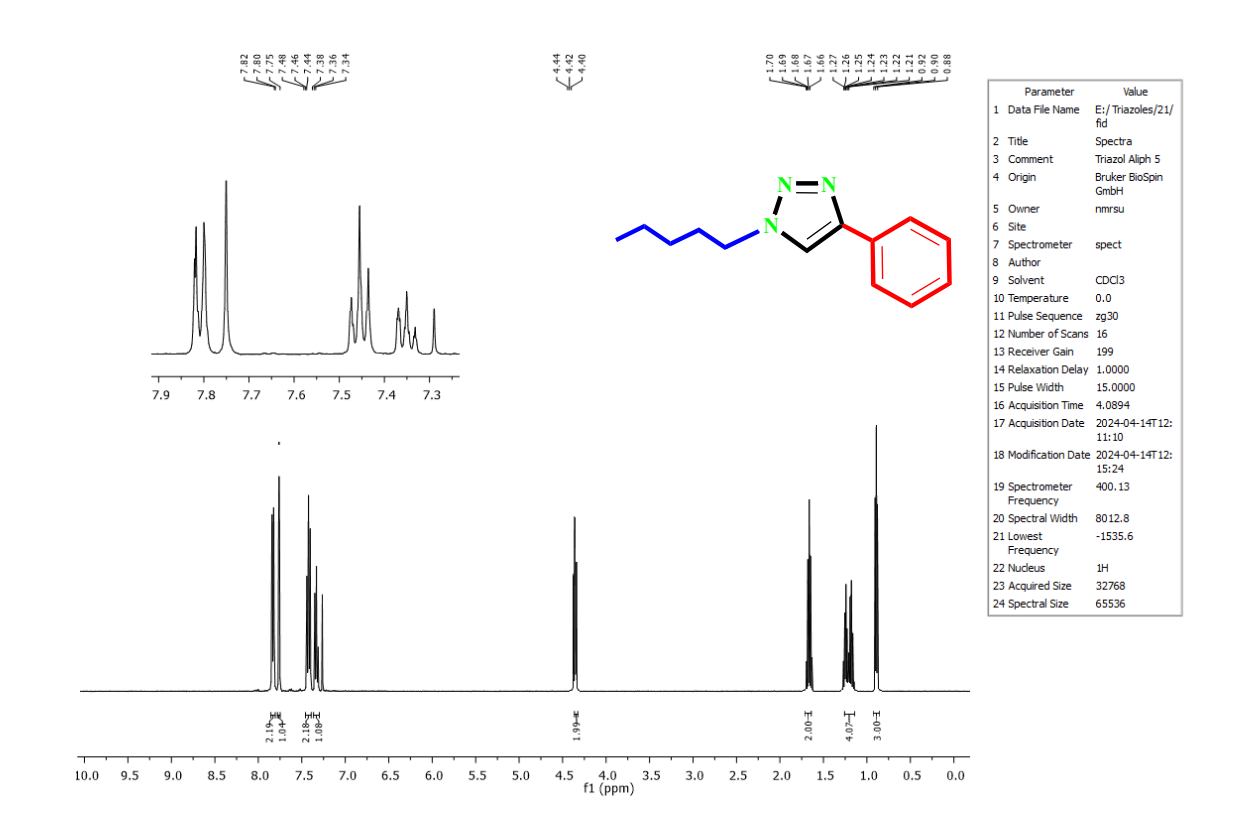
**Annexure 3(p)** <sup>13</sup>C NMRspectrumof 4-(4-methoxyphenyl)-1-phenyl-1*H*-1,2,3-triazole



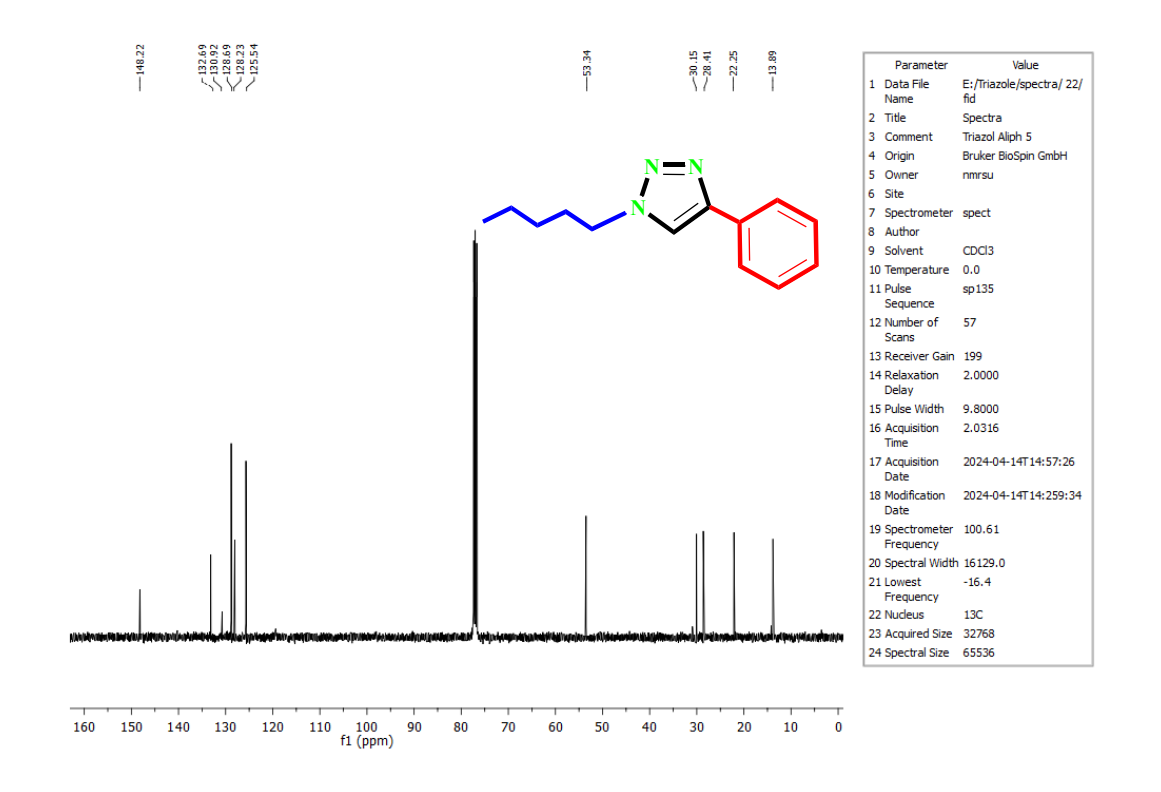
Annexure 3(q) <sup>1</sup>H NMRspectrum of 1-Butyl-4-phenyl-1*H*-1,2,3-triazole



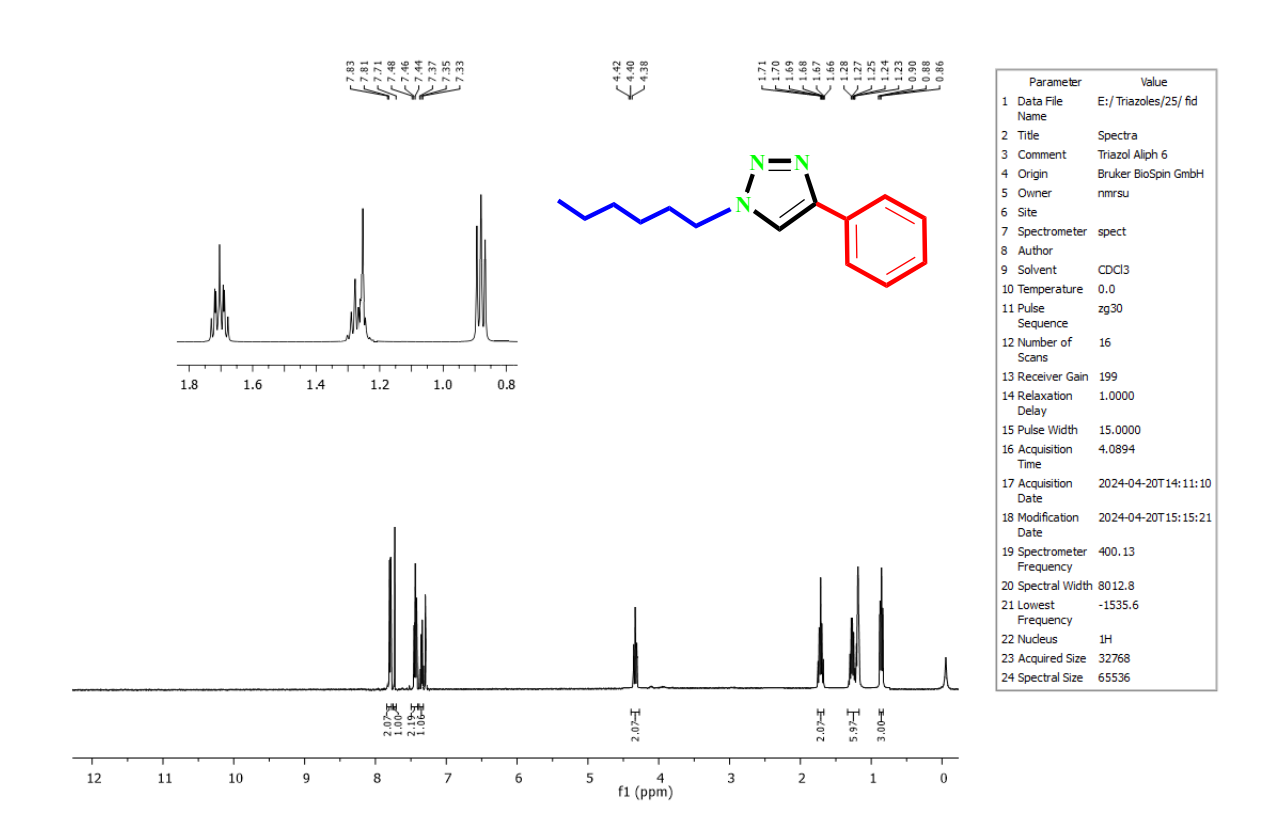
Annexure 3(r) <sup>13</sup>C NMR spectrumof 1-Butyl-4-phenyl-1*H*-1,2,3-triazole



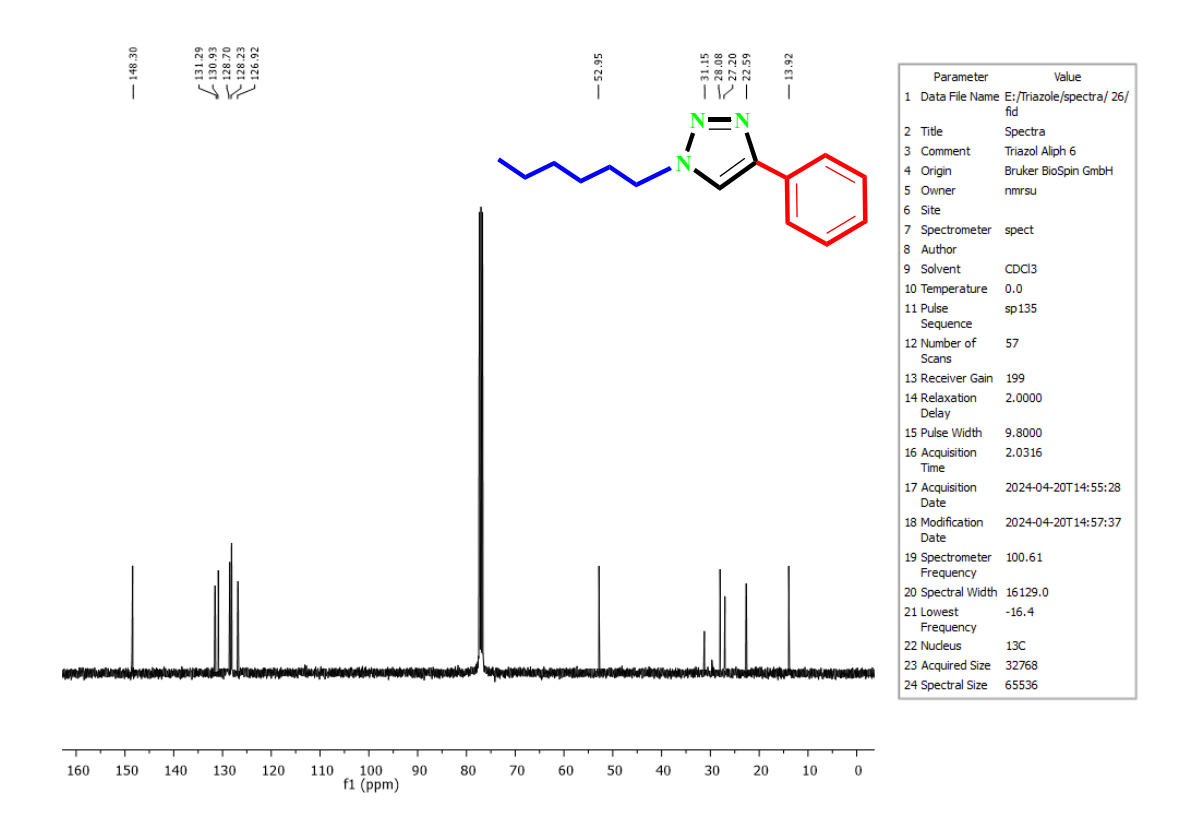
Annexure 3(s) <sup>1</sup>H NMRspectrum of 1-Pentyl-4-phenyl-1*H*-1,2,3-triazole



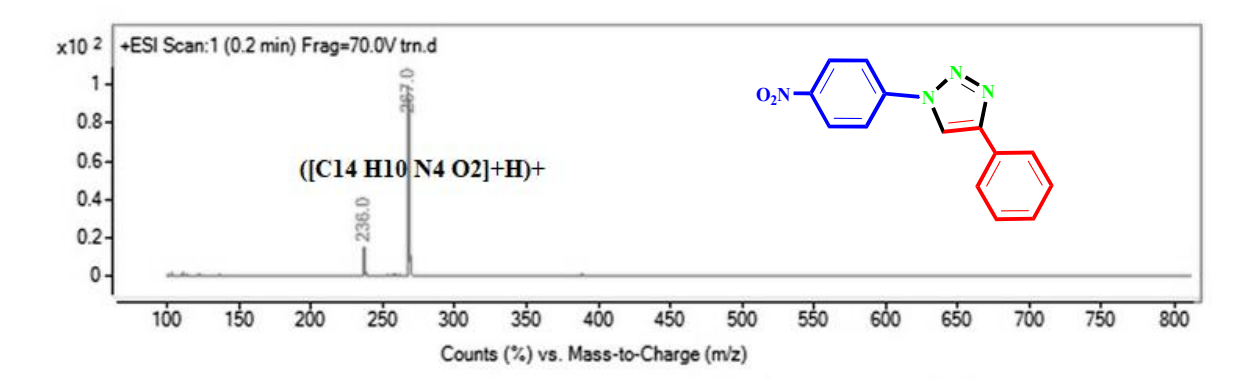
Annexure 3(t) <sup>13</sup>C NMRspectrum of 1-Pentyl-4-phenyl-1*H*-1,2,3-triazole



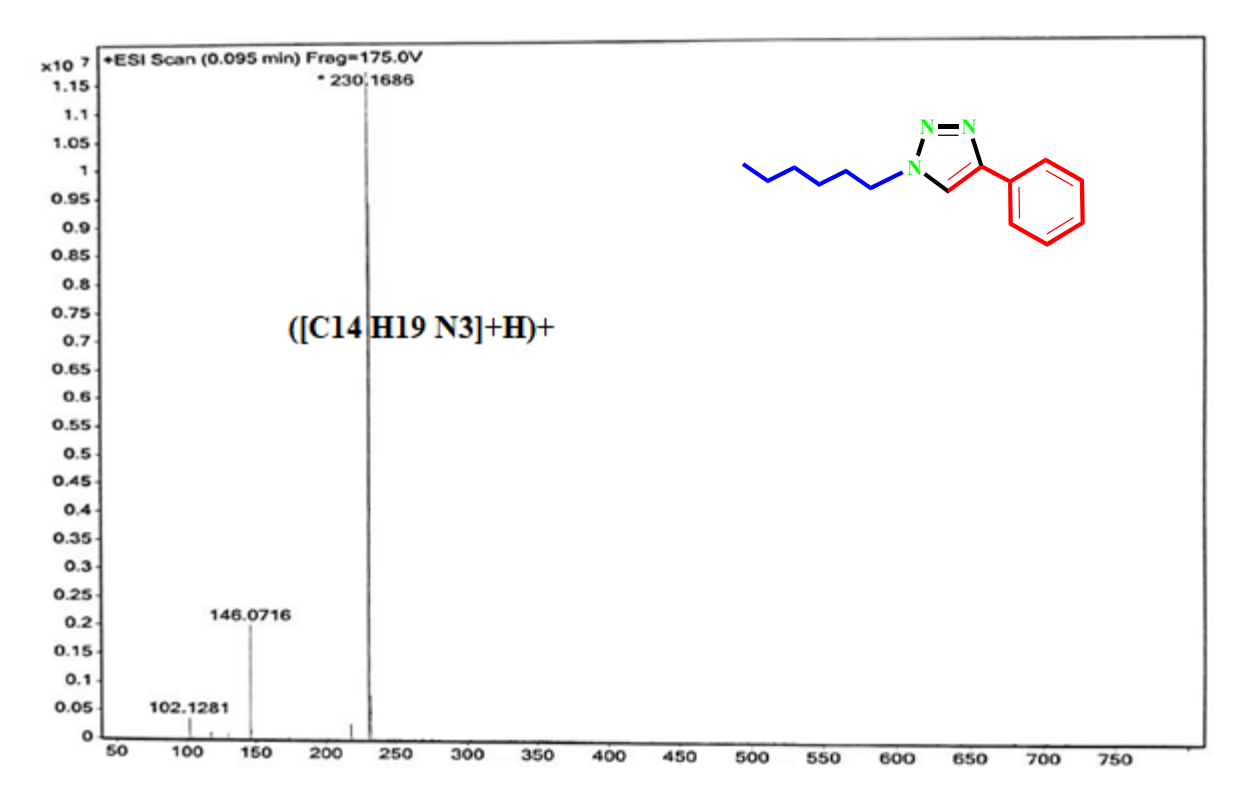
**Annexure 3(u)** <sup>1</sup>H NMRspectrumof 1-Hexyl-4-phenyl-1*H*-1,2,3-triazole



**Annexure 3(v)** <sup>13</sup>CNMRspectrum of 1-Hexyl-4-phenyl-1*H*-1,2,3-triazole



**Annexure 3(w)**Mass spectrum of 1-(3-nitrophenyl)-4-phenyl-1*H*-1,2,3-triazole.



Annexure 3(x) Mass spectrum of 1-hexyl-4-phenyl-1*H*-1,2,3-triazole

# Chapter 4

This chapter gives details about the synthetic procedure of Zn@CS-SB/Fe<sub>3</sub>O<sub>4</sub>-SiO<sub>2</sub>, its characterization, and applications.

### Section 4.1 Synthesis and characterization of Zn (II) onto Chitosan Schiff base metal complex

#### Zn@CS-SB/Fe<sub>3</sub>O<sub>4</sub>-SiO<sub>2</sub>[Zn@CS-SB/Fe<sub>3</sub>O<sub>4</sub>-SiO<sub>2</sub>]

We have synthesized a novel catalyst system i.e., Zn (II) onto Chitosan Schiff base metal complex [Zn@CS-SB/Fe<sub>3</sub>O<sub>4</sub>-SiO<sub>2</sub>]. The synthetic process of CS-SB/Fe<sub>3</sub>O<sub>4</sub>-SiO<sub>2</sub> is represented in **Figure 4.1**. First, the Fe<sub>3</sub>O<sub>4</sub> nanoparticles were prepared by coprecipitating Fe<sup>3+</sup> and Fe<sup>2+</sup> salts, and then silica was coated onto the surface of the Fe<sub>3</sub>O<sub>4</sub> nanoparticles using TEOS. Chitosan, an important biomaterial characterized by its biodegradability and wide chemical-modifying capacity, was then bound with Fe<sub>3</sub>O<sub>4</sub>-SiO<sub>2</sub>. The surface of chitosan-bound silica magnetic nanoparticles was then functionalized with salicaldehyde via the formation of a Schiff base to get CS-SB/Fe<sub>3</sub>O<sub>4</sub>-SiO<sub>2</sub>. Finally, ZnCl<sub>2</sub> was refluxed with Chitosan Schiff base magnetic complex to get Schiff base Zn@CS-SB/Fe<sub>3</sub>O<sub>4</sub>-SiO<sub>2</sub>. The developed catalyst was characterized by numerous techniques like SEM imaging and mapping, EDX, HRTEM, XPS, FTIR, XRD, TGA, BET, VSM, ICP-AES, and CHN analysis.

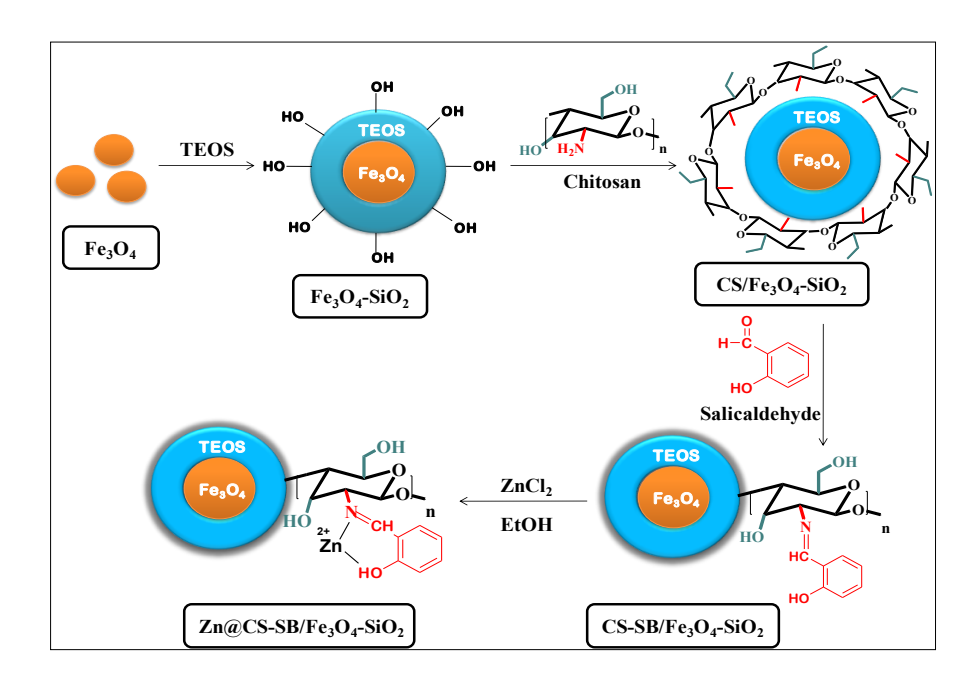


Figure 4.1. Proposed Scheme for the synthesis of Zn@CS-SB/Fe<sub>3</sub>O<sub>4</sub>-SiO<sub>2</sub>

### **Materials and Instrumentation**

All the reagents used were purchased from Merck or Aldrich Chemical Companies. All the FTIR spectra were recorded on FTIR spectrophotometer of Perkin-Elmer make. XRD data was recorded on D2 PHASER Rigaku X-ray diffractometer in 2 theta scale of 10-80°. XPS spectra of the prepared catalyst was recorded on Thermoscientific NEXA Surface analyser. While CHNS was recorded on Model Elementar, UNICUBE whereas the thermal behavior (TGA) was recorded on Perkin Elmer, Diamond TG/DTA with a heating rate of 10 °C min<sup>-1</sup>. BET analysis was done on Quantachrome make (Anton Paar). FEG-SEM analysis and EDX were carried out using Hitachi S-3000N Scanning electron microscope. TEM analysis was done on FEI of Talos make. The amount of metal loading was obtained by ICP-AES analysis using ARCOS, Simultaneous ICP spectrometer. The magnetism (magnetic moment) was calculated using a vibrating sample magnetometer (VSM) bearing Model: 7410series, Lakeshore at room temperature from -10,000 to +15,000 Oe. H and 13C NMR data was recorded using Bruker Avance (100 MHz and 400 MHz).

### 4.1.1 General procedure for the preparation of Zn@CS-SB/Fe<sub>3</sub>O<sub>4</sub>-SiO<sub>2</sub>

### Synthesis of Magnetic Nanoparticles (Fe<sub>3</sub>O<sub>4</sub> NPs)

The salts of Iron chloride, i.e., FeCl<sub>3</sub> (5.0 g) and FeCl<sub>2</sub> (2.5 g), were taken in the ratio of 2:1 and successively dissolved in distilled water (30 mL) in a beaker. The resultant solution so obtained was then added drop by drop to an aq. NaOH sol. under vigorous stirring for 30 min. This results in the precipitation and formation of nanoferrites. After 20 min, the precipitated mixture of ferrites was separated using a magnet and washed with distilled water so as to maintain its pH at 7.0 and vacuum dried at 60° C overnight.

### Synthesis of TEOS coated Magnetic Nanoparticles (Fe<sub>3</sub>O<sub>4</sub>-SiO<sub>2</sub>)

In a round bottom flask (250 mL), Fe<sub>3</sub>O<sub>4</sub> NPs (2 g) was dispersed in water (40 mL), ethanol (130 mL), ammonia (7 mL) and TEOS i.e., tetraethyl orthosilicate (7 mL) were added successively and the mixture was vigorously stirred and refluxed for 8 h. The resultant Fe<sub>3</sub>O<sub>4</sub>@SiO<sub>2</sub> mass was magnetically separated and washed repeatedly

with distilled water and ethanol and finally, the product was vacuum dried at 60 °C overnight.

### Synthesis of Chitosan coated Silica Magnetic Nanoparticles (CS/Fe<sub>3</sub>O<sub>4</sub>-SiO<sub>2</sub>)

Chitosan (1 g) was suspended in 50 mL of acetic acid (2%, w/v) in a round botton flask (100 mL) and magnetically stirred at room temperature for 1 h to give a homogeneous gel-like solution. After that, 50 mg of prepared Fe<sub>3</sub>O<sub>4</sub>@SiO<sub>2</sub> and Na<sub>2</sub>SO<sub>4</sub> (15%, w/v) was added to the Chitosan gel solution and magnetically stirred at room temperature for 1.5 h. The Chitosan coated Silica Magnetic Nanoparticles (CS/Fe<sub>3</sub>O<sub>4</sub>-SiO<sub>2</sub>) thus obtained were separated using an external magnet and washed with methanol and water respectively dried in a vacuum at 60 °C for 6 h.

### Synthesis of Schiff base functionalized Chitosan coated Silica Magnetic Nanoparticles (CS-SB/Fe<sub>3</sub>O<sub>4</sub>-SiO<sub>2</sub>)

Initially, 2 g of CS/Fe<sub>3</sub>O<sub>4</sub>-SiO<sub>2</sub> was suspended in 100 mL of acetic acid (2%, w/v) and magnetically stirred at room temperature for 1 h. Then, salicylaldehyde (1 mmol, 0.12 g) was added to it and stirred under a magnetic stirrer at 60°C for 24h. The support (CS-SB/Fe<sub>3</sub>O<sub>4</sub>-SiO<sub>2</sub>) thus prepared was separated via magnet and washed with acetone and water, respectively and vacuum dried at 60 °C overnight.

### Synthesis of Zn@CS-SB/Fe3O4-SiO2

1 g of CS-SB/Fe<sub>3</sub>O<sub>4</sub>-SiO<sub>2</sub> and 0.13 g of Zn(II)Cl<sub>2</sub> were added into 45 mL of ethanol in a round-bottom flask (100 mL), and the resulting mixture was refluxed at 60°C for 16 h. Finally, Zn@CS-SB/Fe<sub>3</sub>O<sub>4</sub>-SiO<sub>2</sub>was collected from the reaction mixture using an external magnet and washed with EtOH and acetone, respectively, and vacuum dried at 70°C overnight.

### 4.1.2 Characterization of Zn@CS-SB/Fe<sub>3</sub>O<sub>4</sub>-SiO<sub>2</sub>

### HR-SEM

The surface morphological appearance of the synthesized catalyst was determined using HR-SEM analysis (**Figure 4.2**). HR-SEM images of the support i.e., CS-SB/Fe<sub>3</sub>O<sub>4</sub>-SiO<sub>2</sub> (**Figure 1a and 1b**),indicate the uniform dispersion of spherical particles with a slightly rough surface. Further, the HR-SEM images of the developed

catalyst i.e., Zn@CS-SB/Fe<sub>3</sub>O<sub>4</sub>-SiO<sub>2</sub> revealed its homogeneous nature, in which the lower magnified images revealed the presence of quasi-spherical structures (**Figure 4.2c**). However, the higher magnification view revealed the fibre-like structures (**Figure 4.2d**), which could be attributed to the imprinting of Zinc metal ions on the surface of CS-SB/Fe<sub>3</sub>O<sub>4</sub>-SiO<sub>2</sub>which has been reported to form fibre-like structures in many cases.

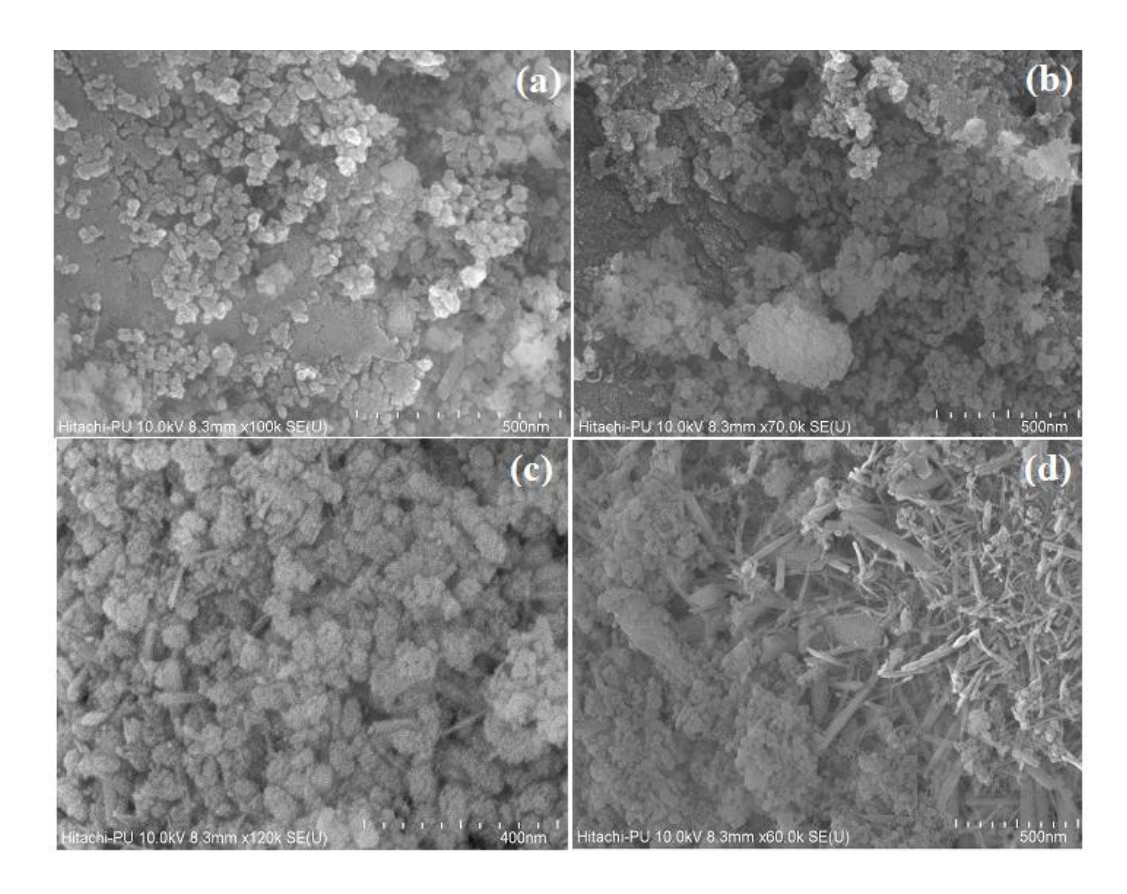


**Figure 4.2** HR-SEM images of (a and b) CS-SB/Fe<sub>3</sub>O<sub>4</sub>-SiO<sub>2</sub> (c and d) Zn@CS-SB/Fe<sub>3</sub>O<sub>4</sub>-SiO<sub>2</sub>

The distribution of various elements present in Zn@CS-SB/Fe<sub>3</sub>O<sub>4</sub>-SiO<sub>2</sub> was investigated using SEM elemental mapping (**Figure 4.3**). The corresponding images revealed the co-existence of Fe, Si, C, N, and Zn elements, demonstrating uniform distribution of all the elements in Zn@CS-SB/Fe<sub>3</sub>O<sub>4</sub>-SiO<sub>2</sub>.

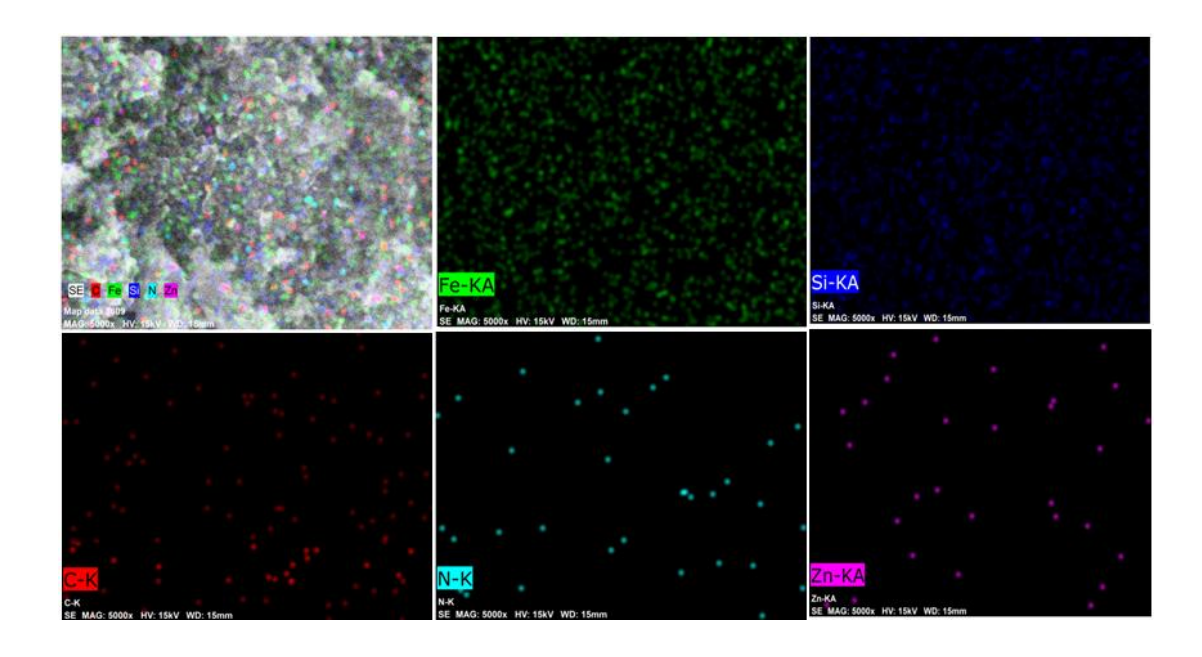


Figure 4.3 SEM Elemental Mapping of Zn@CS-SB/Fe<sub>3</sub>O<sub>4</sub>-SiO<sub>2</sub>

### **TEM**

Transmission Electron Microscopic images TEM (**Figure 4.4**) showed the presence of small black dots in the form of Zn(II) particles uniformly distributed over the surface of CS-SB/Fe<sub>3</sub>O<sub>4</sub>-SiO<sub>2</sub> support. Moreover, the light grey area surrounding the dark core of Fe<sub>3</sub>O<sub>4</sub>-SiO<sub>2</sub> confirmed the successful formation of chitosan-based Schiff base ligand onto the surface of Fe<sub>3</sub>O<sub>4</sub>-SiO<sub>2</sub>.

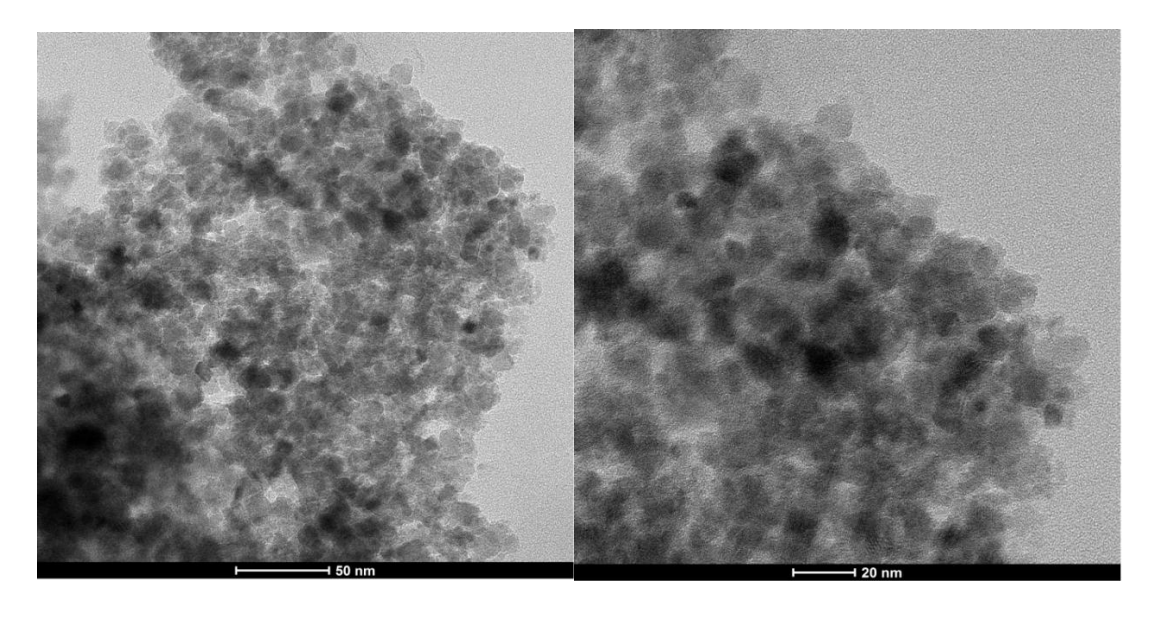


Figure 4.4. TEM images of Zn@CS-SB/Fe<sub>3</sub>O<sub>4</sub>-SiO<sub>2</sub>

### **EDX**

EDX profile of Zn@CS-SB/Fe<sub>3</sub>O<sub>4</sub>-SiO<sub>2</sub> demonstrated the presence of Fe, O, C, Si, N, and Zn as its main constituent elements (**Figure 4.5**). The developedcatalystwas considered to be pure, as no other peak of impurity was observed. Further, Inductively Coupled Plasma Atomic Emission Spectroscopy (ICP-AES analysis of Zn@CS-SB/Fe<sub>3</sub>O<sub>4</sub>-SiO<sub>2</sub> was carried out to ascertain its precise elemental composition. The results indicated that the amount of Zn loaded onto the support material CS-SB/Fe<sub>3</sub>O<sub>4</sub>-SiO<sub>2</sub> was found to be 1.8 wt%.

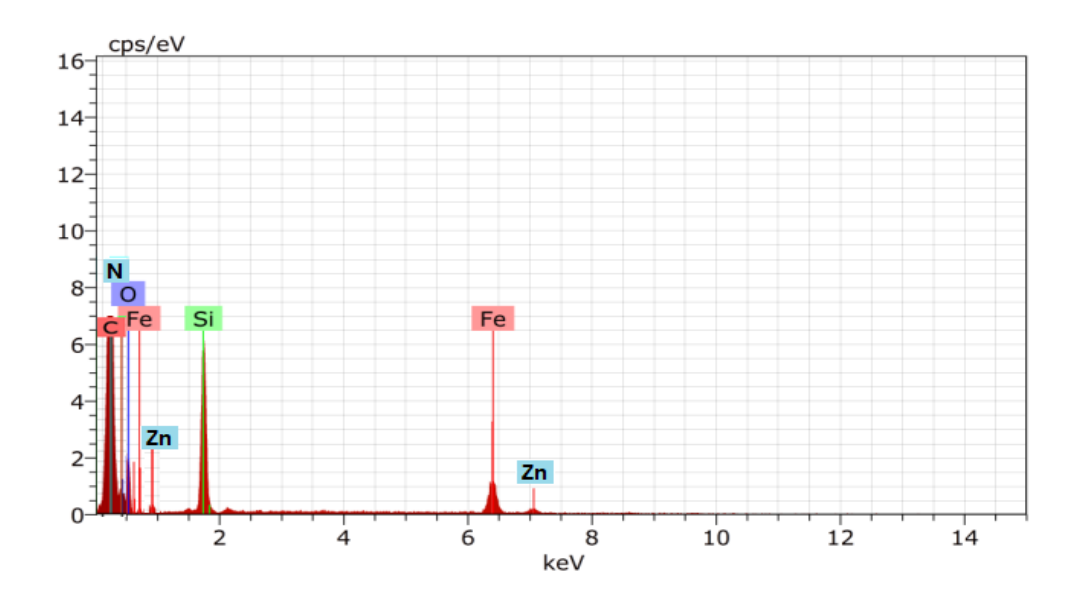


Figure 4.5 EDX Spectrum of Zn@CS-SB/Fe<sub>3</sub>O<sub>4</sub>-SiO<sub>2</sub>

### **BET**

To investigate the surface area as well as the porosity of the developed catalyst,Brunauer-Emmett-Teller (BET) analysis was done. According to the IUPAC classification, the Nitrogen adsorption-desorption curve of Zn@CS-SB/Fe<sub>3</sub>O<sub>4</sub>-SiO<sub>2</sub> exhibited type IV isotherm [1], suggesting its mesoporous nature (**Figure 4.6**). From the BET data, it was also inferred that Zn@CS-SB/Fe<sub>3</sub>O<sub>4</sub>-SiO<sub>2</sub> has a specific surface area of 146.79 m<sup>2</sup> g<sup>-1</sup>, a mean pore diameter of 15.89 nm, and a total pore volume of 0.377 cm<sup>3</sup> g<sup>-1</sup>, respectively.

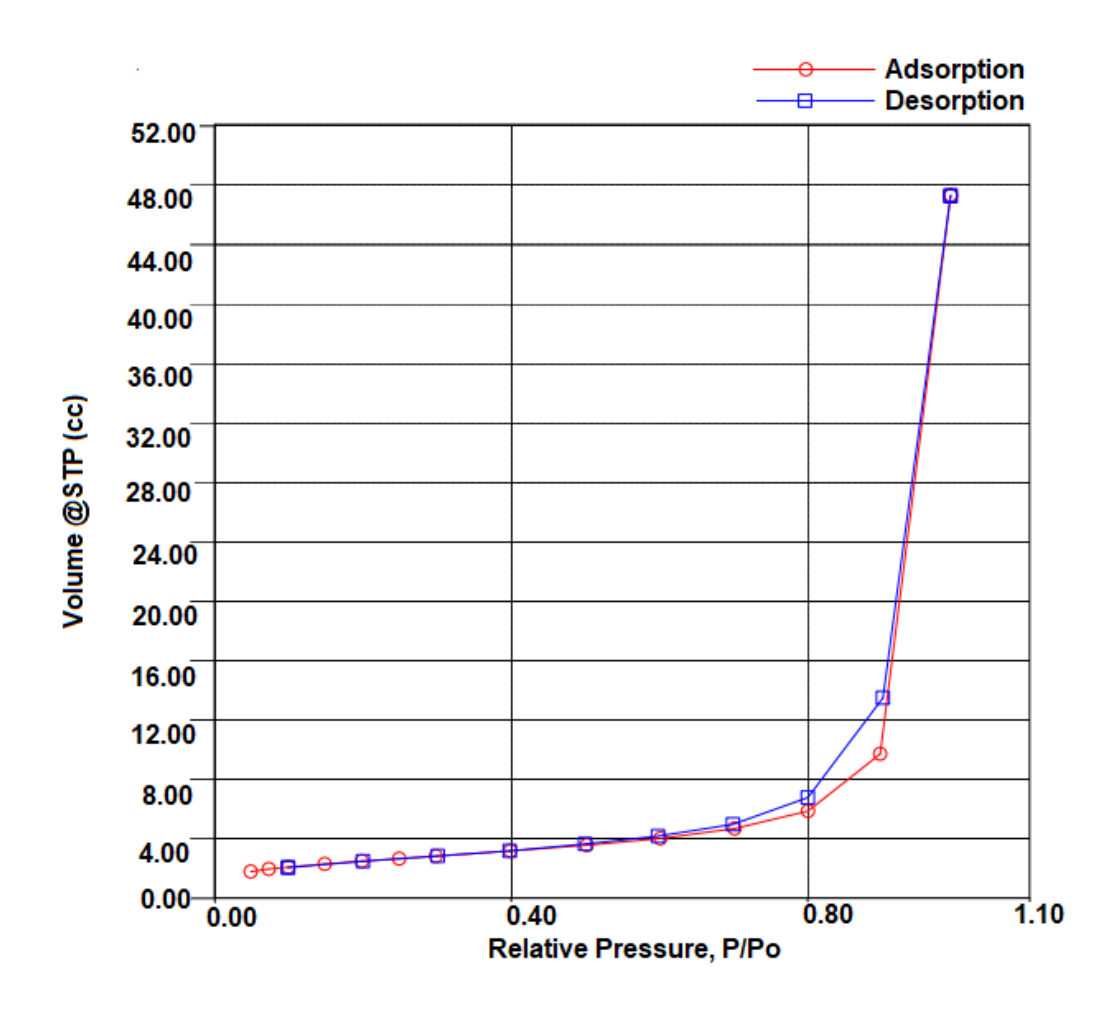


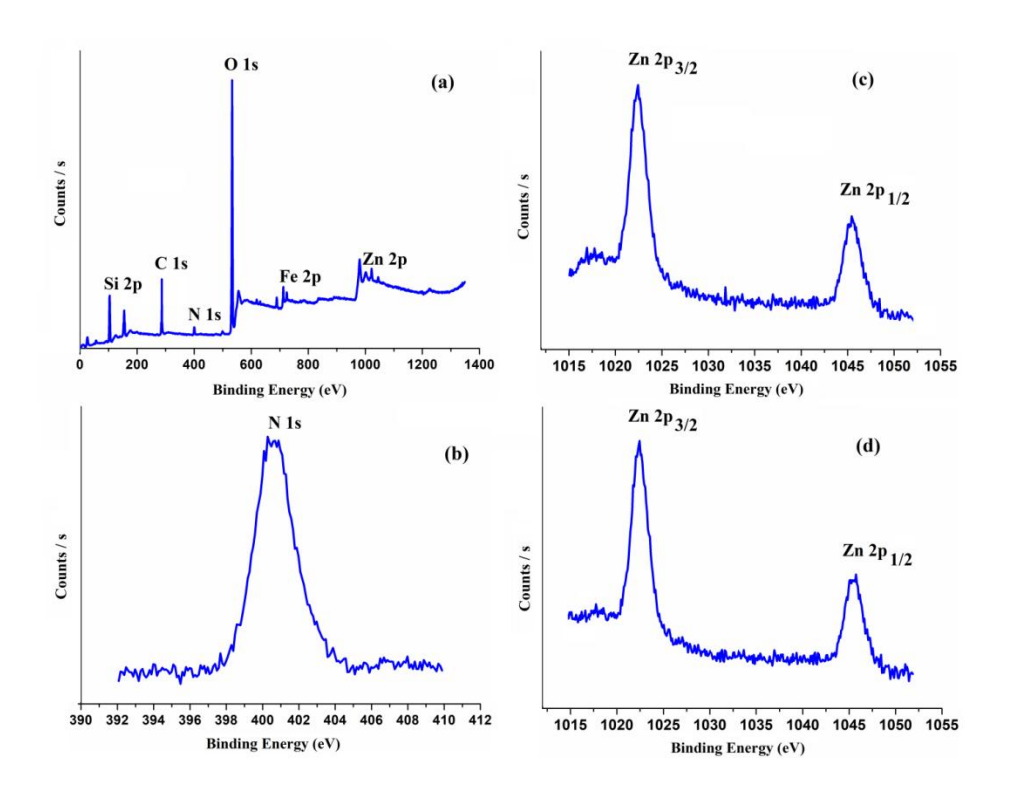
Figure 4.6 Nitrogen adsorption-desorption isotherm of Zn@CS-SB/Fe<sub>3</sub>O<sub>4</sub>-SiO<sub>2</sub>

### XPS

The binding energy and oxidation state (electronic properties) of Zn@CS-SB/Fe<sub>3</sub>O<sub>4</sub>-SiO<sub>2</sub>were investigated by X-ray photoelectron spectroscopy (XPS) technique. The overall survey spectrum (**Figure 4.7a**) confirms the presence of all the expected elements with binding energy peaks corresponding to Fe 2p (711.4 eV), Si 2p (103.6 eV), O 1s (531 eV), N 1s (399 eV) and Zn 2p (1021 eV) are well observed. **Figure 4.7b** represents N 1s region with a binding energy peak at 401 eV [2]. **Figure 4.7c** typically displayed two characteristic absorption peaks of Znat 1021 eV and 1044 eV for 2p<sub>3/2</sub> and 2p<sub>1/2</sub>, respectively with a binding energy difference of 23 eV, thereby confirming the +2oxidation state of Zn [3]. Further, the deconvoluted XPS spectrum of Zn 2p also showed two doublets of peaks at 1021.6 and 1044.7 eV attributed to +2

oxidation state of Zn. Moreover, the shifting of binding energy peaks of O (1s) and N (1s) at 532 eV and 399 eV may be attributed to the Zn-O and Zn-N bonds, respectively [4]. These outcomes certify that Zn metal could be successfully coordinated with N and O species on the surface of CS-SB/Fe<sub>3</sub>O<sub>4</sub>-SiO<sub>2</sub>and not by physical adsorption.

XPS analysis of the recycled catalyst (Figure **4.7d**, after six consecutive runs) indicated no significant changes in their binding energy patterns in comparison to the fresh catalyst, and thus representing a stable electronic structure around Zn<sup>2+</sup> in recycled catalyst, indicating the excellent recyclability of Zn@CS-SB/Fe<sub>3</sub>O<sub>4</sub>-SiO<sub>2</sub>.



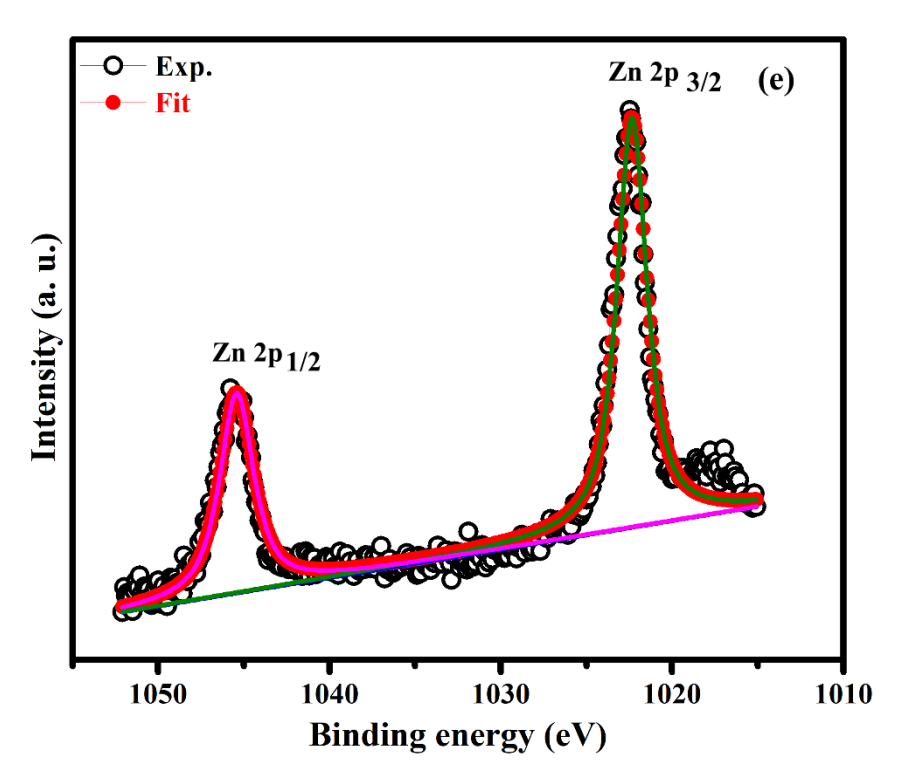


**Figure 4.7.** XPS of Zn@CS-SB/Fe<sub>3</sub>O<sub>4</sub>-SiO<sub>2</sub>; (a) Overall survey spectrum (b) N 1s region (c) Core level spectrum of Zn 2p (Fresh) (d) Core level spectrum of Zn 2p (reused after 6 runs) (e) DeconvulatedXPS spectrum of Zn 2p.

### **VSM**

The magnetic properties of Fe<sub>3</sub>O<sub>4</sub>-SiO<sub>2</sub> and Zn@CS-SB/Fe<sub>3</sub>O<sub>4</sub>-SiO<sub>2</sub> were examined using vibrating sample magnetometry (VSM) at room temperature. The VSM curves indicate that both samples exhibit zero coercivity, demonstrating superparamagnetic behavior [5] (**Figure 4.8**). The magnetic saturation values for Fe<sub>3</sub>O<sub>4</sub>-SiO<sub>2</sub> and Zn@CS-SB/Fe<sub>3</sub>O<sub>4</sub>-SiO<sub>2</sub> were measured to be 32.0 emu/g and 28.0 emu/g, respectively. The reduction in the magnetic saturation value for Zn@CS-SB/Fe<sub>3</sub>O<sub>4</sub>-SiO<sub>2</sub> is likely due to the presence of a significant amount of non-magnetic material on the surface of Fe<sub>3</sub>O<sub>4</sub>-SiO<sub>2</sub>. The inset image in **Figure 4.8** shows that the magnetic properties of the catalyst facilitate easy separation from the reaction mixture, allowing for redispersion into solution without significant aggregation in subsequent reaction cycles.

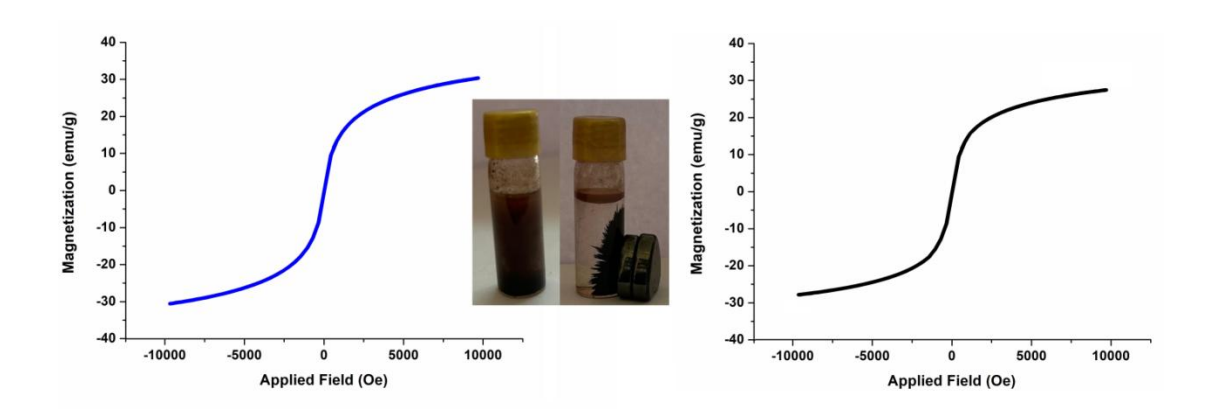
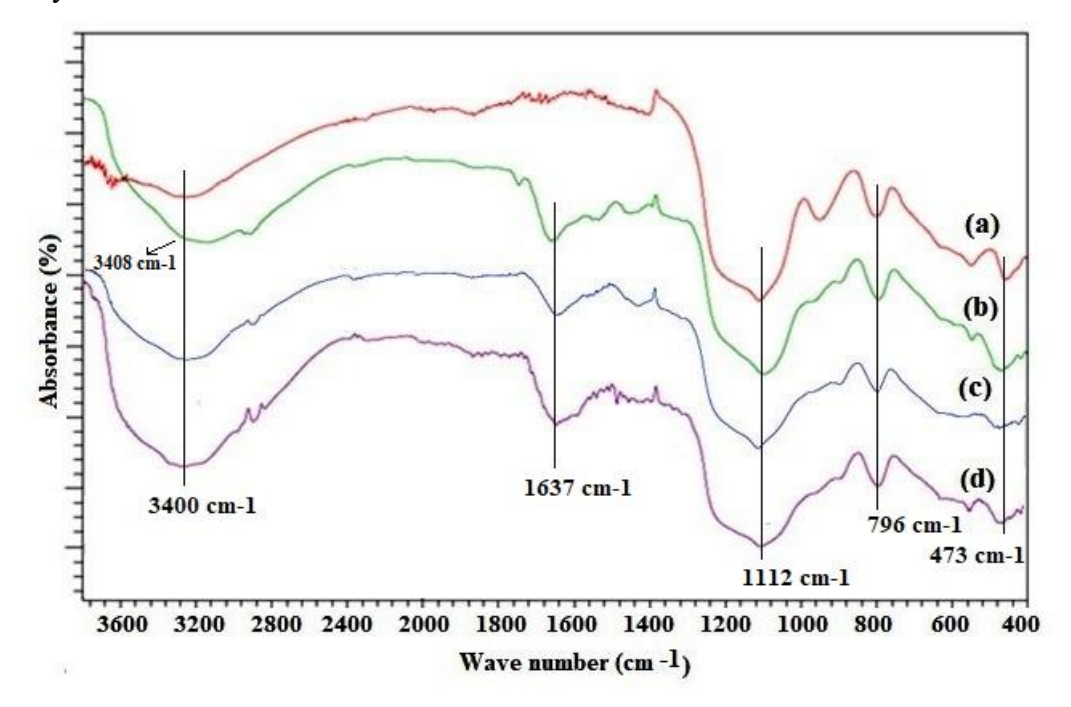


Figure 4.8 VSM spectra (a) Fe<sub>3</sub>O<sub>4</sub>-SiO<sub>2</sub> b) Zn@CS-SB/Fe<sub>3</sub>O<sub>4</sub>-SiO<sub>2</sub>

### **FTIR**

To probe various functionalities, present in the synthesized materials, FTIR spectroscopy was used and the corresponding spectra of (a) Fe<sub>3</sub>O<sub>4</sub>-SiO<sub>2</sub>, (b) CS-SB/Fe<sub>3</sub>O<sub>4</sub>-SiO<sub>2</sub> (c) Zn@CS-SB/Fe<sub>3</sub>O<sub>4</sub>-SiO<sub>2</sub> (Fresh), (d) Zn@CS-SB/Fe<sub>3</sub>O<sub>4</sub>-SiO<sub>2</sub> (reused after 6 runs) are presented in Figure 4.9. The characteristic stretching vibration at 548 cm<sup>-1</sup> is attributed to the Fe-O-Fe bond, and the peaks around 1112, 796, and 473 cm<sup>-1</sup> are probablyattributed to the Si-O-Si symmetric and asymmetric stretching vibrations, indicating the existence of a SiO<sub>2</sub> layer around the Fe<sub>3</sub>O<sub>4</sub> nanoparticles [6]. Figure 4.9 (b) demonstrated a characteristic broad band at 3408 cm<sup>-1</sup>, which corresponds to the overlapping stretching vibrations of -NH2 and -OH functional groups present in chitosan. Also, the characteristic broad absorption peak around 3400 cm<sup>-1</sup> is an envelope of stretching vibrations for O-H of the adsorbed water and silanol is observed in all the spectra, Figure 4.9 (a, b, c and d). The FTIR spectra of CS-SB/Fe<sub>3</sub>O<sub>4</sub>-SiO<sub>2</sub> and Zn@CS-SB/Fe<sub>3</sub>O<sub>4</sub>-SiO<sub>2</sub> (Figure 4.9b and c) showed the appearance of a new absorption peak at 1637 cm<sup>-1</sup> and 1522 cm<sup>-1</sup> which corresponds to the stretching vibrations of the C=N group and C-O group of phenol confirms the successful binding of chitosan functionalized Schiff base onto the surface of Fe<sub>3</sub>O<sub>4</sub>-SiO<sub>2</sub> magnetic nanoparticles. The formation of Zn(II) metal complex with coordinating N and O atoms of the Schiff base ligand on the modified surface of CS-SB/Fe<sub>3</sub>O<sub>4</sub>-SiO<sub>2</sub> was confirmed by the shift in the -C=N- stretching frequency by 12 cm<sup>-1</sup> in the FTIR spectrum of the Zn@CS-SB/Fe<sub>3</sub>O<sub>4</sub>-SiO<sub>2</sub> (Figure 4.9c).Further, the FTIR spectra (Figure 4.9d) of the reused catalyst (after six consecutive runs) in the degradation of dyes were carried out and the outcome clearly indicated no considerable changes, and peaks were observed in the same region as in the fresh catalyst.



**Figure4.9** FTIR spectra (a) Fe<sub>3</sub>O<sub>4</sub>-SiO<sub>2</sub>, (b) CS-SB/Fe<sub>3</sub>O<sub>4</sub>-SiO<sub>2</sub> (c) Zn@CS-SB/Fe<sub>3</sub>O<sub>4</sub>-SiO<sub>2</sub> (Fresh), (d)Zn@CS-SB/Fe<sub>3</sub>O<sub>4</sub>-SiO<sub>2</sub> (re-used after 6 runs).

### TGA

The thermal stability of the support materials, as well as the catalyst, was evaluated by carrying out thermogravimetric analysis (TGA). **Figure 4.10** shows the comparison of the TGA profiles of Fe<sub>3</sub>O<sub>4</sub>-SiO<sub>2</sub>, CS-SB/Fe<sub>3</sub>O<sub>4</sub>-SiO<sub>2</sub>, and Zn@CS-SB/Fe<sub>3</sub>O<sub>4</sub>-SiO<sub>2</sub>. The initial weight loss of about 4 wt% below 200°C in all the TGA curves is due to the desorption of physiosorbed and chemisorbed moisture. Further decrease in weight up to 10 % in Fe<sub>3</sub>O<sub>4</sub>-SiO<sub>2</sub> can be attributed to the elimination of adsorbed water, intact organic solvents, and hydroxyl groups from 200°C up to 600°C. Except, Fe<sub>3</sub>O<sub>4</sub>-SiO<sub>2</sub> (**Figure 4.10 a**), the other two thermograms(**Figure 4.10 b and c**) showed a two-stage thermal decomposition process. In the primary stage of thermal decomposition, weight loss in the temperature range below 350°C, could be attributed to the decomposition of the organic moieties present in chitosan-coated Schiff base ligand on the surface of Fe<sub>3</sub>O<sub>4</sub>-SiO<sub>2</sub>. In the secondary stage, weight loss of above 400 °C accounts for the degradation of aromatic framework and unreacted molecules from

the developed catalyst. It has been observed that anchoring of Zn (II) onto the surface of CS-SB/Fe<sub>3</sub>O<sub>4</sub>-SiO<sub>2</sub> decreased the overall thermal constancy of Zn@CS-SB/Fe<sub>3</sub>O<sub>4</sub>-SiO<sub>2</sub>, which could be ascribed to the thermal degrading of the metal species resulting in the lowering of the activation energy. After 600 °C, no significant weight loss was observed in all the thermograms, proving the thermal stability of developed materials at alleviated temperatures.

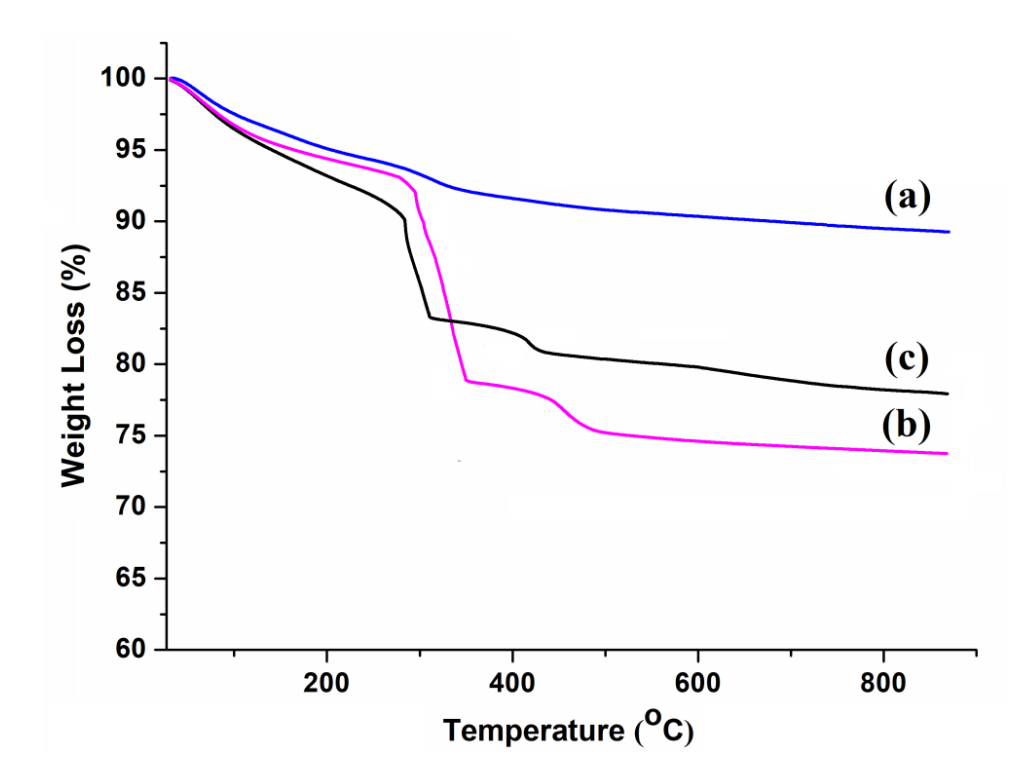


**Fig 4.10.** TGA curves (a) Fe<sub>3</sub>O<sub>4</sub>-SiO<sub>2</sub> (b) CS-SB/Fe<sub>3</sub>O<sub>4</sub>-SiO<sub>2</sub> (c) Zn@CS-SB/Fe<sub>3</sub>O<sub>4</sub>-SiO<sub>2</sub>

### XRD

The phase purity and the crystallinity of Zn@CS-SB/Fe<sub>3</sub>O<sub>4</sub>-SiO<sub>2</sub> was confirmed through X-ray powder diffraction (XRD) analysis. **Figure 4.11** showed three reflection patterns at  $2\theta$ = 34.3, 47.5, and 56.4° corresponding to the [002], [102] and [110] crystalline planes of ZnO [4].Thus, XRD and XPS outcomes confirmed that Zn<sup>2+</sup> is present in the form of ZnO.Further, the diffraction peaks at  $2\theta$ = 30.2, 35.6, 42.3, 53.4 and 62.3° corresponds to the [111], [220], [311], [422] and [511] planes of cubic phase of Fe<sub>3</sub>O<sub>4</sub> lattice which was confirmed by the JCPDS No. 75–1609 [7] and

some enhanced peak intensity was caused by overlapping of peaks of Zn and Fe<sub>3</sub>O<sub>4</sub> respectively. In addition to it, a broad diffraction band at  $2\theta = 15$ -29° and centred at  $2\theta = 22.0$ ° is the characteristic peak assigned to amorphous silica coated on the surface of Fe<sub>3</sub>O<sub>4</sub> nanospheres (JCPDS No. 29-0085) [8].

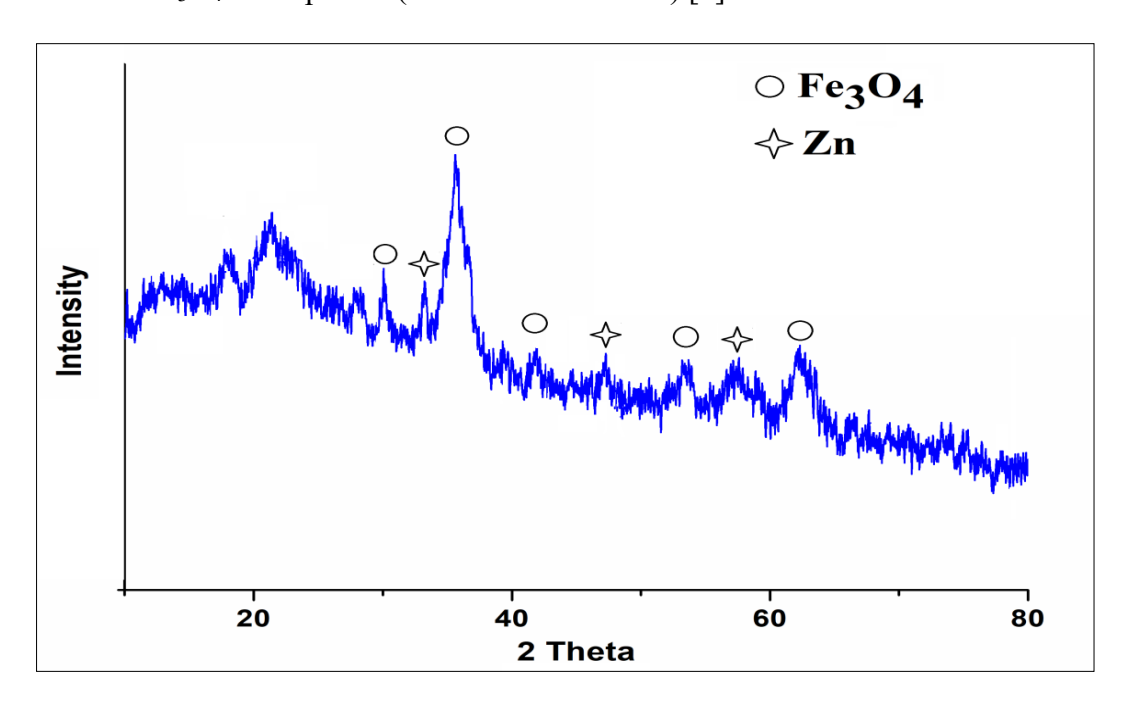


Figure 4.11. XRD spectrum of Zn@CS-SB/Fe<sub>3</sub>O<sub>4</sub>-SiO<sub>2</sub>

### 4.1.3 Reference

- [1]. Ambroz, F., Macdonald, T.J., Martis, V. and Parkin, I.P., 2018. Evaluation of the BET Theory for the Characterization of Meso and Microporous MOFs. *Small methods*, 2(11), pp1800173.
- [2]. Abd El Khalk, A.A., Betiha, M.A., Mansour, A.S., Abd El Wahed, M.G. and Al-Sabagh, A.M., 2021. High degradation of methylene blue using a new nanocomposite based on zeolitic imidazolate framework-8. *ACS omega*, 6(40), pp 26210-26220.
- [3].Zhao, F., Shan, R., Li, W., Zhang, Y., Yuan, H. and Chen, Y., 2021. Synthesis, characterization, and dye removal of ZnCl<sub>2</sub>-modified biochar derived from pulp and paper sludge. *ACS omega*, 6(50), pp 34712-34723.

- [4]. Ingavale, S., Marbaniang, P., Kakade, B. and Swami, A., 2021. Starbon with Zn-N and Zn-O active sites: An efficient electrocatalyst for oxygen reduction reaction in energy conversion devices. *Catalysis Today*, 370, pp 55-65.
- [5]. Sezer, N., Arı, İ., Bicer, Y. and Koc, M., 2021. Superparamagnetic nanoarchitectures: Multimodal functionalities and applications. *Journal of Magnetism and Magnetic Materials*, 538, pp 168300.
- [6]. Ahangaran, F., Hassanzadeh, A. and Nouri, S., 2013. Surface modification of Fe<sub>3</sub>O<sub>4</sub>@SiO<sub>2</sub> microsphere by silane coupling agent. *International Nano Letters*, 3, pp 1-5.
- [7]. Hasan, K., Joseph, R.G., Shehadi, I.A. and Patole, S.P., 2023. Fe<sub>3</sub>O<sub>4</sub>-chitosan immobilized Cu (II) Schiff base catalyst for the microwave-assisted amination of aryl halides in water. *Arabian Journal of Chemistry*, 16 (12), pp 105317.
- [8].Jia, P.Y., Liu, X.M., Li, G.Z., Yu, M., Fang, J. and Lin, J., 2006. Sol-gel synthesis and characterization of SiO2@ CaWO4, SiO2@ CaWO4: Eu3+/Tb3+core-shell structured spherical particles. *Nanotechnology*, *17*(3), p.734.

# Section 4.2 Zn (II) onto Chitosan Schiff base metal complex [Zn@CS-SB/Fe<sub>3</sub>O<sub>4</sub>-SiO<sub>2</sub>] as an efficient magnetically retrievable catalyst for the degradation of organic dyes

Organic pollutants have a significant impact on the environment and are among the major concerns of the modern world. Dyes, in particular, are a primary contributor to water pollution. A substantial quantity of both man-made and aromatic dyes is used in various industries. These dyes are toxic, carcinogenic, and mutagenic, posing serious risks to both the environment and living beings [1,2]. For instance, inhaling methylene blue (MB) dye can lead to symptoms such as dizziness, vomiting, excessive sweating, and mental confusion [3,4]. Additionally, dyes can hinder the photosynthesis of aquatic organisms, posing a severe threat to ecosystems. Dyes can be classified into two main categories: natural dyes and synthetic dyes. Natural dyes are derived from plant sources (leaves, stems, bark, roots, and flowers), as well as animal and mineral sources [5]. In contrast, synthetic dyes are further divided into three subcategories (Figure 4.12): (i) cationic (basic) dyes; (ii) anionic dyes (which include reactive, water-soluble acid, and direct dyes); and (iii) non-ionic dyes (such as solvent dyes, disperse dyes, and pigments) [6]. Many of these synthetic dyes are highly toxic to humans and aquatic organisms [7], highlighting the urgent need for effective degradation methods to remove these harmful substances from industrial waste under mild reaction conditions.

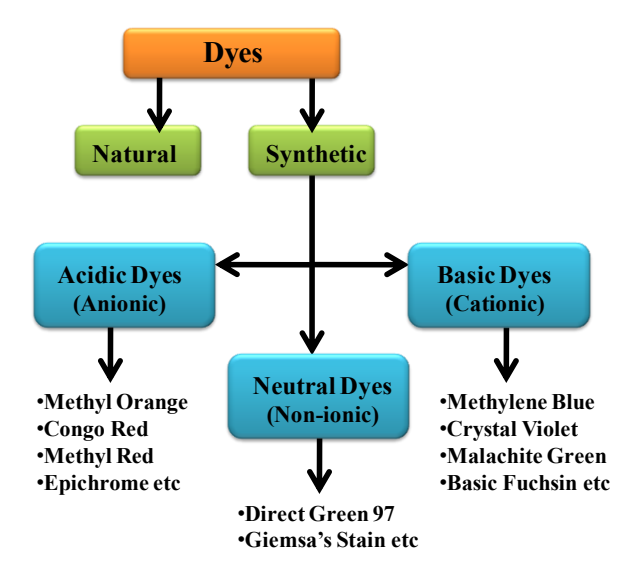
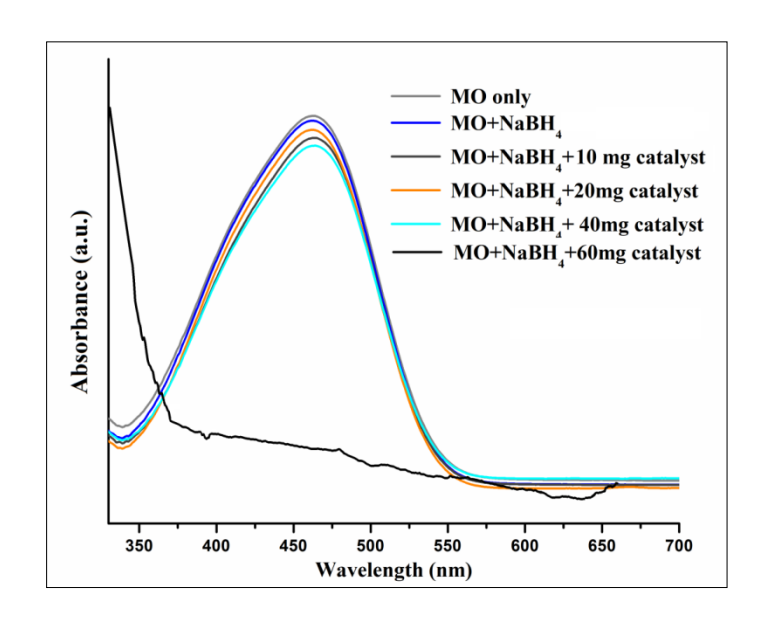


Figure 4.12 Classification of Dyes

Environmental pollutants, particularly dyes and related dyestuffs emerging from the textile industries, are highly mutagenic, carcinogenic, and toxic [8-10]. They are also non-biodegradable, leading to significant health issues such as skin irritation, kidney and liver damage, and poisoning of the central nervous system in both humans and animals [11-14]. Some dyes are challenging to degrade due to their complex aromatic structures and synthetic origins. Therefore, it is essential to develop a sustainable heterogeneous catalyst for the removal of the toxic dyes and dyestuffs from wastewater. Keeping in view the above considerations, we have developed a novel catalyst system i.e., Zn (II) onto Chitosan Schiff base metal complex [Zn@CS-SB/Fe<sub>3</sub>O<sub>4</sub>-SiO<sub>2</sub>] as a highly efficient magnetic catalyst for the degradation of organic dyes. The developed catalyst showed superior activity for the reduction of various dyes like methylene blue (MB), methyl orange (MO), methyl red (MR) and pnitrophenol (PNP) dyes.

### 4.2.1 Results and Discussion

To optimize the reaction conditions, the reduction of methyl orange dye (MO) at a concentration of  $3 \times 10^{-5}$  M in the presence of sodium borohydride (NaBH<sub>4</sub>) (0.05 g) in an aqueous solution was used as a test reaction to investigate the catalytic performance of our catalyst, Zn@CS-SB/Fe<sub>3</sub>O<sub>4</sub>-SiO<sub>2</sub>. The test reaction was probed using UV-Vis spectroscopy, and the absorbance of MO at 465 nm was monitored carefully. Before the addition of sodium borohydride and the catalyst, the dilute aqueous solution of the dye exhibited a specific color. As soon as the reaction started, the color of the solution began to fade within seconds, indicating dye degradation. This color change correlates with a shift in absorption frequency (\lambda max), as recorded by the UV-Vis spectrophotometer. Initially, a blank experiment was conducted without using Zn@CS-SB/Fe<sub>3</sub>O<sub>4</sub>-SiO<sub>2</sub> and sodium borohydride. The subsequent addition of NaBH4 to the MO solution revealed that NaBH4 alone did not affect the absorbance spectra, even after 10 minutes. Therefore, the gathered absorption spectra showed that MO is not efficiently reduced by NaBH<sub>4</sub> alone (Figure 4.13). Additionally, the progress of the catalytic degradation was monitored at different time intervals, using varying concentrations of the catalyst and sodium borohydride, with a UV-Vis spectrophotometer. Figure 4.13demonstrates the photocatalytic degradation of MO using Zn@CS-SB/Fe<sub>3</sub>O<sub>4</sub>-SiO<sub>2</sub> and NaBH<sub>4</sub>. The addition of NaBH<sub>4</sub> alongside 60 mg of the catalyst resulted in a significant color change in the solution within 5 minutes, as well as noticeable alterations in the absorption spectra.NaBH<sub>4</sub>dissociates to produce Na<sup>+</sup> and BH<sub>4</sub>-ions. These ions, along with the dyes, are diffused from aqueous solution onto the surface of the catalyst. Hydrogen ions produced from BH<sub>4</sub>-ions and adsorbed on the catalyst attack the -C=O- and -N=N- functional groups of the dyes. The dyes are finally reduced and detachfrom the catalyst's surface. In conclusion, our results indicate that negligible catalytic conversion was observed with NaBH<sub>4</sub> alone, while the introduction of the catalyst significantly enhanced the catalytic conversions, confirming that Zn@CS-SB/Fe<sub>3</sub>O<sub>4</sub>-SiO<sub>2</sub> is an efficient catalyst for the reduction of methylorange (MO) dye.



**Figure 4.13** Zn@CS-SB/Fe<sub>3</sub>O<sub>4</sub>-SiO<sub>2</sub>catalyzed photocatalytic degradation of Methyl orange Dye under UV-Vis light

After optimizing the reaction conditions, we have selected other mutagenic and noxious, organic dyes, such as methyl red (MR), methylene blue (MB), and p-nitrophenol (PNP), to demonstrate the catalytic versatility of the developed catalyst. The degradation or reduction of MB (3.2×10<sup>-5</sup> M) using NaBH<sub>4</sub> (0.05 g) was conducted at room temperature in the presence of Zn@CS-SB/Fe<sub>3</sub>O<sub>4</sub>-SiO<sub>2</sub> (0.06 g). It was evident that upon adding the catalyst to the reaction medium, the characteristic blue color of the MB dye disappeared within 10 minutes due to the degradation of

MB to leuco methylene blue [15], and it is also reflected by a rapid decline in the absorption intensity around 660 nm (Figure 4.14a). Similarly, the catalytic efficacy of the synthesized catalyst was explored for the catalytic reduction of MR (3.6×10<sup>-5</sup> M) and PNP (7.1×10<sup>-5</sup> M)dyes using 0.05 g of NaBH<sub>4</sub>. The characteristic red color of MR with corresponding absorption peak at 430 nm vanished within 10 minutes upon the addition of the catalyst (Figure 4.14 b). For PNP, the aqueous solution exhibited a pale-yellow color with an absorption band at 317 nm under UV-visible light, which was shifted to 400 nm on the addition of Zn@CS-SB/Fe<sub>3</sub>O<sub>4</sub>-SiO<sub>2</sub> owing to the formation of 4-nitrophenolate, and the colour altered to bright yellow [16]. Further, on adding NaBH<sub>4</sub>, the absorption peak at 400 nm disappeared and a fresh peak at 298 nm formed due to the creation of 4-aminophenol [17] within 8 minutes (Figure 4.14 c). It is a recognized fact that the activity of a catalyst is strongly influenced by the number of active sites present in it. In our case, the existence of C=N/C=C and -OH functional groups and active metal, i.e., Zn2+ may combine with electron-acceptor sites present in the dyes via donor-acceptor  $\pi$ -electron interaction to facilitate the reduction of organic dyes efficiently [18].

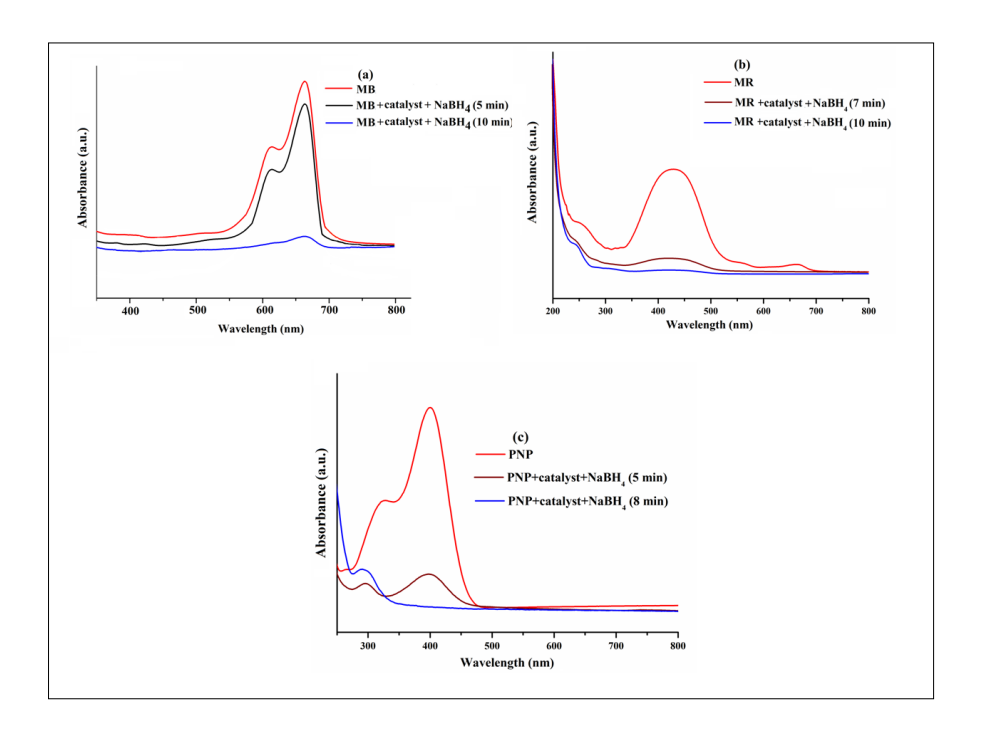


**Figure 4.14** Zn@CS-SB/Fe<sub>3</sub>O<sub>4</sub>-SiO<sub>2</sub>catalyzed photocatalytic degradation of (a) Methylene blue (MB); (b) Methyl red (MR); (c) para-nitrophenol (PNP) under UV-Vis light

### Recyclability

To determine the recyclability of our catalyst and to fulfil the goal of sustainability, the reduction of methyl orange (MO) using Zn@CS-SB/Fe<sub>3</sub>O<sub>4</sub>-SiO<sub>2</sub> was performed for six consecutive runs (**Figure 4.15**). Following the completion of the MO dye degradation, Zn@CS-SB/Fe<sub>3</sub>O<sub>4</sub>-SiO<sub>2</sub> was separated from the reaction mixture using a magnet and simply washed with ethyl acetate (2×10 mL) and water (3×10 mL), vacuum dried, and then reused for subsequent reaction under similar conditions. The results confirm that the developed catalyst used for the reduction of MO dye was reusable up to six cycles without significant loss in its activity,demonstrating the outstanding recyclability of the catalyst.

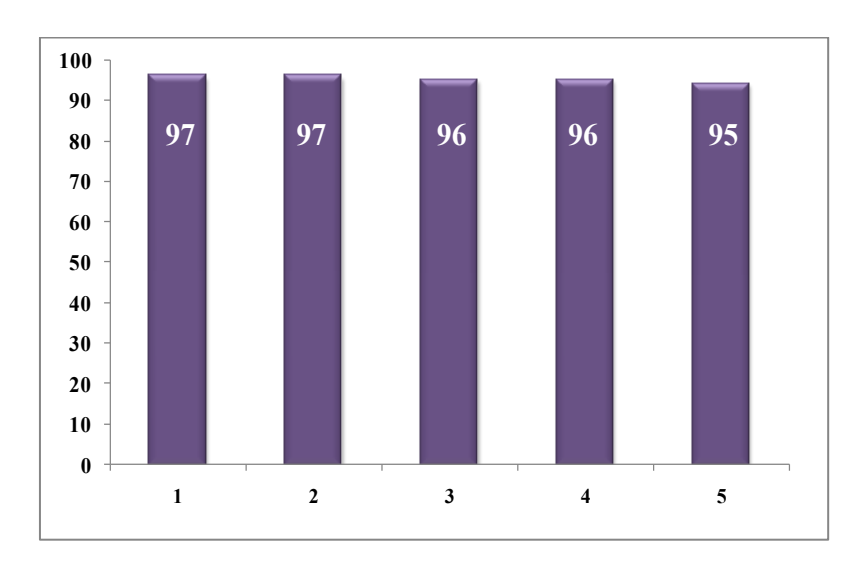


**Figure 4.15** Recyclability of Zn@CS-SB/Fe<sub>3</sub>O<sub>4</sub>-SiO<sub>2</sub> for the degradation of MO dye under optimized reaction conditions.

### 4.2.2 Conclusion

The present study aimed to synthesize the novel magnetic catalyst system Zn@CS-SB/Fe<sub>3</sub>O<sub>4</sub>-SiO<sub>2</sub> bygraftingZn (II) onto Chitosan Schiff base metal complex. Experimental analysis demonstrated that the developed catalyst exhibited excellent catalytic performance for the degradation of various organic dyes such as MO, MB, MR, and PNP under mild reaction conditions, using NaBH<sub>4</sub> as the reducing agent. Zn@CS-SB/Fe<sub>3</sub>O<sub>4</sub>-SiO<sub>2</sub> achieved high efficiency in short reaction times, proving effective even with low metal loading. The enhanced activity of the magnetic composite can be attributed to the combined effects of its high surface area and

improved dye adsorption on the catalyst surface. Furthermore, the catalyst can be easily recycled and reused up to six times without a significant loss in its catalytic activity and selectivity.

### General procedure for the Zn@CS-SB/Fe<sub>3</sub>O<sub>4</sub>-SiO<sub>2</sub> catalyzed degradation of dyes

In a solution of organic dye (0.001 g) in 100 mL of water, Zn@CS-SB/Fe<sub>3</sub>O<sub>4</sub>-SiO<sub>2</sub> (0.06 g) was added. The resultant solution was stirred at room temperature for 30 minutes in the dark to establish an adsorption/desorption equilibrium between the catalyst's surface and the dye molecules. Following this, NaBH<sub>4</sub> (0.05 g) was introduced to the mixture. After various intervals, 5 mL samples were withdrawn from the reaction mixture for analysis. The samples were analyzed using UV-Vis absorption spectroscopy. The catalyst was then separated from the suspension through centrifugation and successfully reused for subsequent catalytic cycles.

### 4.2.3 References

- [1]. Du, J., Arwa, A.H., Cao, Y., Yao, H., Sun, Y., Garaleh, M., Massoud, E.E.S., Ali, E., Assilzadeh, H. and Escorcia-Gutierrez, J., 2024. Green synthesis of zinc oxide nanoparticles from Sida acuta leaf extract for antibacterial and antioxidant applications, and catalytic degradation of dye through the use of convolutional neural network. *Environmental Research*, 258, p.119204.
- [2]. Liu, Y., Jin, W., Zhao, Y., Zhang, G. and Zhang, W., 2017. Enhanced catalytic degradation of methylene blue by α-Fe2O3/graphene oxide via heterogeneous photo-Fenton reactions. *Applied Catalysis B: Environmental*, 206, pp 642-652.
- [3]. Wang, L., Zhang, J. and Wang, A., 2011. Fast removal of methylene blue from aqueous solution by adsorption onto chitosan-g-poly (acrylic acid)/attapulgite composite. *Desalination*, 266(1-3), pp 33-39.
- [4]. El-Sharkawy, E.A., Soliman, A.Y. and Al-Amer, K.M., 2007. Comparative study for the removal of methylene blue via adsorption and photocatalytic degradation. *Journal of colloid and interface science*, 310(2), pp 498-508.
- [5]. Saxena, S. and Raja, A.S.M., 2014. Natural dyes: sources, chemistry, application and sustainability issues. In *Roadmap to sustainable textiles and*

- clothing: eco-friendly raw materials, technologies, and processing methods (pp 37-80). Singapore: Springer Singapore.
- [6]. Pereira, L. and Alves, M., 2012. Dyes-environmental impact and remediation. *Environmental protection strategies for sustainable development*, pp 111-162.
- [7]. Seey, T.L. and Kassim, M.J.N.M., 2012. Characterization of mangrove bark as a potentially low-cost adsorbent for reactive dye removal from aqueous solutions: Equilibrium, mechanisms and kinetics. *International Journal of Pure and Applied Sciences and Technology*, 9(1), pp 9.
- [8]. Mazaheri, H., Ghaedi, M., Azqhandi, M.A. and Asfaram, A.J.P.C.C.P., 2017. Application of machine/statistical learning, artificial intelligence and statistical experimental design for the modeling and optimization of methylene blue and Cd (II) removal from a binary aqueous solution by natural walnut carbon. *Physical Chemistry Chemical Physics*, 19(18), pp 11299-11317.
- [9]. Asfaram, A., Ghaedi, M., Azqhandi, M.H.A., Goudarzi, A. and Hajati, S., 2017. Ultrasound-assisted binary adsorption of dyes onto Mn@ CuS/ZnS-NC-AC as a novel adsorbent: application of chemometrics for optimization and modeling. *Journal of Industrial and Engineering Chemistry*, 54, pp 377-388.
- [10]. Eren, Z., Ince, N.H. and Acar, F.N., 2010. Degradation of textile dyes, dyebaths and dyeing wastewater by homogeneous and heterogeneous sonophotolysis. *Journal of Advanced Oxidation Technologies*, 13(2), pp 206-211.
- [11]. Eren, Z., 2012. Degradation of an azo dye with homogeneous and heterogeneous catalysts by sonophotolysis. *Clean–Soil, Air, Water*, 40(11), pp 1284-1289.
- [12]. Jabeen, S., Sufaid Khan, M., Khattak, R., Zekker, I., Burlakovs, J., Rubin, S.S.D., Ghangrekar, M.M., Kallistova, A., Pimenov, N., Zahoor, M. and Khan, G.S., 2021. Palladium-supported zirconia-based catalytic degradation of rhodamine-b dye from wastewater. *Water*, *13*(11), pp 1522.

- [13]. Kassem, A.A., Abdelhamid, H.N., Fouad, D.M. and Ibrahim, S.A., 2020. Hydrogenation reduction of dyes using metal-organic framework-derived CuO@ C. *Microporous and Mesoporous Materials*, 305, pp 110340.
- [14]. Veisi, H., Abassi, P., Mohammadi, P., Tamoradi, T. and Karmakar, B., 2021. Gold nanoparticles decorated biguanidine modified mesoporous silica KIT-5 as recoverable heterogeneous catalyst for the reductive degradation of environmental contaminants. *Scientific Reports*, 11(1), pp 2734.
- [15]. Kora, A.J. and Rastogi, L., 2016. Catalytic degradation of anthropogenic dye pollutants using palladium nanoparticles synthesized by gum olibanum, a glucuronoarabinogalactan biopolymer. *Industrial Crops and Products*, 81, pp 1-10.
- [16]. Choudhary, M.K., Kataria, J. and Sharma, S., 2018. Evaluation of the kinetic and catalytic properties of biogenically synthesized silver nanoparticles. *Journal of cleaner production*, 198, pp 882-890.
- [17]. Francis, S., Joseph, S., Koshy, E.P. and Mathew, B., 2017. Synthesis and characterization of multifunctional gold and silver nanoparticles using leaf extract of Naregamia alata and their applications in the catalysis and control of mastitis. *New Journal of Chemistry*, 41(23), pp 14288-14298.
- [18]. Zhao, F., Shan, R., Li, W., Zhang, Y., Yuan, H. and Chen, Y., 2021. Synthesis, characterization, and dye removal of ZnCl<sub>2</sub>-modified biochar derived from pulp and paper sludge. *ACS omega*, 6(50), pp 34712-34723.

## Chapter 5

This chapter gives details about the synthetic procedure ofPd@SB/Fe<sub>3</sub>O<sub>4</sub>-TiO<sub>2</sub>, its characterization,and applications

## Section 5.1 Synthesis and characterization of Schiff base functionalized Pd (II) complex onto titania grafted magnetic nanoparticles [Pd@SB/Fe<sub>3</sub>O<sub>4</sub>-TiO<sub>2</sub>]

This section presents a novel magnetic heterogeneous catalyst based on Schiff base functionalized Pd (II) complex onto titania grafted magnetic nanoparticles [Pd@SB/Fe<sub>3</sub>O<sub>4</sub>-TiO<sub>2</sub>]. The synthetic route of Pd@Fe<sub>3</sub>O<sub>4</sub>-TiO<sub>2</sub>/SB is shown in **Figure 5.1**. Initially, Fe<sub>3</sub>O<sub>4</sub> nanoparticles were synthesized by the co-precipitating salts of Fe<sup>3+</sup> and Fe<sup>2+</sup> in alkaline media. Thereafter, to prevent agglomeration, titania was coated onto the surface of Fe<sub>3</sub>O<sub>4</sub> nanoparticles via ultrasonication. The surface of the magnetic TiO<sub>2</sub> coated nanoparticles were functionalized using ethane-1,2-diamine (EDA). The surface –NH<sub>2</sub> groups of EDA/Fe<sub>3</sub>O<sub>4</sub>-TiO<sub>2</sub> were then condensed with salicylaldehyde to give Schiff base functionalized TiO<sub>2</sub> coated magnetic nanoparticles. Finally, palladium acetate was treated with SB/Fe<sub>3</sub>O<sub>4</sub>-TiO<sub>2</sub> under N<sub>2</sub> atm. to give Pd@SB/Fe<sub>3</sub>O<sub>4</sub>-TiO<sub>2</sub> as the heterogeneous magnetic nanocatalyst. The developed novel catalyst, Pd@SB/Fe<sub>3</sub>O<sub>4</sub>-TiO<sub>2</sub> was characterized using various spectroscopic techniques viz. SEM, XPS, TEM, XRD, BET, TGA, FT-IR, EDX, CHN, VSM and ICP-AES analysis.

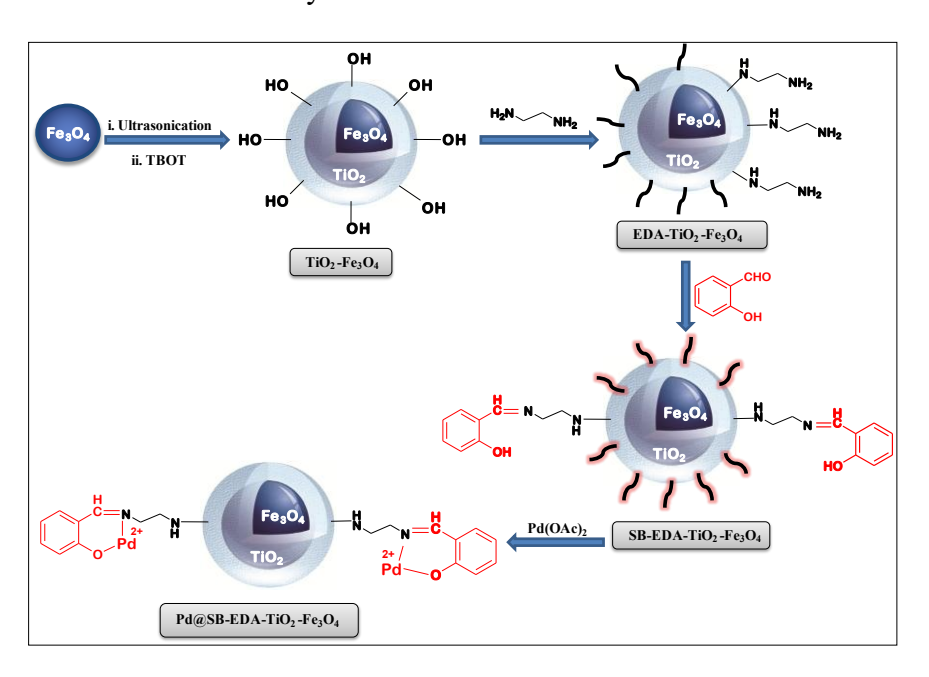


Figure 5.1. General scheme for the preparation of Pd@SB/Fe<sub>3</sub>O<sub>4</sub>-TiO<sub>2</sub>

### 5.1.1 General procedure for the synthesis of Pd@SB/Fe<sub>3</sub>O<sub>4</sub>-TiO<sub>2</sub>

### Preparation of Fe<sub>3</sub>O<sub>4</sub> nanoparticles

To 30 mL of distilled water in a beaker, 5 g of FeCl<sub>3</sub> and 2.5 g of FeCl<sub>2</sub> were dissolved. The solution so obtained was added drop by drop to an aq. NaOH solution for 30 minutes under continuous stirring. Precipitation occurred, and the metal salt was transformed into corresponding hydroxides, which were converted into nano ferrites. The precipitated nano ferrites were separated after 15 minutes using an external magnet and subsequently washed so as to maintain their pH at 7.0 using distilled water and vacuum dried at 60°C.

### Preparation of Fe<sub>3</sub>O<sub>4</sub>-TiO<sub>2</sub>

For the preparation of Fe<sub>3</sub>O<sub>4</sub>-TiO<sub>2</sub>, 1 g of ferrite nanoparticleswas added into a mixture of NH<sub>4</sub>OH (5.0 mL) and ethanol (40 mL) and the resultant suspension was made to undergo ultrasonication for 0.5 h. The resultant solution was poured into an R.B.F. (100 mL), and to it,tetrabutylorthotitanate (4.0 mL) in EtOH (30 mL) was added dropwise and the resultant solution was stirred for 24 h at 45 °C. The resultant composite of Fe<sub>3</sub>O<sub>4</sub>-TiO<sub>2</sub> was separated via magnet and washed with H<sub>2</sub>O and EtOH and oven dried overnight at 60 °C.

### Preparation of EDA/Fe<sub>3</sub>O<sub>4</sub>-TiO<sub>2</sub>

A mixture comprising Ethane-1,2-diamine (EDA) (5 mL) and Fe<sub>3</sub>O<sub>4</sub>-TiO<sub>2</sub> (1 g) was taken in an R.B.F. (50 mL), and to it was added deionized water (10 mL). The reaction mixture was stirred for 8 h at 120 °C. The resultant amine functionalized support of Fe<sub>3</sub>O<sub>4</sub>-TiO<sub>2</sub> was separated using magnet and washed with EtOH and H<sub>2</sub>O successively. It was finally vacuum dried at 60 °C to get EDA/Fe<sub>3</sub>O<sub>4</sub>-TiO<sub>2</sub> as light brown powder.

### Preparation of [SB/Fe<sub>3</sub>O<sub>4</sub>-TiO<sub>2</sub>]

To the suspension of EDA/Fe<sub>3</sub>O<sub>4</sub>-TiO<sub>2</sub> (1 g) in ethanol (30 mL), salicylaldehyde (1.50 mmol) was added and the resultant mixture was refluxed for 24 h. The composite of Schiff base functionalized TiO<sub>2</sub> coated magnetic nanoparticles (SB/Fe<sub>3</sub>O<sub>4</sub>-TiO<sub>2</sub>), thus obtained after the condensation reaction of amine functionality of EDA/Fe<sub>3</sub>O<sub>4</sub>-TiO<sub>2</sub>

with salicylaldehyde was separated using magnet and washed with EtOH and H<sub>2</sub>O. The Fe<sub>3</sub>O<sub>4</sub>-TiO<sub>2</sub>/SB support was finally vacuum dried overnight at 60°C.

### Synthesis of [Pd@SB/Fe<sub>3</sub>O<sub>4</sub>-TiO<sub>2</sub>]

To 1 g of Schiff base functionalized TiO<sub>2</sub> coated magnetic nanoparticles support (Fe<sub>3</sub>O<sub>4</sub>-TiO<sub>2</sub>/SB), a sol. of Pd(OAc)<sub>2</sub> (0.1 g) in toluene (25 mL) was added. The reaction mixture was made to undergo stirring for 16 h under nitrogen atmosphere at 70°C. The resulting Pd@Fe<sub>3</sub>O<sub>4</sub>-TiO<sub>2</sub>/SB complex so obtained was separated via magnet followed by washing with EtOH and H<sub>2</sub>O and vacuum dried overnight.

### 5.1.2 Characterization of Pd@SB/Fe<sub>3</sub>O<sub>4</sub>-TiO<sub>2</sub>

### FE-SEM

It can provide the morphology, size, and distribution of grains of materials. From the FE-SEM images (**Figure 5.2**) of Pd@SB/Fe<sub>3</sub>O<sub>4</sub>-TiO<sub>2</sub>, it was found that the developed catalyst consists of small uniformly distributed quasi-spherical particles with slightly rough structure.

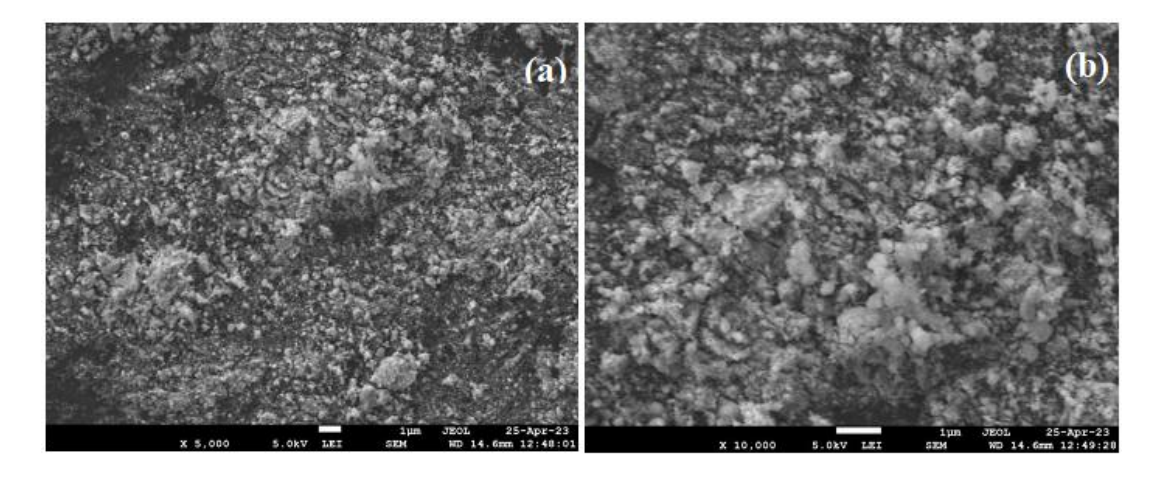


Figure 5.2 FEG-SEM images of Pd@SB/Fe<sub>3</sub>O<sub>4</sub>-TiO<sub>2</sub>

### **TEM**

To understand the morphology and the crystalline properties of Pd@SB/Fe<sub>3</sub>O<sub>4</sub>-TiO<sub>2</sub>, we have used transmission electron microscopy (TEM) with selected area electron diffraction (SAED) pattern analysis (**Figure 5.3**). TEM micrographs indicated the uniform presence of Pd in the form of small well dispersed black dots onto the Fe<sub>3</sub>O<sub>4</sub>-

TiO<sub>2</sub>/SB support (**Figure 5.3a**). The light grey area behind the black dots confirms the presence of SB/Fe<sub>3</sub>O<sub>4</sub>-TiO<sub>2</sub>. Moreover, the average size distributions of Pd@SB/Fe<sub>3</sub>O<sub>4</sub>-TiO<sub>2</sub> werefound to be in the range of 25 to 30 nm (Inset image, **Figure 5.3b**), which was analyzed by plotting a histogram. Further, the concentric rings with bright diffraction spots as shown by the SAED pattern confirmed that the synthesized catalyst has polycrystalline nature. The calculated lattice fringe spacing measured 0.29 nm and 0.26 nm which agree well with (220) and (311) lattice planes present in Fe<sub>3</sub>O<sub>4</sub> [1,2]. Furthermore, the interplanar space values measuring 0.37 nm and 0.23 nm corresponds to the (220) and (111) crystal planes of Pd (**Figure 5.3c**) [3,4].

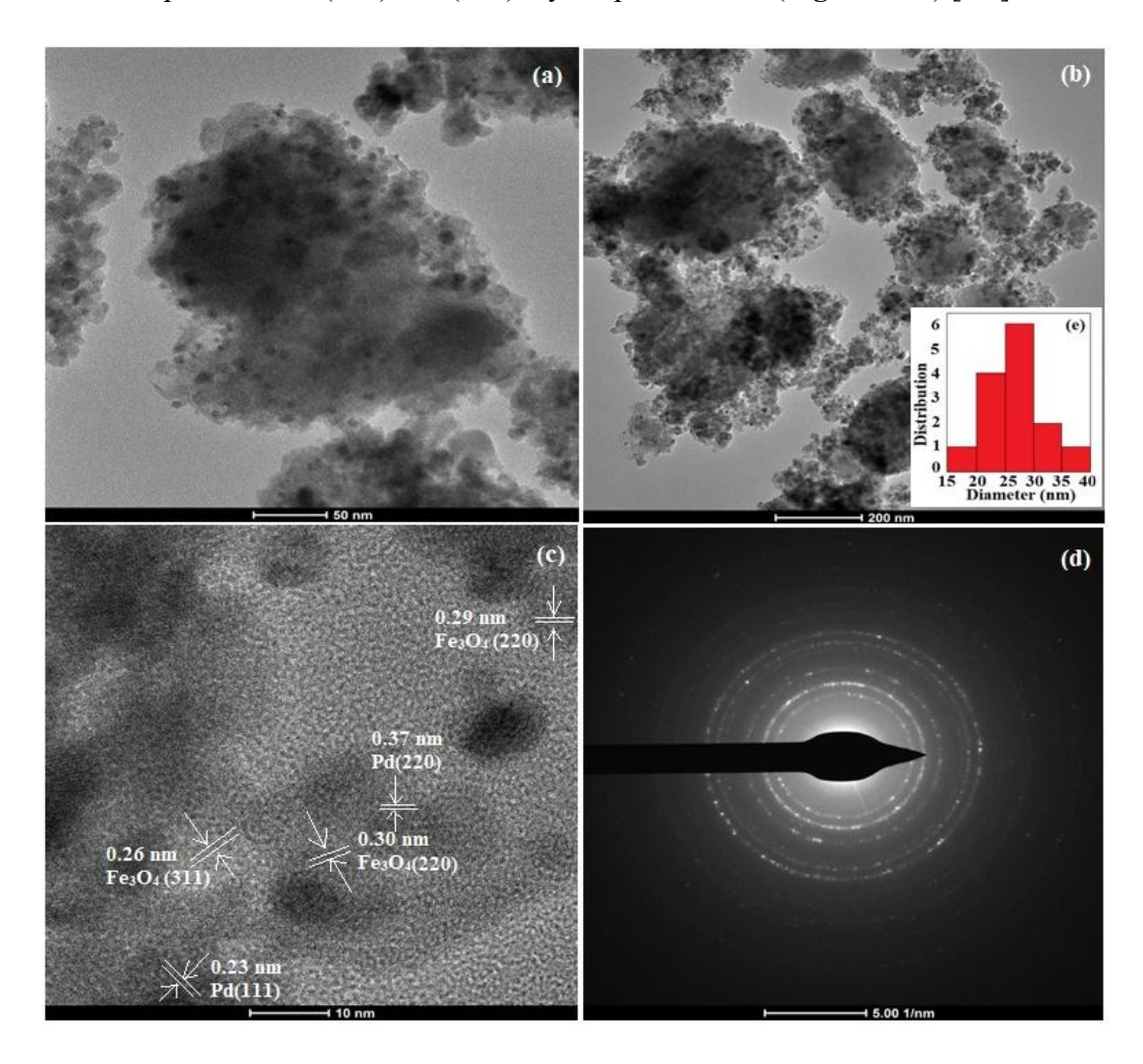
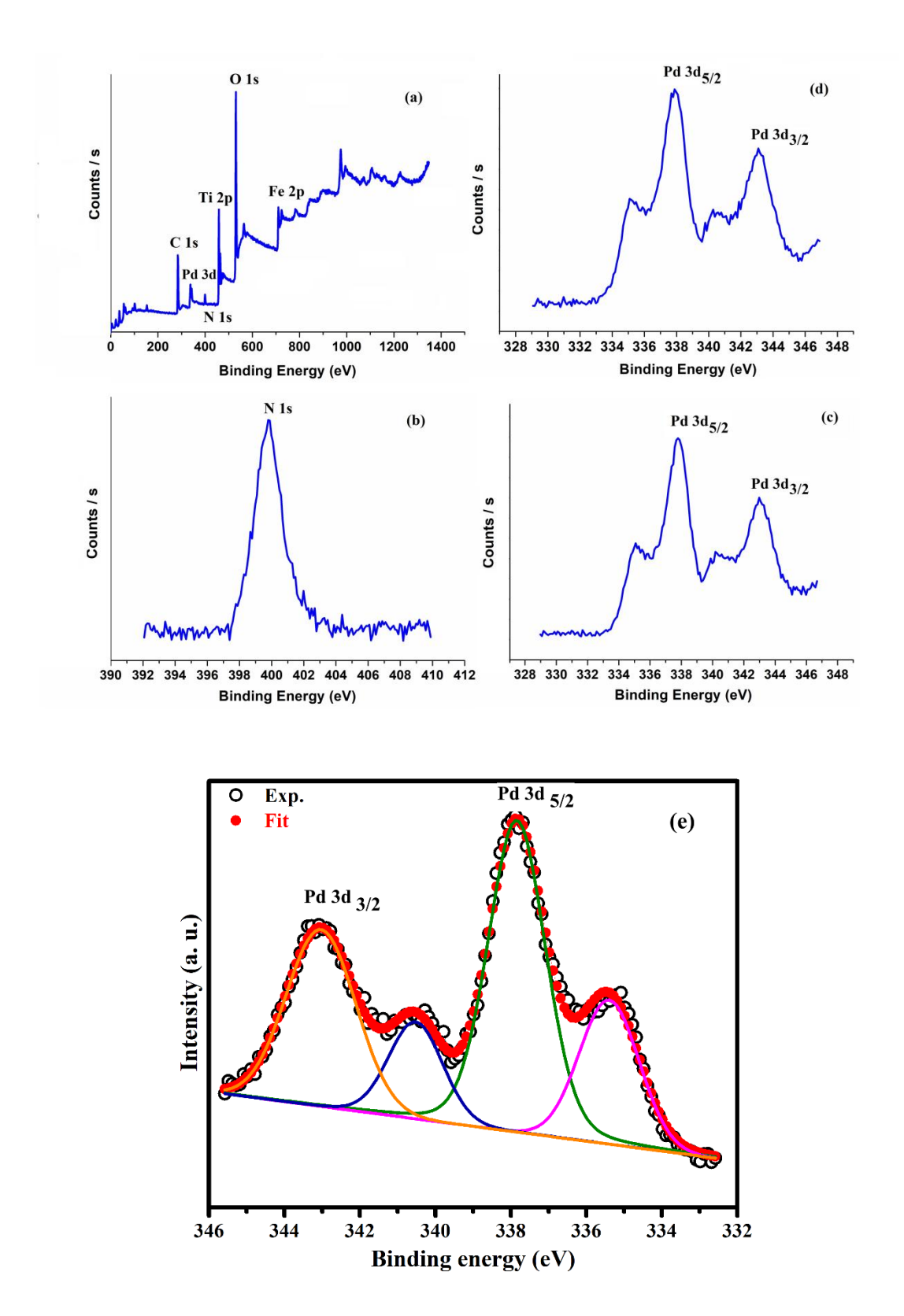


Figure 5.3 TEM images of Pd@SB/Fe<sub>3</sub>O<sub>4</sub>-TiO<sub>2</sub> (a to c); SAED pattern (d)

### XPS

The binding energy and oxidation state (electronic properties) of Pd@SB/Fe<sub>3</sub>O<sub>4</sub>-TiO<sub>2</sub> were analyzed by X-ray photoelectron spectroscopy (XPS) technique. The overall survey spectrum (Figure 5.4a) confirms the presence of all the expected elements with binding energy peaks corresponding to Fe 2p (712.1 eV), Ti 2p (458 and 464 eV), O 1s (531 eV), N 1s (401 eV) and Pd 3d (338 eV) are well observed. Figure **5.4b** typically displayed two characteristic absorption peaks at 338 eV and 343 eV for  $3d_{5/2}$  and  $3d_{3/2}$  respectively, which are consistent with the +2 oxidation state of Pd [5]. Furthermore, the deconvoluted XPS spectrum of Pd 3d also showed two doublets of peaks at 338.2 and 343.4 eV attributed to +2 oxidation state of Pd for 3d<sub>5/2</sub> and 3d<sub>3/2</sub>respectively (**Figure 5.4e**). In comparison to pure Pd(OAc)<sub>2</sub> with binding energy peaks at 337.5 and 342.9 eV, the Pd(II) binding energy of the catalyst, Pd@SB/Fe<sub>3</sub>O<sub>4</sub>-TiO<sub>2</sub> negatively shifted by 0.5 eV, signifying that Pd(II) was binded to the N and O elements of Schiff base functionalized support (SB/Fe<sub>3</sub>O<sub>4</sub>-TiO<sub>2</sub>) [6]. Moreover, the shifting of binding energy peaks of O (1s) and N (1s) at 531 eV and 401 eV may attributes to the Pd-O and Pd-N bonds respectively. These outcomes certify that Pd metal could be successfully coordinated with N and O species on the surface of SB/Fe<sub>3</sub>O<sub>4</sub>-TiO<sub>2</sub>and not by physical adsorption.

XPS analysis of the recycled catalyst (after six consecutive run) indicated no significant changes in their binding energy patterns in comparison to the fresh catalyst, and thus representing a stable electronic structure around Pd<sup>2+</sup> in recycled catalyst, indicating the excellent recyclability of Pd@SB/Fe<sub>3</sub>O<sub>4</sub>-TiO<sub>2</sub> (**Figure 5.4d**).



**Figure 5.4.** XPS of Pd@SB/Fe<sub>3</sub>O<sub>4</sub>-TiO<sub>2</sub>; (a) Overall survey spectrum (b) N 1s region (c) Core level spectrum of Pd 3d (Fresh) (d) Core level spectrum of Pd 3d (re-used after 6 runs) (e) Deconvulated XPS spectrum of Pd3d.

### XRD

The phase purity and the crystallinity of Fe<sub>3</sub>O<sub>4</sub>-TiO<sub>2</sub>, SB/Fe<sub>3</sub>O<sub>4</sub>-TiO<sub>2</sub>and Pd@SB/Fe<sub>3</sub>O<sub>4</sub>-TiO<sub>2</sub> was determined by XRD analysis (Figure 5.5). The XRD spectra of Fe<sub>3</sub>O<sub>4</sub>-TiO<sub>2</sub> (**Figure 5.5a**) showed diffraction peaks at 30.3°, 35.6°, 57.3° and 63.1° may be due to the crystal faces of Fe<sub>3</sub>O<sub>4</sub> nanoparticles with corresponding indices at (220), (311), (511) and (440) respectively and it was confirmed by the JCPDS card No. 75–1609 [7], whereas the peaks at 48.1° and 53.7° corresponds to the (200) and (105) cubic planes of TiO<sub>2</sub> [8]. Further, in the XRD spectra of Pd@SB/Fe<sub>3</sub>O<sub>4</sub>-TiO<sub>2</sub> (Figure 5.5c), appearance of two new diffraction peaks at  $2\theta = 39.9^{\circ}$  and  $43.1^{\circ}$  from crystalline planes (111) and (200) of face centered Pd were observed in addition to the peaks of Fe<sub>3</sub>O<sub>4</sub> and TiO<sub>2</sub> [9].It is quite noticeable that the characteristic diffraction peaks due to Fe<sub>3</sub>O<sub>4</sub> and TiO<sub>2</sub> were retained after grafting Schiff base functionalized Palladium (II) complex onto TiO<sub>2</sub> coated magnetic nanoparticles, which indicates that introducing Pd(II) has not interfered the crystalline phases of Fe<sub>3</sub>O<sub>4</sub> and TiO<sub>2</sub> although their intensities had been slightly reduced. Furthermore, the XRD of the recycled catalyst (following six consecutive runs) in Suzuki coupling and hydrogenation of aromatic nitro compounds was also carried out and the outcomes clearly specified no considerable changes in the XRD peaks in contrast to the fresh catalyst (Figure 5.5d).

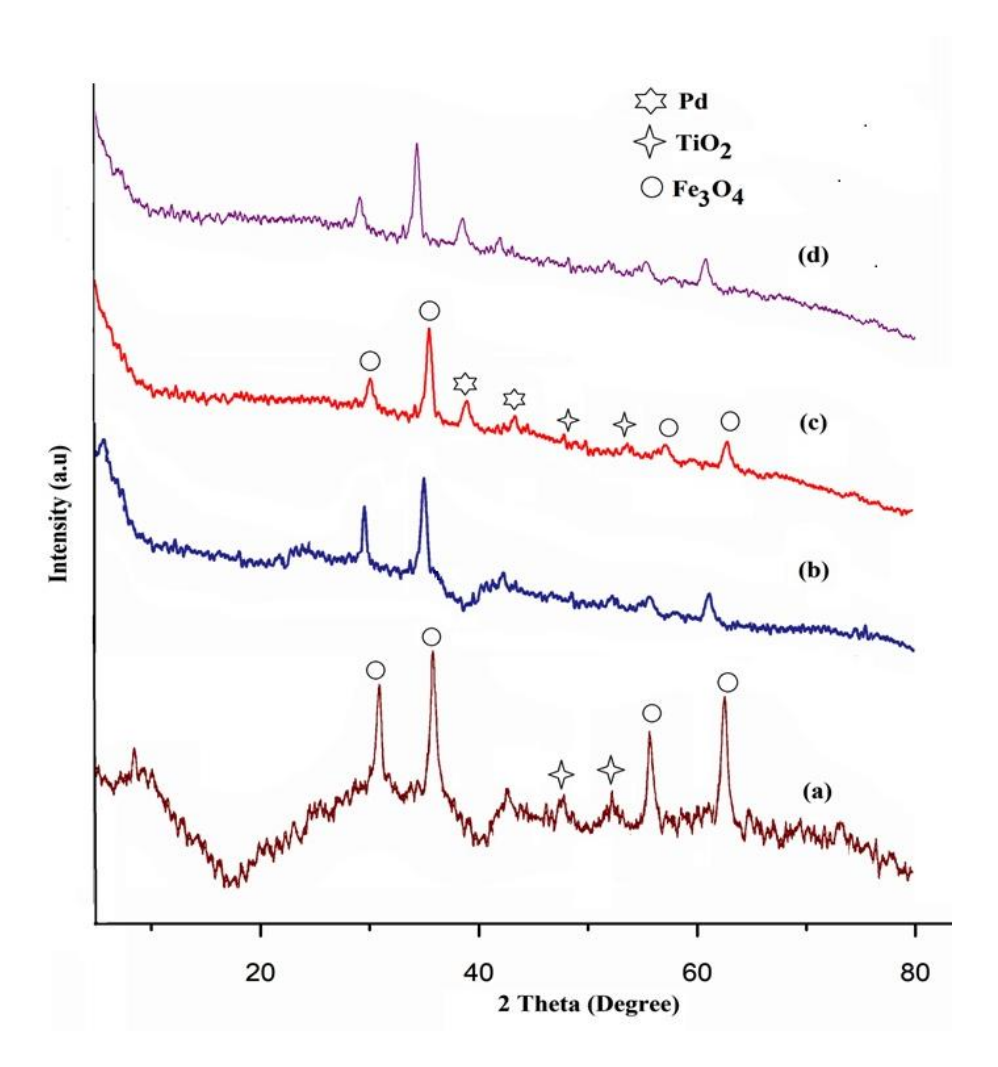


**Figure 5.5.** XRD spectra (a) Fe<sub>3</sub>O<sub>4</sub>-TiO<sub>2</sub>, (b) SB/Fe<sub>3</sub>O<sub>4</sub>-TiO<sub>2</sub>(c) Pd@SB/Fe<sub>3</sub>O<sub>4</sub>-TiO<sub>2</sub> (Fresh), (d)Pd@SB/Fe<sub>3</sub>O<sub>4</sub>-TiO<sub>2</sub> (re-used after 6 runs).

### **TG**A

The thermal constancy of the developed catalyst has been evaluated by thermogravimetric analysis. **Figure 5.6** presents the TGA curves of the different stages. The initial loss in weight of 5.0 wt% below 200 °C in all the three spectra was attributed to the removal of residual solvent and physically adsorbed water molecules from the surface. Further, in the TGA curve of SB/Fe<sub>3</sub>O<sub>4</sub>-TiO<sub>2</sub>, a sharp decrease in weight with a loss of 15.72 wt% between 300 °C and 400 °C was observed due to loss of covalently bonded organic moieties. The degradation continued further till 500 °C with 9wt% loss due to the decomposition of aromatic framework and unreacted molecules. Anchoring of Pd (II) onto the surface of SB/Fe<sub>3</sub>O<sub>4</sub>-TiO<sub>2</sub> decreased the thermal constancy of Pd@SB/Fe<sub>3</sub>O<sub>4</sub>-TiO<sub>2</sub> further. This overall decrease in the thermal

stability of developed catalyst could be ascribed to the thermal degrading in presence of the metal species resulting in the lowering of the activation energy [10]. Nevertheless, the synthesized material could be used upto 310 °C for catalyzing the organic reactions.

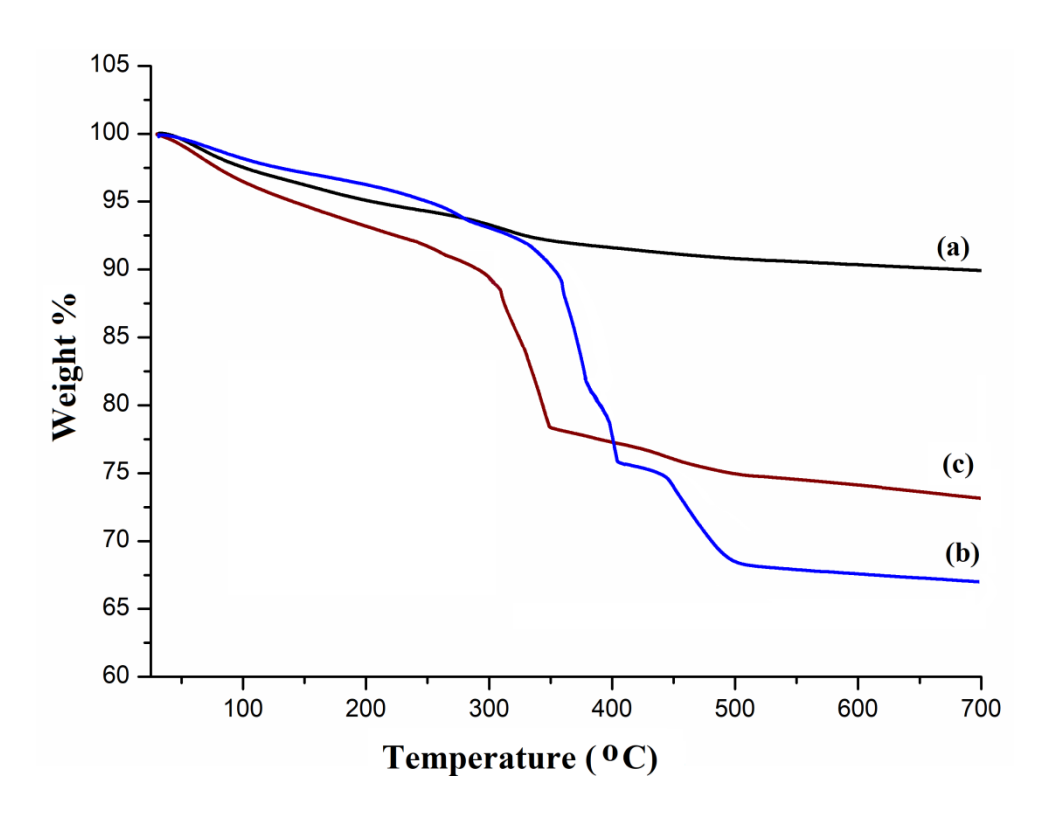


**Figure 5.6** TGA curves (a) Fe<sub>3</sub>O<sub>4</sub>-TiO<sub>2</sub>, (b) SB/Fe<sub>3</sub>O<sub>4</sub>-TiO<sub>2</sub>(c) Pd@SB/Fe<sub>3</sub>O<sub>4</sub>-TiO<sub>2</sub> **BET** 

N<sub>2</sub> adsorption-desorption measurements by BET analysis to determine the surface area as well as the porosity of Pd@SB/Fe<sub>3</sub>O<sub>4</sub>-TiO<sub>2</sub> was done. According to the IUPAC classification, the plot of Pd@SB/Fe<sub>3</sub>O<sub>4</sub>-TiO<sub>2</sub> exhibited type IV, suggesting the mesoporous nature of the developed catalyst (**Figure 5.7**). As evident from the BET data, Pd@SB/Fe<sub>3</sub>O<sub>4</sub>-TiO<sub>2</sub> gives specific surface area of 114.62 m<sup>2</sup> g<sup>-1</sup>, mean pore diameter of 17.23 nm and total pore volume of 0.49 cm<sup>3</sup>/g, respectively.

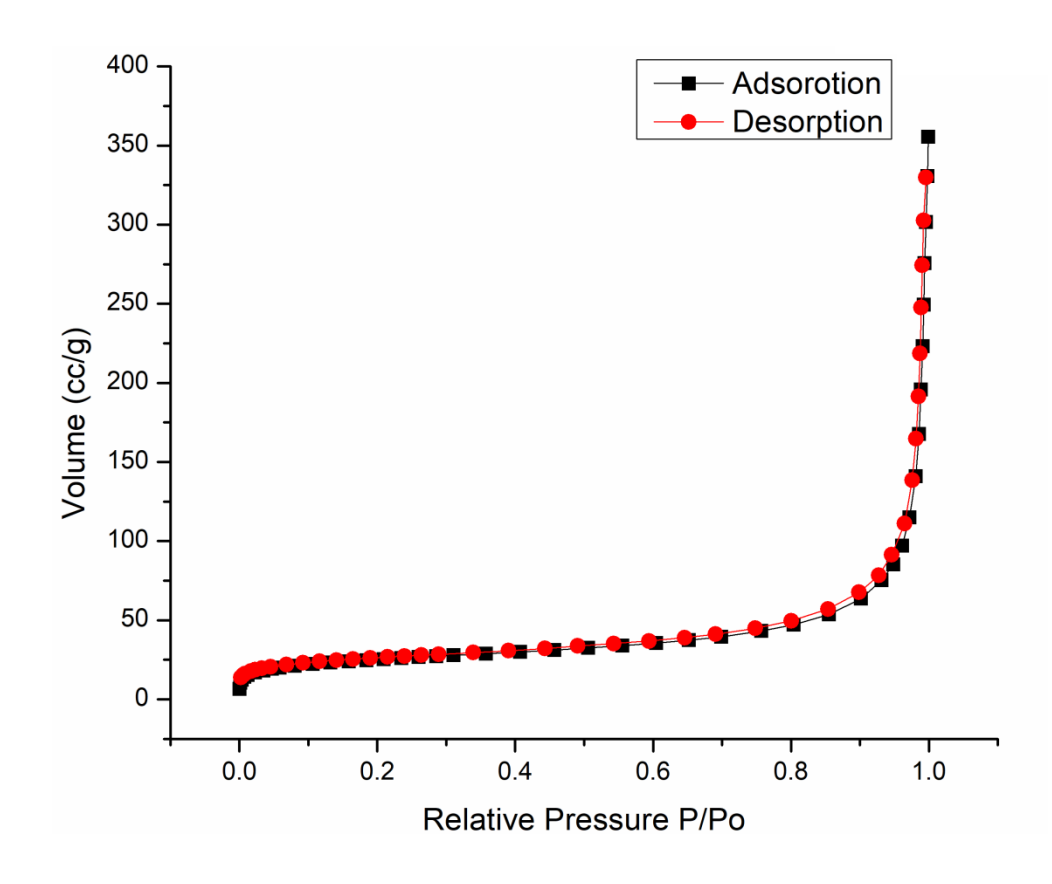
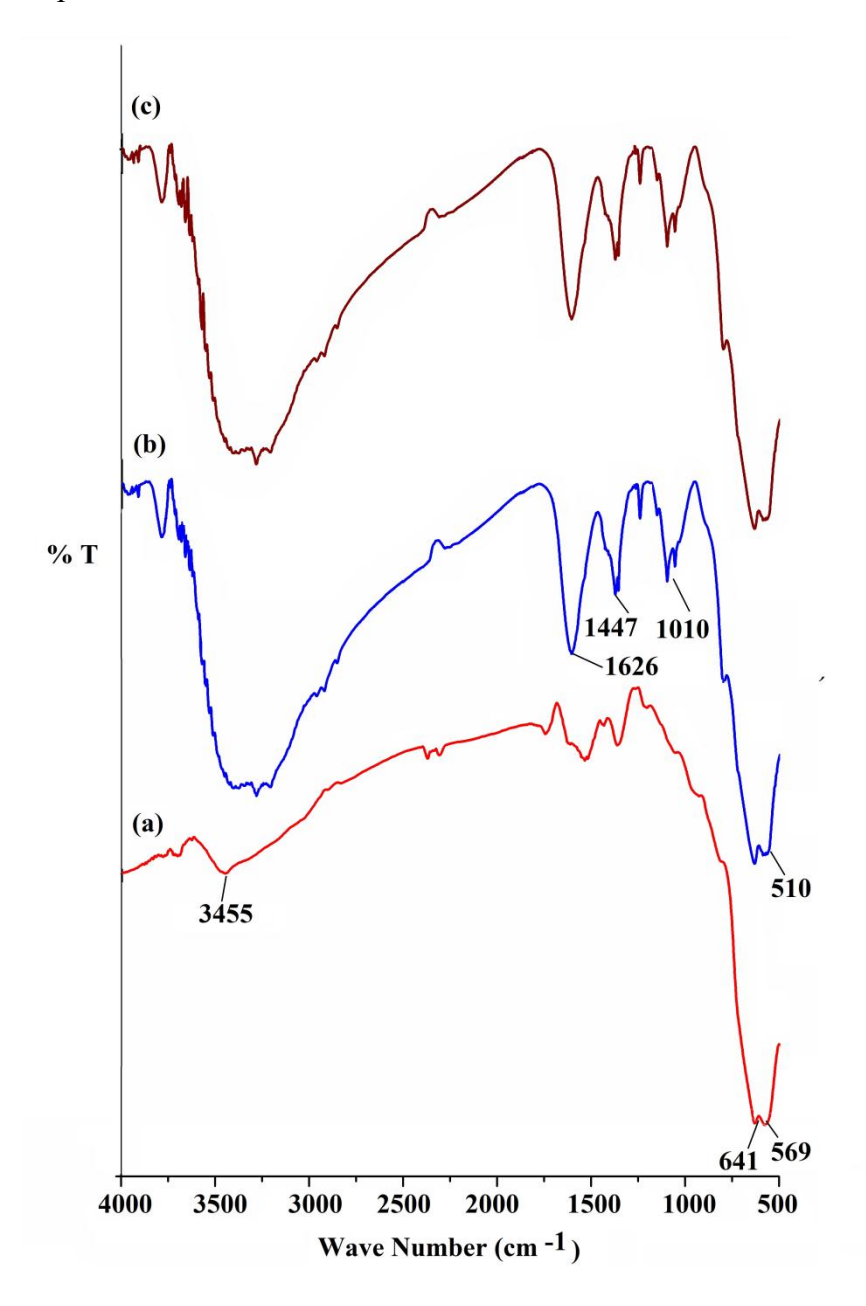


Figure 5.7 N<sub>2</sub> adsorption-desorption isotherm of Pd@SB/Fe<sub>3</sub>O<sub>4</sub>-TiO<sub>2</sub>

### FT-IR

The FT-IR spectral data of (a) Fe<sub>3</sub>O<sub>4</sub>-TiO<sub>2</sub>, (b) Pd@SB/Fe<sub>3</sub>O<sub>4</sub>-TiO<sub>2</sub> (Fresh), (c) Pd@SB/Fe<sub>3</sub>O<sub>4</sub>-TiO<sub>2</sub> (re-used after 6 runs) are shown in **Figure 5.8**. The peaks at 569 and 641 cm<sup>-1</sup> in Fe<sub>3</sub>O<sub>4</sub>-TiO<sub>2</sub> attributes to the stretching vibration in Fe-O [11] while the appearance of broad peak at 3455 cm<sup>-1</sup> corresponds to the absorbed H<sub>2</sub>O molecules. Further, a broad band due to Ti-O of the TiO<sub>2</sub> appeared around 510-640 cm<sup>-1</sup> which corresponds to the binding of TiO<sub>2</sub> with the magnetic nanoparticles [12]. In the FTIR spectrum of Pd@SB/Fe<sub>3</sub>O<sub>4</sub>-TiO<sub>2</sub> (**Figure 5.8b**) a new peak at 1626 cm<sup>-1</sup> corresponds to the azomethine (C=N) stretching confirming the successful grafting of Schiff base functionalized Palladium (II) complex onto TiO<sub>2</sub> coated Fe<sub>3</sub>O<sub>4</sub> magnetic nanoparticles [13]. The C=C stretching frequencies at 1500-1400, 1100-1050 and 900-700 cm<sup>-1</sup> confirms the existence of phenyl rings in the Schiff base functionalized catalyst [14,15]. Further, the FTIR spectra (**Figure 5.8c**) of the recycled catalyst (after six consecutive runs) in Suzuki coupling and hydrogenation of aromatic nitro

compounds was also carried out and the results indicated no significant changes in the spectral patterns.



**Figure 5.8** FTIR spectra (a)Fe<sub>3</sub>O<sub>4</sub>-TiO<sub>2</sub>, (b)Pd@SB/Fe<sub>3</sub>O<sub>4</sub>-TiO<sub>2</sub> (Fresh), (c)Pd@SB/Fe<sub>3</sub>O<sub>4</sub>-TiO<sub>2</sub> (re-used after 6 runs).

### **VSM**

The magnetic properties of synthesized materials were performed using vibrating sample magnetometry (VSM) at room temperature (Figure 5.9). Fe<sub>3</sub>O<sub>4</sub>-

TiO<sub>2</sub> showed super paramagnetic behaviour with saturation magnetization value of about 34.1 emu/g. It is worth mentioning that the TiO<sub>2</sub> coating on Fe<sub>3</sub>O<sub>4</sub> magnetic nanoparticles fairly prevents them from being oxidised, thereby reinforcing their magnetic stability and enabling their rapid dispersal in the absence of magnetic field. Moreover, after the grafting of Schiff base functionalized Palladium (II) complex onto TiO<sub>2</sub> coated magnetic nanoparticles to get Pd@SB/Fe<sub>3</sub>O<sub>4</sub>-TiO<sub>2</sub>, the paramagnetic behavior decreased to 25.3 emu/g. This decrease in saturation value attributes to the coating of the non-magnetic material onto magnetic Fe<sub>3</sub>O<sub>4</sub>-TiO<sub>2</sub> nanoparticles while synthesizing the developed catalyst, but still the novel catalyst is magnetically sound to be detached using magnet.

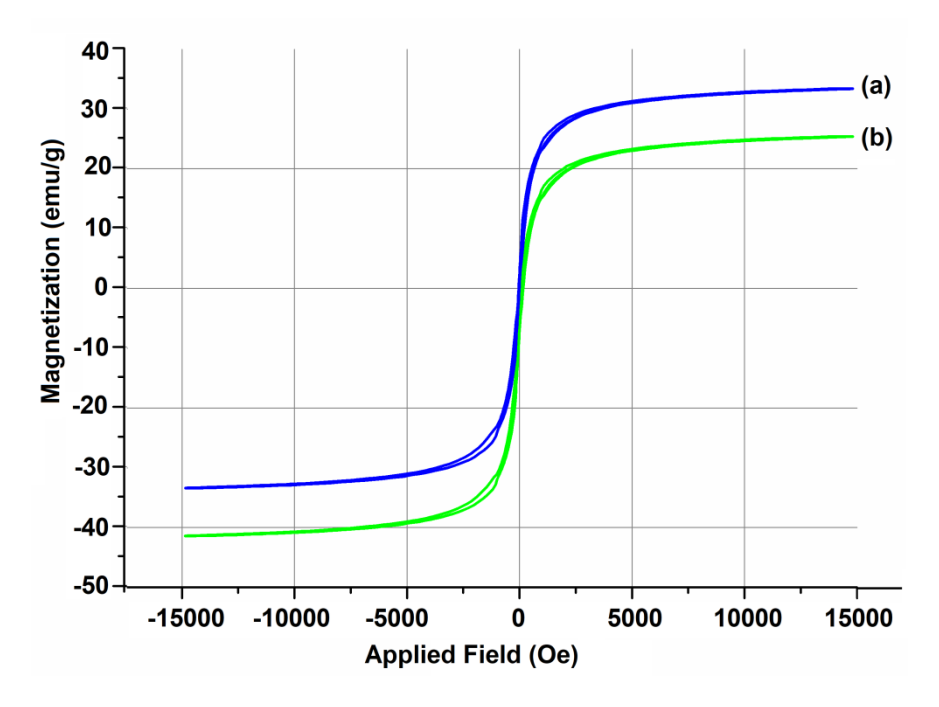


Figure 5.9 VSM spectra (a)Fe<sub>3</sub>O<sub>4</sub>-TiO<sub>2</sub>, (b) Pd@SB/Fe<sub>3</sub>O<sub>4</sub>-TiO<sub>2</sub>

### CHN Analysis

The successful synthesis of Schiff base functionalized TiO<sub>2</sub> coated magnetic nanoparticles-based support was further confirmed by Carbon, Hydrogen and Nitrogen analysis. The results showed that the catalyst contains 3.58 % of Carbon, 0.92 % of Hydrogen and 1.38 % of Nitrogen element.

### **EDX**

This study allows the elemental composition of the specimen to be measured. The EDX spectrum of Pd@Fe<sub>3</sub>O<sub>4</sub>-TiO<sub>2</sub>/SB demonstrates the presence of Pd on SB/Fe<sub>3</sub>O<sub>4</sub>-TiO<sub>2</sub> in addition to the presence of other elements like C, O, N, Fe and Ti (**Figure 5.10**). The high purity of Pd@SB/Fe<sub>3</sub>O<sub>4</sub>-TiO<sub>2</sub> was confirmed as no peaks for other element were observed.

### **ICP-AES**

The amount of Palladium loading on Pd@SB/Fe<sub>3</sub>O<sub>4</sub>-TiO<sub>2</sub>, was examined by Inductively Coupled Plasma Atomic Emission Spectroscopy (ICP-AES). The obtained results correspond to 2.10 wt% of Pd loading onto SB/Fe<sub>3</sub>O<sub>4</sub>-TiO<sub>2</sub>.

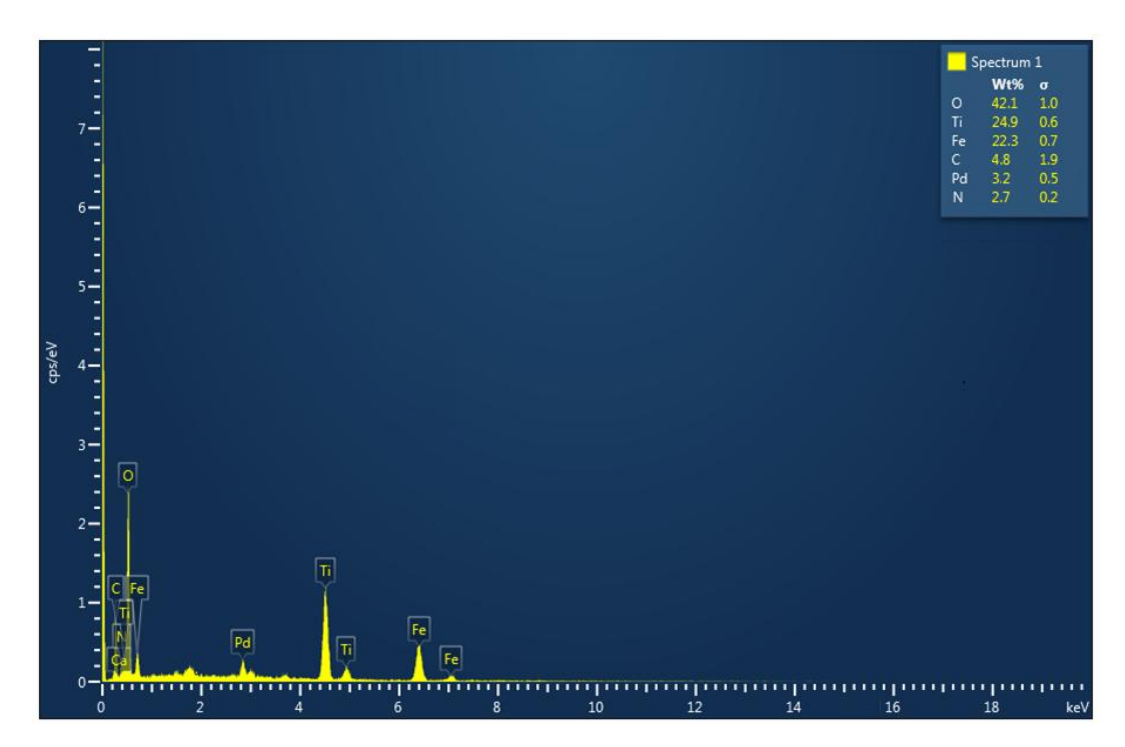


Figure 5.10 EDX spectrum of Pd@SB/Fe<sub>3</sub>O<sub>4</sub>-TiO<sub>2</sub>

### **5.1.2 References**

[1]. Yasmin, S., Roy, N., Kabir, M.H. and Jeon, S., (2022). Nitrogen-functionalized carbon nanotube based palladium nanoparticles as an efficient catalyst for oxygen reduction and ethanol oxidation reaction. *Applied Surface Science Advances*, 9, 100235.

- [2]. Sobhani, S., Falatooni, Z.M., Asadi, S. and Honarmand, M., (2016). Palladium-Schiff base complex immobilized covalently on magnetic nanoparticles as an efficient and recyclable catalyst for Heck and Suzuki cross-coupling reactions. *Catalysis Letters*, 146, 255-268.
- [3]. Sharma, S., Sharma, C., Kaur, M. and Paul, S., (2021). The in situ fabrication of ZIF-67 on titania-coated magnetic nanoparticles: a new platform for the immobilization of Pd (ii) with enhanced catalytic activity for organic transformations. *New Journal of Chemistry*, 45(43), 20309-20322.
- [4]. Bi, J., Chen, J., Dong, Y., Guo, W., Zhu, D. and Li, T., (2018). Polymer-supported palladium (II) containing N2O2: An efficient and robust heterogeneous catalyst for C–C coupling reactions. *Journal of Polymer Science Part A: Polymer Chemistry*, 56(20), 2344-2353.
- [5]. Zhang, S., Ye, J., Liu, Z., Lu, H., Shi, S., Qi, Y. and Ning, G., (2020). Superior antibacterial activity of Fe<sub>3</sub>O<sub>4</sub>@copper (ii) metal–organic framework core–shell magnetic microspheres. *Dalton Transactions*, 49(37), 13044-13051.
- [6]. Archana, K., Pillai, N.G., Rhee, K.Y. and Asif, A., 2019. Super paramagnetic ZIF-67 metal organic framework nanocomposite. *Composites Part B: Engineering*, 158, pp.384-389.
- [7]. Hasan, K., Joseph, R.G., Shehadi, I.A. and Patole, S.P., 2023. Fe<sub>3</sub>O<sub>4</sub>-chitosan immobilized Cu (II) Schiff base catalyst for the microwave-assisted amination of aryl halides in water. *Arabian Journal of Chemistry*, *16* (12), pp 105317.
- [8]. Khan, S.B., Ali, F., Kamal, T., Anwar, Y., Asiri, A.M. and Seo, J., (2016). CuO embedded chitosan spheres as antibacterial adsorbent for dyes. *International journal of biological macromolecules*, 88, 113-119.
- [9]. Sajjadi, M., Nasrollahzadeh, M. and Tahsili, M.R., 2019. Catalytic and antimicrobial activities of magnetic nanoparticles supported N-heterocyclic palladium (II) complex: A magnetically recyclable catalyst for the treatment of environmental contaminants in aqueous media. *Separation and Purification Technology*, 227, p.115716.
- [10]. Sharma, H., Mahajan, H., Jamwal, B. and Paul, S., (2018). Cu@ Fe3O4-TiO2-L-dopa: a novel and magnetic catalyst for the Chan-Lam cross-coupling reaction in ligand free conditions. *Catalysis Communications*, 107, 68-73.

- [11]. Gürbüz, D., Cinarli, A., Tavman, A. and Birteksz, A.S., (2012). Spectral Characterization and Antimicrobial Activity of Some Schiff Bases Derived from 4-Methyl-2-aminophenol. *Chinese Journal of Chemistry*, 30(4), 970-978.
- [12]. Cui, Y., Dong, X., Li, Y., Li, Z. and Chen, W., (2012). Synthesis, structures and urease inhibition studies of Schiff base metal complexes derived from 3, 5-dibromosalicylaldehyde. *European journal of medicinal chemistry*, 58, 323-331.
- [13]. Yıldız, M., Karpuz, Ö., Zeyrek, C.T., Boyacıoğlu, B., Dal, H., Demir, N., Yıldırım, N. and Ünver, H., 2015. Synthesis, biological activity, DNA binding and anion sensors, molecular structure and quantum chemical studies of a novel bidentate Schiff base derived from 3, 5-bis (triflouromethyl) aniline and salicylaldehyde. *Journal of Molecular Structure*, 1094, pp.148-160.
- [14]. Yang, H., Zhang, L., Wang, P., Yang, Q. and Li, C., 2009. The enantioselective cyanosilylation of aldehydes on a chiral VO (Salen) complex encapsulated in SBA-16. *Green Chemistry*, 11(2), pp.257-264.
- [15]. Bhardwaj, M., Sharma, H., Paul, S. and Clark, J.H., (2016). Fe 3 O 4@ SiO 2/EDAC–Pd (0) as a novel and efficient inorganic/organic magnetic composite: sustainable catalyst for the benzylic C–H bond oxidation and reductive amination under mild conditions. *New Journal of Chemistry*, 40(6), 4952-4961.

# Section 5.2 Schiff base functionalized Pd (II) complex onto titania grafted magnetic nanoparticles as an efficient heterogeneous catalyst for Suzuki coupling reaction in water

Synthesis of biaryl motif via Suzuki coupling is a vital core of many biologically important molecules, and has been the center of attention of chemists for many years [1]. This motif has proven activity towards a large variety of therapeutic classes, including anti-fungal, anti-inflammatory, anti-rheumatic, anti-tumor, and anti-hypertensive agents [2]. However, the method for the biaryl synthesis has been a challenging task in the field of synthetic chemistry for over a century. Beginning from Ullmann's earliest reports about the biaryl synthesis via coupling of aryl halides using copper bronze, a large number of important methodologies have been reported [3]. Perhaps, the palladium catalysed Suzuki-Miyaura coupling of arylboronic acids with electrophiles such as triflates, alkenyl or aryl halides using base is the most widely used method both in laboratory and industrial biaryl synthesis [4].

Keeping in view the importance of green procedures in organic synthesis, herein we present the synthesis of Schiff base functionalized Pd (II) complex onto TiO<sub>2</sub> coated magnetic nanoparticles [Pd@SB/Fe<sub>3</sub>O<sub>4</sub>-TiO<sub>2</sub>] as an efficient nanocatalyst and its activity, selectivity and heterogeneity is studied for the biaryl synthesis using Suzuki coupling and for hydrogenation of aromatic nitro compounds under sustainable reaction conditions (**Figure 5.11**).

$$R_1 + (HO)_2B$$

$$R_2 \longrightarrow R_2$$

$$R_2 \longrightarrow R_1$$

$$R_1 \longrightarrow R_2$$

$$R_1 \longrightarrow R_2$$

Figure 5.11 Pd@SB/Fe<sub>3</sub>O<sub>4</sub>-TiO<sub>2</sub>catalyzed Suzuki coupling reaction

### 5.2.1 Results and discussion

# Optimization of the reaction conditions

The catalytic efficiency of Pd@SB/Fe<sub>3</sub>O<sub>4</sub>-TiO<sub>2</sub> was explored for the biaryl synthesis via Suzuki cross-coupling reaction. To optimize the reaction conditions, parabromoacetophenone and phenyl boronic acid were chosen as test substrates, and the reaction was monitored in terms of different parameters, viz., different catalysts, catalyst amount, and reaction temperature (**Table 5.1**). Without the catalyst, no product formation was detected (**Table 5.1**, entry 1). When the reaction was carried

out using different supports, viz. Fe<sub>3</sub>O<sub>4</sub>, Fe<sub>3</sub>O<sub>4</sub>-TiO<sub>2</sub>, EDA/Fe<sub>3</sub>O<sub>4</sub>-TiO<sub>2</sub>, and SB/Fe<sub>3</sub>O<sub>4</sub>-TiO<sub>2</sub>, again, no conversion of reactants was observed. (**Table 5.1**, **entry 2-5**). While in the presence of the synthesized palladium-based catalysts, at different reaction temperatures, a remarkable change in yield of the products was obtained (**Table 5.1**, **entries 6-9**), but the most favorable results were obtained with Pd@SB/Fe<sub>3</sub>O<sub>4</sub>-TiO<sub>2</sub> as a catalyst (**Table 5.1**, **entry 10**). Further optimization was carried out with different amounts of Pd@SB/Fe<sub>3</sub>O<sub>4</sub>-TiO<sub>2</sub>. viz,0.05 g (1 mol% Pd), 0.1 g (1.9 mol% Pd) and 0.15 g (2.8 mol% Pd) (**Table 5.1**, **entries 10-12**). It was found that about 0.1 g (1.9 mol% Pd) of the catalyst shows the optimal efficiency in terms of time and yield (Table 1, entry 10). An increase in the amount of catalyst to 0.15 g did not result in any further increase in the yield of the product (**Table 5.1**, **entry 12**). Thus, 0.1 g (1.9 mol% Pd) of Pd@SB/Fe<sub>3</sub>O<sub>4</sub>-TiO<sub>2</sub> was chosen as the optimal amount of catalyst to carry out the Suzuki coupling reaction.

**Table 5.1.** Evaluation of the activity of the different catalysts and their amount at different temperatures for Suzuki coupling reaction<sup>a</sup>

Entry	Catalyst	Catalyst	Time	Yield <sup>b</sup>
		amount (g)	(min)	(%)
1	No catalyst	-	60	N.R.
2	$Fe_3O_4$	0.1	60	N.R.
3	Fe <sub>3</sub> O <sub>4</sub> -TiO <sub>2</sub>	0.1	60	N.R.
4	EDA/Fe <sub>3</sub> O <sub>4</sub> -TiO <sub>2</sub>	0.1	60	N.R
5.	SB/Fe <sub>3</sub> O <sub>4</sub> -TiO <sub>2</sub>	0.1	60	N.R
6.	$PdCl_2$	0.1	30	72
7.	$Pd(OAc)_2$	0.1	30	78
8.	Pd@Fe <sub>3</sub> O <sub>4</sub> -TiO <sub>2</sub>	0.1	30	82
9.	Pd@SB/Fe <sub>3</sub> O <sub>4</sub> -TiO <sub>2</sub>	0.1	15	88
10.	Pd@SB/Fe <sub>3</sub> O <sub>4</sub> -TiO <sub>2</sub>	0.1	30	93
11.	Pd@SB/Fe <sub>3</sub> O <sub>4</sub> -TiO <sub>2</sub>	0.05	30	72
12.	Pd@SB/Fe <sub>3</sub> O <sub>4</sub> -TiO <sub>2</sub>	0.15	30	94

<sup>&</sup>lt;sup>a</sup>Reaction conditions: Para-bromoacetophenone (1 mmol), phenylboronic acid (1.5 mmol), K<sub>2</sub>CO<sub>3</sub> (1 mmol) in H<sub>2</sub>O (5 mL); <sup>b</sup>Isolated Yield.

Global research trends are shifting their focus to impose environmentally sustainable conditions so as to replace the harmful and toxic chemicals and solvents [5]. To fulfill the requirements, the reaction was further optimized w.r.t. different solvents and the amount of base, and the results are reported in **Table 5.2**. H<sub>2</sub>O and EtOH were chosen as preferred solvents while K<sub>2</sub>CO<sub>3</sub> was used as base as it is mild, easy to handle, non-expensive, and readily available. From the obtained (**Table 5.2**), it was observed that the reaction performed well in polar solvents like acetone, acetonitrile, MeOH, and EtOH, but maximum yield was obtained with water as solvent, while 0.1 mmol of K<sub>2</sub>CO<sub>3</sub> gave the best conversion rate (Table 2, entry 6).

**Table 5.2.** Optimization of reaction conditions in terms of different solvents and amount of base for Suzuki coupling reaction<sup>a</sup>

Entry	Solvent	K <sub>2</sub> CO <sub>3</sub> (mmol)	Time (min)	Yield <sup>b</sup> (%)
1	Toluene	1	30	65
2	Acetonitrile	1	30	91
3	Acetone	1	30	72
4	MeOH	1	30	87
5.	EtOH	1	30	89
6.	$H_2O$	1	30	93
7.	$H_2O$	0.25	30	68
8.	$H_2O$	0.50	30	75
9.	$H_2O$	0.75	30	85
10.	$H_2O$	1.5	30	93

<sup>&</sup>lt;sup>a</sup>Reaction conditions: Para-bromoacetophenone (1 mmol), phenylboronic acid (1.5 mmol), Pd@Fe<sub>3</sub>O<sub>4</sub>-TiO<sub>2</sub>/SB (0.1 g, 1.9 mol% Pd) and Solvent (5 mL).

Using the optimized reaction conditions, the Suzuki coupling reaction was carried out by employing various aryl halides and phenylboronic acids substituted with both electron-donating as well as electron-withdrawing groups, and the results are compiled in **Table 5.3**. It was analysed that the reaction gave a faster conversion rate with para-substituted phenylboronic acids (**Table 5.3**, **entries 5-7**) in comparison to

<sup>&</sup>lt;sup>b</sup>Isolated Yield.

the ortho and meta-substituted phenylboronic acids (**Table 5.3**, **entries 9-11**). Further, the reaction worked well with heteroarylboronic acids as well and gave good results (**Table 5.3**, **entries 12-13**).

**Table 5.3** Pd@Fe<sub>3</sub>O<sub>4</sub>-TiO<sub>2</sub>/SB catalyzed Suzuki coupling between arylhalides and boronic acids using water<sup>a</sup>

Entry	Aryl Halide	Aryl Boronic Acid	Product	Time (min)	Yield (%) <sup>b</sup>
1.	Br	(HO) <sub>2</sub> B	$H_3C$	30	93
2.	O H	(HO) <sub>2</sub> B	O <sub>H</sub>	35	92
3.	NC — Br	(HO) <sub>2</sub> B	NC \	30	94
4.	Ph Br	(HO) <sub>2</sub> B	O <sub>Ph</sub>	35	92
5.	$H_3C$ $Br$	(HO) <sub>2</sub> B F	$H_3C$	45	91
6.	$H_3C$ $Br$	(HO) <sub>2</sub> B————————————————————————————————————	$H_3C$ $OCH_3$	35	90
7.	O H	(HO) <sub>2</sub> B — OCH <sub>3</sub>	O H	45	88
8.	Br	(HO) <sub>2</sub> B		35	93

9.	$H_3C$ $Br$	(HO) <sub>2</sub> B	O H <sub>3</sub> C	50	87
10.	$H_3C$ $Br$	H <sub>3</sub> CO (HO) <sub>2</sub> B	H <sub>3</sub> CO H <sub>3</sub> C	55	88
11.	Br	(HO) <sub>2</sub> B	O H	60	85
12.	O H	(HO) <sub>2</sub> B	O <sub>H</sub> S	50	84
13.	$H_3C$ $Br$	(HO) <sub>2</sub> B	O H <sub>3</sub> C	45	85

<sup>a</sup>Reaction conditions: Para-bromoacetophenone (1 mmol), phenylboronic acid (1.5 mmol), Pd@SB/Fe<sub>3</sub>O<sub>4</sub>-TiO<sub>2</sub> (0.1 g, 1.9 mol% Pd) K<sub>2</sub>CO<sub>3</sub> (1 mmol) in H<sub>2</sub>O (5 mL). <sup>b</sup>Isolated Yield.

The plausible mechanism for the Suzuki coupling reaction has been proposed (**Figure 5.12**), which involves the initial preactivation of Pd@SB/Fe<sub>3</sub>O<sub>4</sub>-TiO<sub>2</sub>. Preactivation typically involves the reduction of Pd(II) precursor to Pd(0) species, which can be accomplished by the addition of reducing agent, electron rich ligands or organometallic coupling partners [4, 6-7]. Herein, the active Pd(0) was generated insitu from Pd(II) in Pd@SB/Fe<sub>3</sub>O<sub>4</sub>-TiO<sub>2</sub> using arylboronic acid which played the dual role i.e., associate reducing agent as well as coupling partner. The similar reduction of Pd(II) precursor to Pd(0) by phenylboronic acid was observed and reported by various authors. Jin et al. have reported the reduction of palladium(II) acetate by phenylboronic acid [8]; Saha et al. have reported Suzuki coupling catalyzed by in situ-generated Pd(0) nanoparticles using boronic acids which acted as the reducing agent [9]. Pharande and co-workers have also reported that the Cellulose

Schiff base-supported Pd(II) was reduced insitu to Pd(0) using arylboronic acid which acted as associate reducing agent and coupling partner as well [10]. The Pd(0) species formed after the preactivation of Pd@Fe<sub>3</sub>O<sub>4</sub>-TiO<sub>2</sub>/SB activates the C-X bond by an oxidative addition, which provides an organo Pd (II) complex prone to react with nucleophiles. This step is followed by transmetallation and finally, reductive elimination to afford the corresponding product.

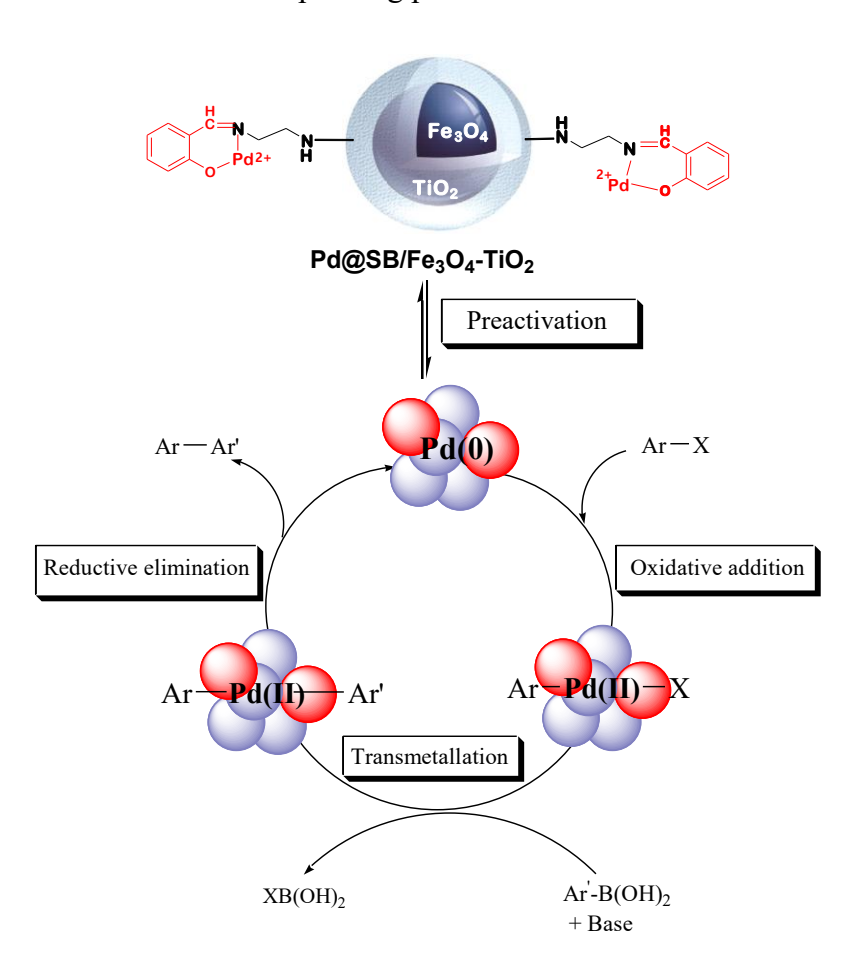


**Figure 5.12** Plausible mechanism for the Pd@SB/Fe<sub>3</sub>O<sub>4</sub>-TiO<sub>2</sub> catalyzed Suzuki coupling.

### Recyclability

Recyclability of the heterogeneous catalyst is a significant aspect in addition to its catalytic activity. Hence, to check the reusability and stability of Pd@SB/Fe<sub>3</sub>O<sub>4</sub>-TiO<sub>2</sub>, we examined the test reaction for **Table 5.3**, **entry 1**. After the reaction was complete, the catalyst was separated from the reaction mixture using an external magnet and then washed with EtOAc and EtOH to remove any residual discharge.

The separated catalyst was reused for another set of reactions by adding new substrates using the same reaction conditions. This practice was repeated up to 6 consecutive runs, and no significant variation in its catalytic efficiency was observed up to the 6th cycle, which demonstrates the outstanding recyclability of the catalyst. To further examine the constancy of the recovered catalyst after the 6th run, we analyzed its structure using XPS, FTIR, and XRD, studies, and the results indicated that the reused catalyst showed insignificant structural change compared to the fresh one. The leaching of Pd metal from the surface of SB/Fe<sub>3</sub>O<sub>4</sub>-TiO<sub>2</sub> was checked using ICP-AES analysis, and the outcomes clearly showthat the palladium is strongly bound to the Schiff base ligand and there is minimal loss even after the 6th consecutive run. To exclude any input of homogeneous catalysis, the reaction (Table 5.3, entry 1) was performed until its conversion was 50% (15 min). At that stage, the catalyst was separated from the reaction mixture using an external magnet (Hot Filtration Test). The liquid phase was then allowed to react further, but no more conversion occurred. evidence strongly supports that the developed catalyst is purely heterogeneous Figure 5.13.

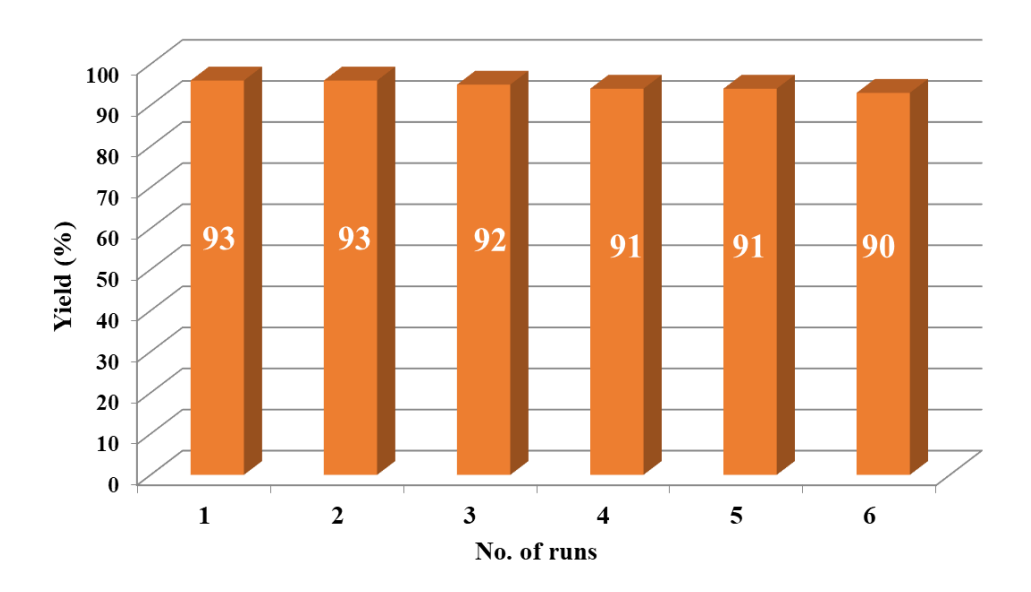


**Figure 5.13** Recyclability of Pd@SB/Fe<sub>3</sub>O<sub>4</sub>-TiO<sub>2</sub> for Suzuki coupling; Reaction conditions: Para-bromoacetophenone (1 mmol), phenylboronic acid (1.5 mmol), Pd@SB/Fe<sub>3</sub>O<sub>4</sub>-TiO<sub>2</sub> (0.1 g, 1.9 mol% Pd), K<sub>2</sub>CO<sub>3</sub> (1 mmol) in H<sub>2</sub>O (5 mL); Isolated Yield.

#### **5.2.2 Conclusion**

This work describes an efficient and operationally simple strategy for the synthesis of Schiff base functionalized Pd (II) complex onto TiO<sub>2</sub> coated magnetic nanoparticles [Pd@SB/Fe<sub>3</sub>O<sub>4</sub>-TiO<sub>2</sub>]. Its excellent catalytic efficiency was explored for the biaryl synthesis via Suzuki coupling. The developed catalytic system resulted in products in excellent yield without any harmful chemical discharge, making it an environmentally benign protocol. In addition to it, the catalyst is cost-effective because it can be simply recovered by means of external magnet and can be recycled up to six consecutive runs devoid of any appreciable change in its structure and morphology. The understanding of such modified catalysts can greatly help further attempts to control and systematically plan the fabrication of efficient catalytic systems for these highly significant organic transformations.

### General procedure for the Pd@SB/Fe<sub>3</sub>O<sub>4</sub>-TiO<sub>2</sub> catalyzed Suzuki Coupling reaction

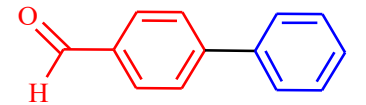
Aryl halide (1 mmol), Phenyl boronic acid (1.5 mmol), Pd@SB/Fe<sub>3</sub>O<sub>4</sub>-TiO<sub>2</sub> (0.10 g, 1.9 mol % Pd), K<sub>2</sub>CO<sub>3</sub> (1 mmol) and H<sub>2</sub>O (5.0 mL) was added in a R.B.F. (25 mL) and then the resultant mixture undergoes magnetic stirring at 100 °C using sand bath for the given time (Table 3). Consequent to the completion of the reaction, the magnetic catalyst was separated and properly washed with double-distilled water and vacuum dried for subsequent use. The reaction mixture was extracted with EtOAc, washed with H<sub>2</sub>O, and afterwards dried over Na<sub>2</sub>SO<sub>4</sub>(anhydrous). The required product was collected after removing solvent under reduced pressure and afterwards crystallization from an appropriate solvent. The structures of the products were confirmed by <sup>1</sup>Hand <sup>13</sup>C NMR and comparison with authentic samples obtained commercially or prepared according to the literature methods.

# Spectral details of the products listed in Table 3

### 4-Acetylbiphenyl (entry 1)

<sup>1</sup>H NMR (400 MHz, CDCl<sub>3</sub>):δ 2.67 (s, 3H, -COCH<sub>3</sub>), 7.41-7.44 (m, 1H), 7.48-7.52 (t, 2H, J = 8.0 Hz), 7.65-7.66 (d, 2H, J = 4.0 Hz), 7.70-7.72 (d, 2H, J = 8.0 Hz), 8.05-8.07 (d, 2H, J = 8.0 Hz); <sup>13</sup>C NMR (100 MHz, CDCl<sub>3</sub>):δ 26.91, 127.25, 127.30, 128.30, 128.98, 129.01, 135.95, 140.32, 145.97, 198.15. ESI-MS: 197 (M+1)<sup>+</sup>.

### Biphenyl-4-carboxaldehyde (entry 2)

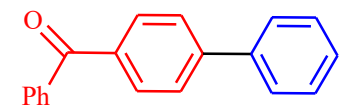


<sup>1</sup>H NMR (400 MHz, CDCl<sub>3</sub>):  $\delta$  7.42-7.46 (t, 1H, J = 8.0 Hz), 7.49-7.53 (t, 2H, J = 8.0 Hz), 7.65-7.67 (d, 2H, J = 8.0 Hz), 7.77-7.79 (d, 2H, J = 8.0 Hz), 7.97-7.99 (d, 2H, J = 8.0 Hz), 10.08 (s, 1H, -CHO); <sup>13</sup>C NMR (100 MHz, CDCl<sub>3</sub>): $\delta$  127.29, 128.14, 128.33, 128.91, 131.23, 138.04, 140.41, 143.52, 191.99. ESI-MS:183 (M+1)<sup>+</sup>.

### 4-Phenylbenzonitrile (entry 3)

<sup>1</sup>H NMR (400 MHz, CDCl<sub>3</sub>): $\delta$  7.44-7.53 (m, 3H), 7.61-7.63 (d, 2H, J = 8.0 Hz), 7.70-7.76 (m, 4H); <sup>13</sup>C NMR (100 MHz, CDCl<sub>3</sub>): $\delta$ 111.44, 119.52, 126.95, 127.15, 127.60, 127.67, 127.85, 128.53, 129.23, 132.63, 139.26, 145.76. **ESI-MS**: 179 (M+1)<sup>+</sup>.

### Phenyl-4-biphenyl ketone(entry 4)



<sup>1</sup>H NMR (400 MHz, CDCl<sub>3</sub>):δ 7.42-7.46 (m, 1H), 7.50-7.55 (m, 4H), 7.62-7.64 (m, 2H) 7.68-7.70 (d, 1H, J = 8.0 Hz), 7.73–7.75 (d, 2H, J = 8.0 Hz), 7.86-7.88 (d, 2H, J = 8.0 Hz), 7.92-7.94 (d, 2H, J = 8.0 Hz); <sup>13</sup>C NMR (100 MHz, CDCl<sub>3</sub>):δ 126.81, 127.08, 127.33, 128.34, 129.00, 130.18, 130.94, 132.62, 136.48, 137.46, 140.07, 145.39, 157.31, 196.88. ESI-MS: 260 (M)<sup>+</sup>.

### 4'-fluoro-4-acetylbiphenyl (entry 5)

$$_{\text{H}_{3}\text{C}}^{\text{O}}$$

<sup>1</sup>H NMR (400 MHz, CDCl<sub>3</sub>): $\delta$ 2.67 (s, 3H, COCH<sub>3</sub>, 7.16-7.21 (t, 2H, J = 8.0 Hz), 7.60-7.67 (m, 4H), 8.04-8.06 (d, 2H, J = 8.0 Hz); <sup>13</sup>C NMR (100 MHz, CDCl<sub>3</sub>): $\delta$ 26.72, 115.84, 116.05, 127.09, 128.91, 129.00, 135.81, 135.98, 136.01, 144.76, 161.75, 164.23, 197.75. **ESI-MS**: 215 (M+1)<sup>+</sup>

### 4'-methoxy-4-acetylbiphenyl (entry 6)

<sup>1</sup>H NMR (CDCl<sub>3</sub>, 400 MHz): $\delta$ 8.02-8.04 (d, J = 8.0 Hz, 2H), 7.66-7.68 (d, J = 8.0 Hz, 2H), 7.60-7.62 (d, J = 8.0 Hz, 2H), 7.02-7.04 (d, J = 8.0 Hz, 2H), 3.89 (s, 3H, OCH<sub>3</sub>), 2.66 (s, 3H, COCH<sub>3</sub>); <sup>13</sup>C NMR (CDCl<sub>3</sub>, 100 MHz): $\delta$  26.66, 114.43, 55.40, 126.62, 128.38, 128.96, 132.25, 135.22, 145.31, 159.93, 198.31. ESI-MS: 227 (M+1)<sup>+</sup>

### 4'-methoxy-biphenyl-4-carboxaldehyde (entry 7)

$$O$$
 $H$ 
 $OCH_3$ 

<sup>1</sup>H NMR (CDCl<sub>3</sub>, 400 MHz): δ10.05 (s, 1H, -CHO), 7.94-7.96 (d, J = 8.0 Hz, 2H), 7.73-7.75 (d, J = 8.0 Hz, 2H), 7.60-7.63 (d, J = 12.0 Hz, 2H), 7.02-7.04 (d, J = 8.0 Hz, 2H), 3.89 (s, 3H, OCH<sub>3</sub>); <sup>13</sup>C NMR (CDCl<sub>3</sub>, 100 MHz):δ 55.41, 114.49, 127.07, 130.35, 128.52, 132.05, 134.63, 146.80, 160.12, 191.63. ESI-MS: 213 (M+1)<sup>+</sup>

### Biphenyl (entry 8)

<sup>1</sup>H NMR (CDCl<sub>3</sub>, 400 MHz): δ 7.36-7.40 (2H, t), 7.46-7.49 (4H, t), 7.62-7.64 (4H, d,J = 8.0 Hz); <sup>13</sup>C NMR (CDCl<sub>3</sub>, 100 MHz): δ 127.29, 128.33, 128.92, 140.41. ESI-MS: 155 (M+1)  $^+$ .

# 2'-fluoro-4-acetylbiphenyl (entry 9)

<sup>1</sup>H NMR (CDCl<sub>3</sub>, 400 MHz):  $\delta$ 8.05-8.07 (d, J = 8.0 Hz, 2H), 7.67-7.69 (d, J = 8.0 Hz, 2H), 7.63 (d, J = 8.0 Hz, 1H), 7.49-7.64 (dd, J = 8.0, 1H), 7.41-47 (t, J = 8.0 Hz, 1H), 7.18-7.24 (m, 1H), 2.67 (s, 3H, -COCH<sub>3</sub>); <sup>13</sup>C NMR (CDCl<sub>3</sub>,100 MHz):  $\delta$  26.59, 116.21, 124.45, 128.51, 129.22, 129.87, 131.92, 136.02, 140.44, 158.65, 160.51, 197.65. ESI-MS: 215 (M+1)<sup>+</sup>

### 2'-methoxy-4-acetylbiphenyl (entry 10)

<sup>1</sup>H NMR (400 MHz, CDCl<sub>3</sub>): δ 8.03-8.05 (d, J = 8.0 Hz, 2H), 7.65-7.67 (d, J = 8.0 Hz, 2H), 7.40-7.51 (m, 2H), 7.05–7.10 (m, 2H), 3.8 5 (s, 3H, -OCH<sub>3</sub>),2.26 (s, 3H, -COCH<sub>3</sub>),; <sup>13</sup>C NMR (100 MHz, CDCl<sub>3</sub>): δ 26.40, 54.93, 111.54, 120.96, 128.09, 129.43, 129.50, 129.83, 130.72, 135.48, 143.92, 156.87, 198.31. **ESI-MS**: 227 (M+1)<sup>+</sup>

### 2'-methoxy-biphenyl-4-carboxaldehyde (entry 11)

<sup>1</sup>H NMR (400 MHz, CDCl<sub>3</sub>): $\delta$ 10.15 (s, 1H, -CHO), 7.93-7.95 (d, J = 8.0 Hz, 2H), 7.72-7.74 (d, J = 8.0 Hz, 2H), 7.35-7.43 (m, 2H), 7.03 – 7.10 (m, 2H), 3.86 (s, 3H, -

OCH<sub>3</sub>); <sup>13</sup>C NMR (100 MHz, CDCl<sub>3</sub>):δ 56.54, 113.97, 120.56, 127.84, 129.12, 129.55, 130.42, 130.63, 135.75, 140.57, 145.59, 191.79. ESI-MS: 213 (M+1)<sup>+</sup>

### 2-(4-Acetylphenyl)thiophene (entry 12)

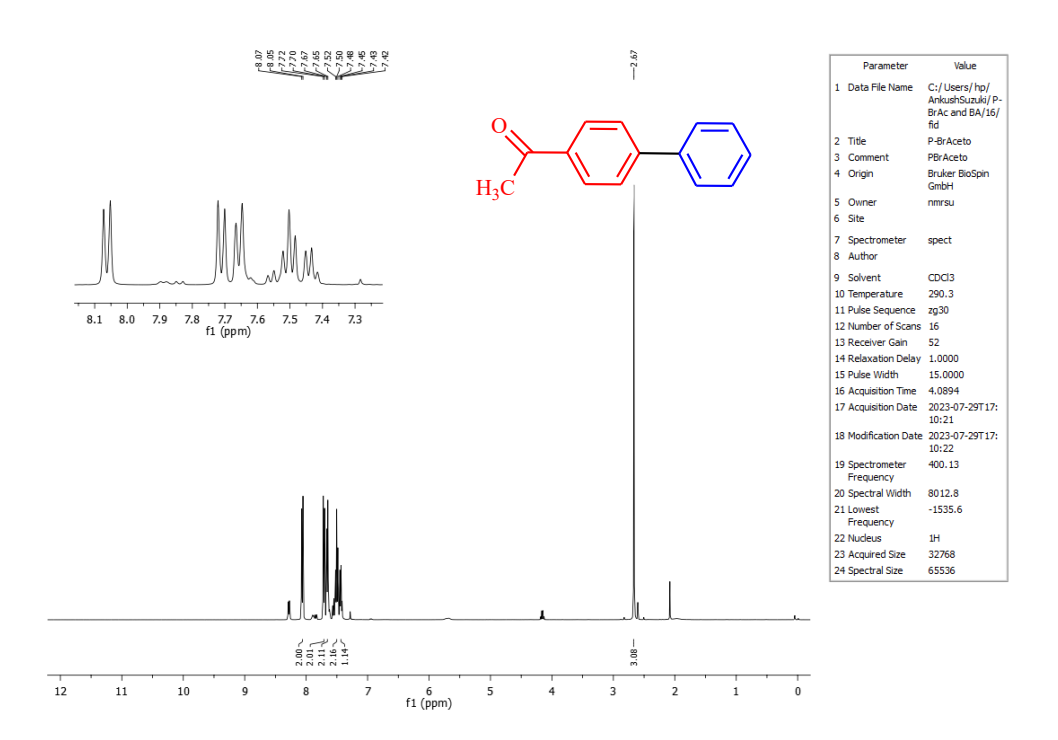
<sup>1</sup>H NMR (400 MHz, CDCl<sub>3</sub>): $\delta$ 8.01-8.03 (d, 2H, J = 8.0 Hz), 7.30-7.32 (d, 2H, J = 8.0 Hz), 7.60-7.61 (m, 1H), 7.44-7.47 (m, 2H), 2.65 (s, 3H, CH<sub>3</sub>); <sup>13</sup>C NMR (100 MHz, CDCl<sub>3</sub>):  $\delta$  26.8, 122.2, 126.6, 126.9, 129.0, 129.3, 135.3, 140.4, 140.9, 197.7. MS-ESI: m/z 203 (M+1)<sup>+</sup>.

### 4.2.3 References

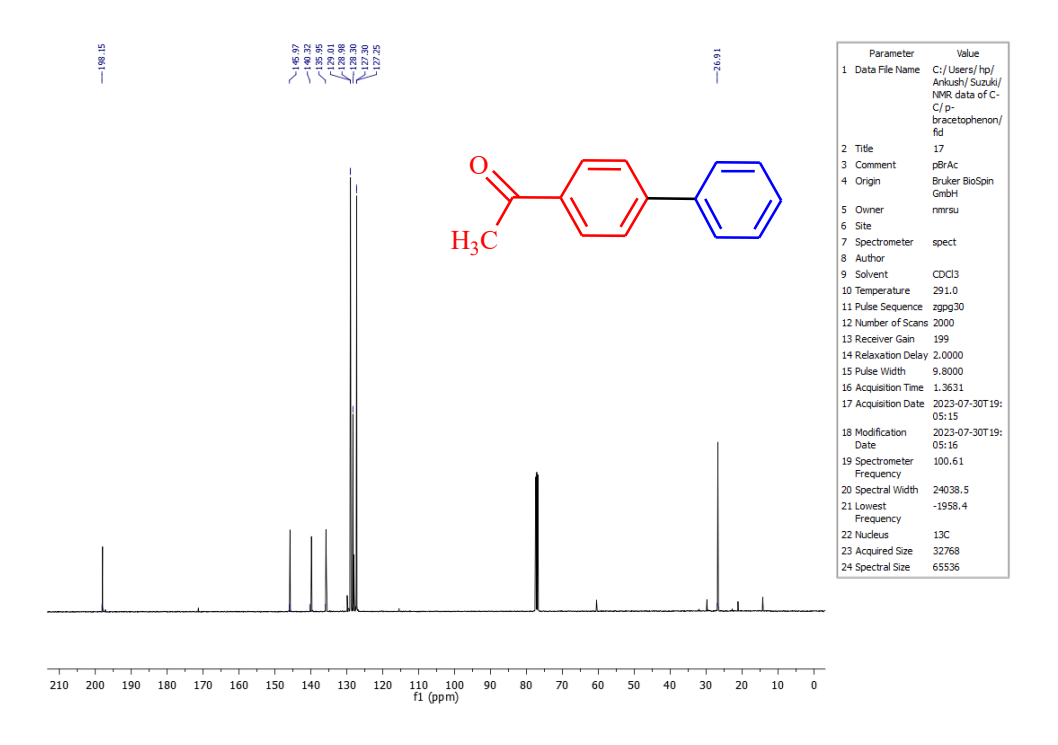
- 1. Maurya, N.K., Singh, A., Sahu, A., Kumar, A., Kant, R., Rao, V.G., Shukla, S.K. and Kuram, M.R., 2025. Suzuki–Miyaura/Mizoroki–Heck coupling cascade to access 2, 2'-bifunctionalized biaryls. *Chemical Communications*, 61(8), pp.1673-1676.
- Roy, V.J., Chakraborty, J. and Raha Roy, S., 2024. Catalytic π–π Interactions
   Triggered Photoinduced Synthesis of Biaryls. *Organic Letters*, 26(1), pp.183187.
- 3. Dubey, A.V. and Kumar, A.V., (2020). A Bio-Inspired Magnetically Recoverable Palladium Nanocatalyst for the Ullmann Coupling reaction of Aryl halides and Arylboronic acids In Aqueous Media. *Applied Organometallic Chemistry*, 34(5), e5570.
- 4. D'Alterio, M.C., Casals-Cruañas, È., Tzouras, N.V., Talarico, G., Nolan, S.P. and Poater, A., (2021). Mechanistic aspects of the palladium-catalyzed Suzuki-Miyaura cross-coupling reaction. *Chemistry–A European Journal*, 27(54), 13481-13493.
- 5. Hessel, V., Tran, N.N., Asrami, M.R., Tran, Q.D., Long, N.V.D., Escribà-Gelonch, M., Tejada, J.O., Linke, S. and Sundmacher, K., (2022). Sustainability of green solvents—review and perspective. *Green Chemistry*, 24(2), 410-437.

- 6. Sun, B., Ning, L. and Zeng, H.C., (2020). Confirmation of Suzuki–Miyaura cross-coupling reaction mechanism through synthetic architecture of nanocatalysts. *Journal of the American Chemical Society*, 142(32), 13823-13832.
- 7. Shaughnessy, K.H., 2020. Development of palladium precatalysts that efficiently generate LPd (0) active species. *Israel Journal of Chemistry*, 60(3-4), pp.180-194.
- 8. Han, W., Liu, C. and Jin, Z., 2008. Aerobic Ligand-Free Suzuki Coupling Reaction of Aryl Chlorides Catalyzed by In Situ Generated Palladium Nanoparticles at Room Temperature. *Advanced Synthesis & Catalysis*, 350(3), pp.501-508.
- 9. Saha, D., Chattopadhyay, K. and Ranu, B.C., 2009. Aerobic ligand-free Suzuki coupling catalyzed by in situ-generated palladium nanoparticles in water. *Tetrahedron Letters*, 50(9), pp.1003-1006.
- 10. Pharande, P.S., Rashinkar, G.S. and Pore, D.M., 2021. Cellulose Schiff base-supported Pd (II): An efficient heterogeneous catalyst for Suzuki Miyaura cross-coupling. *Research on Chemical Intermediates*, 47(11), pp.4457-4476.

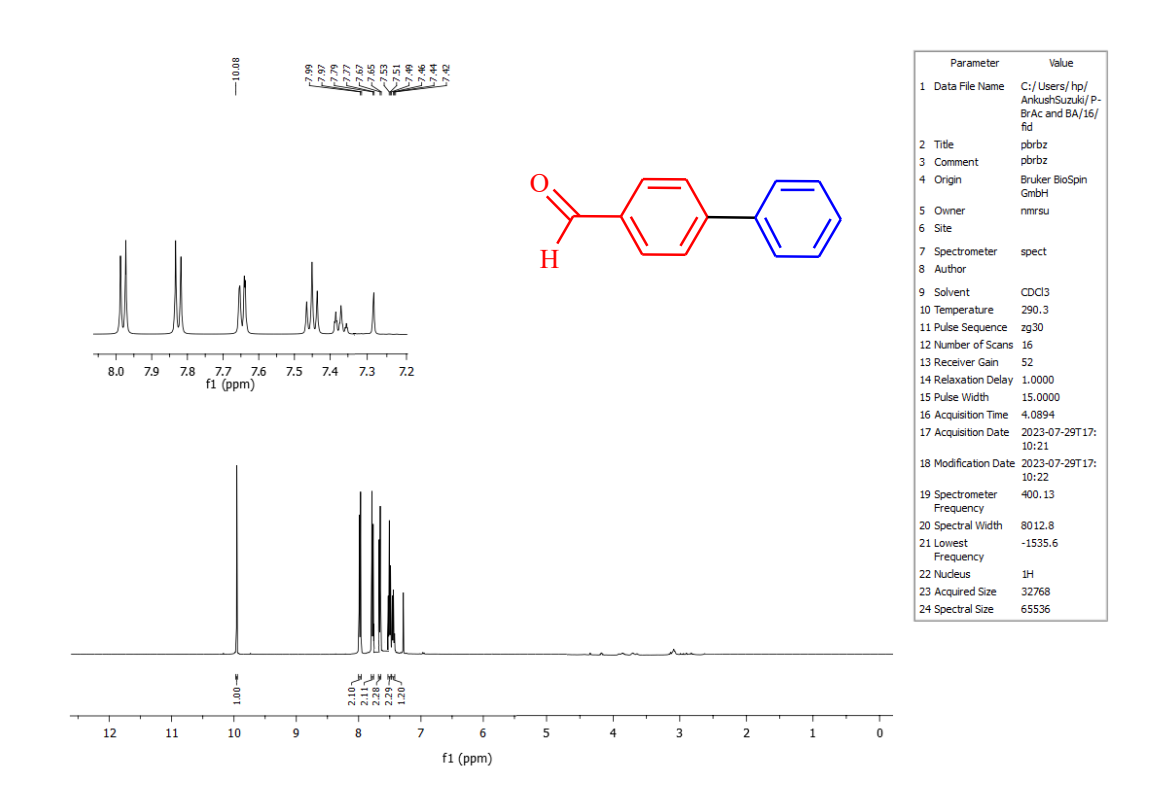
### 4.2.4Annexures



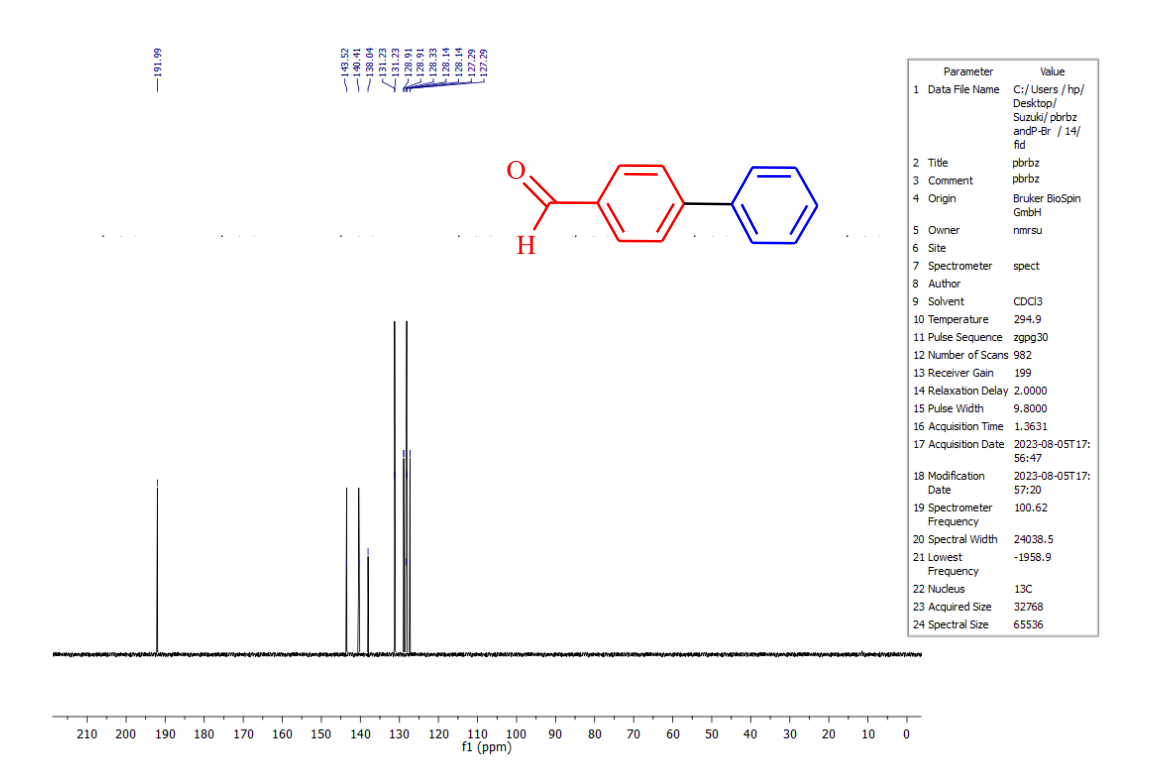
Annexure 5(a) <sup>1</sup>H NMR spectrum of 4-Acetylbiphenyl



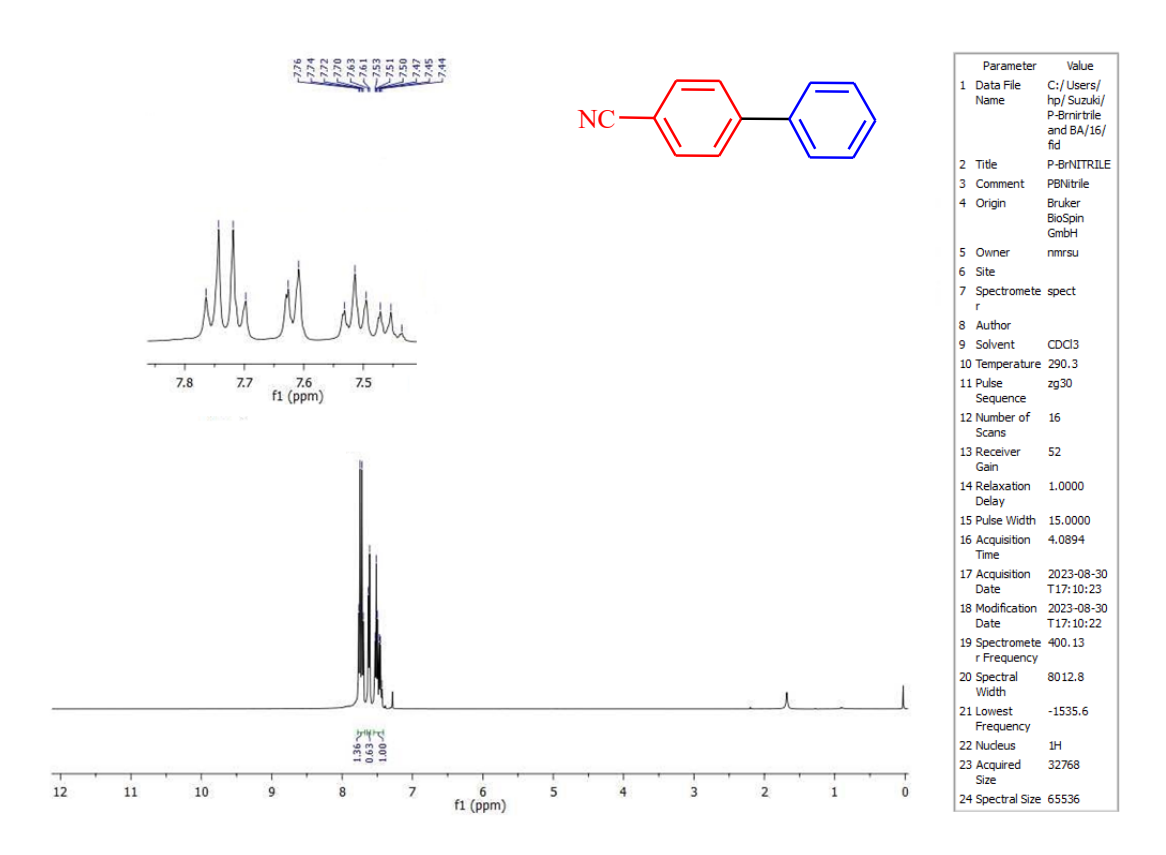
Annexure 5(b) <sup>13</sup>C NMR spectrum of 4-Acetylbiphenyl



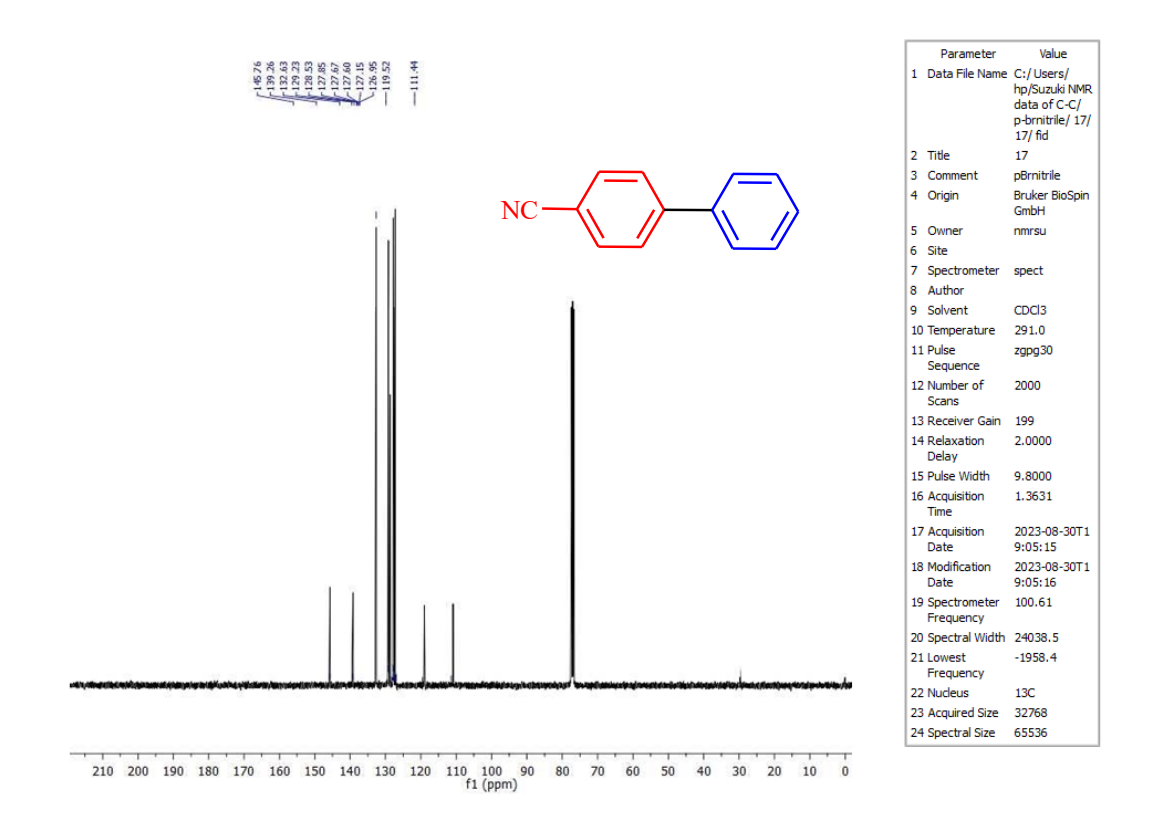
Annexure 5(c) <sup>1</sup>H NMR spectrum of Biphenyl-4-carboxaldehyde



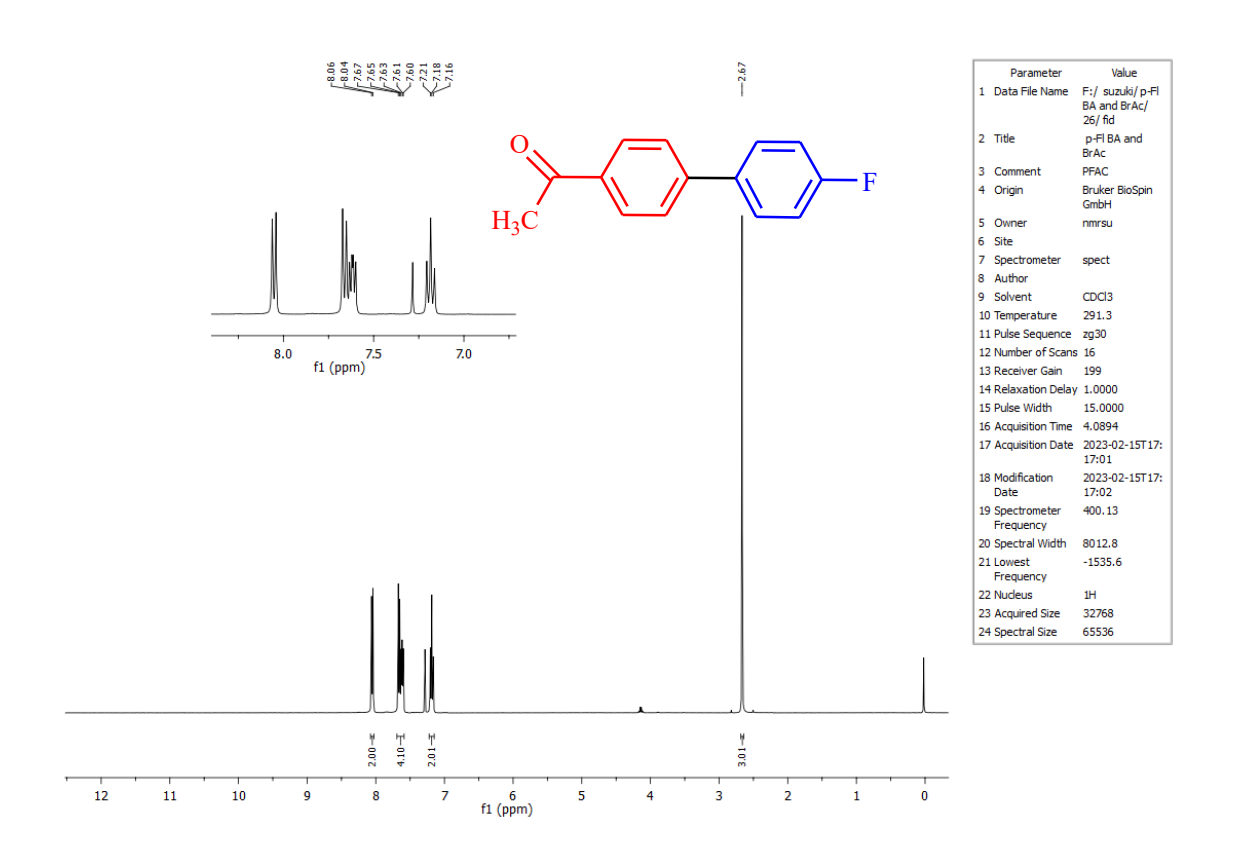
Annexure 5(d) <sup>13</sup>C NMR spectrum of Biphenyl-4-carboxaldehyde



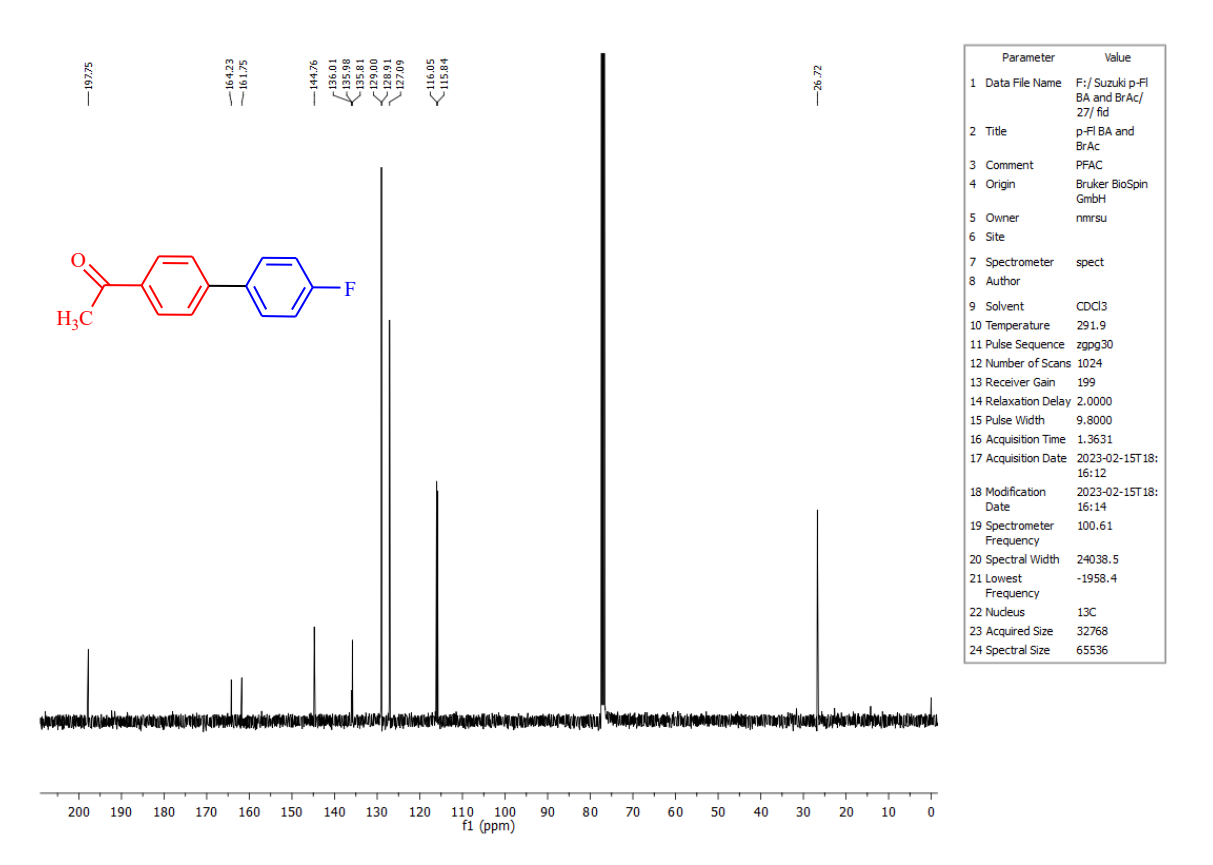
Annexure 5(e) <sup>1</sup>H NMR spectrum of 4-Phenylbenzonitrile



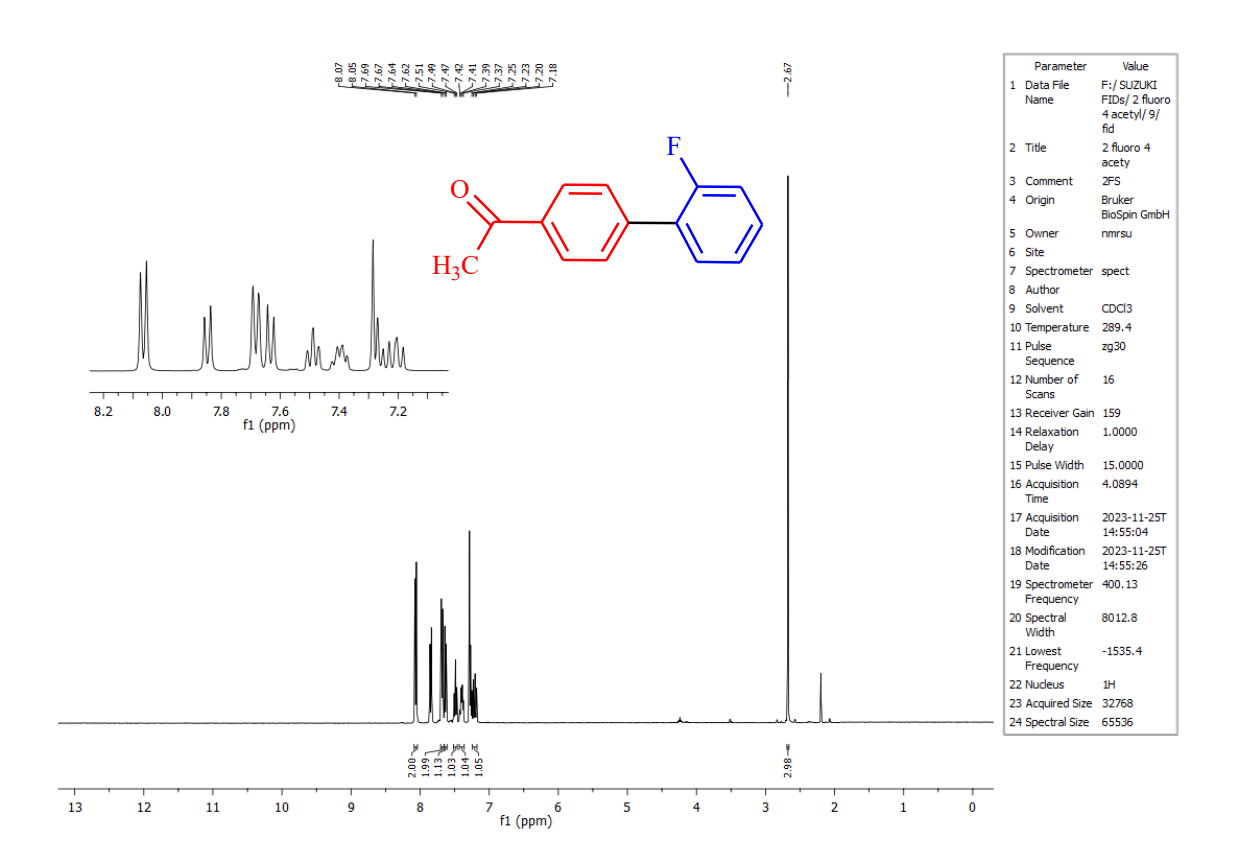
Annexure 5(f) <sup>13</sup>C NMR spectrum of 4-Phenylbenzonitrile



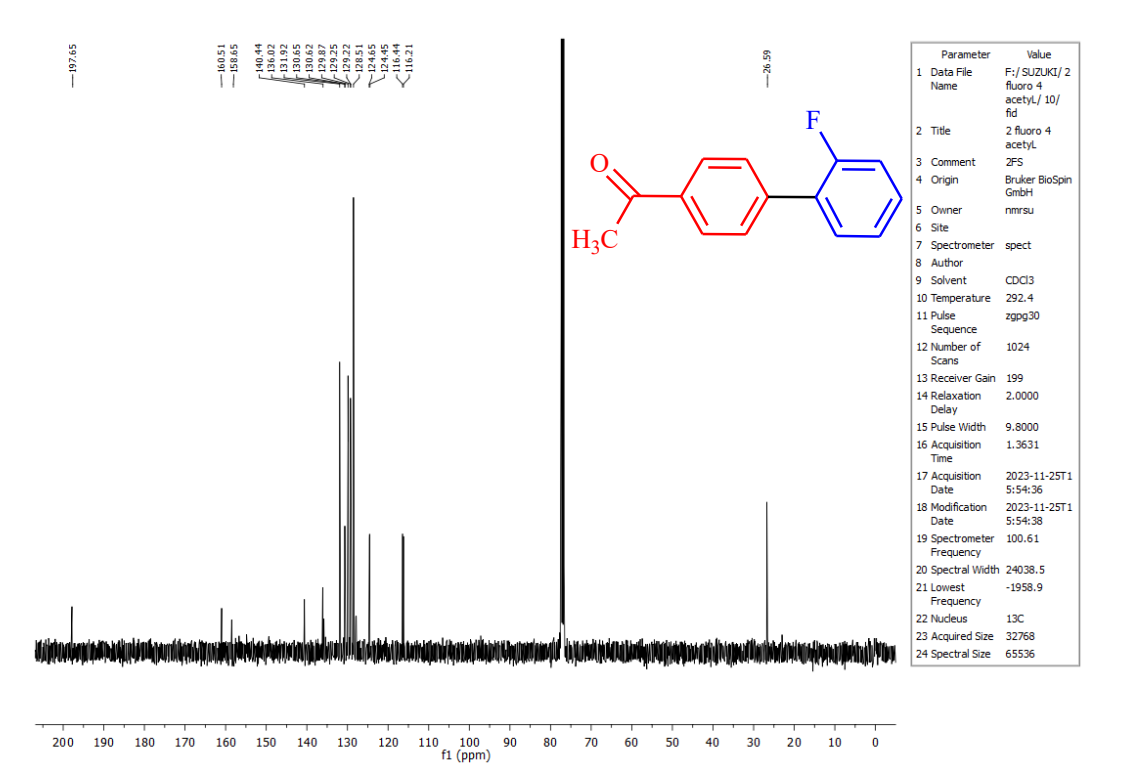
Annexure 5(g) <sup>1</sup>H NMR spectrum of 4'-fluoro-4-acetylbiphenyl



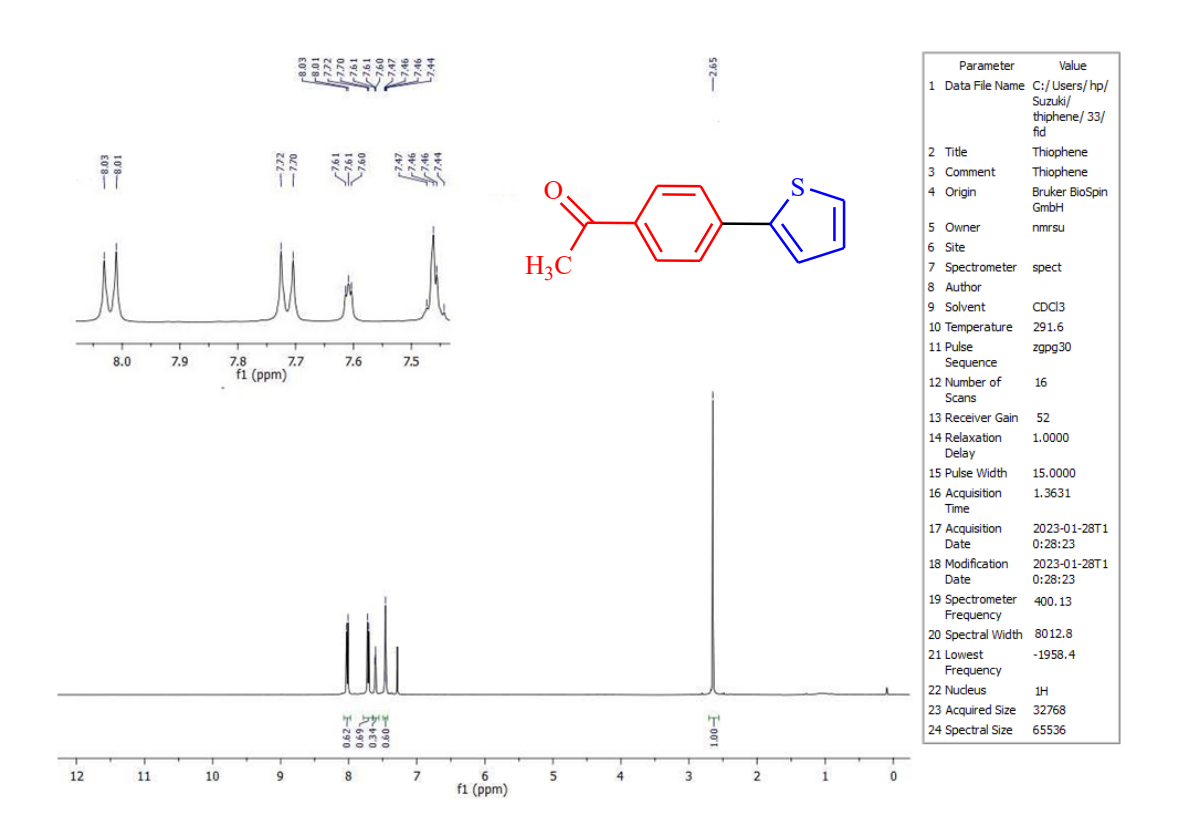
Annexure 5(h) <sup>13</sup>C NMR spectrum of 4'-fluoro-4-acetylbiphenyl



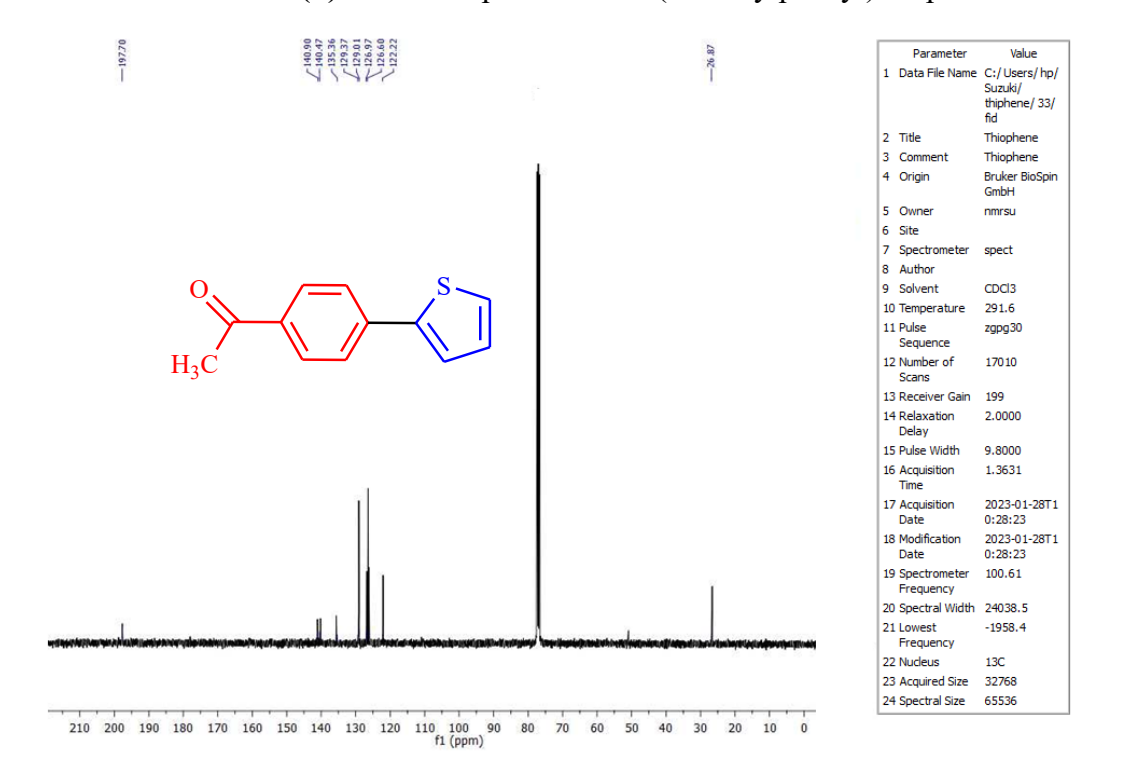
**Annexure 5(i)** <sup>1</sup>H NMR spectrum of 2'-fluoro-4-acetylbiphenyl



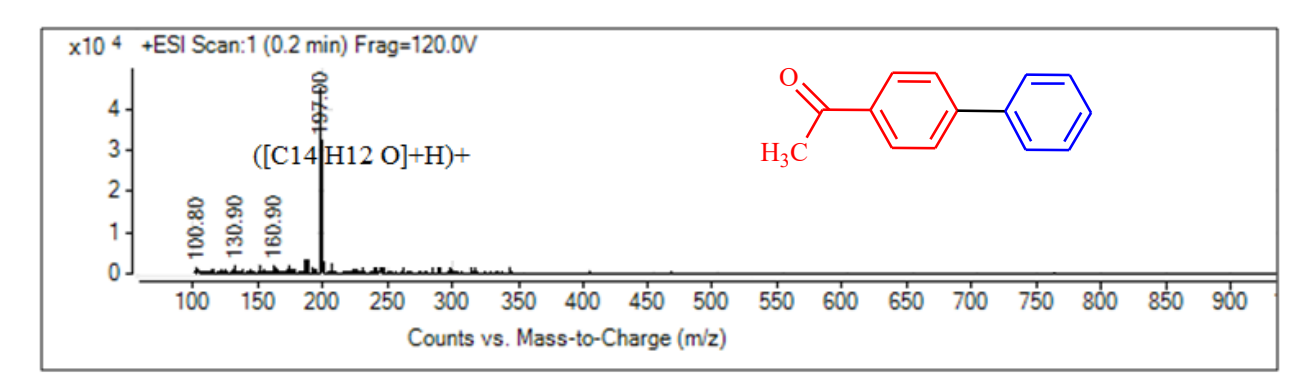
Annexure 5(j) <sup>13</sup>C Spectra of 2'-fluoro-4-acetylbiphenyl



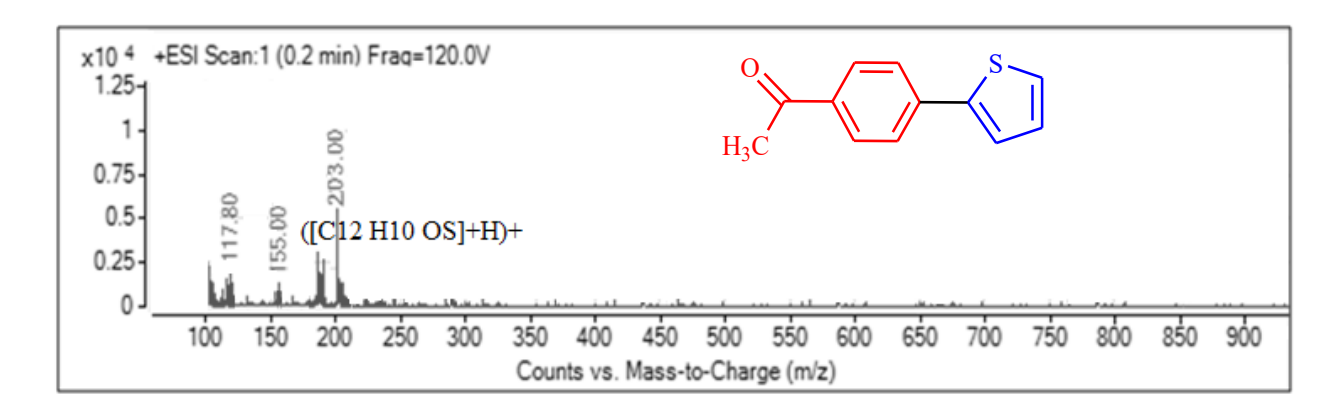
Annexure 5(k) <sup>1</sup>H NMR spectrum of 2-(4-Acetylphenyl)thiophene



Annexure 5(1) <sup>13</sup>C NMR spectrum of 2-(4-Acetylphenyl)thiophene



Annexure 5(m) Mass spectrum of 4-acetylbiphenyl.



Annexure 5(n) Mass spectrum of 2-(4-Acetylphenyl)thiophene

# Section 5.3 Pd@SB/Fe<sub>3</sub>O<sub>4</sub>-TiO<sub>2</sub> as an efficient Schiff base functionalized heterogeneous catalyst for the Hydrogenation of Aromatic Nitro Compounds under mild conditions

Selective hydrogenations, on the other hand, have also attained worldwide significance since they add worth to economic products obtained from diverse processes, and also allow the synthesis of vital compounds for the pharmaceutical, food, petrochemical, and fine chemical industry. Among various hydrogenation reactions, selective catalytic hydrogenation of aromatic nitro compounds finds great importance, since the products obtained are useful in pharmaceutical and medicinal chemistry, and material science [1-3]. Also, selective hydrogenation of aromatic nitro compounds in the company of additional competitive functional groups is a demanding job. For instance, hydrogenation of nitroarenes often ends at an intermediate phase, and thus results in the formation of hydroxyl amines, hydrazines, and azoarenes as by-products[4]. Thus, selective hydrogenation of aromatic nitro compounds using environmentally safe H<sub>2</sub> gas and magnetic catalytic systems is time and again the most desirable transformation in synthetic chemistry [5,6].

To conduct this industrially significant reaction under environmentally friendly conditions, there is anunrelentingrequirement to develop an effective catalytic system for reducing nitro compounds to their corresponding amines while maintaining simple, cost-effective, and green processes. Thus, we present the Pd@SB/Fe<sub>3</sub>O<sub>4</sub>-TiO<sub>2</sub> catalyzed reduction of various aromatic nitro compounds at room temperature, achieving good to excellent yields using molecular hydrogen in an aqueous medium (**Figure 5.14**)

Figure 5.14 Hydrogenation of Nitroarenes

### 5.3.1 Optimization of reaction conditions

Optimized reaction conditions were developed using nitrobenzene as the model substrate under hydrogen atmosphere at room temperature. The effectiveness

of the synthesized catalyst was compared with other known materials like Fe<sub>3</sub>O<sub>4</sub>, Fe<sub>3</sub>O<sub>4</sub>-TiO<sub>2</sub>, EDA/Fe<sub>3</sub>O<sub>4</sub>-TiO<sub>2</sub>, and SB/Fe<sub>3</sub>O<sub>4</sub>-TiO<sub>2</sub> (**Table 5.4**). Palladium-based catalysts in particular, both in homogenous and heterogenous form, showed enhanced activity, but the best results were obtained with the Schiff base functionalized palladium (II) complex onto TiO<sub>2</sub> coated Fe<sub>3</sub>O<sub>4</sub> magnetic nanoparticles, the Pd@SB/Fe<sub>3</sub>O<sub>4</sub>-TiO<sub>2</sub> (**Table 5.4, entry 10**). Further optimization concerningthe amount of catalyst allowed us to select 1.9 mol% Pd as the required amount to give the best results.

**Table 5.4** Evaluation of the activity of the different catalysts and their amount at different temperatures for the reduction of nitrobenzene<sup>a</sup>

Entry	Catalyst	Catalyst amount (g)	Time (h)	Yield <sup>c</sup> (%)
1	No catalyst	-	1.5	N.R.
2	Fe <sub>3</sub> O <sub>4</sub>	0.1	1.5	N.R.
3	Fe <sub>3</sub> O <sub>4</sub> -TiO <sub>2</sub>	0.1	1.5	N.R.
4	EDA/Fe <sub>3</sub> O <sub>4</sub> -TiO <sub>2</sub>	0.1	1.5	Traces
5.	SB/Fe <sub>3</sub> O <sub>4</sub> -TiO <sub>2</sub>	0.1	1.5	Traces
6.	$PdCl_2$	0.1	1	75
7.	$Pd(OAc)_2$	0.1	1	82
8.	$Pd@Fe_3O_4-TiO_2$	0.1	1	86
9.	Pd@SB/Fe <sub>3</sub> O <sub>4</sub> -TiO <sub>2</sub>	0.1	0.5	90
10.	Pd@SB/Fe <sub>3</sub> O <sub>4</sub> -TiO <sub>2</sub>	0.1	0.75	96
11.	Pd@SB/Fe <sub>3</sub> O <sub>4</sub> -TiO <sub>2</sub>	0.05	0.75	72
12.	Pd@SB/Fe <sub>3</sub> O <sub>4</sub> -TiO <sub>2</sub>	0.15	0.75	97

<sup>&</sup>lt;sup>a</sup>Reaction conditions: Nitrobenzene (1 mmol), molecular H<sub>2</sub>, and H<sub>2</sub>O/EtOH (1:1, 5 mL) at room temperature

To find the effect of the solvent system reaction was carried out in EtOH, MeOH, CH<sub>2</sub>Cl<sub>2</sub>, CH<sub>3</sub>CN, and H<sub>2</sub>O. Lower yield of product was obtained with all the pure solvents (**Table 5.5, entries 1-5**). Nevertheless, by employing an

<sup>&</sup>lt;sup>b</sup>Column chromatographic yields.

organic/aqueous co-solvent system, significant improvement in results was obtained (**Table 5.5**, **entries 6-8**). The co-solvent may have a favorable effect that results in the organic substrates being more soluble [7]. From the compiled data, the solvent system was chosen as H<sub>2</sub>O/EtOH in the ratio of (1:1) for carrying out further reactions (**Table 5.5**, **entry 8**).

Table 5.5 Optimization of different solvents for hydrogenation of aromatic nitro compounds<sup>a</sup>

Entry	Solvent	Time (h)	Yield <sup>b</sup> (%)
1	CH <sub>2</sub> Cl <sub>2</sub>	1.5	55
2	CH <sub>3</sub> CN	1.5	75
3	MeOH	1.5	80
4	EtOH	1.5	82
5.	$H_2O$	1.5	88
6.	EtOH/ H <sub>2</sub> O (1:3)	0.75	90
7.	EtOH/ H <sub>2</sub> O (1:2)	0.75	92
8.	EtOH/ H <sub>2</sub> O (1:1)	0.75	96

<sup>&</sup>lt;sup>a</sup>Reaction conditions: Nitrobenzene (1 mmol), molecular H<sub>2</sub>, and Solvent (5 mL), Pd@SB/Fe<sub>3</sub>O<sub>4</sub>-TiO<sub>2</sub> (0.1 g, 1.9 mol% Pd) at room temperature.

Using a variety of substituted aromatic nitro compounds, the activity of the created catalyst was investigated under optimized reaction circumstances (**Table 5.6**). Aromatic nitro compounds containing both electron-withdrawing groups and electron-donating were effective in the established technique. and gave the corresponding products in near quantitative yields. It is worth mentioning that the usual side products obtained during hydrogenation of nitro compounds, viz, azoxy, azo, and hydrazo, azo and azoxy compounds, were not observed in this case. Additionally, there was no dehalogenation occurred throughout the hydrogenation of nitro compounds substituted with halogens, and all the products were obtained in excellent yields.

<sup>&</sup>lt;sup>b</sup>Column chromatographic yields.

A plausible reaction mechanism for the reduction of nitrobenzene to aniline in the presence of Pd@SB/Fe<sub>3</sub>O<sub>4</sub>-TiO<sub>2</sub>involving phenylhydroxylamine as an intermediate has been proposed and depicted in **Figure 5.15**. Initially, nitrobenzene binds with the hydrogenated catalyst **I** to abstract hydrogen atoms from the catalyst surface, leaving water as a by-product and itself reduced to nitrosobenzene intermediate **II**. The nitrosobenzene**II**, then again, undergoes rapid hydrogen transfer from the catalyst to the N=O double bond to form ArNH-OH or hydroxyl amine intermediate **III**, which on abstracting one more molecule of hydrogen from the hydrogenated Pd catalyst yields the final product, amine IV and the catalyst is regenerated.

Table 5.6 Pd@Fe<sub>3</sub>O<sub>4</sub>-TiO<sub>2</sub>/SB catalysed hydrogenation of aromatic nitrocompounds<sup>a</sup>

Entry	Substrate	Product	Time (h)	Yield (%) <sup>b</sup>
1.	$\sim$ NO <sub>2</sub>	$\sim$ NH <sub>2</sub>	0.75	96
2.	H <sub>3</sub> CO NO <sub>2</sub>	H <sub>3</sub> CO NH <sub>2</sub>	0.75	95
3.	H <sub>3</sub> C — NO <sub>2</sub>	$H_3C$ $\longrightarrow$ $NH_2$	1	94
4.	Cl	Cl	1.5	93
	$\sim$ NO <sub>2</sub>	$\sim$ NH <sub>2</sub>		
5.	$CH_3$	$CH_3$	0.75	94
	$\sim$ NO <sub>2</sub>	$\sim$ NH <sub>2</sub>		
6.	$Br \longrightarrow NO_2$	$Br \longrightarrow NH_2$	1.5	93
7.	Cl—NO <sub>2</sub>	Cl—NH <sub>2</sub>	1	95
8.	HO—NO <sub>2</sub>	HO NH <sub>2</sub>	2	90
9.	NO <sub>2</sub>	NH <sub>2</sub>	1.5	92

10.	$O_2N$ $\longrightarrow$ $NO_2$	$H_2N$ $\longrightarrow$ $NH_2$	2	95
-----	---------------------------------	---------------------------------	---	----

<sup>a</sup>Reaction conditions: Aromatic NitroCompound(1 mmol), 0.1 g (1.9 mol% Pd), H<sub>2</sub> atm, and H<sub>2</sub>O/EtOH (1:1, 5 mL) at room temperature.

<sup>b</sup>Column chromatographic yields.

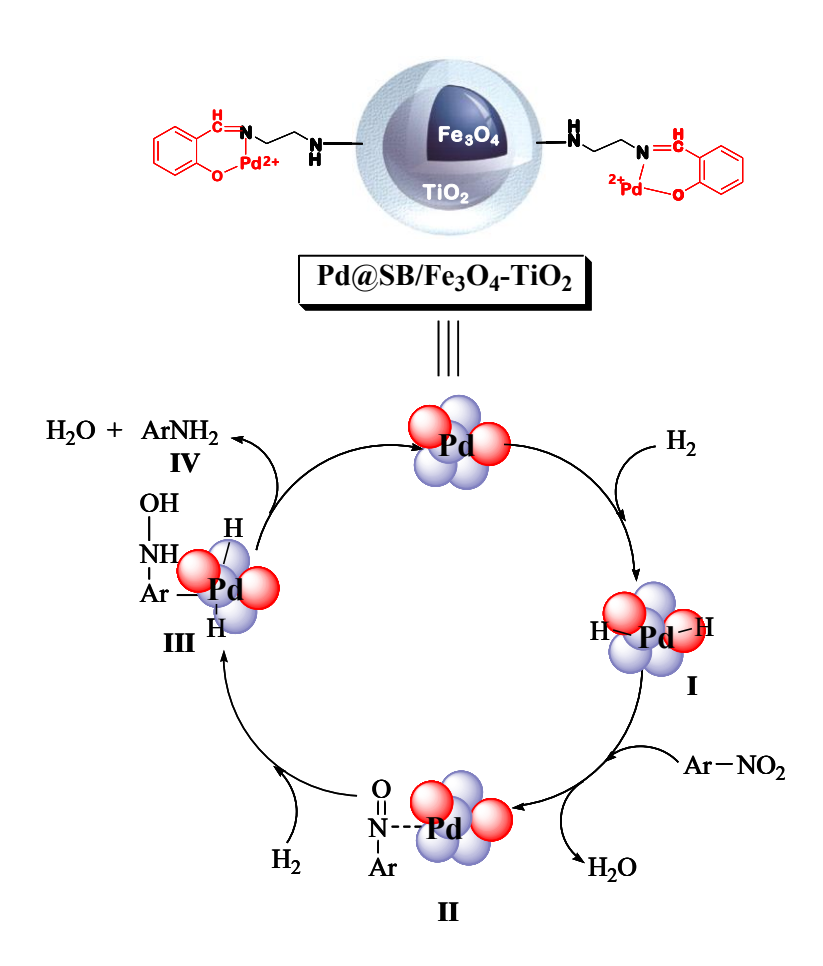
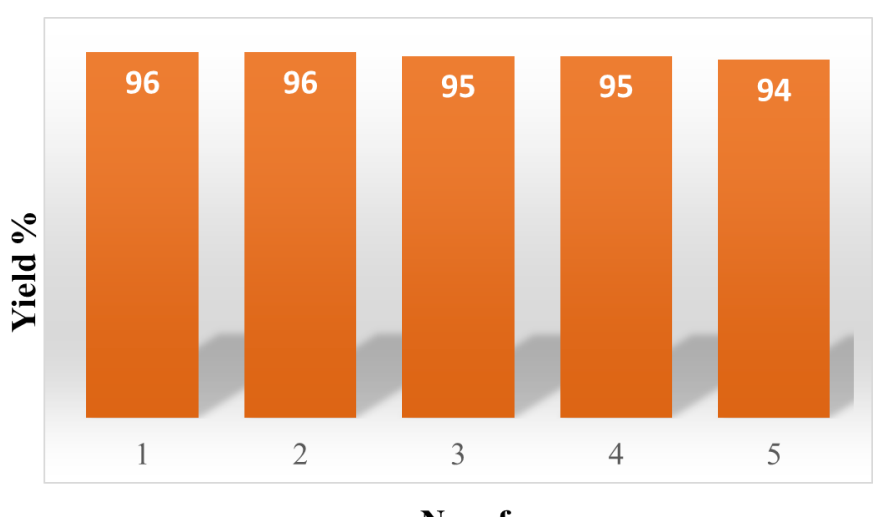


Figure 5.15. Plausible Mechanism for the hydrogenation of nitroarenes

### Recyclability

We investigated the test reaction to verify the stability and reusability of Pd@Fe<sub>3</sub>O<sub>4</sub>-TiO<sub>2</sub>/SB in case of **entry 1**, **Table 5.6.** After the completion of the reaction, the catalyst was recovered from the reaction mixture by using an external magnet, followed by washing with ethyl acetate and ethanol successively so as to remove any residual products. The recovered catalyst was then reused for another set of reactions by adding new substrates under similar reaction conditions. The practice

was repeated for 6 consecutive cycles, and no considerable change in its catalytic activity was observed up to the 6th cycle, demonstrating the superb recyclability of the developed catalyst (**Figure 5.16**). Comparing the recycled catalyst to the new one, FTIR, XRD, and XPS analysis showed no discernible structural changes.



No. of runs

**Figure 5.16** Recyclability ofPd@Fe<sub>3</sub>O<sub>4</sub>-TiO<sub>2</sub>/SB for hydrogenation of nitrobenzene. Reaction conditions: Nitrobenzene (1 mmol), molecular H<sub>2</sub>, and Solvent (5 mL), Pd@SB/Fe<sub>3</sub>O<sub>4</sub>-TiO<sub>2</sub> (0.1 g, 1.9 mol% Pd) at room temperature.

bColumn chromatographic yields.

### 5.3.2 Conclusion

This study outlines a productive and straightforward operational approach for synthesizing Schiff base functionalized palladium (II) complex onto titania-bonded magnetic nanoparticles [Pd@Fe<sub>3</sub>O<sub>4</sub>-TiO<sub>2</sub>/SB], and its excellent catalytic efficiency was explored for the hydrogenation of aromatic nitro compounds in benign reaction conditions. The developed catalytic system gives the desired products in excellent yields without any harmful effluent discharge, making it an environmentally acceptable and greener protocol. In addition to it, the catalyst is cost-effective because it can be easily recovered using external magnet and can be recycled up to six consecutive runs without any appreciable change in its structure and morphology.

# General procedure for the Pd@Fe<sub>3</sub>O<sub>4</sub>-TiO<sub>2</sub>/SB catalyzed hydrogenation of aromatic nitrocompounds

To a round bottom flask (25 mL), aromatic nitro compound (1.0 mmol), Pd@SB/Fe<sub>3</sub>O<sub>4</sub>-TiO<sub>2</sub> (0.1 g,1.9 mol % Pd) and H<sub>2</sub>O:EtOH (1:1), (5.0 mL) was added and then the resultant mixture underwent stirring at room temperature under H<sub>2</sub> atmosphere (Table 5). The catalyst was magnetically removed once the reaction was finished, washed with water, and vacuum-dried for future use. The residual mixture was extracted using EtOAc, washed with H<sub>2</sub>O,and desiccated over sodium sulphate (anhydrous). The crude product thus obtained was further purified using silica gel Column chromatography (ethyl acetate-pet-ether as eluent).

# Comparison with other Schiff base functionalized palladium catalysts reported in the literature with Pd@SB/Fe<sub>3</sub>O<sub>4</sub>-TiO<sub>2</sub>

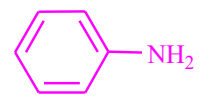
The comparison of the catalytic activity of Pd@SB/Fe<sub>3</sub>O<sub>4</sub>-TiO<sub>2</sub> with other Schiff base functionalized catalyst systems from the literature for the Suzuki coupling reaction and the hydrogenation of aromatic nitro compounds. The results demonstrate the superiority of the developed catalytic system and indicate that the current protocol is highly sustainable. This catalytic system's main benefits include using safe reaction media with a more environmentally friendly hydrogen source, reducing reaction time, and being recyclable and magnetically retrievable.

**Table 5.7** Comparison of the catalytic activity of Pd@SB/Fe<sub>3</sub>O<sub>4</sub>-TiO<sub>2</sub> with other documented Schiff base functionalized catalytic systems for the Suzuki reaction and hydrogenation of aromatic nitro compounds.

Entry	Catalyst	Reaction conditions	Time	Yield (%)	Ref.
1.	Pd-Schiff base@MWCNTs	4-Bromobenzonitrile, K <sub>2</sub> CO <sub>3</sub> (2.0 mmol), DMF/H <sub>2</sub> O (2.0 mL, 1:1)	3h	97	[8]
2.	OCMCS-SB-Pd(II)	Bromobenzene, K <sub>2</sub> CO <sub>3</sub> (1.5 mmol), EtOH/H <sub>2</sub> O, (5 mL, 3:2)	2 h	96	[9]
3.	SB-Pd@MNPs	4-Bromobenzonitrile, Na <sub>3</sub> PO <sub>4</sub> ·12H <sub>2</sub> O (2.2 mmol),EtOH/H <sub>2</sub> O (10 mL, 1:1)	4 h	84	[10]
4.	Pd-Imino-Py-c-Fe <sub>2</sub> O <sub>3</sub>	4-Bromobenzonitrile, Et <sub>3</sub> N (2 mmol), DMF (2 mL)	2.5 h	87	[11]
5.	Schiff-base- Pd@MNPs	4-Bromobenzonitrile, K <sub>2</sub> CO <sub>3</sub> (1.5 mmol) (PEG)-400 (1 ml)	4 h	97	[12]
6.	Pd@SB/Fe <sub>3</sub> O <sub>4</sub> -TiO <sub>2</sub>	Bromobenzene, K <sub>2</sub> CO <sub>3</sub> (1 mmol), H <sub>2</sub> O, (5 mL)	35 min	93	This work
7.	Pd@SB/Fe <sub>3</sub> O <sub>4</sub> -TiO <sub>2</sub>	4-Bromobenzonitrile, K <sub>2</sub> CO <sub>3</sub> (1 mmol), H <sub>2</sub> O, (5 mL)	30 min	94	This work
8.	SB-Pd@MNPs	Nitrobenzene, NaBH <sub>4</sub> (4 mmol), H <sub>2</sub> O, (10 mL), RT	0.03 h	90	[10]
9.	Pd/SBA-15	Nitrobenzene, decane (100 mg), H <sub>2</sub> atm, and EtOH (4 mL), 40 °C	1 h	98	[13]
10.	1T-MoS2	Nitrobenzene, Hydrazine hydrate (40 mmol), and toluene (10 mL)	1.5 h	99	[14]
11.	Pd@SB/Fe <sub>3</sub> O <sub>4</sub> -TiO <sub>2</sub>	Nitrobenzene, H <sub>2</sub> atm., RT and H <sub>2</sub> O/EtOH (1:1, 5 mL)	45 min	96	This work

## Spectral details of the products listed in Table 5.6

## Aniline (entry 1)



<sup>1</sup>H NMR (CDCl<sub>3</sub>, 400 MHz): δ 3.68 (bs, 2H, NH<sub>2</sub>), 6.76-6.78 (d, 2H, J= 8.0 Hz), 6.87-6.91 (t, 1H, J= 8.0 Hz), 7.26-7.30 (t, 2H, J= 8 Hz); <sup>13</sup>C NMR (CDCl<sub>3</sub>, 100 MHz): δ 115.45, 118.52, 129.77, 146.59. ESI-MS: 93 (M)<sup>+</sup>.

### 4-Methoxyaniline (entry 2)

$$H_3CO$$
  $\longrightarrow$   $NH_2$ 

<sup>1</sup>H NMR (CDCl<sub>3</sub>, 400 MHz):  $\delta$  3.44 (s, 3H, -OCH<sub>3</sub>), 3.77 (bs, 2H, NH<sub>2</sub>), 6.66-6.68 (d, 2H, J= 8.0 Hz), 7.76-7.78 (d, 2H, J= 8.0 Hz); <sup>13</sup>C NMR (CDCl<sub>3</sub>, 100 MHz): $\delta$  56.04, 114.97, 115.99, 142.25, 149.90. ESI-MS: 123 (M)<sup>+</sup>.

### 4-Methylaniline (entry 3)

$$H_3C$$
  $\longrightarrow$   $NH_2$ 

<sup>1</sup>H NMR (CDCl<sub>3</sub>, 400 MHz):δ2.28 (s, 3H, CH<sub>3</sub>),3.49 (bs, 2H, NH<sub>2</sub>), 6.64-6.66 (d, 2H, J= 8.0 Hz), 7.00-7.02 (d, 2H, J= 8.0 Hz); <sup>13</sup>C NMR (CDCl<sub>3</sub>, 100 MHz):δ 20.50, 115.31, 127.84, 129.79, 143.82. ESI-MS: 107 (M)<sup>+</sup>.

### 2-Chloroaniline (entry 4)

<sup>1</sup>H NMR (DMSO, 400 MHz):  $\delta$  4.90 (bs, 2H, NH<sub>2</sub>), 6.49-6.53 (t, 1H, J= 8.0 Hz), 6.60-6.62 (d, 1H), 6.93-6.67 (t, 1H, J= 8.0 Hz), 7.01-7.03 (d, 1H); <sup>13</sup>C NMR (DMSO, 100 MHz):  $\delta$  116.12, 118.14, 118.20,127.45, 130.08, 144.02. ESI-MS: 128 (M)<sup>+</sup>, 130 (M+2)<sup>+</sup>.

### 2-Methylaniline (entry 5)

<sup>1</sup>H NMR (CDCl<sub>3</sub>, 400 MHz): $\delta$  2.85 (s, 3H, CH<sub>3</sub>), 3.43 (bs, 2H, NH<sub>2</sub>), 6.78-7.05 (m, 4H); <sup>13</sup>C NMR (CDCl<sub>3</sub>, 100 MHz): $\delta$  45.51, 110.63, 115.20, 118.32, 121.25, 136.21, 147.35. ESI-MS: 107 (M)<sup>+</sup>.

## 4-Bromoaniline (entry 6)

$$\operatorname{Br} - \hspace{-1em} \bigvee - \operatorname{NH}_2$$

<sup>1</sup>H NMR (CDCl<sub>3</sub>, 400 MHz):  $\delta$  3.69 (bs, 2H, NH<sub>2</sub>), 6.57- 6.60 (d, 2H, J= 12 Hz), 7.25-7.27 (d, 2H, J= 8 Hz); <sup>13</sup>C NMR (CDCl<sub>3</sub>, 100 MHz): $\delta$  110.20, 132.03,116.74, 145.45. ESI-MS: 171 (M)<sup>+</sup>

# 4-Chloroaniline (entry 7)

$$CI$$
  $\longrightarrow$   $NH_2$ 

<sup>1</sup>H NMR (CDCl<sub>3</sub>, 400 MHz):  $\delta$  7.11-7.13 (d, 2H, J= 8 Hz), 6.62- 6.64 (d, 2H, J= 8 Hz),3.68 (bs, 2H, NH<sub>2</sub>);<sup>13</sup>C NMR (CDCl<sub>3</sub>, 100 MHz): $\delta$  116.16, 128.94, 120.43, 147.17. ESI-MS: 127 (M)<sup>+</sup>.

### 4-Aminophenol (entry 8)

$$\operatorname{HO} - \hspace{-1em} \bigvee \operatorname{NH}_2$$

<sup>1</sup>H NMR (CDCl<sub>3</sub>, 400 MHz):  $\delta$  3.13 (bs, 2H, NH<sub>2</sub>), 4.68 (bs, 1H, OH), 6.62- 6.64 (d, 2H, J= 8 Hz), 6.11-6.13 (d, 2H, J= 8 Hz); <sup>13</sup>C NMR (CDCl<sub>3</sub>, 100 MHz): $\delta$  116.92, 117.27, 141.78, 148.71. **ESI-MS**: 109 (M)<sup>+</sup>.

## 1-Naphthylamine (entry 9)

<sup>1</sup>H NMR (CDCl<sub>3</sub>, 400 MHz):  $\delta$  4.10 (bs, 2H, NH<sub>2</sub>), 6.82- 6.84 (d, 1H, J= 8 Hz), 7.34-7.41 (m, 2H,), 7.49-7.55 (m, 2H), 7.85-7.89 (m, 2H); <sup>13</sup>C NMR (CDCl<sub>3</sub>, 100 MHz): $\delta$  109.75, 119.03, 120.88, 123.71, 124.93, 125.92, 126.50, 128.62, 134.45, 142.15. ESI-MS: 143 (M)<sup>+</sup>.

### Benzene-1,4-diamine (entry 10)



<sup>1</sup>H NMR (CDCl<sub>3</sub>, 400 MHz):  $\delta$  3.34 (bs, 4H, NH<sub>2</sub>), 6.59 (s, 4H); <sup>13</sup>C NMR (CDCl<sub>3</sub>, 100 MHz):  $\delta$  116.94, 138.57. ESI-MS: 108 (M)<sup>+</sup>.

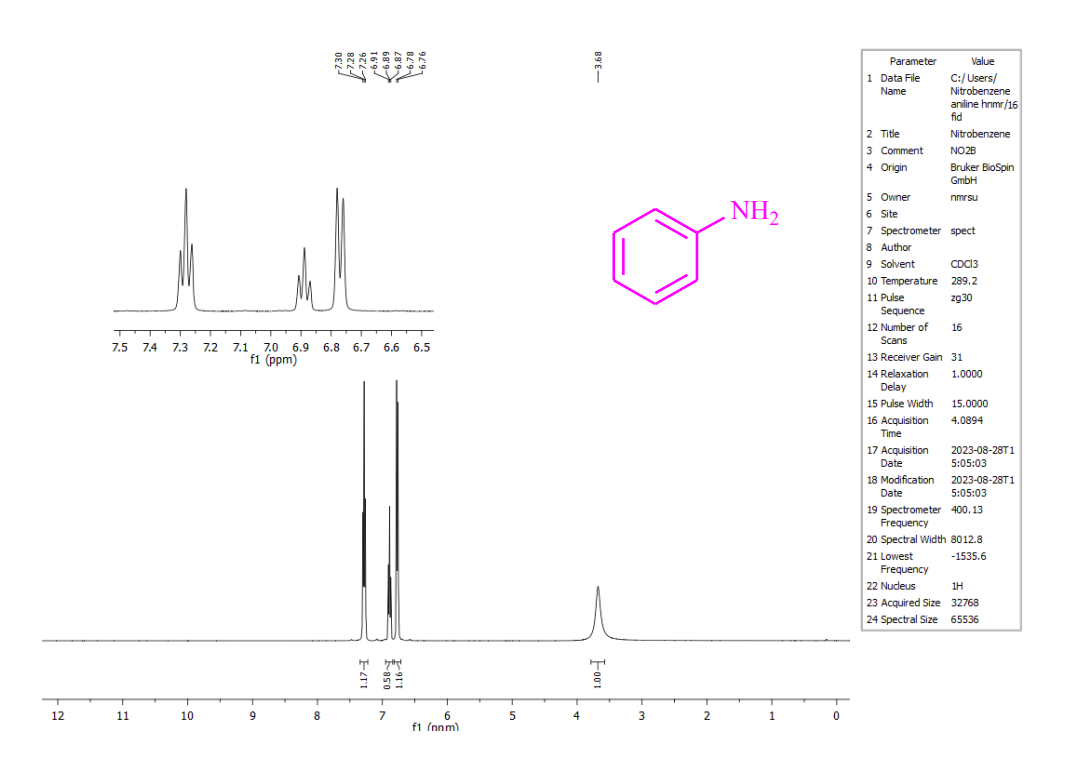
### 4.3.3 References

- [1]. Guo, W., Zheng, Y., Xiang, W. and Zhang, Y., 2025. Advances in catalysis of reduction of nitroaromatics and its mechanism: a tutorial review. *RSC Sustainability*.
- [2]. Gong, W., Ma, J., Chen, G., Dai, Y., Long, R., Zhao, H. and Xiong, Y., 2025. Unlocking the catalytic potential of heterogeneous nonprecious metals for selective hydrogenation reactions. *Chemical Society Reviews*.
- [3]. Kumar, A., Sharma, S., Sharma, S., Bhardwaj, M. and Maji, S., 2024. Novel Pd (II) complex of Schiff base encapsulated on ferrite-titania core [Pd@SB/Fe<sub>3</sub>O<sub>4</sub>-TiO<sub>2</sub>]: a recyclable nanocatalyst for Suzuki coupling and hydrogenation of aromatic nitro compounds. *Research on Chemical Intermediates*, 50(9), pp.4249-4274.
- [4]. Shil, A.K., Sharma, D., Guha, N.R. and Das, P., 2012. Solid supported Pd (0): an efficient recyclable heterogeneous catalyst for chemoselective reduction of nitroarenes. *Tetrahedron Letters*, *53*(36), pp 4858-4861.
- [5]. Zhou, P., Li, D., Jin, S., Chen, S. and Zhang, Z., 2016. Catalytic transfer hydrogenation of nitro compounds into amines over magnetic graphene oxide supported Pd nanoparticles. *international journal of hydrogen energy*, 41(34), pp 15218-15224.
- [6]. Bhardwaj, M., Jamwal, B. and Paul, S., 2016. Novel Cu (0)-Fe <sub>3</sub> O <sub>4</sub>@ SiO <sub>2</sub>/NH<sub>2</sub> cel as an efficient and sustainable magnetic catalyst for the synthesis of

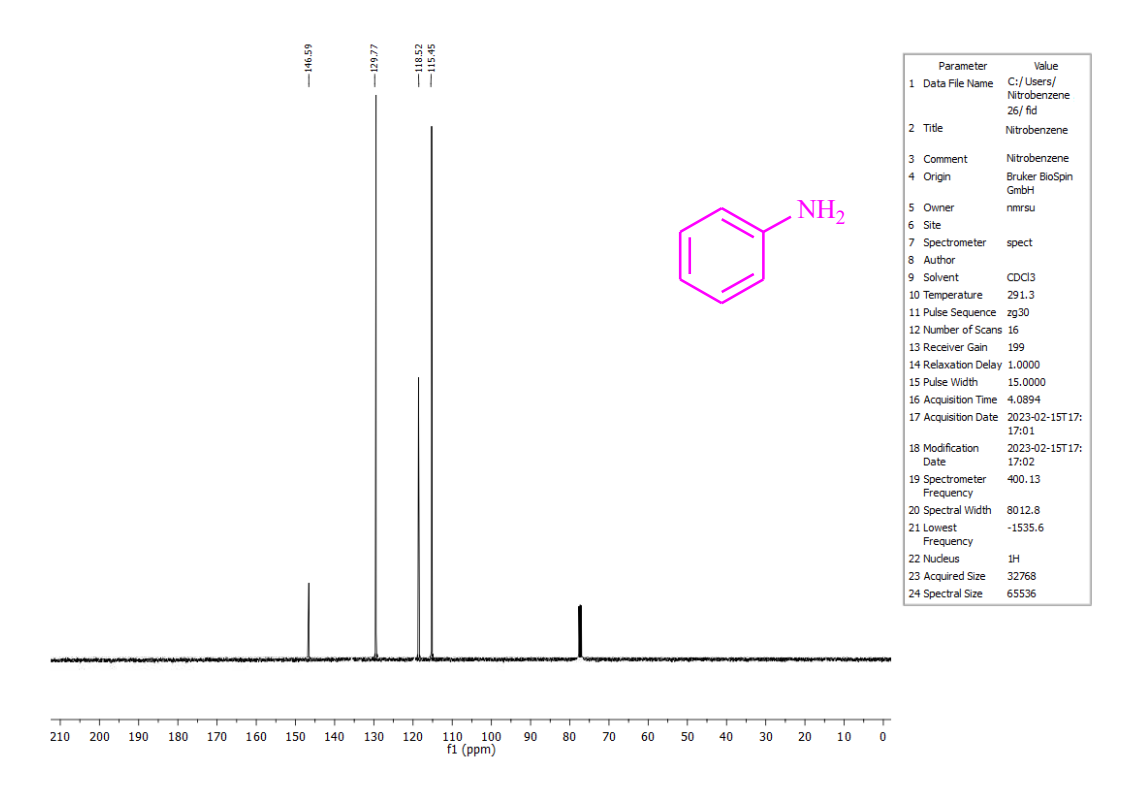
- 1, 4-Disubstituted-1, 2, 3-triazoles and 2-substituted-benzothiazoles via one-pot strategy in aqueous media. *Catalysis Letters*, *146*, pp 629-644.
- [7]. Castro, G.R. and Knubovets, T., 2003. Homogeneous biocatalysis in organic solvents and water-organic mixtures. *Critical Reviews in Biotechnology*, 23(3), pp 195-231.
- [8]. D'Alterio, M.C., Casals-Cruañas, È., Tzouras, N.V., Talarico, G., Nolan, S.P. and Poater, A., 2021. Mechanistic aspects of the palladium-catalyzed Suzuki-Miyaura cross-coupling reaction. *Chemistry–A European Journal*, 27(54), pp.13481-13493.
- [9]. Dong, Y., Bi, J., Ming, S., Zhang, S., Zhu, D., Meng, D. and Li, T., 2021. Functionalized chitosan as a novel support for stabilizing palladium in Suzuki reactions. *Carbohydrate Polymers*, 260, p.117815.
- [10]. Manjunatha, K., Koley, T.S., Kandathil, V., Dateer, R.B., Balakrishna, G., Sasidhar, B.S., Patil, S.A. and Patil, S.A., 2018. Magnetic nanoparticle-tethered Schiff base–palladium (II): Highly active and reusable heterogeneous catalyst for Suzuki–Miyaura cross-coupling and reduction of nitroarenes in aqueous medium at room temperature. *Applied Organometallic Chemistry*, 32(4), p.e 4266.
- [11]. Yasmin, S., Roy, N., Kabir, M.H. and Jeon, S., 2022. Nitrogen-functionalized carbon nanotube based palladium nanoparticles as an efficient catalyst for oxygen reduction and ethanol oxidation reaction. *Applied Surface Science Advances*, 9, p.100235.
- [12]. Navidi, M., Rezaei, N. and Movassagh, B., 2013. Palladium (II)—Schiff base complex supported on multi-walled carbon nanotubes: A heterogeneous and reusable catalyst in the Suzuki–Miyaura and copper-free Sonogashira—Hagihara reactions. *Journal of Organometallic Chemistry*, 743, pp.63-69.
- [13]. Duan, Y., Zheng, M., Li, D., Deng, D., Wu, C. and Yang, Y., 2017. Synthesis of Pd/SBA-15 catalyst employing surface-bonded vinyl as a reductant and its application in the hydrogenation of nitroarenes. *RSC Advances*, 7(6), pp.3443-3449.

[14]. Ramalingam, A., Samaraj, E., Venkateshwaran, S., Senthilkumar, S.M. and Senadi, G.C., 2022. 1T-MoS 2 catalysed reduction of nitroarenes and a one-pot synthesis of imines. *New Journal of Chemistry*, 46(18), pp.8720-8728.

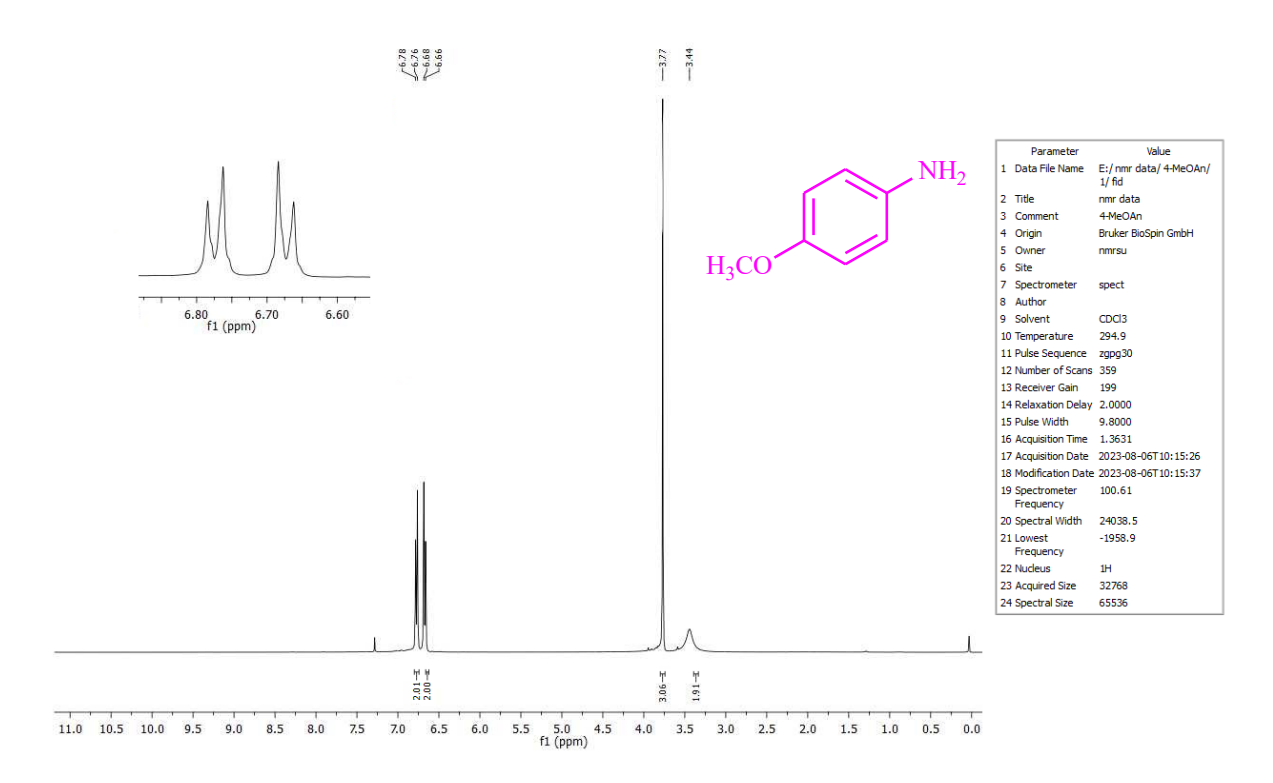
### 4.3.4 Annexures



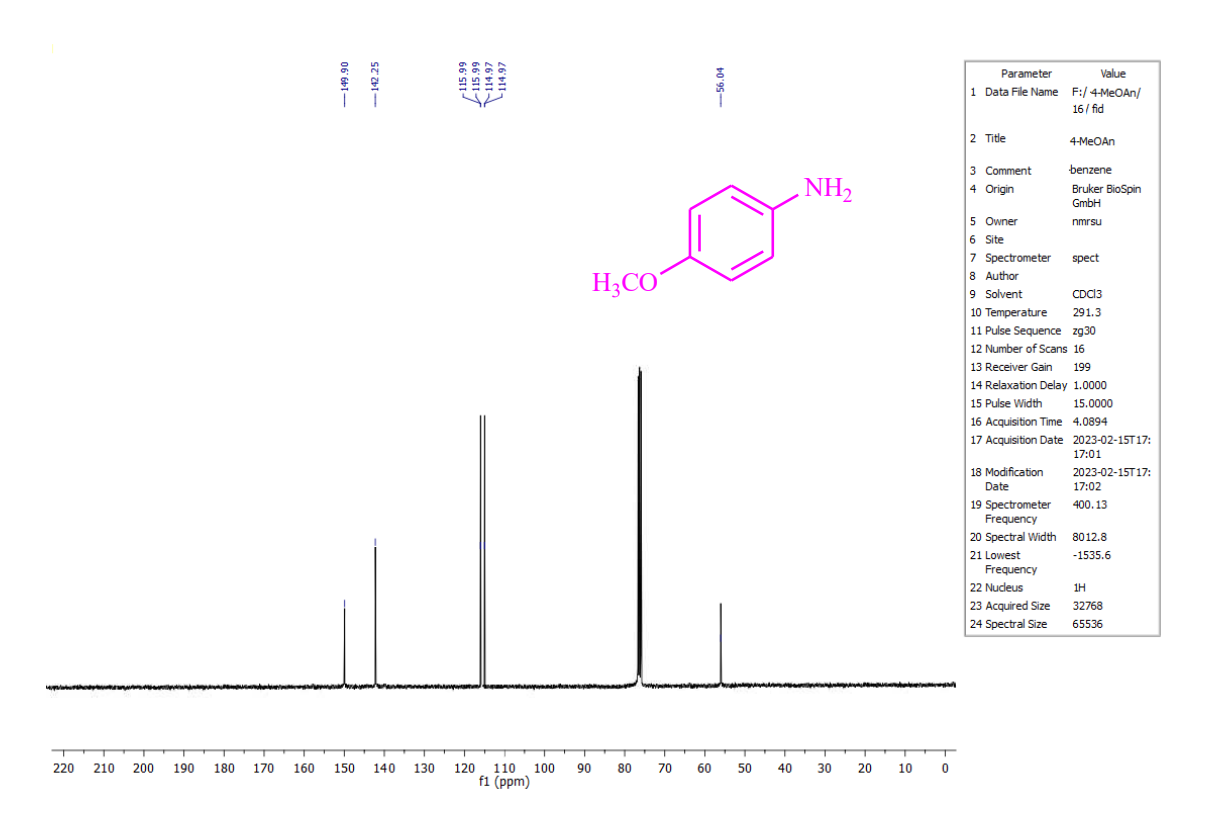
Annexure 5(0)¹H NMR spectrum of Aniline



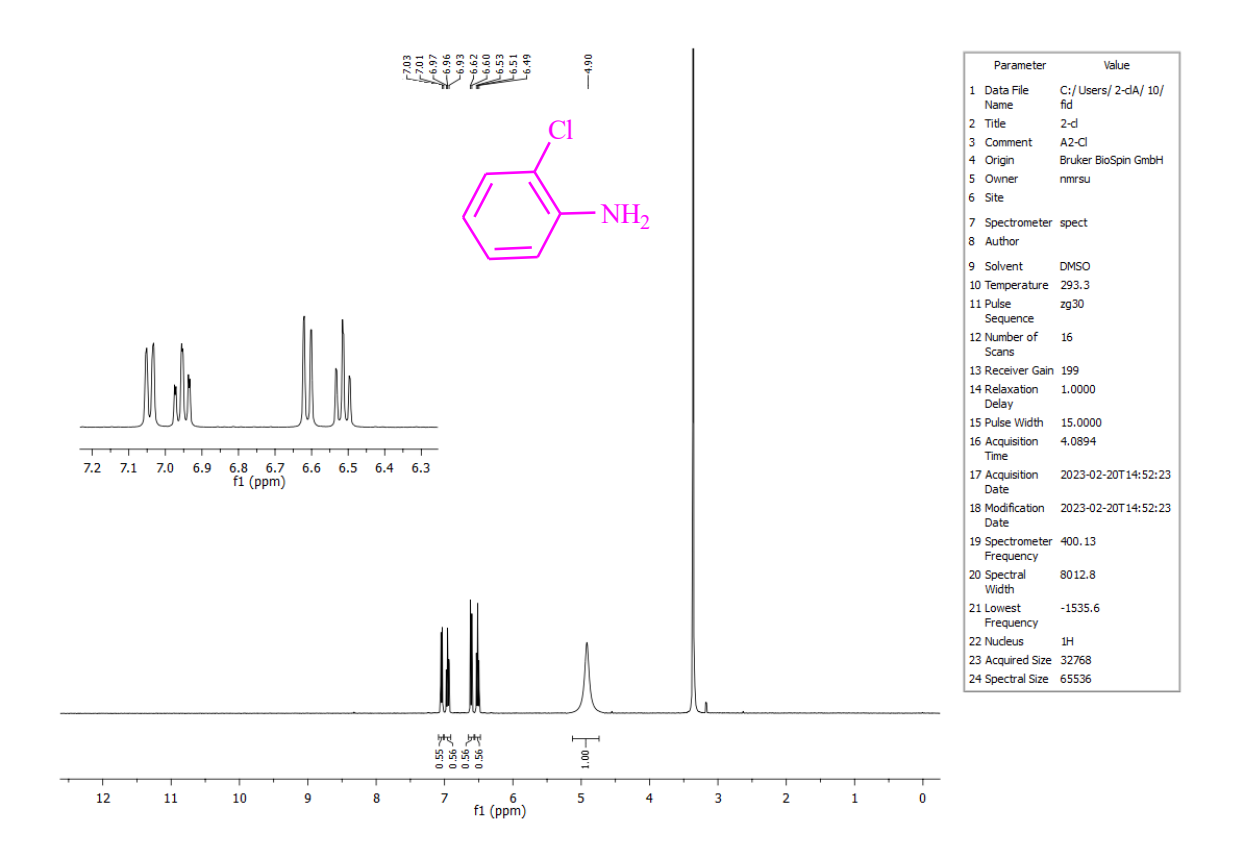
Annexure 5(p)<sup>13</sup>C NMR spectrum of Aniline



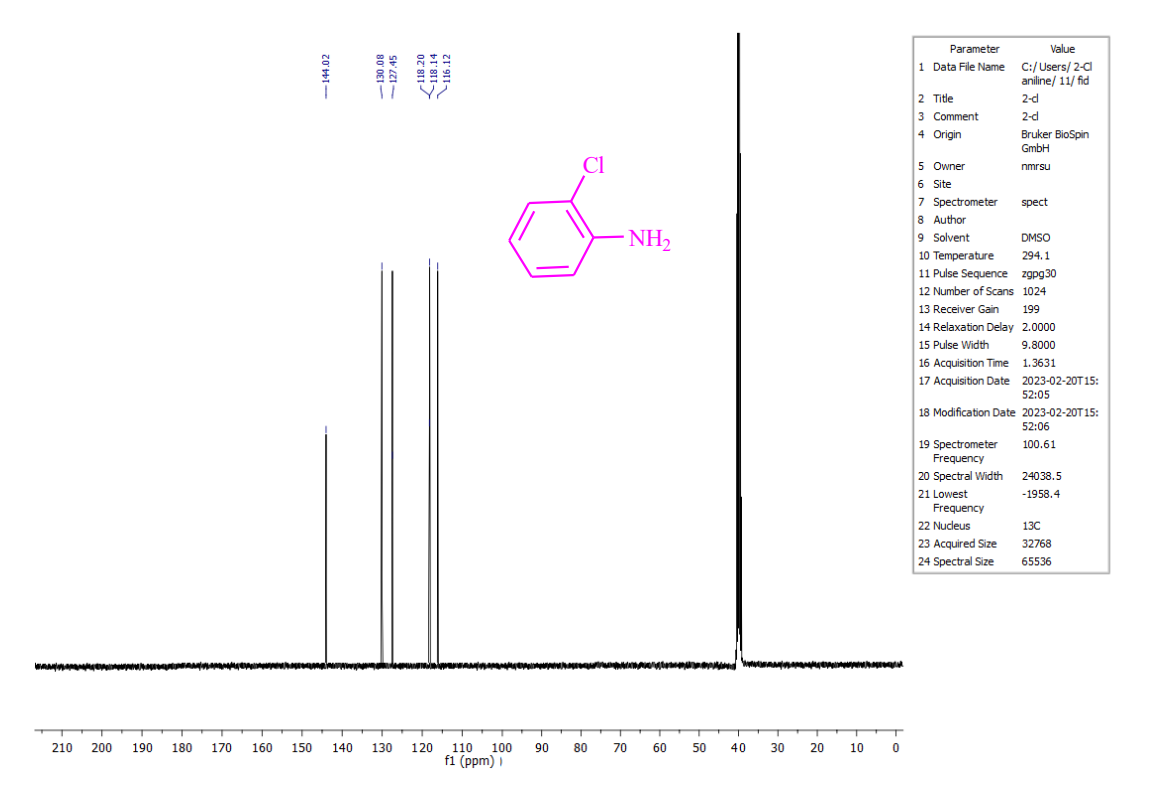
Annexure 5(q)<sup>1</sup>H NMR spectrum of 4-Methoxyaniline



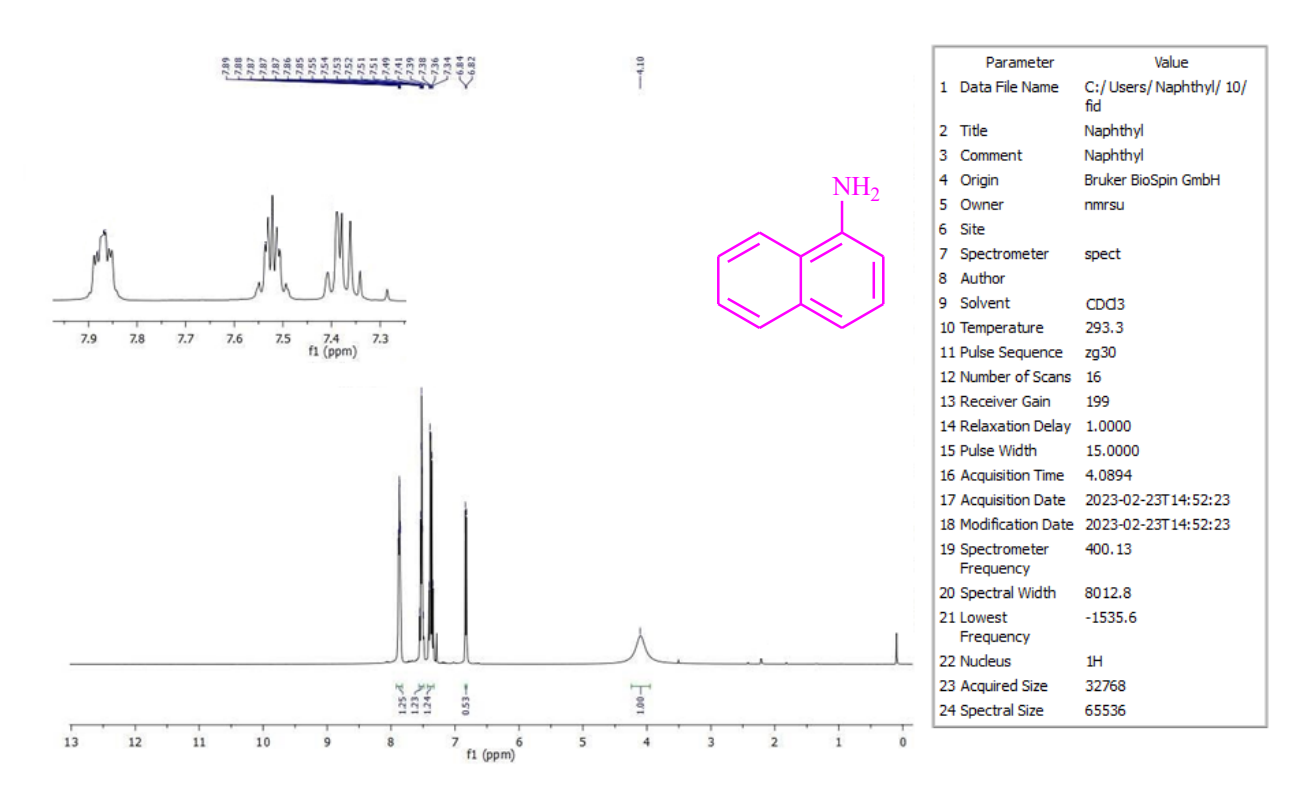
Annexure 5(r)<sup>13</sup>C NMR spectrum of 4-Methoxyaniline



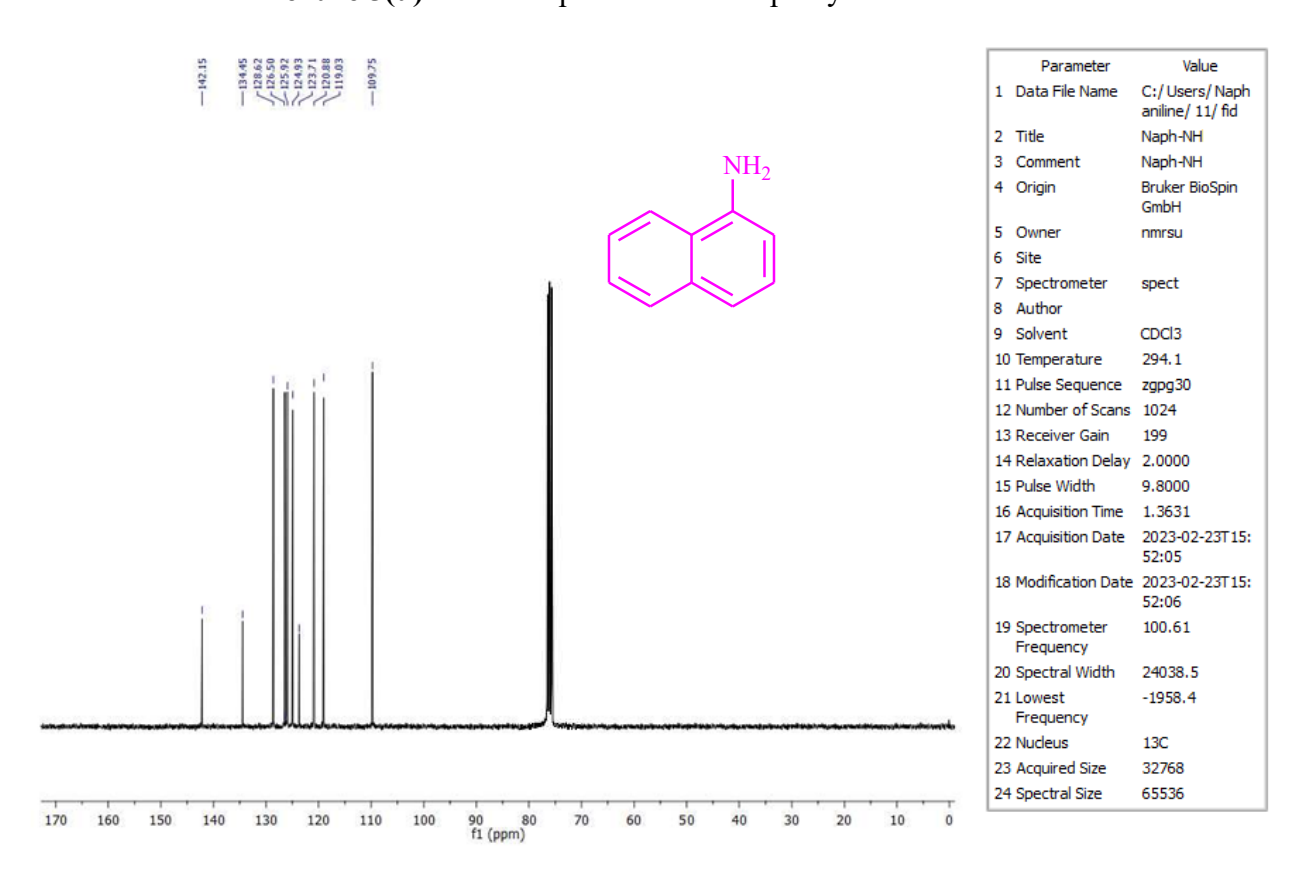
# Annexure 5(s)<sup>1</sup>H NMR spectrum of 2-Chloroaniline



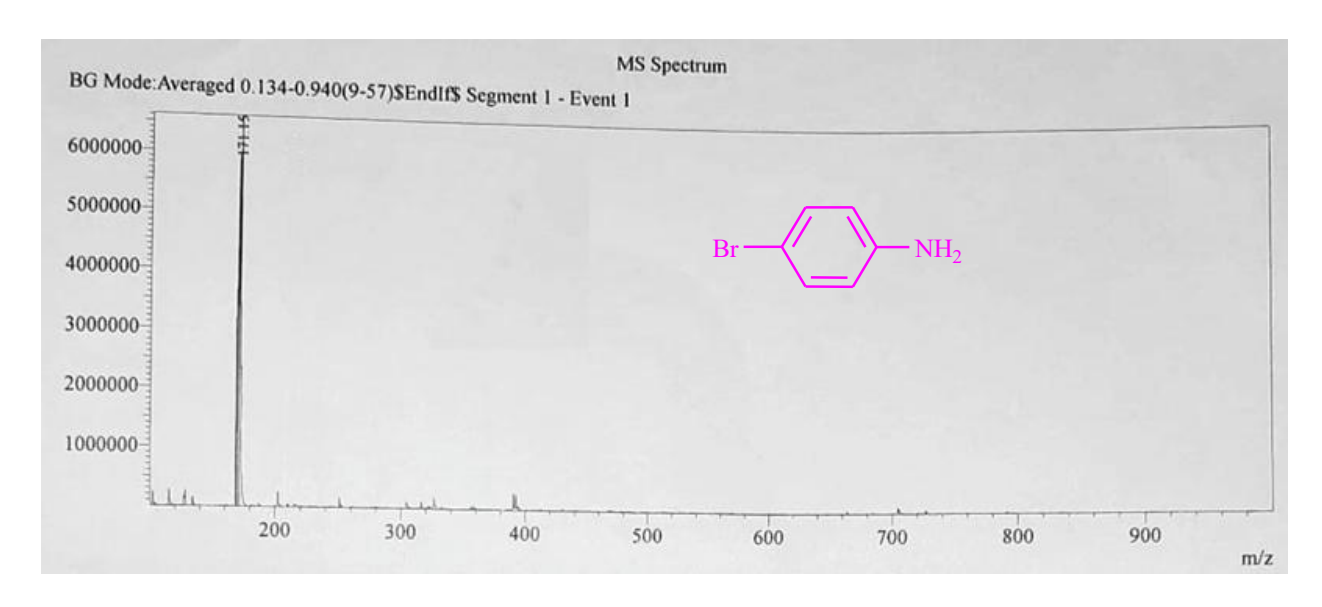
Annexure 5(t)<sup>13</sup>C NMR spectrum of 2-Chloroaniline



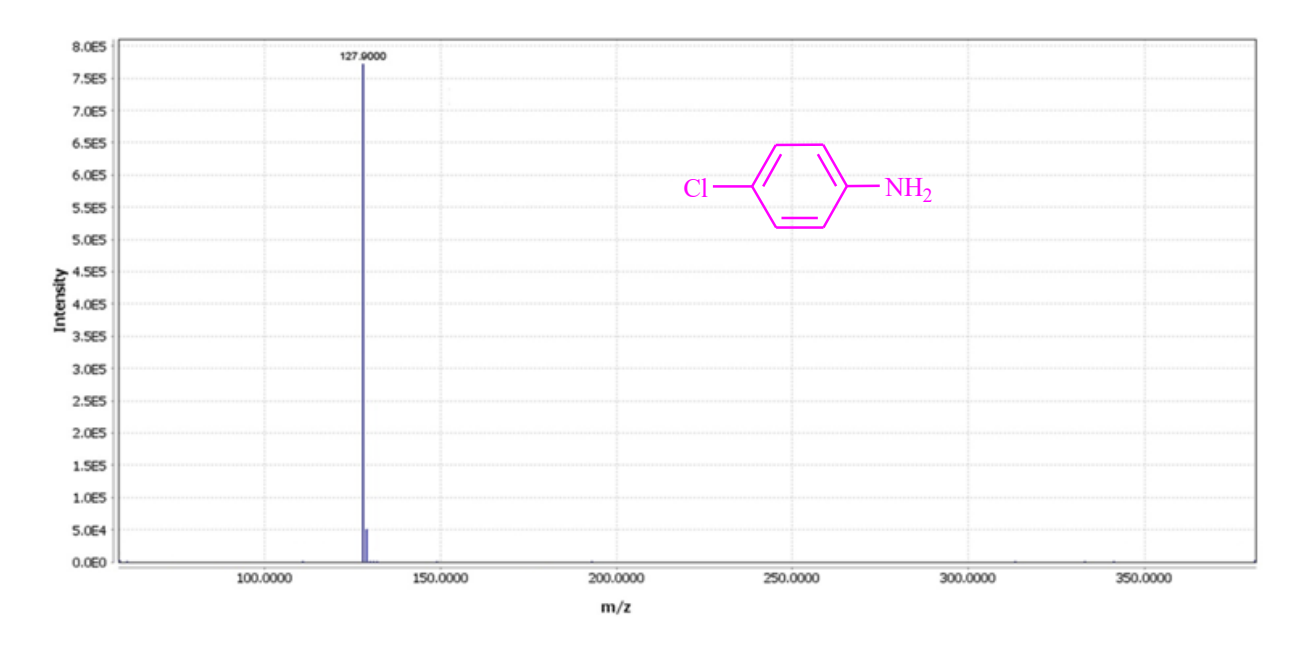
# Annexure 5(u)<sup>1</sup>H NMR spectrum of 1-Naphthylamine



Annexure 5(v)<sup>13</sup>C NMR spectrum of 1-Naphthylamine



Annexure 5(w) Mass spectrum of 4-Bromoaniline



Annexure 5(x) Mass spectrum of 4-Chloroaniline

### **Summary and Overall Conclusion of the Thesis**

Schiff bases have proven to be invaluable as synthetic intermediates in the intricate process of coordinating metal complex synthesis. These compounds are particularly noted for their distinctive imine or azomethine (C=N) functional groups, which emerge from the nucleophilic addition reactions that define Schiff base chemistry. The real intrigue lies in the observation that when carefully selected metals—such as copper (II), zinc (II), and palladium (II)—are combined with Schiff base ligands in controlled ambient conditions, there is a remarkable amplification of the bioactivity associated with these ligands. This thesis embarks on a detailed exploration of the synthesis of both homogeneous and heterogeneous Schiff base metal complexes, emphasizing the unique interactions and characteristics of the metals involved. Advanced spectroscopic methods, including UV-Vis, FTIR, NMR, and X-ray diffraction, are employed to meticulously characterize the resulting complexes, providing insights into their structural properties and stability. Furthermore, the investigation will assess the potential applications of these complexes, specifically their abilities in biocidal activity, DNA binding, and catalysis, thereby highlighting their significance in medicinal chemistry and environmental applications. Each synthesized complex not only showcases the fascinating interplay between metal ions and Schiff bases but also opens up new avenues for research and application in diverse scientific fields.

In this study, we synthesized various metal complexes involving Cu(II), Zn(II), and Pd(II) alongside a Schiff base ligand of the Salen type. The synthesized compounds underwent comprehensive characterization through a range of spectroscopic techniques, which included UV-Vis spectroscopy, IR spectroscopy, and NMR analysis, allowing us to confirm their structures and compositions. Following characterization, the biological activities of the Schiff base ligand and its corresponding metal complexes were rigorously assessed. This evaluation focused on their antibacterial and antifungal properties, using the well disc diffusion method to determine the inhibition zones against specific strains of bacteria and fungi. Additionally, we investigated the DNA binding capabilities of these complexes through multispectroscopic techniques, such as fluorescence and UV-Vis

spectroscopy. Our findings reveal that, among the synthesized metal complexes, the Cu(II) complex demonstrated the most significant biological activities, effectively inhibiting the growth of pathogenic microbes and showcasing a strong interaction with DNA. This indicates its potential as a promising candidate for further biological and pharmaceutical applications.

Heterogeneous metal complexes are increasingly recognized for their remarkable potential in catalysis, rivaling the efficiency of homogeneous transition metal complexes across a diverse range of applications. Their advantages stem from attributes such as sustainability, ease of recovery, and recyclability, making them a compelling choice for modern chemical processes. In our research, we have successfully synthesized an innovative magnetic nanocomposite catalyst, designated as Cu@L-dopaSB/Al<sub>2</sub>O<sub>3</sub>-Fe<sub>3</sub>O<sub>4</sub>. This composite involves the functionalization of copper(II) ions (Cu(II)) with a Schiff base derived from L-dopa, affixed to a support structure of aluminum oxide (Al<sub>2</sub>O<sub>3</sub>) and magnetite (Fe<sub>3</sub>O<sub>4</sub>). This specific combination enhances the catalyst's magnetic properties and facilitates its separation and recovery from reaction mixtures. The characterization of the developed catalyst was comprehensive, employing a variety of advanced analytical techniques. We utilized High-Resolution Scanning Electron Microscopy (HR-SEM) morphological analysis, Energy Dispersive X-ray Spectroscopy (EDX) for elemental composition, Transmission Electron Microscopy (TEM) for structural insights, X-Ray Diffraction (XRD) for crystallographic information, Brunauer-Emmett-Teller (BET) analysis for surface area assessment, Fourier Transform Infrared Spectroscopy (FTIR) for functional group identification, Inductively Coupled Plasma Atomic Emission Spectroscopy (ICP-AES) for metal content determination, and CHN analysis for organic content measurement. Additionally, Thermogravimetric Analysis (TGA) provided insights into thermal stability, while Vibrating Sample Magnetometry (VSM) assessed magnetic properties. Following its characterization, we investigated the catalytic performance of the Cu@L-dopaSB/Al<sub>2</sub>O<sub>3</sub>-Fe<sub>3</sub>O<sub>4</sub> catalyst in the synthesis of 1,4-disubstituted-1,2,3-triazoles, a class of compounds valued for their versatility in pharmaceuticals and materials science. The catalyst demonstrated exceptional

efficiency, yielding outstanding results in the target reactions, underscoring its potential for practical applications in organic synthesis.

Furthermore, a Zn (II)-based catalyst system, consisting of a Chitosan Schiff base metal complex [Zn@CS-SB/Fe<sub>3</sub>O<sub>4</sub>-SiO<sub>2</sub>], has been developed. The new catalyst was characterized using various techniques, including SEM imaging and mapping, EDX, HRTEM, XPS, FTIR, XRD, TGA, BET, VSM, ICP-AES, and CHN analysis. Organic pollutants, particularly dyes, pose significant environmental challenges and are a major concern in today's world. Many industries utilize large quantities of synthetic and aromatic dyes, many of which are highly toxic to humans and aquatic life. This highlights the urgent need for effective methods to degrade and remove these harmful substances from industrial waste under mild reaction conditions. In light of these concerns, the developed magnetic catalyst, Zn@CS-SB/Fe<sub>3</sub>O<sub>4</sub>-SiO<sub>2</sub>, was tested for its ability to degrade organic dyes. The catalyst exhibited remarkable activity for reducing various dyes, including methylene blue (MB), methyl orange (MO), methyl red (MR), and p-nitrophenol (PNP), in the presence of NaBH<sub>4</sub> as the reducing agent. The enhanced performance of this magnetic composite can be attributed to its high surface area and improved dye adsorption properties on the catalyst surface. Additionally, the catalyst demonstrated the ability to be easily recycled and reused up to six times without a significant loss in catalytic activity or selectivity.

To advance our research on the application of transition metal complexes as Schiff base functionalized magnetic catalysts, we have successfully synthesized a novel catalytic system: a palladium (II) complex functionalized with Schiff base on titania-coated magnetic nanoparticles, designated as Pd@SB/ Fe<sub>3</sub>O<sub>4</sub>-TiO<sub>2</sub>. This innovative catalytic system has undergone comprehensive characterization using a variety of analytical techniques, including Field Emission Scanning Electron Microscopy (FE-SEM), Energy Dispersive X-Ray Spectroscopy (EDX), Transmission Electron Microscopy (TEM), X-ray Photoelectron Spectroscopy (XPS), X-ray Diffraction (XRD), Brunauer-Emmett-Teller (BET) surface area analysis, Thermogravimetric Analysis (TGA), Fourier Transform Infrared Spectroscopy (FT-IR), Carbon-Hydrogen-Nitrogen (CHN) elemental analysis, Vibrating Sample

Magnetometry (VSM), and Inductively Coupled Plasma Atomic Emission Spectroscopy (ICP-AES). Biaryls are of paramount importance in the field of organic chemistry, serving as essential building blocks for a vast number of natural products, including various polymers, biologically active alkaloids, useful ligands, and critical medicinal drugs. The presence of biaryl structures in a diverse range of biologically active compounds and functional groups emphasizes their significance and versatility in modern chemical synthesis. Selective hydrogenations have gained considerable attention globally, as they enhance the economic value of products derived from different chemical processes. Additionally, they facilitate the synthesis of key compounds that are vital within the pharmaceutical, food, petrochemical, and fine chemical industries. In particular, the selective catalytic hydrogenation of aromatic nitro compounds has become increasingly important due to the high demand for the resulting aromatic amines, which have significant applications in pharmaceutical and medicinal chemistry as well as material science. To evaluate the catalytic performance of our synthesized Pd@SB/Fe<sub>3</sub>O<sub>4</sub>-TiO<sub>2</sub> catalyticsystem, we investigated its efficiency in two crucial reactions: the Suzuki coupling reaction aimed at synthesizing biaryls through carbon-carbon coupling, and the selective hydrogenation reaction targeting aromatic nitro compounds to produce aromatic amines. The results obtained were outstanding, showcasing the catalyst's efficacy under sustainable reaction conditions and highlighting its potential for practical applications in organic synthesis.

In conclusion, this thesis decisively addresses all targeted objectives, thoroughly investigating the antimicrobial properties of Schiff base metal complexes, their DNA binding capabilities, and their catalytic activities in crucial reactions. The study rigorously focuses on carbon-carbon (C-C) coupling, carbon-nitrogen (C-N) bond formation, and hydrogenation processes, specifically involving metal complexes of copper (Cu), zinc (Zn), and palladium (Pd). These investigations unequivocally demonstrate the significant potential and versatility of these metal complexes in advancing applications within medicinal chemistry and catalysis.

### Future Scope

Schiff base metal complexes are increasingly recognized for their remarkable properties, positioning them as promising candidates for a variety of biological and catalytic applications within both medicinal and industrial sectors. These complexes which exhibit significant biological activities, have been investigated comprehensively. Their antibacterial, antifungal, antiviral. anticancer, neuroprotective, and DNA-binding capabilities highlight their potential in therapeutic settings, offering innovative approaches to combat various diseases. Future endeavors in this field could focus on the design of tailored Schiff base metal complexes aimed at specific disease targets, enabling more effective treatment options. Exploring the synergistic effects of these complexes in conjunction with existing therapeutic agents presents an additional avenue for enhancing treatment efficacy. Furthermore, the development of Schiff base metal complex-based nanoparticles could revolutionize drug delivery systems, improving bioavailability and targeting of drugs to specific tissues. On the other hand, the role of heterogeneous Schiff base catalysts in organic transformations has garnered significant attention due to their efficiency and versatility. A deeper understanding of these catalytic systems is crucial for the design of novel Schiff base structures and supporting materials. This knowledge could facilitate the creation of asymmetric Schiff base catalysts, which are essential for producing enantiomerically pure compounds. Moreover, integrating Schiff base catalysts with cutting-edge technologies—such as metal-free catalysis, the synthesis of hybrid materials, advanced computational design, and photocatalytic applications—holds great promise for expanding their functionality and applicability in various chemical processes.

### **List of Publications**

- [1]. Kumar, A., Ahmed, S., Bhardwaj, M., Imtiaz, S., Kumar, D., Bhat, A.R., Sood, B. and Maji, S., 2024. In vitro Anti-microbial, DNA-binding, In silico Pharmacokinetics and Molecular Docking Studies of Schiff-based Cu (II), Zn (II) and Pd (II) Complexes. *Journal of Molecular Structure*, p.138695.
- [2]. **Kumar**, **A.**, Sharma, S., Sharma, S., Bhardwaj, M. and Maji, S., **2024**. Novel Pd (II) complex of Schiff base encapsulated on ferrite—titania core [Pd@ SB/Fe<sub>3</sub>O<sub>4</sub>—TiO<sub>2</sub>]: a recyclable nanocatalyst for Suzuki coupling and hydrogenation of aromatic nitro compounds. *Research on Chemical Intermediates*, *50*(9), pp.4249-4274.
- [3]. **Kumar**, **A.**, Sharma, V., Bhardwaj, M. and Maji, S., **2025**. Novel Schiff Base Functionalized Cu (II) onto L-dopa/Al<sub>2</sub>O<sub>3</sub>-Fe<sub>3</sub>O<sub>4</sub> as an Efficient Catalyst for One Pot Synthesis of 1, 4-Disubstituted-1, 2, 3-Triazoles using Boronic Acids in Benign Reaction Media. *Journal of Inorganic and Organometallic Polymers and Materials*, pp.1-20.
- [4]. Elhadj-Daouadji, B., Zaoui, F., Zorgani, M.A., Abubakar, S., Siddig, L.A., Abdelhamid, A.S., Bhardwaj, M., Hachemaoui, M., **Kumar, A.**, Bounaceur, B. and Lebsir, F., **2025**. Efficient removal of asphaltene and organic dyes using hybrid magnetic Nanomaterials: Adsorption selectivity and comparative study. *Fuel*, *381*, p.133284.
- [5].Mir, A.A., Wani, Z.A., Baht, A.R., Fahelelbom, K.M., Kumar, A. and Ahmed, S., 2024. Widening spectrum of adverse effects caused by long-term use of proton pump inhibitors: A comprehensive review of literature. *LabMed Discovery*, p.100027.
- [6]. Bhardwaj, M., Mahajan, B., **Kumar**, **A.** and Parcha, V., **2023**. Studies on antioxidant potential and total phenolic contents of dried powder and pulp of raw and ripe Carica papaya fruit. *Biomedicine*, *43*(02), pp.753-758.

### **List of Conferences**

- 1.Oral presentationin 4<sup>th</sup>International Conference on "Recent Advances in Fundamental and Applied Sciences" (RAFAS-2023)held on March 24<sup>th</sup> -25<sup>th</sup>2023 organized by School of Chemical Engineering and Physical Sciences, Lovely Professional University, Punjab.
- 2. Oral presentation in 5<sup>th</sup> International Conference on "Recent Advances in Fundamental and Applied Sciences" (RAFAS-2024) held on April19<sup>th</sup>-20<sup>th</sup> 2024 organized by School of Chemical Engineering and Physical Sciences, Lovely Professional University, Punjab.
- 3. Certificate of Meritfor securing Second PositionPrize in the Oral presentation in 4<sup>th</sup> International Conference on "Recent Advances in Fundamental and Applied Sciences" (RAFAS-2023) held on March 24<sup>th</sup> -25<sup>th</sup> 2023 organized by School of Chemical Engineering and Physical Sciences, Lovely Professional University, Punjab.